UNIVERSIDADE FEDERAL DE GOIÁS (UFG)

INSTITUTO DE CIÊNCIAS BIOLÓGICAS (ICB)

PROGRAMA DE PÓS-GRADUAÇÃO EM GENÉTICA E BIOLOGIA MOLECULAR (PPGBM)

APARECIDO FERREIRA DE SOUZA

Homeostase de ferro em *Paracoccidioides* spp.: novos alvos de estudo e estabelecimento de HSP30 como proteína ligante de hemoglobina

GOIÂNIA

2021

UNIVERSIDADE FEDERAL DE GOIÁS
INSTITUTO DE CIÊNCIAS BIOLÓGICAS

TERMO DE CIÊNCIA E DE AUTORIZAÇÃO (TECA) PARA DISPONIBILIZAR VERSÕES ELETRÔNICAS DE TESES

E DISSERTAÇÕES NA BIBLIOTECA DIGITAL DA UFG

Na qualidade de titular dos direitos de autor, autorizo a Universidade Federal de Goiás (UFG) a disponibilizar, gratuitamente, por meio da Biblioteca Digital de Teses e Dissertações (BDTD/UFG), regulamentada pela Resolução CEPEC nº 832/2007, sem ressarcimento dos direitos autorais, de acordo com a Lei 9.610/98, o documento conforme permissões assinaladas abaixo, para fins de leitura, impressão e/ou download, a título de divulgação da produção científica brasileira, a partir desta data.

O conteúdo das Teses e Dissertações disponibilizado na BDTD/UFG é de responsabilidade exclusiva do autor. Ao encaminhar o produto final, o autor(a) e o(a) orientador(a) firmam o compromisso de que o trabalho não contém nenhuma violação de quaisquer direitos autorais ou outro direito de terceiros.

1. Identificação do material bibliográfico

[ ] Dissertação [x] Tese

2. Nome completo do autor

Aparecido Ferreira de Souza

3. Título do trabalho

Homeostase de ferro em *Paracoccidioides* spp.: novos alvos de estudo e estabelecimento de HSP30 como proteína ligante de hemoglobina

4. Informações de acesso ao documento (este campo deve ser preenchido pelo orientador)

Concorda com a liberação total do documento [x] SIM [ ] NÃO[1]

[1] Neste caso o documento será embargado por até um ano a partir da data de defesa. Após esse período, a possível disponibilização ocorrerá apenas mediante:
a) consulta ao(à) autor(a) e ao(à) orientador(a);
b) novo Termo de Ciência e de Autorização (TECA) assinado e inserido no arquivo da tese ou dissertação.
O documento não será disponibilizado durante o período de embargo.
Casos de embargo:
- Solicitação de registro de patente;
- Submissão de artigo em revista científica;
- Publicação como capítulo de livro;
- Publicação da dissertação/tese em livro.

Obs. Este termo deverá ser assinado no SEI pelo orientador e pelo autor.

Documento assinado eletronicamente por **APARECIDO FERREIRA DE SOUZA**, **Discente**, em 06/07/2021, às 12:49, conforme horário oficial de Brasília, com fundamento no art. 6º, § 1º, do Decreto nº 8.539, de 8 de outubro de 2015.

Documento assinado eletronicamente por **Celia Maria De Almeida Soares**, **Professor do Magistério Superior**, em 29/07/2021, às 13:48, conforme horário oficial de Brasília, com fundamento no art. 6º, § 1º, do Decreto nº 8.539, de 8 de outubro de 2015.

A autenticidade deste documento pode ser conferida no site https://sei.ufg.br/sei/controlador_externo.php?acao=documento_conferir&id_orgao_acesso_externo=0, informando o código verificador **2188504** e o código CRC **B150C169**.

Referência: Processo nº 23070.032676/2021-77 SEI nº 2188504

APARECIDO FERREIRA DE SOUZA

Homeostase de ferro em *Paracoccidioides* spp.: novos alvos de estudo e estabelecimento de HSP30 como proteína ligante de hemoglobina

Tese apresentada ao Programa de Pós-Graduação em Genética e Biologia Molecular, do Instituto de Ciências Biológicas, da Universidade Federal de Goiás (UFG), como requisito para obtenção do título de Doutor em Genética e Biologia Molecular.
Área de concentração: Genética e Biologia Molecular.
Linha de pesquisa: Genômica funcional, estrutural e proteômica.

Orientadora: Professora Doutora Célia Maria de Almeida Soares.

GOIÂNIA

2021

Ficha de identificação da obra elaborada pelo autor, através do
Programa de Geração Automática do Sistema de Bibliotecas da UFG.

Souza, Aparecido Ferreira de
Homeostase de ferro em Paracoccidioides spp.: novos alvos de estudo e estabelecimento de HSP30 como proteína ligante de hemoglobina [manuscrito] / Aparecido Ferreira de Souza. - 2021.
8, 157 f.: il.

Orientador: Profa. Dra. Célia Maria de Almeida Soares.
Tese (Doutorado) - Universidade Federal de Goiás, , Programa de Pós-Graduação em Genética e Biologia Molecular, Goiânia, 2021.
Bibliografia. Anexos. Apêndice.

1. Imunidade nutricional. 2. HSP30. 3. proteínas-CFEM. 4. Sideróforos. I. Soares, Célia Maria de Almeida, orient. II. Título.

CDU 577.2

UNIVERSIDADE FEDERAL DE GOIÁS

INSTITUTO DE CIÊNCIAS BIOLÓGICAS

ATA DE DEFESA DE TESE

ATA DE DEFESA DE TESE

Ata Nº **28** da sessão de Defesa de Tese de **Aparecido Ferreira de Souza** que confere o título de Doutor(a) em **Genética e Biologia Molecular**, na área de concentração em **Genética e Biologia Molecular.**

Ao/s **vinte e oito dias do mês de junho do ano de dois mil e vinte e um**, a partir da(s) **14h00**, por videoconferência, seguindo portaria CAPES no. 36 de 16 de março de 2020 e recomendação da UFG, realizou-se a sessão pública de Defesa de Tese intitulada **"Homeostase de ferro em *Paracoccidioides spp.*: advento de novos alvos de estudo e estabelecimento de HSP30 como proteína ligante de hemoglobina**". Os trabalhos foram instalados pelo(a) Orientador(a), Professor(a) Doutor(a) **Célia Maria de Almeida Soares (ICB/UFG)** com a participação dos demais membros da Banca Examinadora: Professor(a) Doutor(a) **Augusto Schrank (UFRGS)**, membro titular externo; Professor(a) Doutor(a) **Ana Flávia Alves Parente (UnB)**, membro titular externo, Professor(a) Doutor(a) **Elisa Flávia Luiz Cardoso Bailão (UEG)**, membro titular externo; Professor(a) Doutor(a) **Alexandre Melo Bailão (ICB/UFG)**, membro titular interno. Durante a argüição os membros da banca **fizeram** sugestão de alteração do título do **trabalho**. A Banca Examinadora reuniu-se em sessão secreta a fim de concluir o julgamento da Tese tendo sido(a) o(a) candidato(a) **aprovado** pelos seus membros. Proclamados os resultados pelo(a) Professor(a) Doutor(a) **Célia Maria de Almeida Soares**, Presidente da Banca Examinadora, foram encerrados os trabalhos e, para constar, lavrou-se a presente ata que é assinada pelos Membros da Banca Examinadora, ao(s) **vinte e oito dias do mês de junho do ano de dois mil e vinte e um**.

TÍTULO SUGERIDO PELA BANCA

"Homeostase de ferro em *Paracoccidioides spp.*: novos alvos de estudo e estabelecimento de HSP30 como proteína ligante de hemoglobina"

Documento assinado eletronicamente por **Alexandre Melo Bailao**, **Professor do Magistério Superior**, em 28/06/2021, às 18:03, conforme horário oficial de Brasília, com fundamento no art. 6º, § 1º, do Decreto nº 8.539, de 8 de outubro de 2015.

Documento assinado eletronicamente por **Celia Maria De Almeida Soares**, **Professor do Magistério Superior**, em 28/06/2021, às 18:03, conforme horário oficial de Brasília, com fundamento no art. 6º, § 1º, do Decreto nº 8.539, de 8 de outubro de 2015.

Documento assinado eletronicamente por **Elisa Flávia Luiz Cardoso Bailão**,

Usuário Externo, em 28/06/2021, às 18:05, conforme horário oficial de Brasília, com fundamento no art. 6º, § 1º, do Decreto nº 8.539, de 8 de outubro de 2015.

Documento assinado eletronicamente por **Juliana Alves Parente Rocha**, **Coordenadora de Pós-Graduação**, em 28/06/2021, às 18:06, conforme horário oficial de Brasília, com fundamento no art. 6º, § 1º, do Decreto nº 8.539, de 8 de outubro de 2015.

A autenticidade deste documento pode ser conferida no site https://sei.ufg.br/sei/controlador_externo.php?acao=documento_conferir&id_orgao_acesso_externo=0, informando o código verificador **2170676** e o código CRC **4B34FCC7**.

Referência: Processo nº 23070.032676/2021-77 SEI nº 2170676

Dedico esta tese a *Deus*, meu grande *Amigo*; aos meus pais queridos, *Sr. Manoel Jorge de Souza* e *Sra. Jovita Ferreira Brito*; ao amor da minha vida, *Flaviane Muniz Dias*; à minha irmã maravilhosa, *Anália Ferreira de Souza* e ao meu sobrinho amado, *Christopher Souza Andrade*.

"Choose what you love most and let it kill you, if you have to".

(Lara Fabian)

"To fight for the right without question or pause. To be willing to march, march into hell for a heavenly cause".

(The Impossible Dream, Joe Darion)

"Aprenda a ir com tudo, inclusive com calma".

(Aparecido Souza)

AGRADECIMENTOS

A *Deus*, por de forma tão amável ter escolhido me chamar de amigo. Por contrapor a tendência do Universo à desordem, aleatoriedade e ao caos, promovendo eventos outrora impossíveis, favoráveis. Em minha mente ecoa um pensamento: seria a entalpia a própria manifestação Divina? Independente de hipóteses e teorias, aprendi que "O temor do *Senhor* é o princípio da sabedoria, e o conhecimento do *Santo* é prudência" (Provérbios 9,10). Obrigado, meu *Amigo*, por me fazer chegar até aqui e por saber que *Tu* tens para mim planos maiores e melhores que os meus, os quais estão muito além da minha racionalidade.

Aos meus pais, *Sr. Manoel Jorge de Souza* e *Sra. Jovita Ferreira Brito*, por todo o apoio a mim devotado. Foram muitas as dificuldades para que eu pudesse chegar até aqui, mas vosso amor e exemplo de integridade me nutriram para enfrentar os desafios, hora extrínsecos, hora intrínsecos. Aos senhores dedico meu amor!

À minha esposa maravilhosa, *Flaviane Muniz Dias*, por ter abraçado meus sonhos como seus e sempre agir com carinho e compreensão nos momentos mais difíceis desta caminhada. O seu abraço é um esteio para mim, no qual posso repousar em meio às tempestades da vida. Te amo! Aos meus sogros, *Sr. Washington Dias de Araújo* e *Sra. Maria Aparecida Muniz Dias*, por terem me acolhido como filho e agirem sempre de forma empática para comigo.

À minha irmã, *Anália Ferreira de Souza*, por invariavelmente me conceder apoio e ser um exemplo de perseverança em meio às adversidades. Ao meu sobrinho lindo, *Christopher Souza Andrade*, cujo sorriso faz aquecer meu coração.

À minha orientadora, *Profa. Dra. Célia Maria de Almeida Soares*, por todo o apoio dispensado a mim. Foram inúmeras as vezes em que eu pensei em desistir, porém a senhora não desistiu de mim. Agradeço de coração por sua atitude empática frente às minhas limitações intrínsecas. Não poderia deixar de agradecer à senhora por sempre providenciar para mim a compra de todos os reagentes, materiais e insumos que eu precisei para o desenvolvimento de meu trabalho de doutorado (e mestrado). Tenho em minha mente a clareza de que tive acesso a ótimas condições de trabalho bem como a oportunidades de aprendizado ímpares, de valor incalculável. Mais uma vez, meu sincero agradecimento à senhora!

Aos docentes que integram o Laboratório de Biologia Molecular da Universidade Federal de Goiás, por incontáveis momentos de aprendizado que tive junto aos senhores. Agradeço especialmente ao *Prof. Dr. Alexandre Melo Bailão* e à *Profa. Dra. Mirelle Garcia Silva Bailão*, por sempre terem acolhido a mim e às minhas dúvidas de forma cordial e atenciosa, colaborando grandemente para o meu aprendizado nesta jornada do estudo da homeostase de Fe em microrganismos.

Aos companheiros com os quais tive a felicidade de poder trabalhar: *Dr. Juliano Domiraci Paccez*, *Dra. Mariana Vieira Tomazett*, *Me. Kassyo Lobato Potenciano Silva*, *Me. Lana O'Hara Souza Silva*, *Me. Guilherme Algusto Alves Silva*, *Dr. André Luis Elias Moreira*, *Dr. Luiz Paulo Araújo dos Santos*, *Dr. Leandro do Prado Assunção*, *Dr. Kleber Santiago Freitas e Silva*, *Me. Raisa Melo Lima*, *Dra. Juliana Santana de Curcio* e *Dra. Marielle Garcia Silva*. Muito obrigado por compartilharem tanto conhecimento comigo. Pude aprender muito ao vosso lado. O melhor da vida é o que desejo para vocês! Agradeço a todos os colegas do Laboratório de Biologia Molecular da UFG que de alguma forma contribuíram para que eu chegasse até aqui.

Aos coordenadores do PGBM de diferentes períodos de vigência do cargo, por tamanha dedicação na consolidação do programa bem como na atenção dedicada a nós, discentes.

À servidora técnico-administrativa *Lilia Fernanda Fernandes Duarte Barbalho* por de forma tão competente atender às nossas demandas da pós-graduação.

À *Dra. Ana Cristina Guimarães* e ao *Dr. Rafael Borges Mendes* por me apoiarem de forma extremamente profissional no que tange à minha saúde mental.

A queridos amigos que me apoiaram nesta caminhada, cujo número é tão grande que tenho o receio de me esquecer de algum. Minha sincera gratidão a vocês!

À CAPES por conceder minha bolsa de estudos durante o doutorado (e mestrado).

À banca de avaliação desta tese, por ter aceitado de bom grado revisar meu trabalho.

A todos, por tudo, muito obrigado!

SUMÁRIO

LISTA DE FIGURAS

RESUMO

Compreender os mecanismos que regem a interação patógeno-hospedeiro é crucial para o desenvolvimento de novas abordagens terapêuticas e de diagnóstico. Fungos do gênero *Paracoccidioides* são os agentes etiológicos da micose sistêmica paracoccidioidomicose e, quando no hospedeiro, encontram um ambiente desafiador e escasso em nutrientes e micronutrientes, como o Fe, que é indispensável para a sobrevivência do patógeno. Estudos prévios demonstraram que fungos deste gênero, em resposta à privação de Fe, são capazes de sintetizar e captar sideróforos (quelantes de Fe^{3+}), utilizar proteínas do hospedeiro que contêm Fe como fonte do metal e utilizar uma via redutiva não-canônica de assimilação de Fe. Apesar de todos estes achados, ainda há lacunas que precisam ser preenchidas quanto à resposta do patógeno à privação do metal. No presente trabalho, alvos que ainda precisam de estudo neste contexto foram definidos, como o estabelecimento das funções de proteínas do fungo que contêm o domínio CFEM e a determinação da especificidade de receptores de sideróforos. Adicionalmente, mostrou-se que a exposição de *Paracoccidioides* à hemoglobina promove mudança em nível de proteoma de parede celular do fungo, o que é ilustrado pela capacidade aumentada do fungo interagir com macrófagos. Esta abordagem permitiu a bioprospecção da proteína ligante de hemoglobina HSP30, a qual está presente na superfície celular e tem a expressão regulada positivamente quando o fungo é exposto à hemoglobina. Foi demonstrado que o silenciamento de *hsp30* causa diminuição do crescimento do fungo após exposição à hemoglobina. Cabe ainda investigar a função de HSP30 como heme oxigenase. A observação detalhada destas questões, ainda em aberto, pode promover a expansão do conhecimento sobre a biologia de *Paracoccidioides* spp. e, consequentemente, promover a bioprospecção de novos alvos para diagnóstico diferencial e/ou terapia da PCM.

Palavras-chave: Imunidade nutricional; HSP30; proteínas-CFEM; Sideróforos.

ABSTRACT

Understanding the mechanisms that govern host-pathogen interaction is crucial for the development of new therapeutic and diagnostic approaches. Fungi of *Paracoccidioides* genus are the etiological agents of paracoccidioidomycosis, a systemic mycosis and, when in the host, fungi find a hostile environment that is scarce in nutrients and micronutrients, such as Fe, which is indispensable for the survival of the pathogen. Previous studies have shown that fungi of this genus, in response to Fe deprivation, are able to synthesize and capture siderophores (Fe^{3+} chelators), use host proteins that contain Fe as metal's source and use a non-canonical reductive pathway for assimilation of Fe. Despite all these findings, there are still gaps that need to be filled regarding the pathogen's response to Fe deprivation. In the present work, targets that still need to be studied in this context were defined, such as the establishment of the protein functions of the fungus that contain the CFEM domain and the determination of the specificity of siderophore receptors. Additionally, it was shown that the exposure of *Paracoccidioides* to hemoglobin promotes changes at fungal cell wall proteome level, which is illustrated by the increased ability of the fungus to interact with macrophages. This approach allowed the bioprospecting of the hemoglobin-binding protein HSP30, which is present on the cell surface and has its expression regulated positively when the fungus is exposed to hemoglobin. It has been shown that silencing of *hsp30* causes decreased growth of the fungus after exposure to hemoglobin. It is also necessary to investigate the function of HSP30 as heme oxygenase. The detailed observation of those open questions can promote the expansion of knowledge about the biology of *Paracoccidioides* spp. and, consequently, promote the bioprospecting of new targets for differential diagnosis and/or therapy of PCM.

Keywords: Nutritional immunity; HSP30; CFEM-proteins; Siderophores.

1. Introdução / Revisão de literatura

1.1. Interação patógeno-hospedeiro

Arsenais sofisticados, táticas rebuscadas e constantes mudanças estratégicas: o que poderia ser a descrição de um cenário de guerra também serve como conotação para o evento de interação patógeno-hospedeiro (Asehnoune, Villadangos e Hotchkiss, 2016; Gonzalez e Hernandez, 2016). Dentre a miríade de aspectos estudados na interação patógeno-hospedeiro, a imunidade nutricional ocupa lugar de destaque por consistir na habilidade inata do hospedeiro de controlar a biodisponibilidade de nutrientes e micronutrientes essenciais, como o ferro (Fe), afetando a sobrevivência de patógenos (Núñez, Sakamoto e Soares, 2018; Soares e Weiss, 2015; Wang e Cheraryil, 2009).

Fungos do gênero *Paracoccidioides* são os agentes etiológicos da paracoccidioidomicose (PCM), micose sistêmica endêmica da América Latina cujo diagnóstico acurado e abordagem terapêutica de menor tempo ainda são desafios (Shikanai-Yasuda, Mendes, Colombo, Queiroz-telles, Satie, Kono, Paniago, A. M. M., *et al.*, 2017). Estudos prévios demonstraram que a resposta de *Paracoccidioides* à depleção de Fe é um importante atributo de virulência para o patógeno, que uma vez sob depleção do metal, promove modulação de seu metabolismo, primando pela utilização de vias metabólicas independentes de Fe (Parente, Ana F. A. *et al.*, 2011). Os mecanismos que o fungo emprega para obter Fe quando no hospedeiro incluem a capacidade de sintetizar, secretar e captar sideróforos/xenosideróforos; uma via redutiva não-clássica de assimilação de Fe e a capacidade de captar heme/hemoglobina por meio de um receptor GPI-ancorado denominado Rbt5, conforme descrito em trabalhos prévios (Bailão *et al.*, 2014, 2015; Silva-Bailão *et al.*, 2014; Silva *et al.*, 2020).

Apesar da robusta contribuição destes estudos, ainda há a necessidade da ampliar o conhecimento sobre como os fungos deste gênero respondem à depleção de Fe. O presente trabalho elenca eventos que ainda precisam ser investigados no contexto *Paracoccidioides*-privação de Fe e estabelece HSP30 como uma nova proteína ligante de hemoglobina em *Paracoccidioides* spp.

1.2. O micronutriente Fe

Ubiquidade e polivalência são atributos do micronutriente Fe. Este metal de transição é o mais abundante do planeta e o quarto mais encontrado na crosta terrestre.

Devido à sua flexibilidade de estados de oxidação é empregado por sistemas biológicos como cofator de metaloproteínas que atuam em eventos vitais, como o metabolismo energético, biossíntese e reparo de DNA, síntese de outros biopolímeros e muitos outros processos (Baker, Anderson e Baker, 2003; Dlouhy e Outten, 2013). Os íons Fe^{2+} (doador de elétrons) e Fe^{3+} (aceptor de elétrons) são as principais formas do micronutriente encontradas em sistemas biológicos e a interconversão entre estas formas é sobremaneira fácil. Cabe salientar que na presença de água, oxigênio e pH fisiológico (7,2), a forma predominante do metal é Fe^{3+}, sendo a solubilidade deste extremamente limitada (Baker, Anderson e Baker, 2003; Kosman, 2013).

A maneira versátil como a interconversão entre os íons Fe^{2+} e Fe^{3+} ocorre também apresenta um lado negativo: na presença de água e oxigênio, íons livres do metal podem promover a formação de radicais hidroxila, baseada nas reações de Fenton e Haber-Weiss, que causam danos oxidativos a biomoléculas e estruturas celulares (Hentze, Muckenthaler e Andrews, 2004; Papanikolaou e Pantopoulos, 2005). Por ser ao mesmo tempo vital e potencialmente tóxico, o controle da biodisponibilidade de Fe é realizado de maneira equilibrada, com estrito controle da captação, estoque e mobilização do metal. Tal controle em parte é feito pela associação do metal a proteínas do organismo, que limitam a quantidade livre do metal (Kosman, 2020; Tandara e Salamunic, 2012).

1.3. Homeostase de ferro na infecção

A resposta do hospedeiro humano a patógenos, como *Paracoccidioides* spp., é complexa e envolve diversos componentes do sistema imunológico. Células da imunidade inata, como neutrófilos, células NK e macrófagos são mobilizadas para contrapor o agente invasor e uma série de citocinas pró-inflamatórias são produzidas nesse cenário. O padrão de citocinas produzidas (Th1/Th2/Th17) pode ser diferente em indivíduos acometidos e, como esses padrões direcionam a resposta de linfócitos T e B, diferentes desfechos da doença são descritos na literatura (Burger, 2021).

A importância do micronutriente Fe para sistemas biológicos propicia a competição entre patógenos e hospedeiros pelo metal. O hospedeiro humano (assim como demais mamíferos) apresenta como componente integral de sua imunidade inata a chamada imunidade nutricional, que é a capacidade de, na maior parte dos casos, limitar a biodisponibilidade de nutrientes e micronutrientes essenciais para patógenos (Núñez,

Sakamoto e Soares, 2018; Wang e Cheraryil, 2009; Weinberg, 1975). A ligação do metal a proteínas como ferritina, transferrina, lactoferrina, siderocalina e hemoglobina (proteína globular tetramérica abundante que alberga quatro grupos heme, e está presente nos eritrócitos, relacionada ao transporte de oxigênio), é uma forma de ao mesmo tempo evitar efeitos tóxicos e limitar o acesso de patógenos ao metal (Papanikolaou e Pantopoulos, 2005).

Nos cenários de infecção, o organismo promove o aumento da biossíntese de citocinas pró-inflamatórias. Dentre estas citocinas, a interleucina-6 é de importância relevante no que tange ao controle da biodisponibilidade do micronutriente Fe, uma vez que esta citocina estimula hepatócitos a produzirem hepcidina, o hormônio peptídico considerado como o regulador central do metabolismo de ferro em mamíferos (Nemeth *et al.*, 2004; Tandara e Salamunic, 2012). O aumento dos níveis séricos de hepcidina provoca hipoferremia por regular negativamente a proteína de efluxo de Fe de fagócitos e enterócitos, chamada ferroportina (FPN) conforme Figura 1, que consiste em uma representação esquemática do processo.

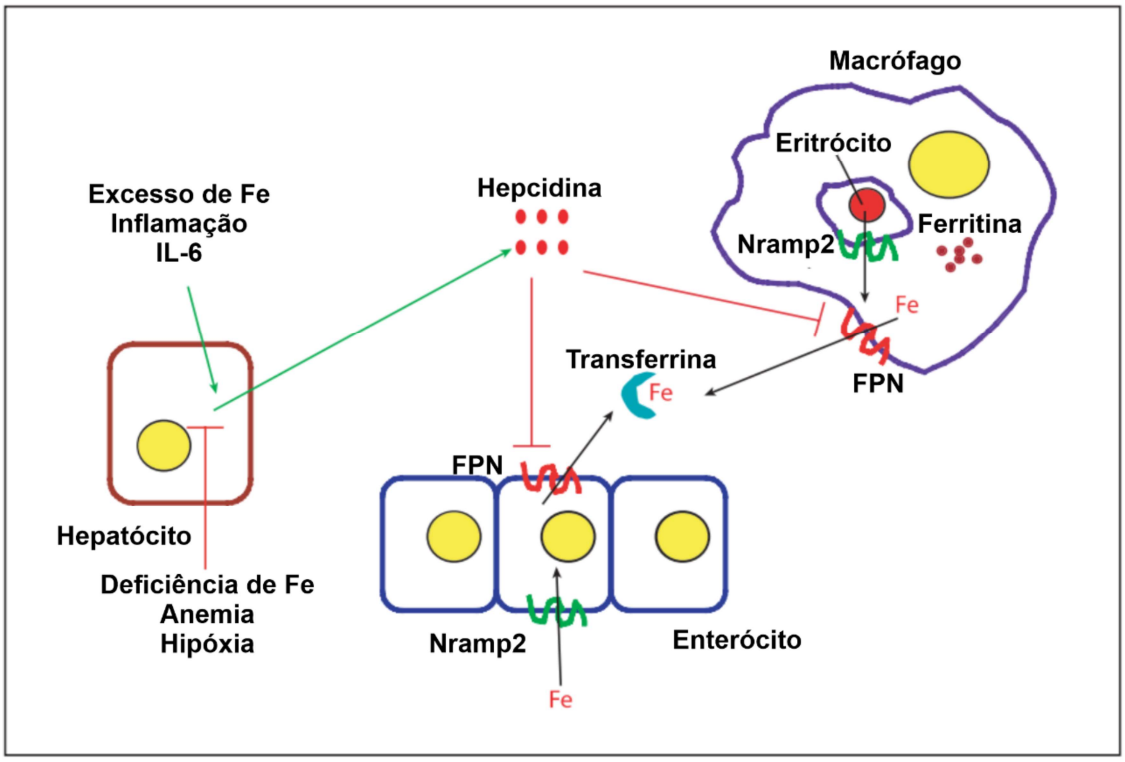

Figura 1. Homeostase de Fe no hospedeiro e a função do hormônio hepcidina. Processos infecciosos desencadeiam inflamação com consequente aumento de IL-6 que por sua vez induz a biossíntese de hepcidina, hormônio peptídico considerado como central na regulação sistêmica de Fe. IL-6: interleucina

6, FPN: ferroportina (exportador de Fe), Nramp2 (importador/exportador de Fe). Adaptado de Wang e Cheraryil, 2009.

Em adição aos eventos previamente descritos, a regulação negativa de FPN também promove o aumento da quantidade intracelular de Fe. Este aumento intracelular do metal leva à ativação de NF-kB e consequente aumento da biossíntese de outras citocinas pró-inflamatórias. Esta estratégia reduz para níveis drásticos os níveis de Fe circulante no organismo, o que caracteriza um fator limitante para a proliferação de patógenos extracelulares (Tandara e Salamunic, 2012).

Patógenos intracelulares também enfrentam limitação de acesso ao Fe, uma vez que a presença destes no interior de macrófagos promove o aumento da expressão dos transportadores Nramp1 e FPN, que atuam respectivamente no efluxo de Fe do interior de fagolisossomos para o citoplasma e no efluxo de Fe do citoplasma para o meio extracelular (Wang e Cheraryil, 2009). Com o decréscimo da quantidade intracelular de Fe, além da inibição do crescimento de patógenos, também ocorre a inibição de NF-kB. Apesar disso, a indução da resposta inflamatória não é inibida, porque ocorre a indução de HIF-1α (fator induzível por hipóxia), que também promove o aumento da biossíntese de citocinas pró-inflamatórias (Wang e Cheraryil, 2009).

1.4. Fungos patogênicos: mecanismos de resposta à depleção de Fe

Frente ao ambiente escasso de Fe encontrado no hospedeiro, fungos patogênicos empregam diferentes estratégias para conseguir ter acesso ao metal, as quais são basicamente: (1) captação de sideróforos ou heme/hemoglobina mediada por receptores, o que caracteriza vias não redutivas de assimilação de Fe e; (2) vias redutivas de assimilação de Fe, que dependem de complexos enzimáticos (transportadores e permeases) que promovem oxidorredução do metal e a captação deste (Caza e Kronstad, 2013).

Sideróforos são quelantes orgânicos de baixo peso molecular que possuem alta afinidade por Fe^{3+} (Neilands, 1993). Alguns fungos, como *Aspergillus fumigatus*, apresentam a capacidade de biossíntese dessas moléculas e as secretam para o sequestro de Fe^{3+} no meio extracelular, realizando após a absorção do complexo sideróforo-Fe^{3+} através de receptores (Haas *et al.*, 2003; Hissen *et al.*, 2004; Raymond-Bouchard *et al.*,

2012; Schrettl *et al.*, 2007; Wallner *et al.*, 2009). Alguns fungos, porém, não são hábeis para a biossíntese de sideróforos, mas apresentam a capacidade de captar sideróforos produzidos por outros organismos (xenosideróforos), sendo exemplos de fungos com tal habilidade *Candida albicans* e *Cryptococcus neoformans* (Heymann *et al.*, 2002; Tangen *et al.*, 2007).

Apesar de ser uma estratégia sofisticada, sideróforos têm afinidade por Fe^{3+}, e a biodisponibilidade de Fe livre no hospedeiro é ínfima, uma vez que o metal se encontra ligado a diversas proteínas do hospedeiro. Frente a esta situação, alguns fungos desenvolveram a capacidade de competir com o hospedeiro pelo ferro contido em algumas proteínas, utilizando para tanto adesinas e vias redutivas de assimilação de Fe, que classicamente são compostas por redutases férricas, ferroxidases dependentes de cobre e ferropermeases de alta afinidade (Bailão *et al.*, 2012). São exemplos de fungos com esta capacidade *C. albicans* e *C. neoformans*, que são hábeis na utilização de transferrina como fonte de Fe (Jung *et al.*, 2008, 2009; Jung e Kronstad, 2008; Knight *et al.*, 2005; Ramanan e Wang, 2000). *C. albicans* em adição à capacidade de utilização de transferrina como fonte de Fe, também é hábil para utilizar ferritina, através de uma adesina chamada Als3, associada às pseudo-hifas produzidas pelo fungo durante a infecção (Almeida *et al.*, 2008). Outra estratégia para captação de Fe por fungos patogênicos é a secreção de redutases férricas, conforme demonstrado em estudos prévios com foco em *Histoplasma capsulatum*, os quais apontaram que esta atividade de redutase férrica é dependente de glutationa, a qual é clivada por uma gama-glutamiltransferase (Ggt1) secretada pelo fungo, evento que gera um dipeptídeo com alto poder redutor (Zarnowski *et al.*, 2008; Zarnowski e Woods, 2005).

Não obstante, fungos patogênicos também apresentam a capacidade de utilizar heme/hemoglobina como fonte de Fe (Caza e Kronstad, 2013; Roy e Kornitzer, 2019). *C. albicans* é o fungo patogênico sobre o qual há o maior número de informações sobre este mecanismo. O fungo é capaz de provocar lise de eritrócitos e utilizar hemoglobina como fonte de Fe (Moors *et al.*, 1992; Pendrak e Roberts, 2007; Tanaka *et al.*, 1997). A identificação e caracterização do fator hemolítico de *C. albicans* apontou que o mesmo consiste em uma manoproteína e que a porção glicosilada desta exerce função crucial para o processo de hemólise (Manns, Mosser e Buckley, 1994; Watanabe *et al.*, 1999).

Dentre as maiores contribuições dos estudos de utilização de heme por *C. albicans*, está a descoberta de uma família de receptores que é essencial para o processo

(Weissman e Kornitzer, 2004). Componentes dessa família, Rbt5 e Pga7 são proteínas que contêm o chamado domínio CFEM (*common in several fungal extracellular membrane proteins*) e estão presentes na parede celular e na membrana do patógeno, as quais realizam um mecanismo de comunicação permitindo a transferência de heme para o meio intracelular (Kulkarni, Kelkar e Dean, 2003; Kuznets *et al.*, 2014; Zhang *et al.*, 2015). Adicionalmente ao sistema, outra proteína que também contém domínio CFEM, denominada Csa2, foi identificada no exoproteoma de *C. albicans* e teve sua importância demonstrada para o processo de captação de heme, por atuar como hemóforo (Okamoto-Shibayama *et al.*, 2014; Sorgo *et al.*, 2010). Csa2 teve sua estrutura cristalográfica determinada, o que contribuiu para o estabelecimento do domínio CFEM como a porção da proteína que se liga ao heme e abriu perspectivas para o estudo de outras proteínas que contêm este domínio e a função destas no processo de patogênese (Nasser *et al.*, 2016). Csa1 e Rbt51 também foram apontadas como componentes da família de receptores de hemoglobina em *C. albicans*, mas a função precisa dessas proteínas em relação à captação de heme não está completamente estabelecida (Weissman e Kornitzer, 2004). Recentemente foi demonstrado que este sistema de receptores é capaz de internalizar heme previamente ligado à albumina, elencando esta como uma fonte nova de heme para o patógeno (Pinsky *et al.*, 2020). A internalização do grupo heme por *C. albicans* é concluída pelo sistema ESCRT de endocitose e, posteriormente, a molécula sofre ação da enzima heme oxigenase, que promove a liberação de Fe, biliverdina e monóxido de carbono (Pendrak *et al.*, 2004; Weissman *et al.*, 2008). A Figura 2 consiste em uma representação esquemática dos processos descritos acima (exceto ação da heme oxigenase).

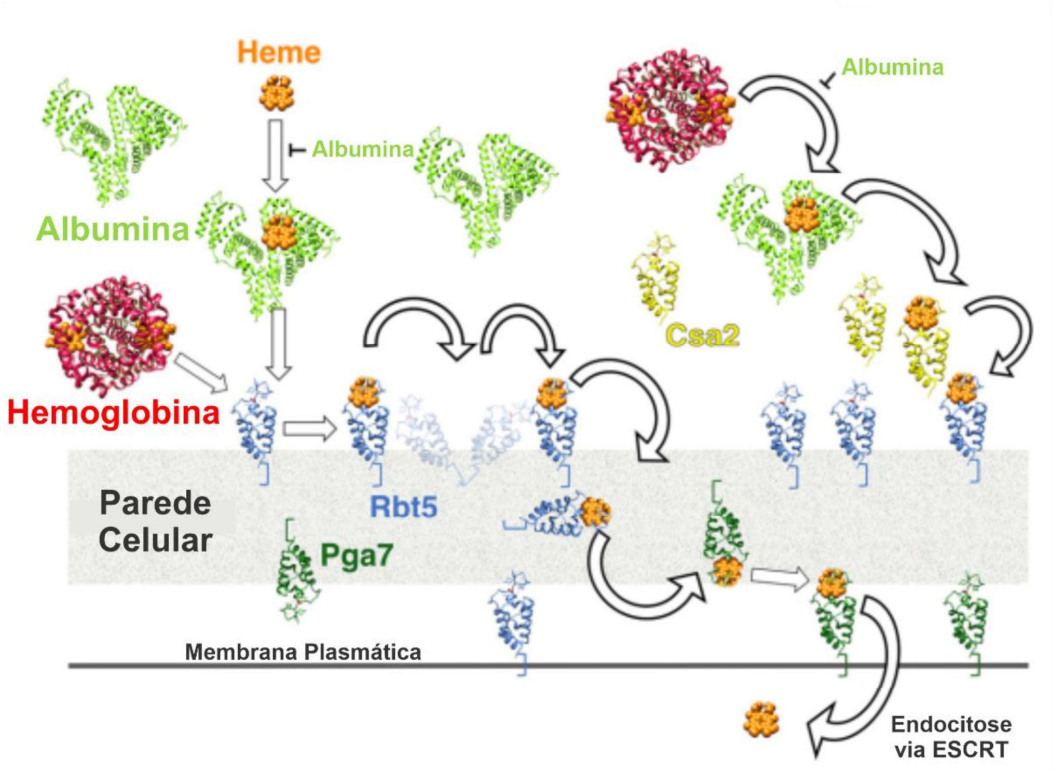

Figura 2. Captação de heme mediada por rede de receptores em *Candida albicans*. Heme oriundo de diversas fontes do hospedeiro, incluindo hemoglobina e albumina, é captado por uma rede de distribuição que inclui o hemóforo Csa2 e os receptores de parede celular/membrana plasmática Rbt5 e Pga7. A internalização do grupo heme é finalizada via sistema ESCRT de endocitose. Adaptado de Pinsky *et al*., 2020.

H. capsulatum também apresenta a capacidade de utilizar heme como fonte de Fe através da ligação da molécula à superfície do fungo, evento que é abolido pelo tratamento do patógeno com Proteinase K, sugerindo que a capacidade de ligação ao heme por *H. capsulatum* é exercida por algum receptor de natureza molecular proteica, porém a caracterização deste ainda não foi realizada (Foster, 2002). *C. neoformans* também é hábil para a utilização de heme, evento que é realizado através de uma manoproteina extracelular denominada Cig1 (Cadieux *et al.*, 2013). Após o contato com Cig1, a exemplo de *C. albicans*, a internalização do grupo heme é propiciada pelo sistema de transporte ESCRT. Mutações de componentes desse sistema reduziram a capacidade de *C. neoformans* crescer na presença de heme como única fonte de Fe, o que aponta para a importância do sistema para o evento (Guanggan *et al.*, 2015; Hu *et al.*, 2013).

1.5. O gênero *Paracoccidioides* e a paracoccidioidomicose

Paracoccidioides spp. consiste em um complexo de fungos termodimórficos composto pelas espécies *Paracoccidioides brasiliensis* (por sua vez composta pelas espécies filogenéticas S1a, S1b, PS2, PS3 e PS4) e *Paracoccidioides lutzii*, sendo todos agentes etiológicos da PCM (Muñoz *et al.*, 2016). Recentemente foi proposta a ascensão taxonômica das espécies filogenéticas PS2, PS3 e PS4 para as espécies *Paracoccidioides americana*, *Paracoccidioides restrepiensis* e *Paracoccidioides venezuelensis*, respectivamente (Turissini *et al.*, 2017). Cabe salientar que a especiação dentro do gênero *Paracoccidioides* já havia sido predita por estudo pioneiro de RAPD (análise de DNA polimórfico amplificado aleatoriamente) de diferentes cepas do fungo (Soares *et al.*, 1995).

A PCM é uma micose sistêmica, endêmica da América Latina, com alta prevalência no Brasil. A doença é adquirida por inalação de conídios ou fragmentos de micélio, forma em que o fungo se encontra no ambiente. Nos pulmões, os propágulos inalados, sob ação da temperatura do hospedeiro, sofrem transição para a forma de

levedura, parasitária (Brummer, Castaneda e Restrepo, 1993). A Figura 3 apresenta os aspectos macro e microscópicos de *P. brasiliensis*.

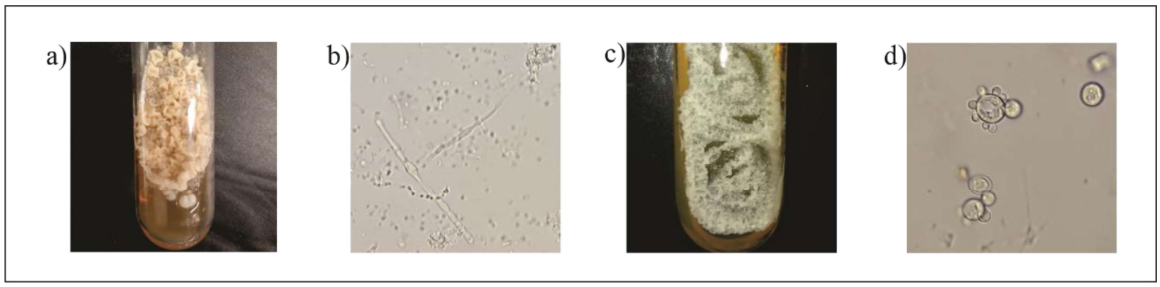

Figura 3. Aspectos macro e microscópicos de *P. brasiliensis* (*Pb18*). a) Aspecto macroscópico de cultura de micélio de *P. brasiliensis*: colônias pequenas, irregulares, de cor branca a bronzeada, que eventualmente podem ser cobertas por micélios aéreos curtos que frequentemente aderem ao ágar, rompendo sua superfície. Cultivado a 26º C em meio Fava-Netto semissólido. **b)** Aspecto microscópico de micélio de *P. brasiliensis*, apresentando hifas septadas hialinas. Aumento de 400 x. **c)** Aspecto macroscópico de cultura de levedura de *P. brasiliensis*: colônias macias, enrugadas e de cor creme. Cultivado a 37º C em meio Fava-Netto semissólido. **d)** Aspecto microscópico de células leveduriformes de *P. brasiliensis*, apresentando células com múltiplos brotamentos, com aspecto de "roda-de-leme". Aumento de 400 x. Imagens registradas pelo próprio autor no Laboratório de Biologia Molecular da Universidade Federal de Goiás.

A PCM desenvolve-se primariamente nos pulmões, porém o fungo pode disseminar-se para outros órgãos e tecidos por via linfática ou hematogênica. Indivíduos afetados pela doença podem sofrer manifestações agudas ou crônicas, que variam de moderadas a graves, podendo haver o desenvolvimento de sequelas, conforme Figura 4. Se não tratada corretamente, a doença pode levar os indivíduos acometidos à morte (Shikanai-Yasuda, Mendes, Colombo, Queiroz-telles, Satie, Kono, Paniago, A. M., *et al.*, 2017).

Figura 4. Manifestações clínicas da PCM. a) PCM fase aguda, **b)** PCM fase crônica, **c)** PCM sequelar, adaptado de Shikanai-Yasuda *et al.*, 2006.

Diversos estudos têm sido conduzidos para a elucidação da interação de *Paracoccidioides* spp. com o hospedeiro, os quais englobam a resposta do patógeno aos estresses osmótico, oxidativo e nitrosativo; privação de zinco e carbono, bem como interação direta com o hospedeiro (murino) e macrófagos, dentre outros (Gonzalez e Hernandez, 2016; Pigosso *et al.*, 2017). A resposta de *Paracoccidioides* spp. à depleção de Fe também tem sido alvo de estudos, conforme exposto na sessão subsequente.

1.6. Homeostase de Fe em *Paracoccidioides* spp.

Estudo pioneiro da resposta de *Paracoccidioides* spp. à depleção de Fe demonstrou que ocorre no patógeno um remodelamento metabólico, no qual o patógeno prima pela utilização de vias metabólicas independentes do metal. Também foi demonstrado que a depleção de Fe promove em *Paracoccidioides* a regulação positiva do fator de transcrição HapX (que em *A. fumigatus* regula a resposta do fungo à privação de Fe), porém ainda não foram completamente elucidados quais mecanismos de controle transcricionais governam a resposta de *Paracoccidioides* à privação do metal (Parente, Ana F. A. *et al.*, 2011; Schrettl *et al.*, 2010). Por enfrentar no hospedeiro um ambiente hostil que inclui a privação de Fe, *Paracoccidioides* spp. também apresenta mecanismos rebuscados como forma de contrapor a imunidade nutricional, conforme Figura 5.

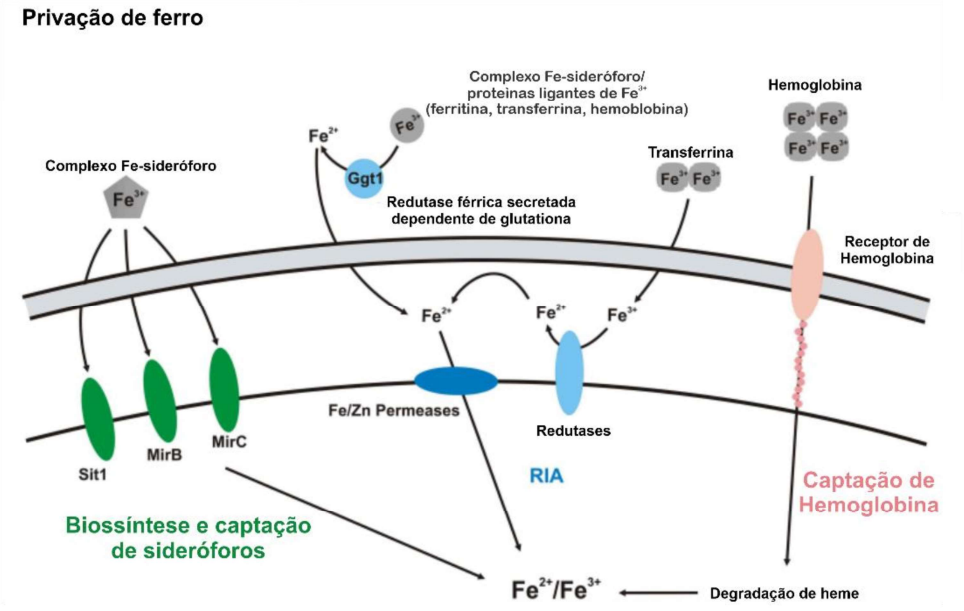

Figura 5. Mecanismos de captação de ferro em *Paracoccidioides* spp. Em resposta à privação de Fe, *Paracoccidioides spp*, é capaz de sintetizar e captar sideróforos (processo destacado em verde), explorar

fontes de Fe do hospedeiro por meio de uma via redutiva de Fe (RIA) não-canônica (processo destacado em azul) bem como captar hemoglobina por meio de um receptor GPI-ancorado (processo destacado em rosa). Ggt1 (gama-glutamiltransferase). Adaptado de Bailão *et al*., 2015.

Estudo prévio baseado em análises *in silico* da homologia de sequências de proteínas relacionadas com a captação de Fe por outros fungos patogênicos, sugeriu que *Paracoccidioides* spp. apresentaria a capacidade de biossíntese e utilização de sideróforos, além de uma via redutiva de assimilação de Fe (Silva *et al.*, 2011). Posteriormente, as proposições feitas nesse estudo foram confirmadas por evidências experimentais, que demonstraram que *Paracoccidioides* spp. produz e secreta sideróforos, bem como apresenta uma via não-clássica de assimilação de Fe, por utilizar Fe/Zn permeases para internalização do metal ao invés de Fe permeases exclusivas para o processo (Bailão *et al.*, 2015; Silva-Bailão *et al.*, 2014; Silva *et al.*, 2020).

Paracoccidioides spp. também possui a capacidade de causar lise de eritrócitos e é hábil para utilizar hemoglobina como fonte de Fe. Análises *in silico* evidenciaram que *Paracoccidioides* spp. apresenta proteínas homólogas à família de receptores de heme/hemoglobina de *C. albicans*: Rbt5, Rbt51, Csa1 e Csa2. Análises transcricionais demonstraram a regulação positiva desses transcritos em *Paracoccidioides* spp., quando exposto à hemoglobina (Bailão *et al.*, 2014). Os autores ainda demonstraram que a proteína Rbt5 de *P. lutzii* é capaz de ligar-se à hemina, bem como investigações de citolocazição apontaram que Rbt5 encontra-se na parede celular do fungo, apontando para a função de receptor. Adicionalmente, mutantes *knockdown* para *PbRbt5* gerados pela estratégia de RNA antisentido ainda apresentaram a capacidade de utilizar hemoglobina como fonte de Fe, o que sugere que, assim como *C. albicans*, *Paracoccidioides* spp. pode apresentar uma complexa rede de receptores que atuam no evento de internalização de heme/hemoglobina (Bailão *et al.*, 2014).

1.7. *Paracoccidioides* spp. e HSP30

Proteínas de choque térmico (HSPs, do Inglês *heat shock proteins*) integram uma família muito ampla de proteínas de diferentes pesos moleculares relacionadas com respostas a estresse celular que não inclui apenas choque térmico, mas diversos outros eventos estressores (Whitley, Goldberg e Jordan, 1999).

Fungos do gênero *Paracoccidioides* apresentam HSPs de diferentes pesos moleculares, como HSP90 que está envolvida na resposta do fungo a diversos estresses, incluindo o oxidativo (Tamayo *et al.*, 2013). Entretanto, *Paracoccidioides* spp. apresenta diversas HSPs cujas funções ainda não foram elucidadas (Nicola, Andrade e Silva-Pereira, 2005).

Dentre essas HSP, a proteína de choque térmico de 30 kDa (HSP30) é um importante alvo de estudo. A justificativa para tal importância está no fato de que em estudo de ESTs (*assembled expressed sequence tags*) de *P. brasiliensis*, HSP30 apresentou o maior número de sequências dentre as ESTs de HSPs analisadas (Nicola, Andrade e Silva-Pereira, 2005). Adicionalmente, análises transcricionais de *P. brasiliensis* exposto a sangue e plasma humano, foi observada a presença de transcritos de HSP30 regulados positivamente (Bailão *et al.*, 2006, 2007). HSP30 também foi identificada como proteína de superfície celular de *P. lutzii* que interage com macrófagos (Tomazett *et al.*, 2019). Esses achados apontam para a importância de HSP30 para a biologia de *Paracoccidioides* spp. e fazem desta proteína um relevante alvo de estudo.

1.8. Sobre a importância de compreender a biologia de *Paracoccidioides* spp.

Apesar de muitas vezes serem subestimadas pela sociedade e seus representantes públicos, infecções fúngicas representam um importante problema de saúde em nível mundial e merecem, portanto, atenção da comunidade científica no que tange à compreensão dos mecanimos que conferem patogenicidade a determinados fungos (Almeida, Rodrigues e Coelho, 2019). Dentre estas infecções fúngicas, a PCM é uma micose sistêmica endêmica da América Latina, de importância relevante no Brasil, causada por fungos do gênero *Paracoccidioides* (Shikanai-Yasuda et al., 2017). Uma vez que autoridades competentes não desenvolvem políticas de enfrentamento e acompanhamento epidemiológico da doença, a PCM continua afetando diversos indivíduos e provocando queda na qualidade de vida, sequelas ou até mesmo a morte destes. Apesar dos esforços da comunidade científica, a PCM ainda não é reconhecida pela Organização Mundial da Saúde como doença tropical negligenciada (Griffiths, Colombo e Denning, 2019). Há inclusive quem considere a PCM uma doença do passado, o que é um grande equívoco, haja vista a grande quantidade de relatos de casos disponíveis na literatura, conforme Figura 6, alguns inclusive mostrando coinfecção por

Paracoccidioides spp, e *Sars-CoV-2*, o que aponta para o fato da PCM ser uma doença contemporânea e digna de atenção (Macedo, de *et al.*, 2020; Santos *et al.*, 2021).

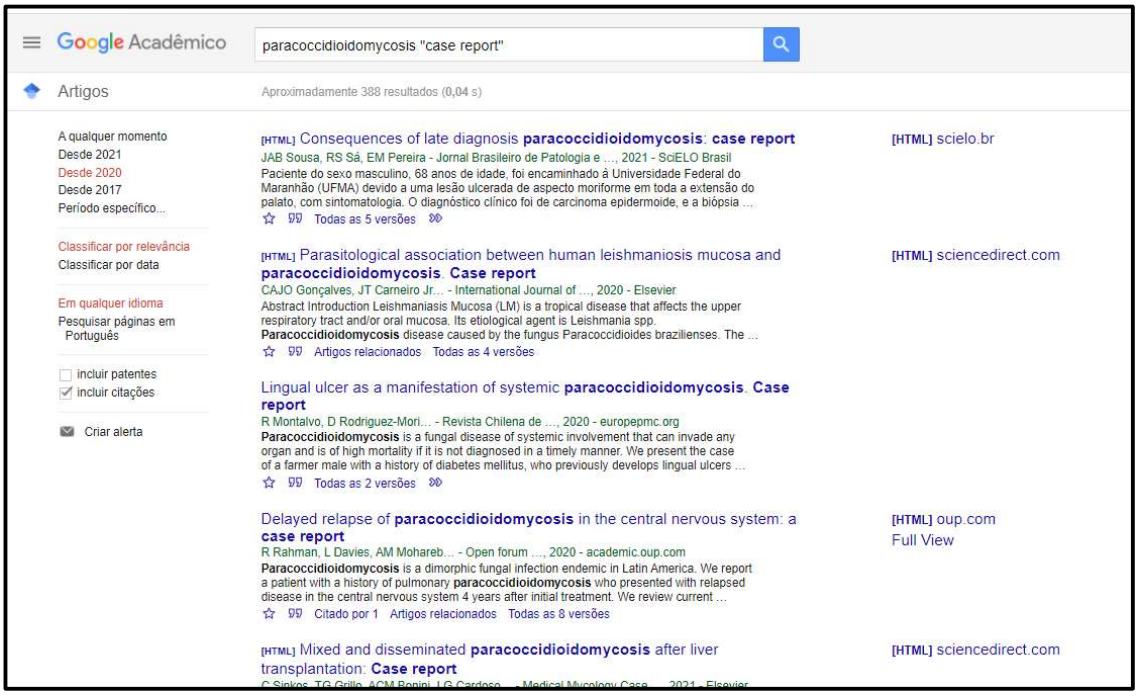

Figura 6. Relatos de caso de PCM publicados nos últimos dois anos. Uma busca simples na base de dados Google Acadêmico (disponível em https://scholar.google.com.br/) utilizando como palavras-chave paracoccidioidomycosis "case report" mostra disponíveis na base 388 relatos de casos, contando apenas os publicados do ano de 2020 até o presente momento. Busca realizada no dia 30 de abril de 2021.

Apesar dos avanços obtidos no entendimento da biologia do patógeno, o diagnóstico acurado da PCM e abordagens terapêuticas mais efetivas no que tange ao tempo de duração destas ainda são desafios atuais, fatos que justificam a continuidade do estudo da biologia de *Paracoccidioides* spp. (Shikanai-Yasuda et al., 2017). Estudos prévios demonstraram que a resposta de *Paracoccidioides* spp. à depleção de Fe constitui um fator relevante para o estabelecimento da PCM e que tal resposta envolve mecanismos complexos que envolvem desde o sensoriamento da biodisponibilidade do metal, adaptação metabólica, mecanismos de alta afinidade e especificidade para a captação do micronutriente além da atuação de microRNAs que atuam no processo (Bailão *et al.*, 2006, 2007, 2014, 2015; Curcio, de *et al.*, 2020; Silva-Bailão *et al.*, 2014; Silva *et al.*, 2011, 2020).

Cabe salientar que apesar destes estudos, ainda há lacunas no que tange à forma como *Paracoccidioides* responde à privação de Fe. Frente a isso, o presente trabalho

elenca eventos que ainda precisam ser investigados no contexto *Paracoccidioides*-privação de Fe e estabelece HSP30 como uma nova proteína ligante de hemoglobina em *Paracoccidioides* spp. Olhar para estas lacunas e novos achados é um fator indispensável para a expansão do conhecimento sobre a biologia de *Paracoccidioides* spp., com a consequente bioprospecção de novos alvos em potencial para o diagnóstico e/ou tratamento da PCM.

2.1. Objetivo geral

Descrever novos alvos para estudo no contexto *Paracoccidioides*-privação de ferro.

2.2. Objetivos específicos

- Definir processos relacionados à resposta de *Paracoccidioides* spp. à privação de Fe que ainda demandam elucidação;
- Avaliar em nível proteômico de parede celular as mudanças provocadas pela exposição de *Paracoccidioides lutzii* à hemoglobina;
- Avaliar a capacidade de adesão a macrófagos de *P. lutzii* previamente exposto a hemoglobina;
- Realizar citolocalização de HSP30 e avaliar a dinâmica de indução de expressão da proteína frente à exposição do fungo à hemoglobina;
- Caracterizar as interações moleculares de HSP30 e hemoglobina;
- Promover ensaio de crescimento de cepas silenciadas para *hsp30* na presença de hemoglobina.

Journal of Fungi

MDPI

Review

The "Little Iron Waltz": The Ternary Response of *Paracoccidioides* spp. to Iron Deprivation

Aparecido Ferreira de Souza, Marcella Silva de Paula, Raisa Melo Lima, Marielle Garcia Silva, Juliana Santana de Curcio, Maristela Pereira and Célia Maria de Almeida Soares *

Laboratório de Biologia Molecular, Instituto de Ciências Biológicas, ICB II, Campus II, Universidade Federal de Goiás, Goiânia 74000-000, Brazil; aparecidofsouza@gmail.com (A.F.d.S.); mar_cella10sp@hotmail.com (M.S.d.P.); raisamelolima@hotmail.com (R.M.L.); mariellegarcias@gmail.com (M.G.S.); julianadecurcio1@gmail.com (J.S.d.C.); maristelaufg@gmail.com (M.P.)
* Correspondence: cmasoares@gmail.com

Received: 17 September 2020; Accepted: 9 October 2020; Published: 12 October 2020

Abstract: *Paracoccidioides* is a genus of thermodimorphic fungi that causes paracoccidioidomycosis. When in the host, the fungus undergoes several challenges, including iron deprivation imposed by nutritional immunity. In response to the iron deprivation triggered by the host, the fungus responds in a ternary manner using mechanisms of high affinity and specificity for the uptake of Fe, namely non-classical reductive iron uptake pathway, uptake of host iron proteins, and biosynthesis and uptake of siderophores. This triple response resembles the rhythmic structure of a waltz, which features three beats per compass. Using this connotation, we have constructed this review summarizing relevant findings in this area of study and pointing out new discoveries and perspectives that may contribute to the expansion of this "little iron waltz".

Keywords: siderophores; CFEM proteins; reductive iron uptake pathway

1. Introduction

One of the greatest things about studying the host–pathogen interaction is to gradually understand that despite the storm of molecular events that support the adaptation process, there is organization! This organization is often referred to as "orchestration" or an "orchestrated response" [1–3]. It truly makes sense to trace an association between molecular events and the performance of music in an orchestrated way; in both cases, there is a myriad of individuals acting, albeit in an organized manner, which provides a final result of completeness. The host, through its immunity, employs several strategies that generate stress to pathogens, which in most cases makes it impossible for microorganisms to persist in it [4,5]. One of these strategies is nutritional immunity, a network of processes that culminate in limiting the bioavailability of nutrients and micronutrients for pathogens [6–8]. Without nutrients, there are two alternatives for microorganisms: succumbing to death or adapting to an environment of scarcity [9].

Iron is one of the micronutrients that is deprived through nutritional immunity. This transition metal is widely employed as a cofactor of several enzymes involved in crucial cellular processes, such as DNA synthesis and repair, energy metabolism, antioxidant systems, and biopolymer synthesis, among many others [10]. Obviously, iron is important for both the host and the pathogen, given its participation in elementary processes for life. This massive recruitment of iron is due to its flexibility of oxidation states, switching from ferric ion (Fe^{3+}) to ferrous ion (Fe^{2+}) with remarked facility [11]. Like a double-edged sword, this transition metal characteristic also makes it harmful if free in the intracellular environment, as this electron movement can damage biomolecules, which require that both host and pathogens employ mechanisms for the strict control of metal's bioavailability [12,13].

In the context of the host–pathogen interface, it is advantageous for the host, through nutritional immunity, to limit the bioavailability of iron to pathogens, given the metal's importance for the maintenance of vital cellular processes; if pathogens do not have access to the metal, the inevitable path is their death [14]. However, pathogens that have infectious success, like pathogenic bacteria and protozoa, are able to supplant nutritional immunity through highly sensitive and specific mechanisms for iron uptake [9,15]. Regarding pathogenic fungi, this is also a reality. In a generalist way, these microorganisms respond to iron deprivation by three main events: (1) the reductive iron assimilation pathway (as described for *Cryptococcus neoformans*); (2) exploration of iron-containing host proteins, such as hemoglobin (as described for *Candida albicans*) and; (3) biosynthesis and uptake of siderophores (as described for *Aspergillus fumigatus*) [16,17].

Latin America is the endemic region of a genus of pathogenic fungi named *Paracoccidioides*, which causes paracoccidioidomycosis (PCM), a systemic mycosis that affects both immunocompetent and immunocompromised individuals and can cause severe sequelae and even death, if proper treatment is not employed [18,19]. Despite the extensive work found in the scientific literature relative to the pathogen's biology and disease's pathobiology, more effective treatments, regarding the duration, are still current challenges [20]. Recent work has shown that the *Paracoccidioides* genus is composed of five species: *Paracoccidioides lutzii*, *Paracoccidioides restrepiensis*, *Paracoccidioides venezuelensis*, *Paracoccidioides americana*, and the cosmopolitan species *Paracoccidioides brasiliensis*, certainly the most investigated among the five species [21].

Paracoccidioides spp., like most living creatures, also need iron for the maintenance of cellular activity and consequently to obtain infectious success. This is evidenced in several ways. For example, the well-known MMcM (McVeigh and Morton) modified medium for growth of *Paracoccidioides* spp. contains in its composition a solution of trace elements, of which iron is the metal that appears in the highest molarity (approximately 3.6 μM; the next most abundant metal is zinc, with approximately 2.8 μM) [22]. Additionally, it has been shown that in the interaction with macrophages, the addition of iron chelators promotes a decrease in the pathogen's survival, which points to the interdependence of the metal's presence and successful parasitism [23,24].

In response to the iron deprivation imposed by the host, *Paracoccidioides* spp. modulate their metabolism prioritizing the use of glycolysis and negatively regulating iron-dependent pathways, such as the tricarboxylic acid cycle [25]. Additionally, the pathogen employs three high affinity and specific pathways for the uptake of iron, which allows the fungus to survive and persist, forming a ternary response [26–28]. Below we discuss these mechanisms and list new findings in this field of knowledge, ones that suggest this "little iron waltz" may mean improving therapeutic approaches to PCM.

2. "Time Signature": The Transcriptional Reprogramming of *Paracoccidioides* spp. Facing Iron Deprivation

The ternary response of *Paracoccidioides* spp., when deprived of iron, resembles the rhythmic structure of a waltz, which features three beats per compass (ternary compass). Following this connotation, in this review we call a "beat" each of the three events that compose *Paracoccidioides* spp. response to iron deprivation. These events are orchestrated from a transcriptional reprogramming that occurs in the face of metal deprivation. Thus, still following the connotation of the performance of orchestrated music, the transcriptional reprogramming works just like the time signature at the beginning of a music sheet, which contains the global information for playing a song.

Iron deprivation suffered by pathogens when in the host leads to a transcriptional response that induces the expression of several proteins involved in obtaining metals from the host during infection. The expression of iron uptake pathways is part of a mechanism finely regulated by fungi, in which several transcriptional factors are activated to produce a rapid response to metal deprivation imposed by the host. As previously mentioned, the acquisition of iron from host by fungi is mediated by three uptake systems, of which one, the reductive iron assimilation pathway, is formed by ferric

reductases [26]. The expression of these proteins is regulated by conditions such as metal deprivation and pH variation. In this way, the pathogenic fungus *C. albicans* has 15 putative ferric reductases, and the expression of some of those genes is under control of transcriptional factors; for example, ferric reductases FRE2p and FRP1p are regulated positively by the transcriptional factor Rim 101, in response to an alkaline environment [29]. In addition to the variation in response to pH, the expression of the ferric reductase FRP1p is increased during iron deprivation and the transcriptional factor Rim 101 also regulates the expression of this protein in *C. albicans* under this condition [30]. In *C. neoformans*, Rim 101 is involved in the use of heme from the host [31]. Additionally, the homeostasis of iron in *C. neoformans* is regulated by several other mechanisms. For example, the global repressor Tup1 is involved in the production of melanin; formation of capsules; and positive regulation of copper uptake transporter (CTR4p), ferric reductase transmembrane component (FRTp1), and siderophore–iron transporter (SIT2p) [32]. In *C. albicans*, Tup1 is also involved in the repression of genes such as *rbt5* for the capture of host heme [33,34]. In fungi of the *Paracoccidioides* complex, the expression of these transcriptional factors is still being elucidated. The expression of *Rim 101* and *Tup1* are induced during iron deprivation, and their expression seems to undergo a regulation mediated by miRNAs, differentially expressed during the deprivation of this metal (de Curcio, personal communication), indicating that these two genes are involved with the fine transcriptional response to iron deprivation, contributing to the control of iron homeostasis in fungi of this complex.

In *A. fumigatus*, the response to iron deprivation is regulated by transcription factors encoded by genes *sreA* and *hapX* [35,36]. The transcription factor SreA is reduced in iron deprivation, promoting the depression of HapX, an essential event for induction of the siderophore biosynthesis pathway [37]. In addition, the influence of SreA on genes involved in iron capture systems was observed [35]. Another gene that plays a role in the adaptation of *A. fumigatus* in low iron is *tptA*, which is homologous to the *Saccharomyces cerevisiae* gene *tpc1*. The study carried out by Huang and collaborators [38] showed that *tptA* loss reduces the expression of *hapX* and that the overexpression of *hapX* in the *tptA* mutant strain restored the growth defect and the production of siderophores.

During iron deprivation, an increase in the expression of the transcriptional regulator *hapX* and in siderophores biosynthesis and uptake genes *sidA* and *sit1*, respectively, was observed in *P. brasiliensis* [25]. After 10 min of iron deprivation, the transcriptional regulator *hapX* level increased 2.3 times and remained increased up to 1 h. The *sidA* expression increased nine fold after 30 min of incubation and remained elevated for 24 h [25]. SrbA of *P. brasiliensis* restored the mutant's defective growth phenotype of a null mutant strain of *A. nidulans*, demonstrating the functionality of this gene during iron deprivation [39]. As mentioned, mobilization of transcription factors orchestrates the response of fungi to Fe deprivation.

3. "The First Beat": The Non-Classical Reductive Pathway of Iron Assimilation in *Paracoccidioides* spp.

The "first beat" of this "little iron waltz", as mentioned above, is a strategy that some fungi use to circumvent iron deprivation, which is conventionally called the reductive pathway for iron assimilation and consists of multi-enzyme complexes that promote oxidation and reduction of the metal and internalize it [9]. Fungi such as *C. albicans* and *C. neoformans* have this ability, which is subsidized by iron reductases, copper-dependent ferroxidases and iron permeases that act together in the process [40,41]. This iron assimilation pathway allows the capture of free Fe^{3+}, which is insoluble and therefore not bioavailable. However, since the amount of free metal in the host is minimal, this pathway is used mainly to sequester iron from host metalloproteins [40]. In *Histoplasma capsulatum*, a extracellular glutathione-dependent ferric reductase activity has been reported, in a process where glutathione is cleaved by a gamma-glutamyl transpeptidase (Ggt1) and a dipeptide with high reductive power is generated, acting on the reduction of Fe^{3+} that feeds the metal's internalization system [42,43].

The investigation of the ability of *Paracoccidioides* spp. to use this reductive pathway began with in silico analyses that pointed to the presence in the fungus genome of ferric reductases (like *fre1*,

fre3, *fre5*, *fre7*, and *frp1*), Ggt1, and copper-dependent ferroxidase orthologues (like *fetp*). However, it was surprising to find that *Paracoccidioides* spp. do not show ferric permeases [44]. As a way of investigating this path in more detail, a specific methodology was employed to accompany the steps of reduction, oxidation, and internalization of the metal in members of the genus *Paracoccidioides* [45]. This methodology, employing ^{59}Fe uptake assays, suggested that the Fe uptake process occurs differently between *P. brasiliensis and P. lutzii*, so that *P. lutzii* has an inefficient reductive iron assimilation (RIA) pathway [26]. The absence of orthologs for ferric permeases also suggests that in the *Paracoccidioides* genus a non-classical reductive iron assimilation pathway (non-classical RIA) occurs [26]. The non-classical term refers to the fact that under iron deprivation, the transcripts of zinc permeases (Zrts) have positive regulation, suggesting that Zrts act in a promiscuous way, transporting both Zn^{2+} and Fe^{2+} during deprivation. In other words, Zrts would not be specific for zinc but a generalist divalent metal carrier [26]. In agreement with the in silico analyses that pointed to the presence of a Ggt1 orthologue in the genomes of *Paracoccidioides* spp., transcriptional data showed that Ggt1 undergoes positive regulation when the fungus is grown in iron deprivation [46]. However, the extent to which Ggt1 acts in conjunction with the non-classical RIA is still unknown. Once this question is resolved, new perspectives will certainly be outlined. This question has been the subject of studies by our group.

4. "The Second Beat": Exploring the Host's Iron-Containing Proteins

The "second beat" of this "waltz" is the ability of *Paracoccidioides* spp. to explore a host's iron-containing proteins directly. In order to limit the toxicity of iron and the bioavailability of the metal for pathogens, the host associates the metal with various proteins, such as hemoglobin and myoglobin (in the form of a heme group), albumin, transferrin, ferritin, and lactoferrin, among others [47]. This variety of iron alternative sources caused pathogens to develop specific mechanisms for metal capture from those sources [9,40].

C. albicans, for example, uses a protein called Als3 to allow iron uptake from ferritin [40,48]. *C. albicans* is also able to use a host's heme-containing proteins, especially hemoglobin and serum albumin, through a network of hemophores (Csa2, Rbt5, Pga7) located on the cell surface that allow the sequestration and internalization of these iron sources [28,33,49,50]. The performance of hemophores is based on the presence of the CFEM (common in several fungal extracellular membrane proteins) domain, which has been reported in other fungal species, such as *Candida glabrata* and *Candida parapsilosis* [51–53]. The internalization of the heme group by *C. albicans* is dependent on the ESCRT (endosomal sorting complex required for transport) endocytosis system [54]. Like *C. albicans*, *C. neoformans* also uses heme through the Cig1 hemophore, which differs from *Candida* spp. hemophores by not presenting the CFEM domain [55]. The internalization of heme by *C. neoformans* is also dependent on the ESCRT system [56,57].

Paracoccidioides spp. are capable of using various iron-containing proteins such as lactoferrin, ferritin, transferrin, and hemoglobin [27]. Regarding hemoglobin uptake, the event occurs through a receptor that also has the CFEM domain, homologous to *C. albicans* Rbt5. The knock-down of *rbt5* compromises the capacity of *Paracoccidioides* spp. survive on macrophages and colonize murine's spleen [27]. Despite these data, it remains to be clarified whether *Paracoccidioides* spp. use only Rbt5 for using heme/hemoglobin or if other hemophores and ancillary proteins may be involved. It is important to highlight that in different *Paracoccidioides* genomes there are at least four sequences that code for proteins that contain the CFEM domain (Table 1). There is still a need for elucidating whether those proteins are involved in the capture of iron-containing proteins from the host. Additionally, it is not clear yet which endocytic system the fungus uses to internalize the molecule. It is also necessary to investigate whether *Paracoccidioides* spp. have other proteins dedicated to the use of specific iron sources in the host.

Table 1. The putative CFEM proteins in *Paracoccidioides* spp. Genomes *.

Species [a]	Gene ID [b]	Product Description [c]	CFEM (E-Value) [d]	GPI Modification Site Prediction? [e]	SignalP [f]	SecretomeP [g]
P. lutzii	PAAG_04763	Hypothetical protein	2.0×10^{-8}	None	Yes	-
	PAAG_11627	Hypothetical protein	2.8×10^{-13}	None	Yes	-
	PAAG_05158	Rbt5 [#]	3.3×10^{-15}	Yes	Yes	-
	PAAG_02225	Csa1 [#]	5.2×10^{-12}	None	Yes	-
	PAAG_00918	Hypothetical protein	5.5×10^{-11}	None	Yes	-
P. brasiliensis	PADG_11659	Hypothetical protein	1.5×10^{-11}	None	-	-
	PADG_05363	Csa1 [#]	1.5×10^{-11}	None	Yes	-
	PADG_02506	Hypothetical protein	1.7×10^{-8}	None	Yes	-
	PADG_03909	Hypothetical protein	2.1×10^{-8}	Yes	Yes	-
	PADG_06374	Hypothetical protein	3.6×10^{-13}	None	-	Yes
	PADG_05000	Rbt5 [#]	4.5×10^{-15}	Yes	Yes	-
P. americana	PABG_12009	Hypothetical protein	1.6×10^{-11}	None	Yes	-
	PABG_00115	Hypothetical protein	1.7×10^{-8}	None	Yes	-
	PABG_01323	Hypothetical protein	2.4×10^{-8}	Yes	Yes	-
	PABG_04599	Rbt51 [#]	4.5×10^{-15}	Yes	Yes	-

* The search for probable CFEM proteins in the genomes of *Paracoccidioides* was carried out using the online tool available at https://fungidb.org/fungidb/ (genes; sequence analysis; protein motif pattern). The term used in the search was CFEM. [a] *Paracoccidioides* species with genomes available in the FungiDB database. [b] Access code of the predicted CFEM-containing sequences. [c] Annotation available on FungiDB. [d] Confidence score of the prediction for CFEM domain presence. [e] Site prediction for GPI anchor modification. The prediction was performed by the online tool big-PI Predictor available at http://mendel.imp.ac.at/gpi/gpi_server.html. [f] Classical secretion prediction performed by the online tool SignalP 4.0 available at http://www.cbs.dtu.dk/services/SignalP-4.0/. [g] Non-classical secretion prediction performed by the online tool SecretomeP 2.0 available at http://www.cbs.dtu.dk/services/SecretomeP/. [#] Names assigned to the sequences as suggested by Bailão et al. (2014) [27].

5. "The Third Beat": Biosynthesis and Uptake of Siderophores by *Paracoccidioides* spp.

Finally, but just as important as the other events described so far, there is the "waltz' third beat": the non-reducing mechanism of iron uptake mediated by siderophores [58]. From the Greek "iron carriers", siderophores are low-molecular-weight (usually 1 KDa) molecules that solubilize ferric iron (Fe^{3+}). Siderophores can also act in the storage of iron [59]. The iron uptake process by this mechanism occurs by excretion of siderophores and binding to the free iron ions, forming the iron–siderophore complex. After uptake, this complex is linked to specific receptor proteins, like Sit1 of *C. albicans* and *C. neoformans* and, MirB and MirC of *Aspergillus nidulans*, present in the cell membrane and through active transport are internalized [60–62]. There are different types of siderophores. Carboxylate siderophores are produced mainly by bacteria such as *Mycobacterium tuberculosis*, which synthesizes carboxymicobactin [63]. Catecholate siderophores are produced mainly by bacteria, like enterobactin (or enterochelin) produced by *Escherichia coli* and other Enterobacteriaceae [64]. However, most of the siderophores produced by fungi belong to the hydroxamate group, with the exception of the rizzoferrin, siderophores of the carboxylate type, which are produced by several *Mucorales* sp., as well as the catecholate-type pistilarin, produced by *Penicillium bilaii* [17].

Hydroxamate siderophores are the most commonly found in nature and are grouped into four structural families: rhodotoluric acid, fusarinines, coprogens, and ferricromes [17]. In bacteria, hydroxamates are composed of acylated and hydroxylated alkylamines, while in fungi they are derived from ornithine, a non-proteinogenic amino acid, which is hydroxylated and alkylated [65]. The importance of siderophores in fungal virulence is well characterized by detailed studies with the pathogen *A. fumigatus*, which produces siderophores belonging to the ferricrome family (ferricrocin), which are intracellular, and fusarinins (fusarinin C, triacetylfusarinica (TAFC)), which are extracellular. The production of intracellular ferricrocin siderophores is coordinated according to the morphology of the fungus; that is, ferricrocin is produced during filamentous growth, while hydroxyferricrocin is produced in spores of conidia, which are the infectious particles [9]. The iron–siderophore complex is transported back to cells via membrane proteins called siderophore transporters. In *A. nidulans*, MirA, MirB, and MirC were characterized as transporters of siderophores, with MirA and MirB being carriers

of enterobactin and TAFC, respectively. Although MirC shows a high degree of conservation with other siderophore transporters, its exact role in capturing siderophores has not yet been found [66].

The mechanisms of iron uptake mediated by siderophores in fungi of the *Paracoccidioides* genus were investigated. These fungi conserve homologues genes related to the biosynthesis and uptake of siderophores, and transcripts of such genes are positively regulated during iron deprivation [44,46]. The genomes of members of the *Paracoccidioides* genus encode the orthologue genes for siderophore biosynthesis, namely sidA, sidF, sidC, sidD, sidI, and sidH, as well as the orthologues for the capture of siderophores, namely sit1, mirB, and mirC. During iron deprivation in *Paracoccidioides* spp., the synthesis and secretion of siderophores of the hydroxamate type coprogen B and dimerumic acid occurs, which are extracellular siderophores, and ferricrocin and ferricromes C, which are intracellular siderophores. The capacity for synthesis and secretion of siderophores by *Paracoccidioides* spp. was attested by a crossfeeding experiment, whereby a strain of *A. nidulans* unable to produce siderophores had its growth restored when grown in MMcM without iron, in co-cultivation with *Paracoccidioides* spp., which pointed out that *A. nidulans* can use siderophores produced and secreted by *P. brasiliensis* [28].

Members of the *Paracoccidioides* genus can use xenosiderophores as a source of iron, such as ferrioxamine B (FOB) [67,68]. In the presence of FOB, the suppression on synthesis of endogenous siderophores occurs, indicating the use of ferric ions linked to FOB as an iron source. Additionally, proteomic and enzymatic analyzes demonstrated that SidA, the enzyme that promotes ornithine hydroxylation during siderophore biosynthesis, was negatively regulated, suggesting the blockade of the pathway due to the alternative source of iron. To investigate the role of siderophore production in fungus virulence, *P. brasiliensis* knockdown strains for *sidA* were obtained, depicting a reduction in the production of siderophores as well as a reduction in the pathogenicity in the *Tenebrio molitor* model of infection, when compared to wild type strains [68].

As mentioned above, members of the *Paracoccicioides* genus can use xenosiderophores [67,68]. Since FOB is a hydroxamate siderophore, a class produced by the genus, it seems interesting to question whether *Paracoccidioides* spp., such as *A. nidulans*, would have the ability to transport siderophores from groups other than hydroxamates, produced by bacteria for example. In this sense, with the intention of pointing out aspects of the response of *Paracoccidioides* spp. to iron deprivation that need to be clarified, we performed molecular dynamics simulation. The three-dimensional structures of the MirB, MirC, and Sit1 proteins of *Paracoccidioides* spp. were subjected to molecular modeling using the I-TASSER server [69]. The structures of the siderophores enterobactin, ferrioxamine B, and carboxymicobactin were obtained in the literature [70–72], and molecular docking was performed between siderophores and proteins using AutoDock Vina [73]. Based on the quality of obtained data (Supplementary Table S1), we present here preliminary results based on molecular dynamics of the *P. brasiliensis* siderophore receptors suggesting capture of hydroxamates, catecholates, or carboxylates, as shown in Figure 1. The energy interaction data are presented in Supplementary Table S2 and suggest that although all *P. brasiliensis* siderophores receptors have the apparent ability to interact with any type of siderophore (for additional information on molecular dynamics experiments, see Supplementary Material), MirB would have a higher affinity for carboxymycobactin (a carboxylate, Figure 1A), and MirC would have a higher affinity for enterobactin (a catecholate, Figure 1B), while Sit1 may have a higher affinity for FOB (a hydroxamate, Figure 1C). In accordance with the molecular dynamics data, we carried out analyzes of the transcripts of the siderophore transporters *sit1*, *mirB*, and *mirC*. For this, *P. brasilienses* yeast cells were incubated in MMcM supplemented with BPS or FOB, and after 6 and 24 h, the cells were collected and extraction of total RNA was performed. Transcriptional analyzes were performed using the standard curve method for relative quantification [74] for calculating the relative expression levels of transcripts of interest. Surprisingly, the transcripts of *sit1*, *mirB*, and *mirC* increased in the first 6 h in the presence of FOB. However after 24 h, it was noticed that the transcript of *sit1* remained elevated, corroborating the possible preferential interaction of Sit1 with FOB (Figure 1D). Obviously, these data are preliminary and require further investigation, but have information that points to the

capacity of *Paracoccidioides* spp. of using any type of siderophore, which is exciting because it could yield discoveries about the biology of the pathogen not explored to date.

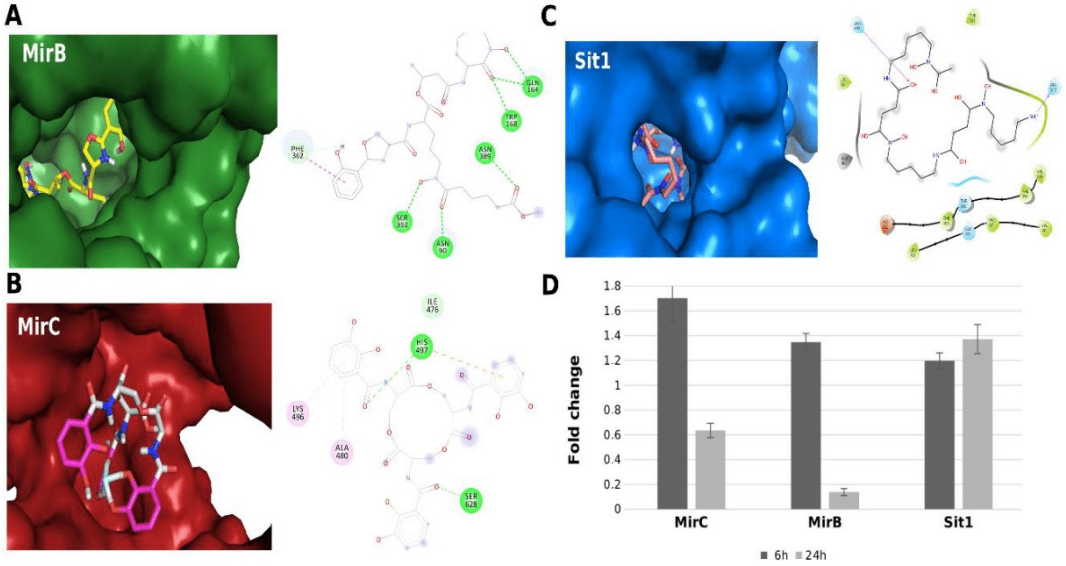

Figure 1. Interactions between three-dimensional models and siderophores. (**A**) Interaction between MirB and carboxymycobactin. The left panel shows the coupling of siderophore in the MirB pocket (green). In the right panel, it is observed that the interaction is maintained by conventional hydrogen bonds (green), carbon–hydrogen bonds (light blue), and pi–pi stacked interaction (pink) between the aromatic rings of carboxymycobactin and PHE362. (**B**) Interaction between MirC and enterobactin. The left panel shows the coupling of the siderophore in the MirC pocket (red). In the right panel, the interaction is maintained by conventional hydrogen (green) and carbon–hydrogen (light blue) bonds, in addition to the pi–alkyl (pink) interaction between the aromatic enterobactin ring and the amino acids LYS496 and ALA480 and the pi–cation interaction (yellow) between the aromatic ring and the HIS497. (**C**) Interaction between Sit1 and ferrioxamine B. The left panel shows the coupling of the siderophore in the Sit1 pocket (blue). In the right panel, it is observed that the ligand ferrioxamine B is maintained mainly by hydrophobic affinity (green) to the pocket of Sit1. (**D**) Levels of transcripts from siderophore transporter genes accessed by RT-qPCR after cultivation of *P. brasiliensis* in Fe deprivation or in the presence of FOB for 6 h and 24 h. For a list of the primers used in the experiments, see Supplementary Table S3. Additional information on this transcriptional analysis is available in the Supplementary Materials.

6. "The Addition of Chialteras": Recent Findings and Future Perspectives on the Response of *Paracoccidioides* spp. to Fe Deprivation

In this review, we compare the response of *Paracoccidioides* spp. to iron deprivation and the execution of a waltz. In music, notes (like chialteras) can suddenly appear and surprise those who hear. Similarly, in science, new discoveries can bring new concepts and break paradigms. It is justified to continue studying the mechanisms that *Paracoccidioides* spp. employ when challenged by iron deprivation, as shown in Figure 2. We also cite some events that occur in other fungal species when subjected to iron deprivation, as summarized in Table 2.

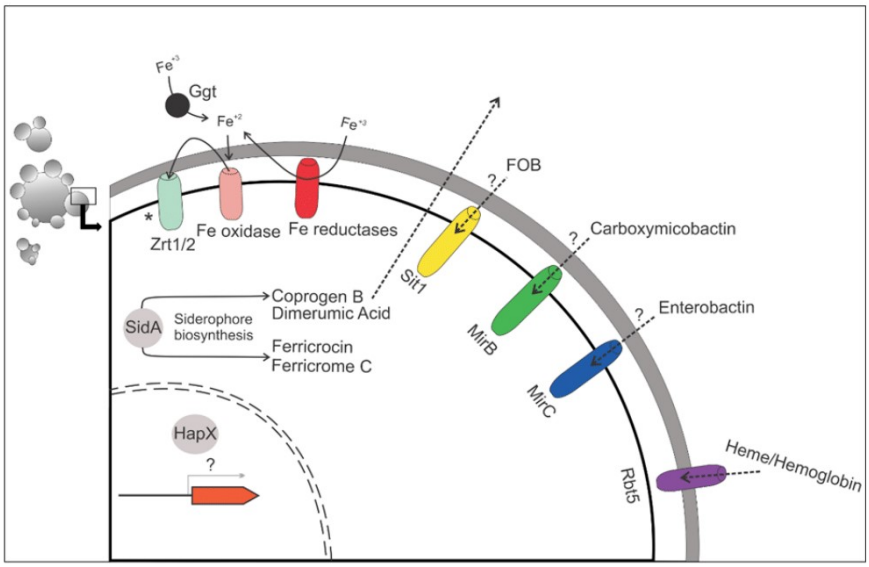

Figure 2. Overview of the mechanisms of iron uptake used in species of the *Paracoccidioides* complex. During iron deprivation *Paracoccidioides* spp. employ several mechanisms of iron uptake, such as siderophore transporters (Sit1, MirB, and MirC); binding to the heme group, mediated by Rbt5; or by iron and zinc transporters and iron-reductases. Rbt5 and SidA are described as virulence factors in *Paracoccidiodes* spp. "*" In *P. lutzii*, RIA is apparently ineffective, because after the metal reduction step, there is no uptake of this. "?" points to aspects that still require elucidation.

Table 2. Mechanisms of fungi response to iron deprivation.

Species	Described Mechanism	Proteins Involved
Paracoccidioides spp.	Non-classical RIA [a,b] Use of host Fe-proteins Biosynthesis and uptake of siderophores	Ferric reductases, ferroxidase, GGT, Zrt1/2 Rbt5 (heme/hemoglobin uptake) SidA, Sit1, MirB, MirC
Candida albicans	RIA Use of host Fe-proteins Uptake of siderophores	Ferric reductases, ferroxidases, ferric permeases Rbt5, Pga7, Csa2 (heme/hemoglobin uptake); Als3 (iron uptake from ferritin) Sit1
Cryptococcus neoformans	RIA Use of host Fe-proteins Uptake of siderophores	Ferric reductases, ferroxidases, ferric permeases Cig1 (heme/hemoglobin uptake) Sit1
Aspergillus spp.	Biosynthesis and uptake of siderophores	SidA, MirA, MirB, MirC

[a] RIA: reductive iron assimilation. [b] Non-classical RIA: in *Paracoccidioides* spp. RIA is referred to as non-classical because the internalization of iron is not performed by a ferric permease but by a zinc/iron permeases called Zrt1/2.

Our group has been working on this challenge, and soon new information about proteins of the pathogen involved in the capture of iron from the host and even the participation of miRNAs in this process will be published. In this review, we also present preliminary data that point out that *Paracoccidioides* spp. is capable of using siderophores of all classes, including carboxymycobactin, a siderophore produced by *M. tuberculosis*, which is a bacterium that has already been described as causing coinfection with *Paracoccidioides* spp. [75,76]. This is a very relevant fact to be studied, considering that in a recent work by our group, it was seen that offering the FOB xenosiderophore to *P. brasiliensis* causes downregulation of SidA, the initial enzyme in the siderophore biosynthesis pathway, which raises questions about how pathogens respond to the presence of xenosiderophores in vivo [68]. In this sense, characterizing the potential xenosiderophores used by the *Paracoccidioides*

complex aggregates information about the mechanisms used by these fungi for the development in conditions of iron deprivation, such as that found during the colonization of the host. In addition, all this data point to the challenge of understanding not only how *Paracoccidioides* spp. interact with the host but also with other pathogenic microorganisms and even the commensal microbiota. Certainly, all these findings will add more and more compasses to this "waltz" and, from a "little iron waltz", soon we will be able to appreciate a "complete symphony".

Supplementary Materials: The following are available online at http://www.mdpi.com/2309-608X/6/4/221/s1, Figure S1: RMSD in molecular dynamics simulations of the models, Figure S2: 3D and 2D interactions between siderophores receptors models and carboxymycobactin, Figure S3: 3D and 2D interactions between siderophores receptors models and enterobactin, Figure S4: 3D and 2D interactions between siderophores receptors models and ferrioxamine B, Table S1: Quality of three-dimensional models after molecular dynamics simulation, Table S2: Scores of binding energies between proteins and siderophores, Table S3: Sequences of forward and reverse oligonucleotides.

Author Contributions: C.M.d.A.S. provided the reagents. A.F.d.S., M.S.d.P., R.M.L., M.G.S., J.S.d.C., M.P., and C.M.d.A.S. contributed to the literature review and writing and to the manuscript formatting. R.M.L. and M.P. performed the analysis of molecular dynamics and generated the figures. A.F.d.S., J.S.d.C. and M.G.S. performed RT-qPCR analyzes. All authors have read and agreed to the published version of the manuscript.

Funding: We thank the CAPES and CNPq for providing fellowships to A.F.S., M.S.P., R.M.L., M.G.S., and J.S.C. CMAS and MP are fellows from Conselho Nacional de Desenvolvimento Científico e Tecnológico (CNPq). This work was supported by grants from Conselho Nacional de Desenvolvimento Científico e Tecnológico (CNPq) and Fundação de Amparo à Pesquisa do Estado de Goiás (FAPEG), Instituto Nacional de Ciência e Tecnologia (INCT) de Estratégias de Interação Patógeno-Hospedeiro (grant number 201810267000022/INCT-FAPEG).

Conflicts of Interest: The authors declare no conflict of interest. The funders had no role in the design or writing of this manuscript.

References

1. Abraham, S.N.; St. John, A.L. Mast cell-orchestrated immunity to pathogens. *Nat. Rev. Immunol.* **2010**, *10*, 440–452. [CrossRef] [PubMed]
2. Audia, J.P.; Webb, C.C.; Foster, J.W. Breaking through the acid barrier: An orchestrated response to proton stress by enteric bacteria. *Int. J. Med. Microbiol.* **2001**, *291*, 97–106. [CrossRef] [PubMed]
3. Lemon, B.; Tjian, R. Orchestrated response: A symphony of transcription factors for gene control. *Genes Dev.* **2000**, *14*, 2551–2569. [CrossRef] [PubMed]
4. Asehnoune, K.; Villadangos, J.; Hotchkiss, R.S. Understanding host–pathogen interaction. *Intensive Care Med.* **2016**, *42*, 2084–2086. [CrossRef]
5. Casadevall, A.; Pirofski, L.A. Host-pathogen interactions: Basic concepts of microbial commensalism, colonization, infection, and disease. *Infect. Immun.* **2000**, *68*, 6511–6518. [CrossRef]
6. Weinberg, E.D. Nutritional Immunity. *J. Am. Mecical Assoc.* **1975**, *231*, 39–41. [CrossRef]
7. Ganz, T. Iron and infection. *Int. J. Hematol.* **2018**, *107*, 7–15. [CrossRef]
8. Cassat, J.E.; Skaar, E.P. Iron in Infection and Immunity. *Cell Host Microbe* **2013**, *13*, 509–519. [CrossRef]
9. Caza, M.; Kronstad, J.W. Shared and distinct mechanisms of iron acquisition by bacterial and fungal pathogens of humans. *Front. Celullar Infect. Microbiol.* **2013**, *3*, 1–23. [CrossRef]
10. Dlouhy, A.C.; Outten, C.E. The Iron Methallome in Eukaryotic Organisms. *Met. Ions Life Sci.* **2013**, *12*, 241–278. [CrossRef]
11. Aisen, P.; Enns, C.; Wessling-Resnick, M. Chemistry and biology of eukaryotic iron metabolism. *Int. J. Biochem. Cell Biol.* **2001**, *33*, 940–959. [CrossRef]
12. Papanikolaou, G.; Pantopoulos, K. Iron metabolism and toxicity. *Toxicol. Appl. Pharmacol.* **2005**, *202*, 199–211. [CrossRef] [PubMed]
13. Tandara, L.; Salamunic, I. Iron metabolism: Current facts and future directions. *Biochem. Medica* **2012**, *22*, 311–328. [CrossRef] [PubMed]
14. Malavia, D.; Crawford, A.; Wilson, D. *Nutritional Immunity and Fungal Pathogenesis: The Struggle for Micronutrients at the Host–Pathogen Interface*, 1st ed.; Elsevier Ltd.: Amsterdam, The Netherlands, 2017; Volume 70.

15. Huynh, C.; Yuan, X.; Miguel, D.C.; Renberg, R.L.; Protchenko, O.; Philpott, C.C.; Hamza, I.; Andrews, N.W. Heme uptake by *Leishmania amazonensis* is mediated by the transmembrane protein LHR1. *PLoS Pathog.* **2012**, *8*, 36. [CrossRef] [PubMed]
16. Bairwa, G.; Hee Jung, W.; Kronstad, J.W. Iron acquisition in fungal pathogens of humans. *Metallomics* **2017**, *9*, 215–227. [CrossRef]
17. Haas, H. Fungal siderophore metabolism with a focus on *Aspergillus fumigatus*. *Nat. Prod. Rep.* **2014**, *31*, 1266–1276. [CrossRef]
18. Shikanai-Yasuda, M.A.; Telles Filho, F.D.Q.; Mendes, R.P.; Colombo, A.L.; Moretti, M.L.; Kono, A.; Tresoldi, A.T.; Wanke, B.; Carvalho, C.R.; Benard, G.; et al. Consenso em paracoccidioidomicose. *Rev. Soc. Bras. Med. Trop.* **2006**, *39*, 297–310. [CrossRef]
19. Brummer, E.; Castaneda, E.; Restrepo, A. Paracoccidioidomycosis: An update. *Clin. Microbiol. Rev.* **1993**, *6*, 89–117. [CrossRef]
20. Shikanai-Yasuda, M.A.; Mendes, R.P.; Colombo, A.L.; Queiroz-telles, F.D.; Satie, A.; Kono, G.; Paniago, A.M.M.; Nathan, A.; Carlos, A.; Bagagli, E. Brazilian guidelines for the clinical management of paracoccidioidomycosis. *Rev. Soc. Bras. Med. Trop.* **2017**. [CrossRef]
21. Turissini, D.A.; Gomez, O.M.; Teixeira, M.M.; Mcewen, J.G.; Matute, D.R. Species boundaries in the human pathogen *Paracoccidioides*. *Fungal Genet. Biol.* **2017**, *106*, 9–25. [CrossRef]
22. Restrepo, A.; Jiménez, B.E. Growth of *Paracoccidioides brasiliensis* yeast phase in a chemically defined culture medium. *J. Clin. Microbiol.* **1980**, *12*, 279–281. [CrossRef] [PubMed]
23. Cano, L.E.; Gomez, B.; Brummer, E.; Restrepo, A.; Stevens, D.A. Inhibitory effect of deferoxamine or macrophage activation on transformation of *Paracoccidioides brasiliensis* conidia ingested by macrophages: Reversal by holotransferrin. *Infect. Immun.* **1994**, *62*, 1494–1496. [CrossRef] [PubMed]
24. Dias-Melicio, L.A.; Calvi, S.A.; Peraçoli, M.T.S.; Soares, Â.M.V.D.C. Inhibitory effect of deferoxamine on *Paracoccidioides brasiliensis* survival in human monocytes: Reversal by holotransferrin not by apotransferrin. *Rev. Inst. Med. Trop. Sao Paulo* **2005**, *47*, 263–266. [CrossRef] [PubMed]
25. Parente, A.F.A.; Bailão, A.M.; Borges, C.L.; Parente, J.A.; Magalhães, A.D.; Ricart, C.A.O.; Soares, C.M.A. Proteomic analysis reveals that iron availability alters the metabolic status of the pathogenic fungus *Paracoccidioides brasiliensis*. *PLoS ONE* **2011**, *6*, e22810. [CrossRef] [PubMed]
26. Bailão, E.F.L.C.; Lima, P.d.S.; Silva-Bailão, M.G.; Bailão, A.M.; Fernandes, G.d.R.; Kosman, D.J.; Soares, C.M.d.A. *Paracoccidioides* spp. ferrous and ferric iron assimilation pathways. *Front. Microbiol.* **2015**, *6*, 1–12. [CrossRef]
27. Bailão, E.F.L.C.; Parente, J.A.; Pigosso, L.L.; de Castro, K.P.; Fonseca, F.L.; Silva-Bailão, M.G.; Báo, S.N.; Bailão, A.M.; Rodrigues, M.L.; Hernandez, O.; et al. Hemoglobin Uptake by *Paracoccidioides* spp. Is Receptor-Mediated. *PLoS Negl. Trop. Dis.* **2014**, *8*, e2856. [CrossRef]
28. Kuznets, G.; Vigonsky, E.; Weissman, Z.; Lalli, D.; Gildor, T.; Kauffman, S.J.; Turano, P.; Becker, J.; Lewinson, O.; Kornitzer, D. A Relay Network of Extracellular Heme-Binding Proteins Drives *C. albicans* Iron Acquisition from Hemoglobin. *PLoS Pathog.* **2014**, *10*, e1004407. [CrossRef]
29. Baek, Y.U.; Li, M.; Davis, D.A. *Candida albicans* ferric reductases are differentially regulated in response to distinct forms of iron limitation by the Rim101 and CBF transcription factors. *Eukaryot. Cell* **2008**, *7*, 1168–1179. [CrossRef]
30. Liang, Y.; Gui, L.; Wei, D.S.; Zheng, W.; Xing, L.J.; Li, M.C. *Candida albicans* ferric reductase FRP1 is regulated by direct interaction with Rim101p transcription factor. *FEMS Yeast Res.* **2009**, *9*, 270–277. [CrossRef]
31. Kronstad, J.W.; Hu, G.; Jung, W.H. An encapsulation of iron homeostasis and virulence in *Cryptococcus neoformans*. *Trends Microbiol.* **2013**, *21*, 457–465. [CrossRef]
32. Lee, H.; Chang, Y.C.; Varma, A.; Kwon-Chung, K.J. Regulatory diversity of TUP1 in *Cryptococcus neoformans*. *Eukaryot. Cell* **2009**, *8*, 1901–1908. [CrossRef] [PubMed]
33. Weissman, Z.; Kornitzer, D. A family of *Candida* cell surface haem-binding proteins involved in haemin and haemoglobin-iron utilization. *Mol. Microbiol.* **2004**, *53*, 1209–1220. [CrossRef] [PubMed]
34. Braun, B.R.; Head, W.S.; Wang, M.X.; Johnson, A.D. Identification and characterization of TUP1-regulated genes in *Candida albicans*. *Genetics* **2000**, *156*, 31–44. [PubMed]
35. Schrettl, M.; Kim, H.S.; Eisendle, M.; Kragl, C.; Nierman, W.C.; Heinekamp, T.; Werner, E.R.; Jacobsen, I.; Illmer, P.; Yi, H.; et al. SreA-mediated iron regulation in *Aspergillus fumigatus*. *Mol. Microbiol.* **2008**, *70*, 27–43. [CrossRef] [PubMed]

36. Hortschansky, P.; Eisendle, M.; Al-Abdallah, Q.; Schmidt, A.D.; Bergmann, S.; Thön, M.; Kniemeyer, O.; Abt, B.; Seeber, B.; Werner, E.R.; et al. Interaction of HapX with the CCAAT-binding complex—A novel mechanism of gene regulation by iron. *EMBO J.* **2007**, *26*, 3157–3168. [CrossRef]
37. Schrettl, M.; Beckmann, N.; Varga, J.; Heinekamp, T.; Jacobsen, I.D.; Jöchl, C.; Moussa, T.A.; Wang, S.; Gsaller, F.; Blatzer, M.; et al. HapX-Mediated adaption to iron starvation is crucial for virulence of *Aspergillus fumigatus*. *PLoS Pathog.* **2010**, *6*, e1001124. [CrossRef] [PubMed]
38. Huang, J.; Ma, Z.; Zhong, G.; Sheppard, D.C.; Lu, L.; Zhang, S. The mitochondrial thiamine pyrophosphate transporter TptA promotes adaptation to low iron conditions and virulence in fungal pathogen *Aspergillus fumigatus*. *Virulence* **2019**, *10*, 234–247. [CrossRef]
39. Lima, P.d.S.; Chung, D.; Bailão, A.M.; Cramer, R.A.; Soares, C.M.d.A. Characterization of the Paracoccidioides Hypoxia Response Reveals New Insights into Pathogenesis Mechanisms of This Important Human Pathogenic Fungus. *PLoS Negl. Trop. Dis.* **2015**, *9*, e0004282. [CrossRef]
40. Almeida, R.S.; Wilson, D.; Hube, B. *Candida albicans* iron acquisition within the host. *FEMS Yeast Res.* **2009**, *9*, 1000–1012. [CrossRef]
41. Han, K.; Do, E.; Jung, W.H. A human fungal pathogen *Cryptococcus neoformans* expresses three distinct iron permease homologs. *J. Microbiol. Biotechnol.* **2012**, *22*, 1644–1652. [CrossRef]
42. Zarnowski, R.; Woods, J.P. Glutathione-dependent extracellular ferric reductase activities in dimorphic zoopathogenic fungi. *Microbiology* **2005**, *151*, 2233–2240. [CrossRef] [PubMed]
43. Zarnowski, R.; Cooper, K.G.; Brunold, L.S.; Calaycay, J.; Woods, J.P. *Histoplasma capsulatum* secreted γ-glutamyltransferase reduces iron by generating an efficient ferric reductant. *Mol. Microbiol.* **2008**, *70*, 352–368. [CrossRef] [PubMed]
44. Silva, M.G.; Schrank, A.; Bailão, E.F.L.C.; Bailão, A.M.; Borges, C.L.; Staats, C.C.; Parente, J.A.; Pereira, M.; Salem-Izacc, S.M.; Mendes-Giannini, M.J.S.; et al. The homeostasis of iron, copper, and zinc in *Paracoccidioides brasiliensis*, *Cryptococcus neoformans* var. *Grubii*, and *Cryptococcus gattii*: A comparative analysis. *Front. Microbiol.* **2011**, *2*, 1–19. [CrossRef] [PubMed]
45. Kosman, D.J.; Bailão, E.F.L.C.; Silva-Bailão, M.G.; Soares, C.M.d.A. 59Fe Uptake Assays in *Paracoccidioides* Species. *Bio-Protocol* **2016**, *6*, e1930. [CrossRef]
46. Bailão, E.F.L.C.; Parente, A.F.A.; Parente, J.A.; Silva-Bailão, M.G.; de Castro, K.P.; Kmetzsch, L.; Staats, C.C.; Schrank, A.; Vainstein, M.H.; Borges, C.L.; et al. Metal Acquisition and Homeostasis in Fungi. *Curr. Fungal Infect. Rep.* **2012**, *6*, 257–266. [CrossRef]
47. Núñez, G.; Sakamoto, K.; Soares, M.P. Innate Nutritional Immunity. *J. Immunol.* **2018**, *201*, 11–18. [CrossRef] [PubMed]
48. Almeida, R.S.; Brunke, S.; Albrecht, A.; Thewes, S.; Laue, M.; Edwards, J.E.; Filler, S.G.; Hube, B. The hyphal-associated adhesin and invasin Als3 of *Candida albicans* mediates iron acquisition from host ferritin. *PLoS Pathog.* **2008**, *4*, e1000217. [CrossRef]
49. Okamoto-Shibayama, K.; Kikuchi, Y.; Kokubu, E.; Sato, Y.; Ishihara, K. Csa2, a member of the Rbt5 protein family, is involved in the utilization of iron from human hemoglobin during *Candida albicans* hyphal growth. *FEMS Yeast Res.* **2014**, *14*, 674–677. [CrossRef]
50. Pinsky, M.; Roy, U.; Moshe, S.; Weissman, Z.; Kornitzer, D. Human Serum Albumin Facilitates Heme-Iron Utilization by Fungi. *MBio* **2020**, *11*, 1–14. [CrossRef]
51. Nasser, L.; Weissman, Z.; Pinsky, M.; Amartely, H.; Dvir, H.; Kornitzer, D. Structural basis of haem-iron acquisition by fungal pathogens. *Nat. Microbiol.* **2016**, *1*, 16156. [CrossRef]
52. Ding, C.; Vidanes, G.M.; Maguire, S.L.; Guida, A.; Synnott, J.M.; Andes, D.R.; Butler, G. Conserved and divergent roles of Bcr1 and CFEM proteins in *Candida parapsilosis* and *Candida albicans*. *PLoS ONE* **2011**, *6*, e28151. [CrossRef] [PubMed]
53. Srivastava, V.K.; Suneetha, K.J.; Kaur, R. A systematic analysis reveals an essential role for high-affinity iron uptake system, haemolysin and CFEM domain-containing protein in iron homoeostasis and virulence in *Candida glabrata*. *Biochem. J.* **2014**, *463*, 103–114. [CrossRef]
54. Weissman, Z.; Shemer, R.; Conibear, E.; Kornitzer, D. An endocytic mechanism for haemoglobin-iron acquisition in *Candida albicans*. *Mol. Microbiol.* **2008**, *69*, 201–217. [CrossRef] [PubMed]
55. Cadieux, B.; Lian, T.; Hu, G.; Wang, J.; Biondo, C.; Teti, G.; Liu, V.; Murphy, M.E.P.; Creagh, A.L.; Kronstad, J.W. The mannoprotein cig1 supports iron acquisition from heme and virulence in the pathogenic fungus *Cryptococcus neoformans*. *J. Infect. Dis.* **2013**, *207*, 1339–1347. [CrossRef] [PubMed]

56. Hu, G.; Caza, M.; Cadieux, B.; Chan, V.; Liu, V.; Kronstad, J. *Cryptococcus neoformans* requires the ESCRT protein Vps23 for iron acquisition from heme, for capsule formation, and for virulence. *Infect. Immun.* **2013**, *81*, 292–302. [CrossRef]
57. Guanggan, H.; Caza, M.; Cadieux, B.; Bakkeren, E.; Do, E.; Jung, W.H.; Kronstad, J.W. The ESCRT machinery influences haem uptake and capsule elaboration in *Cryptococcus neoformans*. *Mol. Microbiol.* **2015**, *96*, 973–992. [CrossRef]
58. Saha, M.; Sarkar, S.; Sarkar, B.; Sharma, B.K.; Bhattacharjee, S.; Tribedi, P. Microbial siderophores and their potential applications: A review. *Environ. Sci. Pollut. Res.* **2016**, *23*, 3984–3999. [CrossRef]
59. Neilands, J.B. Siderophores. *Arq. Biochem. Biophys.* **1993**, *302*, 1–3. [CrossRef]
60. Nevitt, T. War-Fe-re: Iron at the core of fungal virulence and host immunity. *Biometals* **2011**, *24*, 547–558. [CrossRef]
61. Miethke, M.; Marahiel, M.A. Siderophore-Based Iron Acquisition and Pathogen Control. *Microbiol. Mol. Biol. Rev.* **2007**, *71*, 413–451. [CrossRef]
62. Sah, S.; Singh, R. Siderophore: Structural And Functional Characterisation—A Comprehensive Review. *Agriculture* **2015**, *61*, 97–114. [CrossRef]
63. Wells, R.M.; Jones, C.M.; Xi, Z.; Speer, A.; Danilchanka, O.; Doornbos, K.S.; Sun, P.; Wu, F.; Tian, C.; Niederweis, M. Discovery of a Siderophore Export System Essential for Virulence of *Mycobacterium tuberculosis*. *PLoS Pathog.* **2013**, *9*, e1003120. [CrossRef] [PubMed]
64. Raymond, K.N.; Dertz, E.A.; Kim, S.S. Enterobactin: An archetype for microbial iron transport. *Proc. Natl. Acad. Sci. USA* **2003**, *100*, 3584–3588. [CrossRef]
65. Khan, A.; Singh, P.; Srivastava, A. Synthesis, nature and utility of universal iron chelator—Siderophore: A review. *Microbiol. Res.* **2018**, *212–213*, 103–111. [CrossRef]
66. Raymond-Bouchard, I.; Carroll, C.S.; Nesbitt, J.R.; Henry, K.A.; Pinto, L.J.; Moinzadeh, M.; Scott, J.K.; Moore, M.M. Structural requirements for the activity of the MirB ferrisiderophore transporter of *Aspergillus fumigatus*. *Eukaryot. Cell* **2012**, *11*, 1333–1344. [CrossRef] [PubMed]
67. Silva-Bailão, M.G.; Bailão, E.F.L.C.; Lechner, B.E.; Gauthier, G.M.; Lindner, H.; Bailão, A.M.; Haas, H.; Soares, C.M.d.A. Hydroxamate production as a high affinity iron acquisition mechanism in *Paracoccidioides* Spp. *PLoS ONE* **2014**, *9*, e105805. [CrossRef]
68. Silva, M.G.; de Curcio, J.S.; Silva-Bailão, M.G.; Lima, R.M.; Tomazett, M.V.; de Souza, A.F.; Cruz-Leite, V.R.M.; Sbaraini, N.; Bailão, A.M.; Rodrigues, F.; et al. Molecular characterization of siderophore biosynthesis in *Paracoccidioides brasiliensis*. *IMA Fungus* **2020**, *11*, 11. [CrossRef]
69. Yang, J.; Zhang, Y. I-TASSER server: New development for protein structure and function predictions. *Nucleic Acids Res.* **2015**, *43*, W174–W181. [CrossRef]
70. Moynié, L.; Milenkovic, S.; Mislin, G.L.A.; Gasser, V.; Malloci, G.; Baco, E.; McCaughan, R.P.; Page, M.G.P.; Schalk, I.J.; Ceccarelli, M.; et al. The complex of ferric-enterobactin with its transporter from *Pseudomonas aeruginosa* suggests a two-site model. *Nat. Commun.* **2019**, *10*, 3673. [CrossRef]
71. Podkowa, K.J.; Briere, L.A.K.; Heinrichs, D.E.; Shilton, B.H. Crystal and solution structure analysis of FhuD2 from Staphylococcus aureus in multiple Unliganded conformations and bound to ferrioxamine-B. *Biochemistry* **2014**, *53*, 2017–2031. [CrossRef]
72. Agoro, R.; Mura, C. Iron supplementation therapy, a friend and foe of mycobacterial infections? *Pharmaceuticals* **2019**, *12*, 75. [CrossRef] [PubMed]
73. Trott, O.; Olson, A.J. AutoDock Vina: Improving the speed and accuracy of docking with a new scoring function, efficient optimization and multithreading. *J. Comput. Chem.* **2010**, *31*, 455–461. [CrossRef] [PubMed]
74. Bookout, A.L.; Cummins, C.L.; Kramer, M.F.; Pesola, J.M.; Mangelsdorf, D.J. High-Throughput Real-Time Quantitative Reverse Transcription PCR. *Curr. Protoc. Mol. Biol.* **2006**, *73*, 15.8.1–15.8.28.
75. Juan, N.R.; Daniela, S.M.; Tania, V.L.; Sergio, E.G.; Alejandrina, R.F.; Rito, Z.L. Paracoccidioidomicosis y TBC-MR en portador de VIH/VHC. *Rev. Chil. Infectol.* **2010**, *27*, 551–555. [CrossRef]
76. Torres-Pereira, C.; Giovanini, A.F.; Stramandinoli, R.T.; Amenabar, J.M.; Piazzetta, C.M. Oral paracoccidioidomycosis and pulmonary tuberculosis co-infection: Relevance of oral biopsy in establishing the diagnosis and therapeutic approach. *Int. J. Infect. Dis.* **2007**, *13*, 112–114. [CrossRef] [PubMed]

Supplementary material

1. Molecular dynamics

The three-dimensional structures of the MirB, MirC and Sit1 proteins of *Paracoccidioides* spp. have not been experimentally determined so far, therefore, using the I-TASSER server we performed the molecular modeling [1]. Molecular dynamics were performed using the GROMACS package, with AMBER force field (ff99SB-ILDM) and TIP3P water. The molecules were subjected to the simulation of 20 nanoseconds, temperature of 300 K, pressure of 1 atm and time interval of 2 fentoseconds. The analysis of RMSD (root-mean-square deviation of atomic positions) were performed using the software of the GROMACS package [2]. Quality scores and Ramachandran maps of proteins were performed using the MolProbity server [3].

The enterobactin and ferrioxamine B siderophores molecules were obtained from the Protein Data Bank (PDB) in the 6Q5E [4] and 4FIL [5] crystals, respectively. Carboxymicobactin was designed according to the structure described by [6]. Molecular docking was performed between siderophores and proteins using AutoDock Vina [7]. The best anchorage between the molecules, according to the energy score, was chosen for the analysis of interaction. This analysis was performed using the Discovery Studio Visualizer (BIOVIA: Dassault Systèmes, 2020), Pymol (The PyMOL Molecular Graphics System, Version 2.0 Schrödinger, LLC) and Maestro (Maestro, Schrödinger, LLC, New York, NY, 2020) software.

1.2. Results and discussion regarding molecular dynamics

In Supplementary Figure 1, the MirC and Sit1 proteins showed high mean square deviation in relation to their backbone, reaching values above 1 nm. However, the MirB protein performed better in molecular dynamics, with RMSD varying around 0.4 nm. This different behavior may be due to MirB more globular structure, while MirC and Sit1 present more regions of unstructured loops, which provide higher flexibility during the simulation. In addition, high RMSD values in the case of models generated with low similarity between crystallographic structures are expected, since there are regions without homology that were modeled by the template-free method [8].

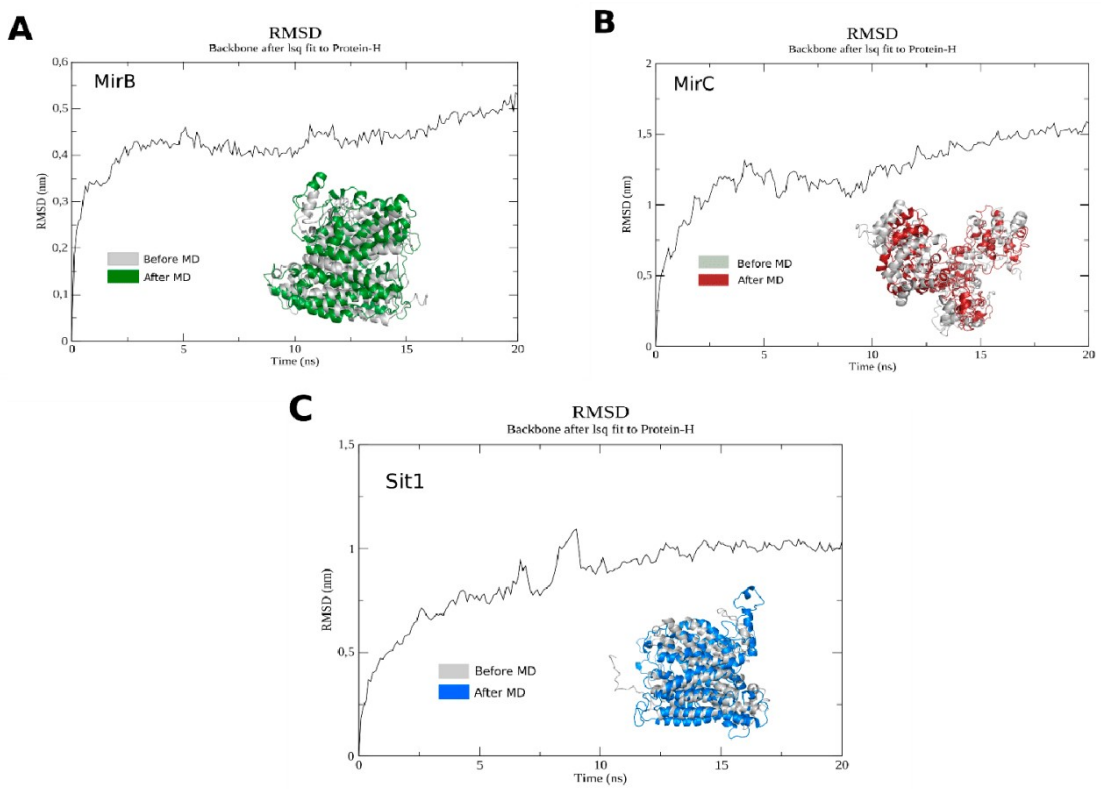

Supplementary Figure S1. RMSD in molecular dynamics simulations of the models: A) MirB showing a fluctuation between 0.4 and 0.5 nm in most of the simulation indicating in this period a more stable conformation of MirB. B) MirC showing a large fluctuation up to 1.5 nm. The Y-shaped MirB structure allowed higher flexibility and consequently higher variation of RMSD. C) Sit1 showing a fluctuation of up to 1 nm of the simulation; but it is possible to observe a stability of the RMSD from 10 ns up to the end. In all cases there is the alignment of the 3D structure, where gray is the model prior to the molecular dynamics and in green, red and blue, respectively, the most representative model of the molecular dynamics.

In molecular dynamics simulation the presence of the solvent induces the molecule to have a dynamic behavior of atoms and it is expected that it will achieve a more favorable three-dimensional structure, with adjustment of the linked and non-linked interactions [9]. In Supplementary Table 1, we note that the amino acids in favorable regions in the Ramachandran map, which refer to the Φ and Ψ angles around the alpha carbon, increased after the molecular dynamics simulation. This fact, together with the reduction of steric shocks and unfavorable interactions, made the molprobity score significantly improve. The molprobity score values achieved are comparable to those of high-quality crystal structures [3].

Supplementary Table S1: Quality of three-dimensional models after molecular dynamics simulation

	Ramachandran favored		Molprobity score	
	before MD	after MD	before MD	after MD
MirB	69.34%	83.65%	4.33	1.95
MirC	66.04%	85.05%	3.81	2.04
Sit1	68.98%	85.42%	4.11	1.93

In Supplementary Figures S2, S3 and S4, we observe the interaction of the carboxymycobactin, enterobactin and ferrioxamine B siderophores, respectively, with MirB, MirC and Sit1. The carboxymycobactin-MirB complex showed the interaction energy score -9.6 Kcal/mol (Supplementary Table 2), compared to the other interactions involving this siderophore. In addition to the pi-pi stacked interaction that occurs with the alignment of two aromatic rings, PHE is also involved in a special hydrogen interaction, where the aromatic ring acts as an electron donor. In this same complex, there are still 5 conventional hydrogen bonds, which are important in intermolecular recognition and in maintaining stability between molecules [10].

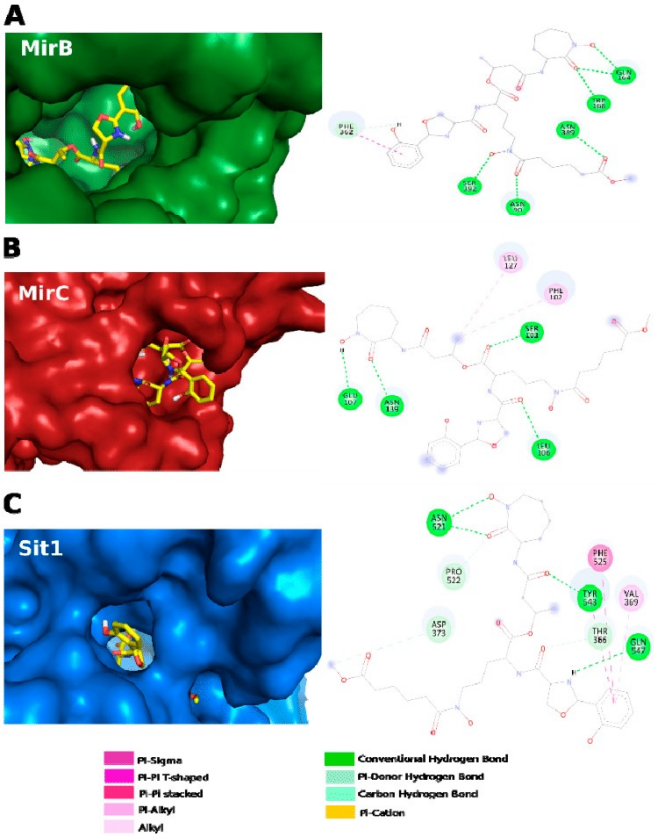

Supplementary Figure S2. 3D and 2D interactions between siderophores receptors models and carboxymycobactin.

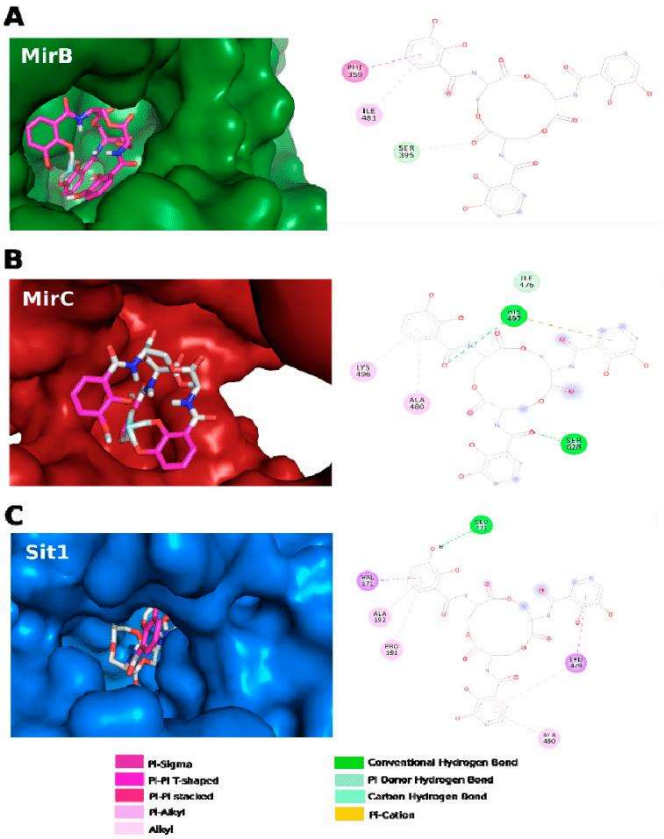

Supplementary Figure S3. 3D and 2D interactions between siderophores receptors models and enterobactin.

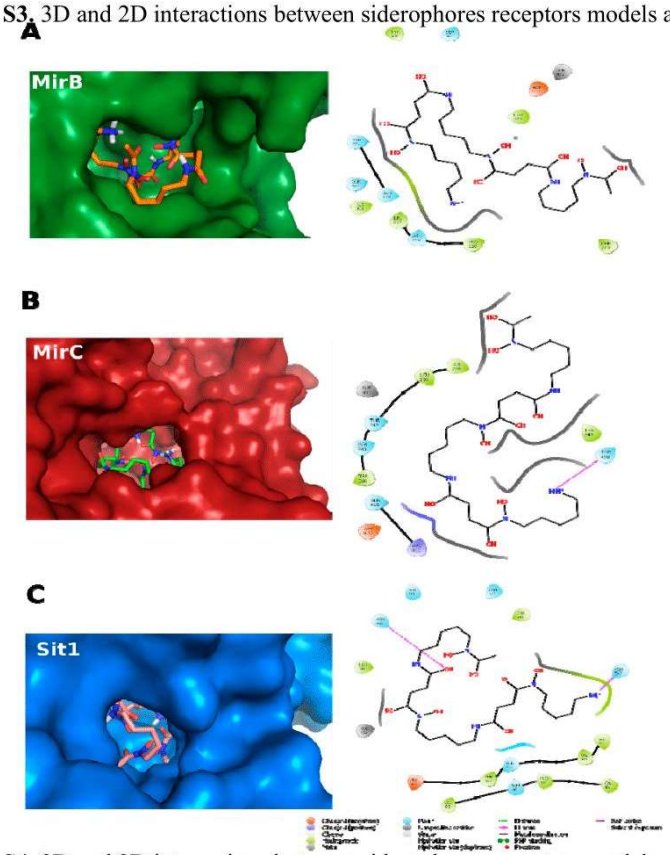

Supplementary Figure S4. 3D and 2D interactions between siderophores receptors models and ferrioxamine B.

Supplementary Table S2: Scores of binding energies between proteins and siderophores

	CMB	EB	FOB
MirB	-9.6	-10.7	-8.7
MirC	-7.1	-10.5	-8.3
Sit1	-8.9	-10.9	-9.8

Energy score = Kcal/mol
CMB = carboxymycobactin
EB = enterobactin
FOB = ferrioxamine B

The complexes in the case of enterobactin showed remarkably similar binding energy scores, as seen in Supplementary Table S2. In general, all complexes formed with enterobactin had several pi-type interactions, mainly because this siderophore has 3 aromatic rings in its chemical structure. It is noted that in the enterobactin-Sit1 complex, pi-alkyl and pi-sigma interactions (Supplementary Figure S3) occur that may have contributed to a slightly better energy value when compared to the other complexes of this siderophore. Among the complexes formed by ferrioxamine B, the ferrioxamine-Sit1 complex had the best energy score of -9.8 Kcal / mol. We noticed that the pocket of the Sit1 protein that interacts with FOB is highly hydrophobic which is especially important in the initial adjustment of the ligand [11].

2. **Strains and Culture Conditions**

For experiments we used yeast cells, strain 18 (ATCC32069) (P*b*18), of *P. brasiliensis*. The cells were maintained in brain heart infusion (BHI) solid medium with 4% (w/v) glucose and grown in liquid BHI for 72 hours, at 36°C. After growth to the exponential phase in liquid BHI and washes with PBS 1X (phosphate buffered saline solution 1X; 1.4 mM KH_2PO_4, 8 mM Na_2HPO_4, 140 mM NaCl, 2.7 mM KCl; pH 7.4) cells were incubated in MMcM (McVeigh/Morton medium) with no iron addition and with 50 µM of ferrous iron-specific chelator (BPS - bathophenanthroline-disulfonic acid; Sigma-Aldrich, Germany), for 24 hours at 36°C with shaking at 150 rpm. After incubation, yeast cells were collected and washed with PBS 1X. Trypan blue was used to determine the viability. For culturing under the conditions of interest was used a total of 10^7 cells/mL. Yeast cells were cultured for 6 and 24 hours in medium with 10 µM of a xenosiderophore (FOB - ferrioxamine B) and in medium with 50 µM of iron chelator BPS.

RNA extraction and quantitative real time PCR (RT-qPCR)

After incubation for 6 and 24 hours in MMcM supplemented with BPS or FOB the yeast cells were collected and total RNA extraction was accomplished using TRIzol (TRI Reagent, Sigma-Aldrich, St. Louis, MO) and mechanical cell rupture (Mini-Beadbeater – Biospec Products Inc., Bartlesville,

OK). Super-Script III Frist-Synthesis SuperMix (Invitrogen, Life Technologies) was used to obtain the cDNAs that were submitted to qRT-PCR in the StepOnePlus real-time PCR System (Applied Biosystems Inc.) using SYBER green PCR master mix (Applied Biosystems, Foster City, CA). Supplementary Table S3 features the sequences of forward and reverse oligonucleotides used. The reaction was performed in triplicate for each cDNA. Data were normalized with the transcript for 28S protein (XP_015701336) [12]. The standard curve method for relative quantification was used for calculating the relative expression levels of transcripts of interest [13]. An aliquot from each cDNA sample was used to obtain the standard curve. Statistical analysis was based in the Student's *t*-test and *P* values of 0.05 or less were considered statistically significant.

Supplementary table S3: Sequences of forward and reverse oligonucleotides

Gene	Sequence
sit1	F: GGCAATCATTTTCCCTGTGTG R: CGCGAAGACTGCAATCAAAAG
mirB	F: GTCTTCTACTGGGTCGGGTAT R: GACCATTCAGGAAGGCTGTC
mirC	F: CAGAATGTGGTGAACGCCGT R: AGAATTTGCAGTCCTGTTGAAC

REFERENCES

1. Yang, J.; Zhang, Y. I-TASSER server: New development for protein structure and function predictions. *Nucleic Acids Res.* **2015**, *43*, W174–W181, doi:10.1093/nar/gkv342.
2. Pronk, S.; Páll, S.; Schulz, R.; Larsson, P.; Bjelkmar, P.; Apostolov, R.; Shirts, M.R.; Smith, J.C.; Kasson, P.M.; Van Der Spoel, D.; et al. GROMACS 4.5: A high-throughput and highly parallel open source molecular simulation toolkit. *Bioinformatics* **2013**, *29*, 845–854, doi:10.1093/bioinformatics/btt055.
3. Williams, C.J.; Headd, J.J.; Moriarty, N.W.; Prisant, M.G.; Videau, L.L.; Deis, L.N.; Verma, V.; Keedy, D.A.; Hintze, B.J.; Chen, V.B.; et al. MolProbity: More and better reference data for improved all-atom structure validation. *Protein Sci.* **2018**, *27*, 293–315, doi:10.1002/pro.3330.
4. Moynié, L.; Milenkovic, S.; Mislin, G.L.A.; Gasser, V.; Malloci, G.; Baco, E.; McCaughan, R.P.; Page, M.G.P.; Schalk, I.J.; Ceccarelli, M.; et al. The complex of ferric-enterobactin with its transporter from Pseudomonas aeruginosa suggests a two-site model. *Nat. Commun.* **2019**, *10*, 1–14, doi:10.1038/s41467-019-11508-y.
5. Podkowa, K.J.; Briere, L.A.K.; Heinrichs, D.E.; Shilton, B.H. Crystal and solution structure analysis of FhuD2 from Staphylococcus aureus in multiple Unliganded conformations and bound to ferrioxamine-B. *Biochemistry* **2014**, *53*, 2017–2031, doi:10.1021/bi401349d.
6. Agoro, R.; Mura, C. Iron supplementation therapy, a friend and foe of mycobacterial infections? *Pharmaceuticals* **2019**, *12*, 1–28, doi:10.3390/ph12020075.

7. Trott, O.; Olson, A.J. AutoDock Vina: improving the speed and accuracy of docking with a new scoring function, efficient optimization and multithreading. *J. Comput. Chem.* **2010**, *31*, 455–461, doi:10.1002/jcc.21334.

8. Carugo, O. How root-mean-square distance (r.m.s.d.) values depend on the resolution of protein structures that are compared. *J. Appl. Crystallogr.* **2003**, *36*, 125–128, doi:10.1107/S0021889802020502.

9. Karplus, M.; McCammon, J.A. Molecular dynamics simulations of biomlecules. *Nat. Struct. Biol.* **2002**, *9*, 646–652, doi:10.1038/nsb0902-646.

10. Chen, D.; Oezguen, N.; Urvil, P.; Ferguson, C.; Dann, S.M.; Savidge, T.C. Regulation of protein-ligand binding affinity by hydrogen bond pairing. *Sci. Adv.* **2016**, *2*, doi:10.1126/sciadv.1501240.

11. Wu, S.; González, M.T.; Huber, R.; Grunder, S.; Mayor, M.; Schönenberger, C.; Calame, M. Molecular junctions based on aromatic coupling. *Nat. Nanotechnol.* **2008**, *3*, 569–574, doi:10.1038/nnano.2008.237.

12. Silva, M.G.; Curcio, J.S. de; Silva-Bailão, M.G.; Lima, R.M.; Tomazett, M.V.; Souza, A.F. de; Cruz-Leite, V.R.M.; Sbaraini, N.; Bailão, A.M.; Rodrigues, F.; et al. Molecular characterization of siderophore biosynthesis in Paracoccidioides brasiliensis. *IMA Fungus* **2020**, *11*, 1–14.

13. Bookout, A.L.; Cummins, C.L.; Kramer, M.F.; Pesola, J.M.; Mangelsdorf, D.J. High-Throughput Real-Time Quantitative Reverse Transcription PCR. In *Current Protocols in Molecular Biology*; 2006; pp. 15.8.1-15.8.28.

Journal of *Fungi*

MDPI

Article

Interacting with Hemoglobin: *Paracoccidioides* spp. Recruits hsp30 on Its Cell Surface for Enhanced Ability to Use This Iron Source

Aparecido Ferreira de Souza [1,†], Mariana Vieira Tomazett [1,†], Kleber Santiago Freitas e Silva [1], Juliana Santana de Curcio [1], Christie Ataides Pereira [1], Lilian Cristiane Baeza [2], Juliano Domiraci Paccez [1], Relber Aguiar Gonçales [3,4], Fernando Rodrigues [3,4], Maristela Pereira [1] and Célia Maria de Almeida Soares [1,*]

1 Laboratório de Biologia Molecular, Instituto de Ciências Biológicas, ICB II, Campus II, Universidade Federal de Goiás, Goiânia 74000-000, Brazil; aparecidofsouza@gmail.com (A.F.d.S.); mvtomazett@gmail.com (M.V.T.); smallbinho@hotmail.com (K.S.F.eS.); julianadecurcio1@gmail.com (J.S.d.C.); christierv@live.com (C.A.P.); julianopaccez@gmail.com (J.D.P.); maristelaufg@gmail.com (M.P.)
2 Centro de Ciências Médicas e Farmacêuticas, Universidade Estadual do Oeste do Paraná, Cascavel 85819-110, Brazil; lilianbaeza@gmail.com
3 Life and Health Sciences Research Institute (ICVS), School of Medicine, University of Minho, 4700-000 Braga, Portugal; relbergoncales@usp.br (R.A.G.); frodrigues@med.uminho.pt (F.R.)
4 ICVS/3B's—PT Government Associate Laboratory, 4800-000 Guimarães, Portugal
* Correspondence: cmasoares@gmail.com
† These authors contributed equally to this work.

Abstract: *Paracoccidioides* spp. are thermally dimorphic fungi that cause paracoccidioidomycosis and can affect both immunocompetent and immunocompromised individuals. The infection can lead to moderate or severe illness and death. *Paracoccidioides* spp. undergo micronutrients deprivation within the host, including iron. To overcome such cellular stress, this genus of fungi responds in multiple ways, such as the utilization of hemoglobin. A glycosylphosphatidylinositol (GPI)-anchored fungal receptor, Rbt5, has the primary role of acquiring the essential nutrient iron from hemoglobin. Conversely, it is not clear if additional proteins participate in the process of using hemoglobin by the fungus. Therefore, in order to investigate changes in the proteomic level of *P. lutzii* cell wall, we deprived the fungus of iron and then treated those cells with hemoglobin. Deprived iron cells were used as control. Next, we performed cell wall fractionation and the obtained proteins were submitted to nanoUPLC-MS^{E}. Protein expression levels of the cell wall F1 fraction of cells exposed to hemoglobin were compared with the protein expression of the cell wall F1 fraction of iron-deprived cells. Our results showed that *P. lutzii* exposure to hemoglobin increased the level of adhesins expression by the fungus, according to the proteomic data. We confirmed that the exposure of the fungus to hemoglobin increased its ability to adhere to macrophages by flow cytometry. In addition, we found that HSP30 of *P. lutzii* is a novel hemoglobin-binding protein and a possible heme oxygenase. In order to investigate the importance of HSP30 in the *Paracoccidioides* genus, we developed a *Paracoccidioides brasiliensis* knockdown strain of HSP30 via *Agrobacterium tumefaciens*-mediated transformation and demonstrated that silencing this gene decreases the ability of *P. brasiliensis* to use hemoglobin as a nutrient source. Additional studies are needed to establish HSP30 as a virulence factor, which can support the development of new therapeutic and/or diagnostic approaches.

Keywords: nutritional immunity; cell wall proteins; molecular dynamics

Citation: de Souza, A.F.; Tomazett, M.V.; Freitas e Silva, K.S.; de Curcio, J.S.; Pereira, C.A.; Baeza, L.C.; Paccez, J.D.; Gonçales, R.A.; Rodrigues, F.; Pereira, M.; et al. Interacting with Hemoglobin: *Paracoccidioides* spp. Recruits hsp30 on Its Cell Surface for Enhanced Ability to Use This Iron Source. *J. Fungi* **2021**, *7*, 21. https://doi.org/10.3390/jof7010021

Received: 23 November 2020
Accepted: 28 December 2020
Published: 1 January 2021

1. Introduction

Iron is one of the micronutrients that is highly essential for the metabolism of almost all organisms, but at high levels, iron is toxic and generates reactive oxygen species (ROS) [1]. Additionally, iron and other metals have their bioavailability strictly controlled by the mammalian host through a process called nutritional immunity, which affects the infectious

success of pathogenic microbes [2]. Hence, microbial iron acquisition is an important virulence attribute [3]. Due to the importance of iron for the biological processes of both hosts and pathogens, but in contrast to the toxic potential of the metal, hosts employ the strategy of binding the metal to several proteins, such as ferritin, transferrin, lactoferrin and hemoglobin, in order to avoid both the metal toxicity and the access of pathogens to it [4].

When challenged by iron deprivation imposed by the host, pathogenic fungi employs mechanisms of high affinity and specificity to capture iron from the host, including reductive iron uptake pathways, biosynthesis, and uptake of siderophores, and the use of host's iron-binding proteins [1,5,6]. Hemoglobin is an abundant host's heme-containing protein and an important iron source for pathogens including fungi. The heme present in the hemoglobin can be removed and totally internalized by the fungi or the iron contained in the heme group can be released and readily internalized by pathogens [7,8]. *Candida albicans* captures hemoglobin-derived heme via a network of receptors that contain the CFEM domain (common in several fungal extracellular membrane proteins) that transfers the heme group to the ESCRT (endosomal sorting complex required for transport)-mediated endocytosis system [9–13]. *Cryptococcus neoformans* is also capable of using heme. The first step in the process is mediated by CIG1, a cell surface protein that, although not containing the CFEM domain, act as a hemophore [14]. Similarly to *C. albicans*, the process of heme endocytosis in *C. neoformans* is dependent on the ESCRT system [15,16]. In addition, recent work showed the importance of the clathrin-mediated endocytosis (CME) mechanism for the uptake of heme and hemoglobin in *C. neoformans*, given that mutants lacking this system are not successful in developing virulence factors. Interestingly, mutants *las17* (a gene encoding for a nucleation-promoting factor for actin assembly) were avirulent in mice infection tests [17].

The *Paracoccidioides* genus comprises thermally dimorphic fungi that grow in a hyphal form in the environment, but exist shift their morphology into budding yeast cells within mammalian hosts [18]. *Paracoccidioides* spp. infect at least 10 million people causing the disease paracoccidioidomycosis (PCM), which is geographically restricted to the subtropical areas of Latin America [19,20]. Members of the *Paracoccidioides* genus include the species *P. brasiliensis*, *P. lutzii*, *P. americana*, *P. restrepiensis,* and *P. venezuelensis*. The disease manifestations range from superficial skin lesions to invasive infections [21,22]. The infection is initiated by inhalation of fungal propagules, which differentiate into yeast cells after reaching the alveolar epithelium [23].

When challenged with iron deprivation, *Paracoccidioides* spp. employs a complex response that encompasses transcriptional and metabolic reprogramming and the expression of high affinity systems for iron uptake, including biosynthesis and uptake of siderophores and a non-canonical iron reductive pathway [24–26]. Additionally, we have demonstrated previously that hemoglobin is the preferential host iron source of the *Paracoccidioides* spp. These fungi have hemolytic activity, able to acquire iron from hemoglobin and endocytize the heme group without releasing iron into the extracellular level. A GPI-anchored receptor, Rbt5, has the primary role of acquiring the essential nutrient iron from the host hemoglobin [27].

Previous studies developed at our laboratory allowed the identification of proteins from *P. lutzii* cell wall by using subcellular fractionation and nanoUPLC-MS^E. Sequential fractionation associated with a proteomic approach allowed the characterization of *P. lutzii* cell wall proteins, such as proteins associated with the cell wall through non-covalent or disulfide bonds (F1) and proteins bound to the cell wall by alkali-labile bonds (F2) [28]. We identified proteins present in the cell wall that belong to several functional categories. Some of these proteins have been previously characterized in the cell wall of *Paracoccidioides* genus playing putative roles in cell wall biogenesis and organization as well as in virulence, adhesion, colonization, survival in hostile environments and evasion of the immune system, thereby allowing the establishment of the disease [29–33]. Another study also carried out in our laboratory allowed the identification of *P. lutzii* cell surface

proteins that interact with macrophages through affinity chromatography based on surface proteomics [34]. The authors obtained F1 cell wall enriched extracts and identified proteins, such as serine proteinase and fructose-1,6-bisphosphate aldolase interacting with macrophage surface proteins, and confirmatory assays showed that these proteins undergo positive regulation during the interaction of the fungus with the host [34]. The studies performed by Araújo et al. (2017) [28] and Tomazett et al. (2019) [34] demonstrated that the identification of the cell wall proteins is a good alternative to list new targets in the context of host–pathogen interaction.

Therefore, in order to investigate changes in the proteomic level of *P. lutzii* cell wall, we deprived the fungus of iron and then treated those cells with hemoglobin. Deprived iron cells were used as control. Next, we performed cell wall fractionation and the obtained proteins were submitted to nanoUPLC-MS^{E}. Protein expression levels of the cell wall F1 fraction of cells exposed to hemoglobin were compared with the protein expression of the cell wall F1 fraction of iron-deprived cells. Our results demonstrated that upregulation of potential adhesins occurs at the cell surface when the fungus is exposed to hemoglobin and revealed that HSP30 of *P. lutzii* is a novel hemoglobin-binding protein. In order to investigate the importance of *Pb*HSP30 in the *Paracoccidioides* genus, we developed a *P. brasiliensis* (*Pb*18) knockdown strain of HSP30 via *Agrobacterium tumefaciens*-mediated transformation (ATMT) and demonstrated that silencing this gene decreases the ability of *P. brasiliensis* to use hemoglobin as a nutrient source. These findings highlight the importance of HSP30 regarding the use of hemoglobin by *Paracoccidioides* spp. and we hypothesize that HSP30 may be important in the context of infection, given that the use of hemoglobin by the fungus is a virulence attribute. To confirm this inference, further investigation is needed. Certainly, these studies will contribute to the expansion of the knowledge regarding *Paracoccidioides*–host interaction, which can culminate in the development of new therapeutic and/or diagnostic approaches.

2. Materials and Methods

2.1. Ethics Statement

All experiments were conducted in accordance with the Brazilian Federal Law 11,794/2008 establishing procedures for the scientific use of animals. All efforts were made to minimize suffering, and the animal experiments were approved by the Ethics Committee on the use of Animal Experimentation (Federal University of Goiás, CEUA-UFG; under protocol number 116/17, approved on 13 November 2017), following the guidelines of the National Council for Control of Animal Experimentation.

2.2. Strains and Growth Conditions

P. lutzii (American Type Culture Collection—ATCC MYA-826—*Pb*01) and *P. brasiliensis* (ATCC 32069—*Pb*18) were maintained in Brain Heart Infusion (BHI) solid broth supplemented with glucose 4% (*w/v*) at 36 °C. To obtain cell wall proteins extracts, *P. lutzii* yeast cells were cultured in BHI liquid medium, supplemented with glucose 4% (*w/v*) for 72 h at 36 °C and under shaking at 120 rpm. Next, 5×10^6 cells/mL were transferred to McVeigh and Morton modified medium (MMcM) chemically defined liquid medium [35] without iron, supplemented with 50 µM of the iron chelator bathophenanthrolinedisulfonic acid (BPS—Sigma-Aldrich, St. Louis, MO, USA) and were maintained in this condition for 36 h in order to establish intracellular iron depletion. Finally, yeasts cells were transferred to MMcM containing bovine hemoglobin 10 µM (Sigma-Aldrich, St. Louis, MO, USA) or BPS 50 µM and maintained for 48 h.

2.3. Extraction of P. Lutzii Cell Wall Proteins (CWPs)

To obtain *P. lutzii* CWPs, we employed the methodology described by Araújo et al., (2017) [28], with some modifications. After 48 h of fungal culture in the presence of hemoglobin (treatment) or in iron deprivation (control), the cultures were collected and centrifuged at 800× *g* for 10 min at 4 °C, and cells were washed 5 times with lysis buffer

(10 mM Tris-HCl pH 8.5, 2 mM $CaCl_2$, 1:10 protease inhibitor). Subsequently, the cells were resuspended in ice-cold 10 mM Tris-HCl buffer, pH 8.0, broken in the presence of liquid nitrogen and the cellular powder was resuspended in ice-cold lysis buffer. Then, glass beads (4 mm) were added to the suspension. The mixture was vortexed for 1 h at 4 °C. After centrifugation at 800× *g* for 10 min at 4 °C, the glass beads were removed and pellets were washed 5 times with ice-cold ultrapure water, 5 times with 0.86 M NaCl, 5 times with 0.34 M NaCl and 5 times with 0.17 M NaCl. The washes performed with NaCl solutions aimed to remove potential contaminants, which can range from extracellular proteins to membrane or cytoplasmic proteins that can be retained on the isolated cell wall by non-specific ionic interactions [36]. The obtained pellets were treated twice with extraction buffer (50 mM Tris-HCl, pH 7.8, 69 mM SDS, 10 mM EDTA and 40 mM Mercaptoethanol) for 10 min at 100 °C and then centrifuged. The supernatants were collected, concentrated using membranes with 10-kDa exclusion level (Amicon Ultra centrifugal filter, Millipore, Bedford, MA, USA) and washed 3 times with ice-cold ultrapure water. Afterwards, treatment with 2-D Clean-Up Kit (GE Healthcare) was performed with another three washes with ice-cold ultrapure water. The obtained extract corresponded to proteins that are non-covalently linked or linked to the cell wall by disulfide bonds.

2.4. Preparation of Complex Samples for NanoUPLC-MS^E

The F1 CWPs extracts were quantified. We added 150 µL of a 0.2 % (*w/v*) RapiGest solution and 10 µL of 50 mM NH_4HCO_3 at pH 8.5 to 300 µg of protein extracts. The mixture was incubated at 80 °C for 15 min and subsequently, 2.5 µL of 100 mM DTT were added, followed by another incubation at 60 °C for 30 min. Next, 2.5 µL of 300 mM of iodoacetamide were added and the samples were maintained for 30 min away from the light at room temperature. Samples were then subjected to tryptic digestion with 60 µL of a 0.05 µg/µL trypsin solution and incubated at 37 °C for 16 h. Then, 60 µL of 5% (*v/v*) trifluoroacetic acid were added and the solution was incubated at 37 °C for additional 90 min. The samples were centrifuged at 13,000× *g* for 30 min at 4 °C and the supernatants were transferred to clean tubes. The centrifugation process was repeated until there was no further precipitate formation. The samples were concentrated in a speed vacuum apparatus, resuspended in 12 µL of ultrapure water, purified on ZipTip Pipette Tips (ZipTip C18 Pipette Tips, Millipore, Bedford, MA, USA) following the manufacturer's instructions, and again concentrated in a speed vacuum concentrator. The obtained peptides were resuspended in 60 µL of 20 mM ammonium formiate, at pH 10, containing 200 fmol/µL phosphorylase B (PHB) (Waters Corporation, Manchester, UK) (MassPREPTM protein), used as the internal control. The obtained samples were submitted to nanoUPLC-MS^E, as described in the subsequent session.

2.5. Data Acquisition by NanoUPLC-MS^E

The samples were subjected to a high-resolution liquid chromatography at the nanoscale through the ACQUITY UPLC® M-Class system (Waters Corporation, Manchester, UK). The fractionation of the peptides was performed in an XBridge® Peptide 5 µm BEH130 C18, 300 µm × 50 mm reverse phase pre-column (Waters Corporation, Manchester, UK). The first dimension of the system was maintained in a flow rate of 0.5 µL/min with an initial condition of 3% acetonitrile (ACN). The peptides were submitted to five fractions (F1–F5) of an ACN gradient (F1–11.4%, F2–14.7%, F3–17.4%, F4–20.7%, and F5–50%). For the second dimension, each fraction was eluted on a 2D Symmetry® 5 µm BEH100 C18, 180 µm × 20 mm trapping column (Waters Corporation, Manchester, UK) and passed through the analytical column Peptide CSH$^{TM.}$BEH130 C18 1.7 µm, 100 µm × 100 mm (Waters Corporation, Manchester, UK), in a flow of 0.4 µL/min at 40 °C. The human (Glu1)-fibrinopeptide B (GFB-Sigma-Aldrich, St. Louis, MO, USA) protein was used for the mass calibration, which was measured every 30 s and in a constant flow of 0.5 µL/min. GFB was used at the concentration of 200 fmol/µL. Peptide identification and quantification were carried out in a Synapt G1 MSTM (Waters Corporation, Machester, UK) mass spectrometer

equipped with a NanoElectronSpray source and two mass analyzers [a first quadrupole and the second time of flight (TOF). Three experimental replicates were performed.

2.6. Spectra Processing and Proteomic Analysis

After nanoUPLC-MS^E, data processing was performed using ProteinLynx Global Server version 3.0.2 software (PLGS) (Waters Corporation, Manchester, UK), which allowed the determination of the exact mass retention time (EMRT) of the peptides and their molecular weight, by mass/charge ratio (m/z). For identification of the peptides, the obtained spectra (along with reverse sequences) were compared with sequences available in the database of *P. lutzii* (*Pb*01) (https://www.uniprot.org/proteomes/UP000002059). To refine protein identification, we employed the detection of at least two ions per peptide fragments, five by protein fragments, the determination of at least one peptide per protein, false positive rate of 4%, carbamidomethylation of cysteine, oxidation of methionine, phosphorylation of serine, threonine and tyrosine and a trypsin-lost cleavage site was allowed. The tolerable mass error for identification of the peptides was set to 50 ppm. The quality graphics for the races were generated through MassPivot software v1.0.1 (kindly provided by Dr. André Murad), FBAT software (https://sites.google.com/view/fbat-web-page), Spotfire® v8.0 (TIBCO Software Inc.©, Palo Alto, CA, EUA) and Microsoft Office Excel (Microsoft®, Redmond, Washington, DC, USA). Proteins present in at least two of the three experimental replicates of extracts were included in the subsequent differential expression analysis. Proteins that presented the lowest coefficient of variance and that were detected in all the replicates were used for the normalization of intensity and the Expression Algorithm (Expression^E, Waters Corporation, Manchester, UK), which is part of the PLGS software [37], was used for the differential expression analysis. Proteins classified as regulated presented fold change $\pm$ 0.5 between the quantification of the extract obtained in the presence of hemoglobin $\times$ Fe deprivation. Homology investigation of identified hypothetical proteins was performed using the BLASTp online tool (Basic Local Alignment Search Tool—https://blast.ncbi.nlm.nih.gov/Blast.cgi?PAGE=Proteins). Protein sequences were further subjected to in silico analysis for signal peptide prediction using the Signal P 4.0 Server online tool (http://www.cbs.dtu.dk/services/SignalP-4.0/). For the prediction of proteins secreted by non-classical pathways, the online tool Secretome P 2.0 was used. The prediction of potential adhesins was performed using the online FaaPred tool (http://bioinfo.icgeb.res.in/faap/). Heatmap graphic was generated by Microsoft Office Excel (Microsoft®, Redmond, Washington, DC, USA). The HSP30 protein was an important finding in our proteomic data and we decided to investigate this result further.

2.7. Expression of the Recombinant HSP30 Protein in Escherichia Coli, Protein Purification, and Polyclonal Antibodies

Total RNA was extracted from fungal yeast cells using the TRIzol reagent (TRI Reagent®, Sigma-Aldrich, St. Louis, MO, USA) and mechanical cell rupture (MiniBeadbeater—BioSpec Products), as described by the manufacturer's protocol. From the extracted RNA, cDNA was synthetized following the manufacturer recommendation of the Super Script® Reverse Transcriptase Kit (Invitrogen™, Waltham, MA, USA). The cDNA was used to amplify the HSP30 protein (PAAG_00871) using the polymerase High Fidelity (Invitrogen™, Waltham, MA, USA). The oligonucleotides sense sequence was 5′GGTTCCGCGTGGATCCATGTTCT CTCGTCGAGCC′3 and the antisense was 5′GGGAATTCGGGGATCCCTACTCAATCGTA ATCTTCTT′3. The amplification cycle comprised denaturation at 94 °C for 2 min followed by 40 cycles of denaturation at 94 °C for 30 s, annealing at 54 °C for 30 s and extension at 72 °C for 1 min and 30 s, followed by a final extension at 72 °C for 5 min. The cDNA product obtained by RT-PCR was cloned into the expression vector pET-32a. Bacterial cells, strain *Escherichia coli* C43, harboring the recombinant plasmid were grown in Luria-Bertani (LB) medium supplemented with 100 µg/mL ampicillin (*w/v*) under agitation at 37 °C until the optical density (OD) reached an absorbance of 0.6 at a wavelength of 600 nm. The reagent Isopropyl-β-D-thiogalactopyranoside (IPTG) was added to the growing culture to a final concentration of 0.1 mM. The bacterial cells were harvested by centrifugation

at 10,000× *g* for 10 min after 16 h of incubation at 15 °C and resuspended in phosphate buffered saline (PBS) 1X. The recombinant HSP30 protein fused to Trx-His-Tag was used for the production of polyclonal antibodies in 4 BALB/c male mice aged 6–8 weeks. The fusion protein was removed from SDS-PAGE gels and injected into mice along with Freund's adjuvant three times at intervals of 15 days. Serum containing polyclonal antibodies was collected and stored at −20 °C. The protein was produced in inclusion bodies and was solubilized using 50 µL of a 20% (*w/v*) *N*-Lauroylsarcosine sodium salt (Sigma Aldrich, Missouri, KS, USA) solution for 5 mL of bacterial extracts and sonicated (5 times, 10 min). SDS-PAGE analysis showed the protein in the soluble fraction and then, the protein was purified by a nickel resin chromatography system (Qiagen Inc., Germantown, MD, USA).

2.8. Far-Western Blot Analyses

We used the protocol described by [38] to perform far-western blot analysis. The recombinant HSP30 protein and bovine hemoglobin were transferred to Hybond nitrocellulose membranes (GE Healthcare, Piscataway, NJ, USA) and incubated for 1 h at room temperature with bovine hemoglobin diluted at 35 µg/mL in blocking buffer containing 10% (*w/v*) skim milk powder and 0.1% (*v/v*) Tween-20 in PBS 1X. Washing of the membrane was performed, followed by incubation with the primary monoclonal antibody anti-human hemoglobin produced in mice (Abcam Plc, Cambridge, UK) and diluted 1:100 in blocking buffer. Another washing series was performed and the membrane was incubated with anti-mouse alkaline phosphatase conjugated secondary antibody (1:10,000) for 1 h at room temperature and protected from light. The revelation step was performed employing 5-bromo-4-chloro-3-indolyl phosphate/p-nitroblue tetrazolium chloride (BCIP/NBT).

2.9. Flow Cytometry and Immunofluorescence Assays

P. lutzii yeast cells were cultivated in the presence of 10 µM of hemoglobin or 50 µM of BPS. Two additional conditions were included, which were 10 µM of $FeSO_4$ and 10 µM of Bovine Serum Albumin (BSA). Flow cytometry was performed according to the methodology described by [34]. Murine macrophages of the lineage RAW 264.7 were cultured in RPMI medium containing bovine fetal serum 10% (*v/v*) and MEM non-essential amino acid solution (Sigma Aldrich, Missouri, KS, USA) at 36 °C and 5% CO_2 until complete confluence. The experiment was performed in 12-well polypropylene plates (Greinner Bio-One, Monroe, NC, USA). We plated 10^5 macrophages per well in Roswell Park Memorial Institute (RPMI) medium containing gamma interferon (IFN-γ) (1 U/mL) (Sigma-Aldrich, St. Louis, MO, USA) following incubation for 24 h at 36 °C and 5% CO_2 for adherence and activation. Then, the medium was replaced by a fresh RPMI medium containing IFN-γ (1 U/mL) and 5 × 10^5 *P. lutzii* yeast cells per well were added to the macrophages. The cells were incubated for 4 h at 36 °C and 5% CO_2. Macrophages were washed with PBS 1X to remove unbound fungal cells, fixed with cold methanol for 2 h at −80 °C and the cells were collected by scraping. The cells were washed three times with PBS 1X, incubated with 100 µg/mL Congo Red (Sigma-Aldrich, St. Louis, MO, USA) for 15 min and washed 3 times again with PBS 1X. The number of yeast cells of *P. lutzii* adhered/internalized to macrophages was identified by flow cytometry assay and the instrument Guava® easyCyte (Merck Millipore, Darmstadt, Germany) acquired a minimum of 10,000 cells per sample. Proportion test was used for statistical comparison between the conditions analyzed [39].

For the immunofluorescence assays, *P. lutzii* yeast cells were grown in the absence or presence of hemoglobin at 10 µM for 48 h at 36 °C under agitation. Subsequently, the cells were centrifuged, and the pellet washed with PBS 1X. Cells were counted in a Neubauer's chamber and 10^6 cells/mL were fixed with ice-cold methanol for 2 h at −80 °C. Then, cells were washed three times with PBS 1X, blocked for 30 min with PBS 1X containing BSA (3% (*w/v*)) and tween-20 (0.2% [*v/v*]) at room temperature and washed 3 times again with PBS 1X. The cells were incubated for 1 h at room temperature with anti-HSP30 protein polyclonal antibodies, produced in mice and diluted 1:100 in blocking buffer. Following 3 washes with PBS 1X, the cells were incubated for 1 h at room temperature with anti-

mouse IgG coupled with fluorescein isothiocyanate (FITC- Sigma-Aldrich, St. Louis, MO, USA) diluted 1:100 in blocking buffer. The cells were washed with PBS 1X 3 times and observed under an Axio Scope A1 fluorescence microscope at bright field and 470/440 nm wavelength. Digital images were acquired using the software AxioVision (Carl Zeiss AG, Berlin, Germany).

2.10. Structural Alignment of HSP30 and Human Heme Oxygenase

The sequence alignment of HSP30 (PAAG_00871) and human heme oxygenase 1 (P09601) was obtained by the ClustalX 2.1 program [40]. In order to perform protein structure comparisons we used the TM-align algorithm [41]. This approach was based on the generation of an enhanced residue-to-residue alignment through dynamic simulations considering the backbone alpha-carbon coordinates of the HSP30 and hemoglobin. The best model was then produced via superposition of the structures under study and a TM-score was generated. The sequence identity cutoff was set to 95% and gap penalties were eliminated to circumvent fragmentation caused by the topological complexity of helices. The PDB output was used in PyMOL (pymol.org) to compare the alignment results from the TM-align server.

2.11. Preparation of Three-Dimensional (3D) Structures and Molecular Docking

The Iterative Threading Assembly Refinement (I-TASSER) server [42] was used to model the three-dimensional structure of HSP30 from *P. lutzii*. The server models protein structures based on templates of homologous proteins experimentally determined and deposited on the PDB (protein data bank) database. I-TASSER applies fold recognition via Monte Carlo simulations in order to rank homologous fragments and the procedure follows basic steps consisting of prediction of secondary structure by Protein Secondary Structure Prediction (PSSpred) and identification of threading templates by Local Meta-Threading-Server (LOMETS). Fragments are assembled in clusters according to conformation and energy levels to detect native similar structures. Finally, the modeled structure undergoes molecular dynamics refinement and prediction of biological function by COACH. The quality of the HSP30 three-dimensional structure was assessed through the MolProbity server.

The *Homo sapiens* hemoglobin structure was retrieved from the PDB under the accession number 1A3N. The ClusPro protein–protein anchor server [43] was used to determine the best protein complex conformations between HSP30 and hemoglobin. After the assembly of the complexes, the next step was to identify the amino acids involved in the interaction. We used the KFC2 server [44] to recognize all residues from the interaction interface from the complex formed by HSP30 and hemoglobin.

2.12. Molecular Dynamics Simulations

Molecular dynamics simulations determined a stable structure of the complex, similar to the native structure model. The protein complex under study was submitted to molecular dynamics using the software GROMACS 4.5.5, AMBER force field (ff99SB-ILDM) with the presence of explicit water TIP3P solvent [45]. The first step of the simulation is the minimization of the overall free energy to remove unfavorable contacts, carried on until 1000 kJ/mol or until the system reached the number of pre-determined steps. We performed a 100 ps NVT (mol, volume, and temperature) simulation followed by a 100 ps NPT (mol, pressure, and temperature) simulation in order to guarantee the balance of the thermodynamic variables. The NVT simulation allowed the pressure of the system to vary and at this step, the temperature was set to 300 K and velocities were calculated through Maxwell's equations. During the NPT simulation, the volume is variable and the pressure was maintained by the Parrinello–Rahman barostat.

After the preparation of the system was completed, the complex formed by HSP30 and hemoglobin was submitted to a simulation of 200 ns, 300 K, 1 atm and time interval of 2 fs. No conformation restriction was applied at this point. Molecular dynamics analysis of trajectories was performed by root mean square deviation (RMSD) in relation to the initial

structure by the *gromos* algorithm [46]. The g_cluster program (GROMACS package) was used to determine the most frequent conformations of the structure during the simulation. We used a cut-off of 0.6 nm to distinguish the conformational sets based on the RMSD profile. The cluster analysis and the RMSD allowed the analysis of the protein profile throughout the simulation and the most representative conformational mode was selected to undergo further analysis. Before the calculation of RMSD evolution and before analyzing clusters form the simulation trajectories, the structures were centered and fitted accordingly.

2.13. Construction of P. Brasiliensis HSP30 Antisense (AsHSP30) Strain

To obtain the silenced strain for the *P. brasiliensis HSP30* gene, the ATMT methodology was used as previously described [27,47,48]. DNA of *P. brasiliensis* was obtained after culturing the cells in BHI medium at 36 °C for 72 h at 150 rpm. The oligonucleotides used to amplify the sequence corresponding to aRNA of *Pb*HSP30 were HSP30 forward 5′ CTCGAGCGGGCTCCAAAGA 3′ and HSP30 reverse 5′ GGCGCGCCGGATGCTCAT 3′. The amplified fragment was inserted into the pCR35 plasmid under the control of the promoter region of the calcium-binding protein gene (CBP-1) from *Histoplasma capsulatum* [49]. Next, the CBP-1 promoter-AS cassette was subcloned into the pUR5750 plasmid, harboring a hygromycin B phosphotransferase as a selection mark. We used this system as a parental binary vector to harbor the aRNA cassette within the transfer DNA (T-DNA) [50]. These constructions were introduced into *A. tumefaciens* LBA1100 strains by electroporation and isolated via kanamycin selection (100 mg/mL). *P. brasiliensis* yeast cells were co-cultivated with transformed *A. tumefaciens* for 3 days at 25 °C and the selection of *P. brasiliensis* transformed cells was performed in BHI solid media containing hygromycin B (75 mg/mL) after 15 days of incubation at 36 °C. For the mitotic stability, randomly selected colonies of *P. brasiliensis* were grown for nine additional cycles in BHI solid medium, alternating absence and presence of 75 mg/mL of hygromycin.

2.14. Characterization of the Knockdown Strain

The HSP30 knockdown strain was characterized according to the level of transcript, growth in different media and cell viability analysis. For the transcriptional analyzes, wild tipe (WT) and silenced HSP30 strains were cultured in MMcM containing hemoglobin at 10 μM. After RNA extraction with TRIzol, the samples were treated with DNAse (RQ1 RNase-free DNase, Promega) and subjected to in vitro reverse transcription (SuperScript III First-Strand Synthesis SuperMix; Invitrogen, Life Technologies), using Oligo(dT). cDNAs were used in the RT-qPCR reaction through the QuantStudio Real-Time PCR (Thermo Fisher Scientific) with a mixture of SYBR green PCR master mix (Applied Biosystems, Foster City, CA, USA). The normalizing gene was the transcript encoding to glyceraldehyde-3-phosphate dehydrogenase (GenBank XM_015846519.1) as determined by Norm-Finder test [51]. The oligonucleotides are depicted in Supplementary Table S1. Cultures were grown in BHI medium and cellular density was measured in triplicates in a spectrophotometer Ultrospec 2000 (Pharmacia Biotech, Piscataway, NJ, USA). The viability of strains was determined by propidium iodide staining and detected by fluorescence microscopy (493/636 nm) in an Axioscope A1 microscope (Carl Zeiss AG, Berlin, Germany) [48]. To evaluate the ability of silenced strains to use hemoglobin, we subjected them to the above described culture condition and plated in triplicate in solid BHI medium. Colony forming units (CFU) were determined by counting. Statistical analysis was performed by the Student's T test and p values ≤ 0.05 were considered statistically significant.

3. Results

3.1. Hemoglobin Promotes Changes at the P. Lutzii Cell Wall Proteome

P. lutzii yeast cells were incubated with hemoglobin or BPS (control) and a specific protocol for the isolation of cell wall proteins was employed, as described in the MM section. Protein extracts were submitted to nanoUPLC-MS^E and the proteomic data were analyzed regarding experimental quality standards that validated the analysis, as shown

in Supplementary Figure S1 [37]. We found 83 proteins upregulated when yeast cells were in the presence of hemoglobin, as shown in Supplementary Table S2. To refine the results, bioinformatics tools were used to analyze which of the identified proteins had predicted secretion signal sequences, i.e., that potentially were addressed to the cell surface. This analysis revealed 33 proteins predicted to reach the fungal cell surface, representing 39.8% of the identified proteins.

For subsequent analysis, we selected proteins with positive prediction of secretion and with increased expression in the presence of hemoglobin. Table 1 and Figure 1A summarize the 33 proteins with predicted secretion. Aspartate-tRNA (Asn) ligase (PAAG_05117; XP_015699700) showed the highest fold change (5.53). Six proteins were identified exclusively in the presence of hemoglobin: HSP30 (PAAG_00871; XP_002797012.2), 40S ribosomal protein S17 (PAAG_01413; XP_002796405.1), 40S ribosomal protein S26E (PAAG_07847; XP_002790158.1), membrane-associated progesterone receptor component 1 (PAAG_01861; XP_002795973.1), protein disulfide-isomerase domain (PAAG_11504; XP_015703276.1) and pyruvate dehydrogenase protein X component (PAAG_02769; XP_002795293.1). Figure 1A presents the heatmap of upregulated proteins predicted as secreted in the presence of hemoglobin.

In order to correlate protein and transcript levels, firstly, we analyzed the transcript expression of HSP30 (PAAG_00871). The results showed that within 24 h, *P. brasiliensis* expresses approximately 20% more HSP30 transcripts in the presence of hemoglobin when compared to the control (BPS) (Figure 1B), but there was a decrease in the level of its expression after 48 h. Hence, mRNA levels increase after 24 h of treatment before protein levels increase.

Next, we determined which upregulated proteins were potential adhesins (Table 1) using bioinformatics tools. Our search revealed 7 potential adhesins and three of them were identified solely in yeast cells submitted to hemoglobin treatment: disulfide-isomerase domain protein (PAAG_11504; XP_015703276.1), pyruvate dehydrogenase protein X component (PAAG_02769; XP_002795293.1) and HSP30 (PAAG_00871; XP_002797012.2). In order to confirm the increase in the adhesion capacity of *P. lutzii*, we pretreated yeast cells with hemoglobin and assessed the ability of cells to interact with macrophages by flow cytometry, as shown in Figure 2. Statistical analysis using proportion test showed that the three conditions analyzed showed a significant difference when compared to the control condition (BSA). However, using the same test, the difference in the ratio between BSA and hemoglobin was 0.54. For BPS and $FeSO_4$, conditions also tested, this difference was 0.11 and 0.02, respectively. Thus, a comparison between the conditions showed that the treatment of *P. lutzii* cells with hemoglobin increased the interaction with macrophages by 5 and 25 times when compared with BPS and $FeSO_4$, respectively. This finding demonstrates that hemoglobin strongly modulates the ability of *P. lutzii* to adhere to macrophages.

Table 1. Up-regulated proteins in Fraction 1 (F1) of the cell wall predicted as secreted, following *Paracoccidioides lutzii* yeast cells exposition to hemoglobin and bathophenanthrolinedisulfonic acid (BPS) for 48 h.

Accession [a]	Description [b]	Score [c]	Expression LevelsRatio (Hb/BPS) [d]	SignalP [e]	SecretomeP [f]
PAAG_00871	30 kDa heat shock protein (HSP30) •	754.8	*	-	0.786
PAAG_08955	40S ribosomal protein S1	672.2	1.62	-	0.720
PAAG_01413	40S ribosomal protein S17	1850.1	*	-	0.738
PAAG_03322	40S ribosomal protein S20	1303.5	1.63	-	0.750
PAAG_07847	40S ribosomal protein S26E	409.6	*	-	0.613
PAAG_00468	4-aminobutyrate aminotransferase	977.2	1.75	-	0.601
PAAG_00430	60S ribosomal protein L2	360.1	1.55	-	0.853
PAAG_00952	60S ribosomal protein L20	1022.6	1.67	-	0.712
PAAG_07786	Acetyl-CoA acetyltransferase	1043.1	4.10	-	0.655
PAAG_05117	Aspartate-tRNA (Asn) ligase	565.1	5.53	-	0.609
PAAG_04838	ATP synthase subunit 4, mitochondrial	663.4	1.51	-	0.781
PAAG_04511	ATP-dependent RNA helicase SUB2	2259.1	1.60	-	0.722
PAAG_03701	BAR domain-containing protein	844.8	2.48	-	0.614
PAAG_01262	Chaperone DnaK	2982.3	1.57	0.864	-
PAAG_03292	Cytochrome c peroxidase, mitochondrial •	3045.4	1.60	-	0.809
PAAG_00173	Electron transfer flavoprotein subunit alpha	465.5	1.88	-	0.642
PAAG_00850	Glutamine-fructose-6-phosphate transaminase (isomerizing)	1305.8	1.65	-	0.693
PAAG_00126	Histone H4.2	4337.0	1.62	0.792	-
PAAG_00053	Malate dehydrogenase, NAD-dependent	1037.2	1.62	-	0.651
PAAG_00481	Membrane biogenesis protein Yop1	922.3	1.93	-	0.902
PAAG_01861	Membrane-associated progesterone receptor component 1	443.0	*	-	0.735
PAAG_12076	NAD(P)H:quinone oxidoreductase, type IV •	1770.3	1.55	0.718	-
PAAG_05735	NADH-ubiquinone oxidoreductase 49 kDa subunit, mitochondrial	668.4	2.05	-	0.675
PAAG_01321	Oxidoreductase 2-nitropropane dioxygenase family •	2254.9	1.79	-	0.707
PAAG_00739	Peptidyl-prolyl cis-trans isomerase B	583.7	1.65	0.641	-
PAAG_08082	Plasma membrane ATPase	738.9	1.93	-	0.712
PAAG_07957	Pre-mRNA splicing factor •	539.9	2.69	-	0.801
PAAG_11504	Protein disulfide-isomerase domain •	364.5	*	-	0.783
PAAG_02769	Pyruvate dehydrogenase protein X component •	325.5	*	-	0.685
PAAG_00417	Succinyl-CoA ligase subunit alpha	1400.3	1.88	-	0.624
PAAG_02921	Translation elongation factor Tu	990.0	1.70	-	0.773
PAAG_04901	Ubiquitin-conjugating enzyme	555.9	1.79	-	0.883
PAAG_12424	Voltage-dependent anion channel protein 1	2827.7	1.54	-	0.761

[a] Protein accession number in NCBI, available at https://www.ncbi.nlm.nih.gov/protein. [b] Description of the protein in the *Paracoccidioides* spp. databank, available in https://www.uniprot.org/uniprot/?query=paracoccidioides+lutzii&sort=score. [c] Score of the quality of protein identification. [d] Ratio between quantification of proteins identified in hemoglobin/iron deprivation. Values $\geq$ 1.5 indicate upregulated proteins; (*) indicates that the protein was identified only upon hemoglobin treatment. [e] Prediction of signal peptide presence; score $\geq$ 0.45; prediction performed by SignalP 4.1 available at http://www.cbs.dtu.dk/services/SignalP/. (-) indicates that the signal peptide was not identified. [f] Prediction of protein secretion by non-classical pathways; score 0.6; prediction performed by SecretomeP 2.0 available at http://www.cbs.dtu.dk/services/SecretomeP/. (-) indicates that the protein was not predicted as secreted by non-classical pathways. • Prediction of adhesin function; score ≥ -0.8; predicted by the FaaPred tool available at http://bioinfo.icgeb.res.in/faap/.

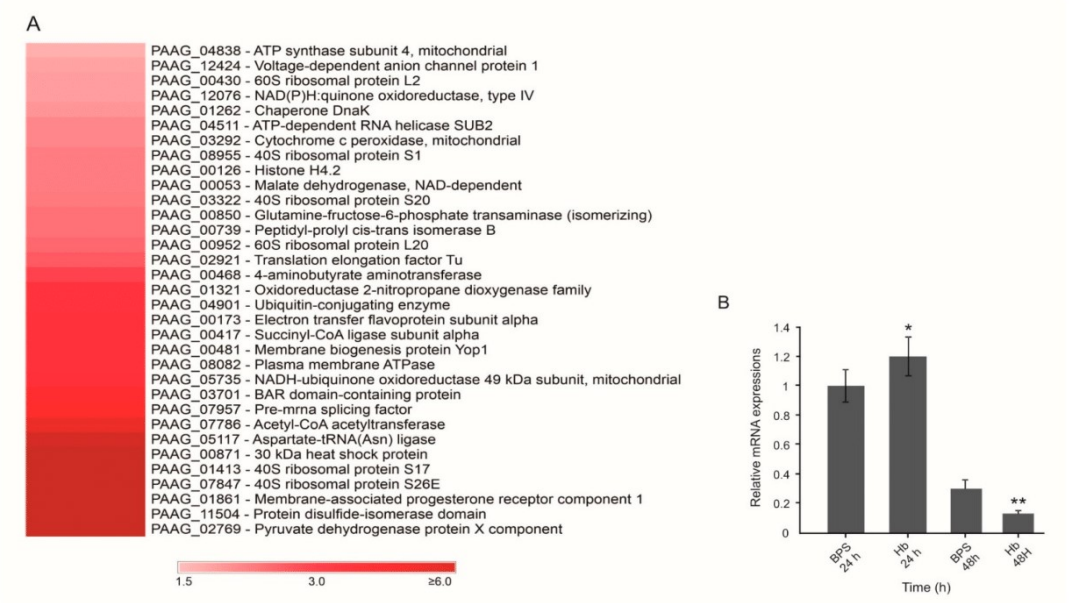

Figure 1. Heatmap of up-regulated proteins predicted as secreted and HSP30 transcriptional analysis. (**A**) The chart was generated using Microsoft Excel tools. Scale: ratio between Hb/BPS conditions. (**B**) HSP30 transcriptional analysis of WT strains of *P. brasiliensis* in the presence of hemoglobin. The yeast cells were grown in liquid Brain Heart Infusion (BHI) medium for 72 h and subsequently in McVeigh and Morton modified medium (MMcM) containing hemoglobin for 24 and 48 h. The control comprised cells grown in the presence of BPS under the same conditions. GraphPad Prism software (GraphPad Software, Inc., La Jolla, CA, USA) was used for the statistical analysis and Student's *t*-test was applied considering p values ≤ 0.05 statistically significant. (*, **) denotes statistically significant differences.

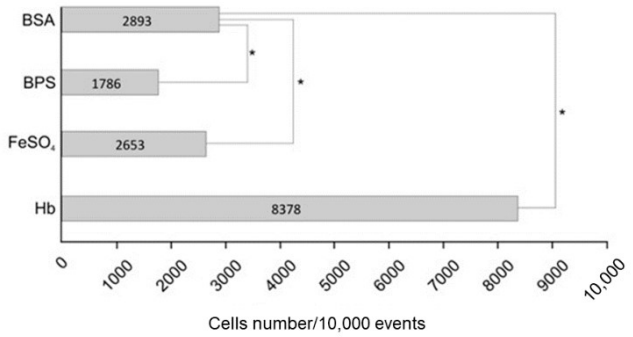

Figure 2. *P. lutzii* interaction with macrophages assessed by flow cytometry. *P. lutzii* yeast cells were grown in the presence of BPS, hemoglobin or $FeSO_4$ and incubated for 4 h with RAW 264.7 macrophages. BSA was used as control. Methanol fixed, non-permeabilized cells were incubated with 100 µg/mL of Congo Red. The amount of *P. lutzii* cells that interacted with macrophages was assessed by flow cytometry using the instrument Guava® easyCyte (MERK). Proportion test was used for statistical comparison between the conditions analyzed. (*) denotes a statistically significant difference.

3.2. Hemoglobin Increases HSP30 Expression at Cell Surface

The treatment of yeast cells with hemoglobin increases the fungal cell adhesion capacity to macrophages. The 30-kDa protein, present at the fungus F1 cell wall fraction, showed potential adhesin properties. The recombinant protein was produced in bacteria, purified, confirmed by spectrometry, and used for polyclonal antibodies production in mice, as depicted in Supplementary Figure S2. Yeast cells were employed for immunofluorescence analysis, as depicted in Figure 3. Fluorescence of HSP30 and its recognition by antibodies at

the fungal cell surface increased when the fungus was previously cultivated in the presence of hemoglobin, which corroborates our proteomic data. No reaction was obtained by using the non-immune sera, as expected.

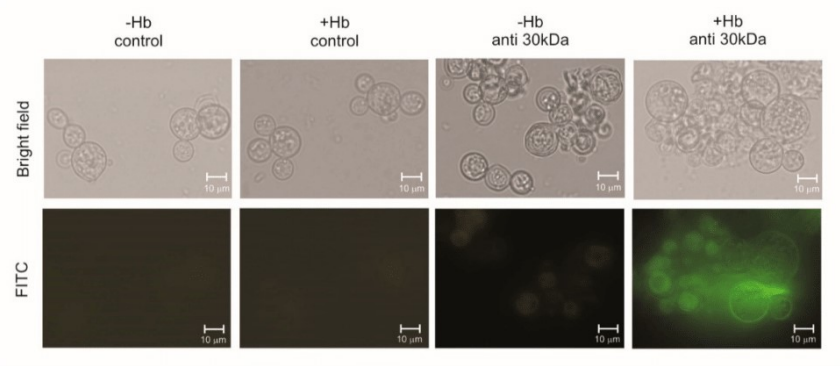

Figure 3. Analysis of hemoglobin influence on HSP30 protein expression at the cell surface of *P. lutzii*. Yeast cells were grown in the presence or absence of hemoglobin. Methanol fixed, non-permeabilized cells were incubated with anti-HSP30 antibodies or with pre immune serum for control. The pictures were taken in bright field and at 450/490 nm of fluorescein isothiocyanate (FITC) probe. All representative pictures were taken using an Axioscope microscope (Carl Zeiss AG, Berlin, Germany) and magnified 400×.

3.3. HSP30 Binds to Hemoglobin at the Fungus Cell Wall by Hydrogen Bonds

As previously shown, HSP30 expression increased when *P. lutzii* cells were grown in the presence of hemoglobin. This finding led us to question whether these proteins interact directly. Hence, we performed analyzes of molecular dynamics. At first, the simulation performed on the complex formed by HSP30 and hemoglobin showed that the evolution of the system achieved a better conformation and provided insight into the molecular motion of the complex on an atomic scale. Before molecular dynamics, the system presented 85 unfavored rotamers and after the simulation, this number reduced 83%. Similarly, the number of favored rotamers before and after the simulation was improved by 200% (Supplementary Table S3).

Molecular dynamics allowed the trajectories of atoms and bonds in the HSP30-hemoglobin complex to be determined numerically through Newton's equations of motion. The forces between the proteins and their potential energies were calculated based on interatomic potentials and force field (AMBER). We determined 103 poor quality bonds within the complex before the simulation and this number fell to zero after the molecular dynamics, showing the best quality of the resultant complex conformation. In addition, there were 11 twisted peptides identified in the complex before the simulation and five after the simulation.

Ramachandran plots were used to analyze energetically allowed regions for backbone angles and amino acid residues in the complex structure. The number of amino acid residues in energetically favored regions increased from 82.7% to 90.4% after the molecular dynamics; regarding allowed regions, the number of residues increased from 95.8% to 98.8% (Supplementary Figure S3). This indicates a stereochemical improvement of the three-dimensional model of the complex.

The quality of the complex formed by the interaction between HSP30 and hemoglobin was assessed by RMSD and cluster analysis after the molecular dynamics simulation. The analyses of the trajectories allowed identifying the equilibration period, the quality of the simulation and the clusters with similar conformations. The simulations became more stable for RMSD at a value of 0.5 nm regarding the complex formed by the interaction between HSP30 and hemoglobin (Supplementary Figure S4A, red line). Analyzed individually, the simulation of hemoglobin achieved stability around and RMSD value

of 0.6 nm (Supplementary Figure S4A, green line) and HSP30 achieved stability around 1.2 nm (Supplementary Figure S4A, black line). These results show that the conformational stability of the complex is higher compared to the structures of the proteins when they are not interacting. According to the trajectories of the simulations, we identified 18 conformational clusters. Cluster analysis showed that the complex conformation of the first three clusters are more stable. In addition, the first cluster remained stable for a longer period than the other clusters, persisting throughout the simulation of the trajectory (Supplementary Figure S4B).

We predicted the interaction between HSP30 and hemoglobin in silico. The interface of interaction between the proteins is large (Figure 4) and maintained by several amino acid residues that interact via hydrogen and polar bonds. Figure 4A shows the surface of the complex and the interaction interface between HSP30 and hemoglobin. Figure 4B shows the cartoon view of the complex and the secondary structures of each protein involved in the interaction. The most important residues that contribute to the free energy of the complex are highlighted in Figure 4 and they interact through hydrogen bonds ranging from 1.5 to 2.8 Å. Asparagine (N80) of hemoglobin interacts with glutamic acid (E232) of HSP30 via a 2.5 Å hydrogen bond (Figure 4C). Arginine (R199) of hemoglobin interacts with phenylalanine (F45) of HSP30 distant 2.4 Å (Figure 4D). The residue F46 of hemoglobin performs two hydrogen bonds with tyrosine (Y222) and E230 of HSP30, distant 2.8 and 2.4 Å, respectively. In addition, the amino acid residue E230 interacts with another residue from hemoglobin, R40, through a hydrogen bond of 1.8 Å (Figure 4E). Finally, H2 (histidine) and Y545 of hemoglobin interacts with V338 and S339, via hydrogen bonds distant 2.5 and 1.7 Å, respectively (Figure 4F). Additionally, we investigated if the interaction of these two molecules would occur in vitro. Through far-western analysis, we demonstrate that HSP30 can bind to hemoglobin, reinforcing the role of this molecule as a potential adhesin, according to the in silico analysis (Figure 4G).

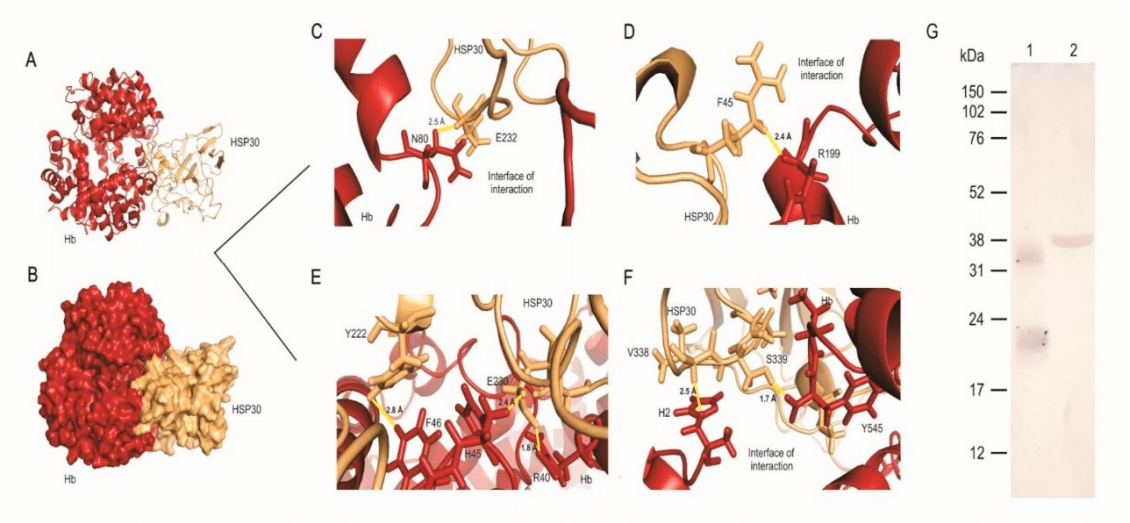

Figure 4. HSP30 is a hemoglobin-binding protein. (**A**) Cartoon view of the interaction showing the secondary structures of both proteins and the secondary structures that maintain the interface of interaction stable. (**B**) Surface view of the complex formed by HSP30 (beige) and hemoglobin (red). The interaction is maintained by a large interface of interaction between the proteins under study and by several amino acids within the interface of interaction. (**C**) Asparagine (N80) interacting with glutamic acid (E232) by a 2.5 Å hydrogen bond. (**D**) Arginine (R199) interacting with phenylalanine (F45) by a 2.4 Å hydrogen bond. (**E**) F46 interacts with tyrosine (Y222) and E230 through two hydrogen bonds, distant 2.8 and 2.4 Å, respectively. E230 also interacts with R40, distant 1.8 Å. (**F**) H2 (histidine) and Y545 interacts with V338 and S339, via hydrogen bonds distant 2.5 and 1.7 Å, respectively. (**G**) Far western analysis showing hemoglobin binding to PbHSP30. 1—Bovine hemoglobin recognition by anti-human hemoglobin monoclonal antibody. 2—Binding of hemoglobin to recombinant HSP30.

3.4. Knockdown of HSP30 Promotes Decreased Cell Growth Post Cultivation in Medium Containing Hemoglobin as Sole Iron Source

To generate *AsHSP30 P. brasiliensis* yeast cells, we used the ATMT methodology. The yeast cells of the *P. brasiliensis* wild type strain were transformed with T-DNA containing *AsHSP30* (Figure 5A). The silenced strain grown in BHI medium showed similar growth and viability levels to the wild type (Figure 5B). However when in the presence of hemoglobin the HSP30 silenced strain showed a decrease in mRNA levels, compared to the wild strain (Figure 5C). In addition, in order to evaluate if the silenced strain presented any defect in the ability to use hemoglobin, we deprived such cells of iron, exposed them to hemoglobin, and evaluated their growth by colony forming units (CFU) counting in BHI medium. The silenced strain had a lower number of CFU when compared to the wild type (Figure 5D). This finding reiterates the role of HSP30 in the use of hemoglobin by *Paracoccidioides*.

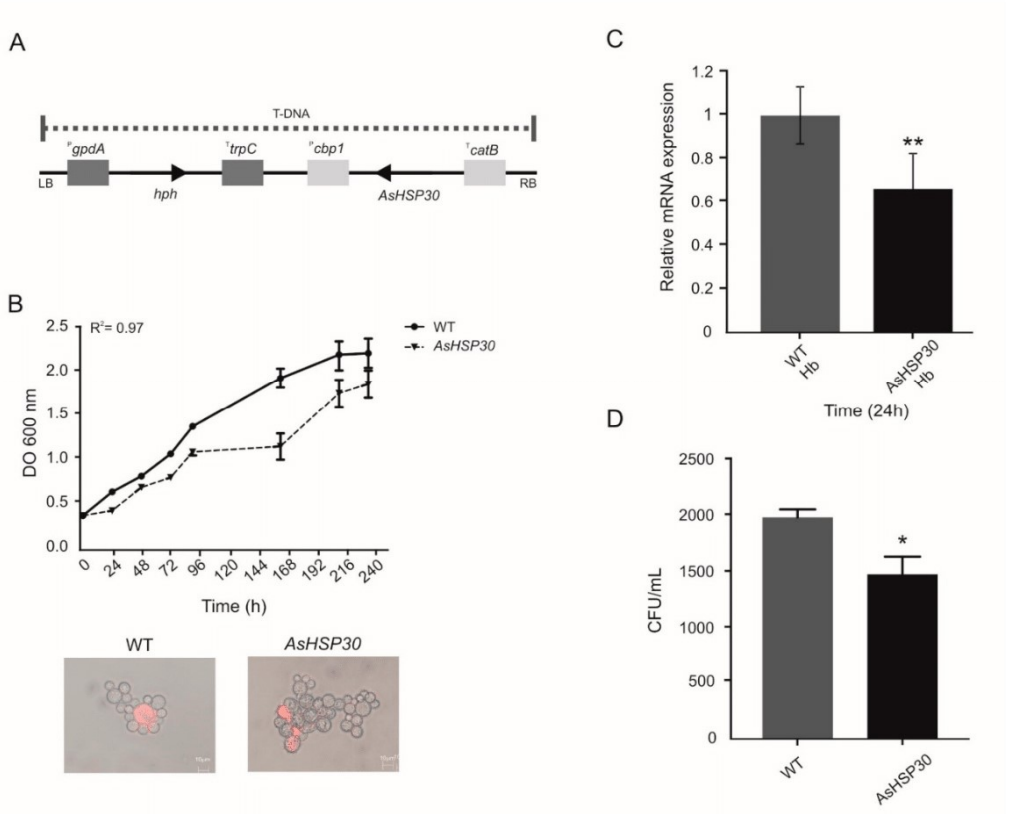

Figure 5. *HSP30* silencing in *P. brasiliensis* cells. (**A**) Integration DNA cassette scheme. The asRNA of *Pb*HSP30 was flanked by the calcium-binding protein promoter region (^{P}*cbp1*) of *Histoplasma capsulatum* and by the cat-B termination region (^{T}*catB*) of *Aspergillus fumigatus*. The hygromycin resistance gene used as a selection mark was flanked by the glyceraldehyde-3-phosphate dehydrogenase promoter region (^{P}*gapdA*) and the trpC termination region (^{T}*trpC*) of *Aspergillus nidulans*. (**B**) Growth and viability of *P. brasiliensis* strains. Yeast cells of WT and AsHSP30 were grown in liquid Brain Heart Infusion (BHI) medium for 10 days and the OD was measured daily at 600 nm. Cellular viability was examined by propidium iodide staining. (**C**) Transcriptional analysis of WT and AsHSP30 strain in the presence of hemoglobin. The strains were grown in liquid BHI medium for 72 h and subsequently in MMcM medium containing hemoglobin. The relative mRNA expression was evaluated at 24 h. (**D**) Number of WT and AsHSP30 CFUs recovered after growth in the presence of hemoglobin. After culturing in the presence of hemoglobin, WT and AsHSP30 cells were plated in solid BHI medium and the colony forming units were counted after 7 days. GraphPad Prism software (GraphPad Software, Inc., La Jolla, CA, USA) was used for statistical analysis and Student's t-test was applied considering p values ≤ 0.05 statistically significant. (*, **) denotes statistically significant differences.

4. Discussion

The host–pathogen interaction is remarkably complex and molecular mechanisms on both sides promote a real competition for survival. The host's nutritional immunity and the mechanisms that pathogens use to overcome it, occupy a prominent place in this context, as demonstrated for several pathogenic bacteria and fungi [5,7]. Previous works by our group have shown that fungi of the *Paracoccidioides* genus employ different strategies to counteract iron limitation, such as the remodeling of the metabolism prioritizing non-iron dependent pathways for energy production, biosynthesis, secretion and uptake of siderophores and the reductive pathway of iron assimilation [24–26,48].

Paracoccidioides spp. are also able to explore host proteins as iron sources, such as ferritin, transferrin, lactoferrin, and hemoglobin. However, hemoglobin available in the culture medium promotes the most robust growth of the fungus, compared to other host Fe proteins. This finding associated with the fact that *Paracoccidioides* spp. presents hemolytic potential and may have contact with hemoglobin/heme by hematogenous dissemination or when phagocytosed, inside macrophages, points to the fungal preference for hemoglobin/heme as an iron source [27,52,53]. In addition, the uptake of hemoglobin depends on a receptor-mediated mechanism, in a process similar to that described for *C. albicans* [11,27]. At the cytoplasmic proteomic level, fungal exposure to hemoglobin promotes the upregulation of enzymes related to the metabolism of amino acids, nitrogen, and sulfur and the downregulation of enzymes related to biosynthesis of porphyrin. This demonstrates that the fungus uses the molecule of hemoglobin not only as an iron source, but also as a source of nitrogen, sulfur and porphyrins [27]. Despite all of these findings, the changes on the surface of fungal cells triggered by the presence of hemoglobin had not been investigated yet.

The cell wall of *Paracoccidioides* spp. is the interface of contact between pathogen and the host. Therefore, the elucidation of the cell wall proteome is relevant for the identification of targets that are essential for the infectious process, which is preferably done under conditions that mimic the environment faced by the pathogen within the host. As an example, the study of the cell wall proteome of *C. albicans* after submission of the fungus to iron deprivation allowed the identification of several proteins related to Fe uptake from host sources, including the hemoglobin-receptors Rbt5 and Pga7, highlighting the importance of this type of approach [54]. Given the complexity of the heme/hemoglobin uptake event by *Paracoccidioides* spp., the objective of this study was to perform proteomic analyses of the pathogen's cell wall, after treatment with hemoglobin and using Fe deprivation as control, in order to investigate other proteins, besides *Pb*Rbt5 that could contribute to this process.

Several proteins identified in the cell wall of *P. lutzii* are related to processes classically characterized at the cytoplasmic level (Table 1, Supplementary Table S1), such as ribosomal proteins, enolase, involved in glycolysis, as well histones related to DNA processing and nucleosome structure, among others. Although intriguing, our results are in accordance with findings in the literature. Approaches of the cell wall proteomes of *P. brasiliensis* and *C. albicans* also evidenced the presence of classic cytoplasmic proteins in the cell wall [28,55,56]. Some authors argue that the presence of these proteins in the cell wall could be due to the methodology used to obtain the protein extracts. Others argue that the occurrence of these proteins is due to the fact that they are bi or multifunctional (moonlighting) proteins, with different functions depending on the subcellular location there are expressed [57,58]. The process used in the present work to obtain cell wall proteins was based on extensive washes of the extracts with decreasing concentrations of NaCl solutions, in order to remove cytoplasmic contaminants associated to the cell wall by non-specific interactions [28,36].

In addition to the possible absence of cytoplasmic contaminants, the identified proteins were submitted to the analysis of prediction of secretion (by classical and/or non-classical route), which corroborated the proteins identified at the cell surface. Moreover, 39.8% of the proteins were predicted to be secreted via classical and/or non-classical pathways and they were grouped mainly as secreted by non-classical pathways (those that are independent of

a signal peptide in the N-terminal portion of the protein), which are not fully understood yet. Several proteins might be secreted by mechanisms that still demand elucidation and consequently are not yet included in the search algorithms of the tools applied here [57,59].

Regarding the use of heme/hemoglobin by *P. lutzii*, *Pb*Rbt5 and other proteins related to iron uptake was not identified by the present proteomic approach [27]. This is due to the fact that Rbt5 is a receptor present in the cell wall retained by a remnant of GPI. To obtain cell wall samples enriched with anchored GPI proteins, other strategies are employed, such as treatment with hydrofluoric acid-pyridine [36]. Despite the absence of *Pb*Rbt5, other up-regulated proteins were predicted as potential adhesins (Table 1). The elongation factor-Tu (EF-Tu) was up-regulated (Table 1). Although it was not identified as an adhesin by the bioinformatics tools applied here, this protein was characterized as an adhesin in a previous work, contributing to the host–pathogen interaction [60]. Recent work performed by our group identified *P. lutzii* surface proteins that interact with macrophages [34]. We found that 25 out of 33 up-regulated proteins predicted to be secreted, were also identified as surface proteins interacting with macrophages by Tomazett et al. (2019) [34]. The upregulation of adhesins allows the inference that the pathogen treatment with hemoglobin mimics conditions found in the host. Thus, the fungus increases the expression of adhesins to improve interaction with the host and establish the infection [61]. We performed flow cytometry to confirm the increase in the adhesion capacity of *P. lutzii* in the presence of hemoglobin (Figure 2), which reiterates the importance of the hemoglobin molecule to the fungus.

We identified a differentially expressed HSP30 protein when the fungus is exposed to hemoglobin (Table 1 and Figure 1A). The HSP30's orthologue in *P. brasiliensis* also presented positive regulation at the transcriptional level when the fungus was grown in the presence of hemoglobin (Figure 1B). Immunofluorescence analysis corroborated these findings, a strong fluorescence and recognition of HSP30 by polyclonal antibodies was observed at the cell surface of *P. lutzii* cells in the presence of hemoglobin (Figure 3). Interestingly, heme oxygenase proteins belong to the HSP30 family [62–65], a fact that deserves attention due to the cultivation condition employed in the present study. To investigate whether HSP30 is a heme oxygenase, we performed sequence and structural alignments with human heme oxygenase 1 (Supplementary Figure S5). We found a level of similarity between these molecules, which suggests conserved functions. Despite a promising result, this in silico analysis require experimental validation.

We employed molecular dynamics analysis to determine the best conformation of interaction between HSP30 and hemoglobin. The pattern of interactions performed by heme-bound proteins influences several biological processes, such as signaling pathways and diseases. Several of those interactions have been identified over the past decades but their molecular basis and their consequences to infectious diseases such as PCM are poorly understood. In addition, the heme-regulatory motif is found within the structure of several proteins that interact with hemoglobin [66]. This motif contains a heme-coordination site and is placed on the surface of the protein facilitating its interaction with its partner [67]. The binding of heme groups to such motifs is able to change protein stability leading to a catalytically active heme-protein-protein complex. The histidine (H) and tyrosine (Y)-based motifs are the most prominent representatives for the interaction of heme-proteins [67,68]. Here, we found the residues Y222 interacting with F46 (phenylalanine), H45 with E230 (glutamic acid) and Y545 interacting with S339 (serine) (Figure 4E,F). Additionally, confirming the in silico findings, we showed that hemoglobin physically binds to the recombinant HSP30 by far-western (Figure 4G).

We investigated the importance of HSP30 in the context of hemoglobin utilization by *Paracoccidioides* spp. at the genetic level. The genetic manipulation of the *Paracoccidioides* genus is based on antisense RNA technology coupled with an ATMT [69]. This technology relies on targeted down-regulation of gene expression and allowed to point the relevance of the Rho-like GTPase PbCDC42 as a virulence determinant [70], to map SCONC (negative regulator of the inorganic sulfur assimilation pathway) of the sulfur metabolism [71] and

the involvement of cytochrome c peroxidase to *P. brasiliensis* virulence [47] among others. In addition, this knock-down system evidenced the involvement of Rbt5 in the hemoglobin utilization by *Paracoccidioides* spp. [27] and the role of the biosynthesis of siderophores for the fungus virulence [48]. Although relatively recent, this technology has been of the current method of choice to manipulate *Paracoccidioides* spp. genetically [72–78].

Based on this methodology, we silenced *HSP30* in *P. brasiliensis* yeast cells. Under usual cultivation conditions, the silenced strain showed similar growth behavior and viability to the WT (Figure 5B). However, there was a 40% reduction in the transcriptional level of HSP30 in the silenced strain in the presence of hemoglobin, confirming the silencing event (Figure 5C). We observed that the AsHSP30 strain generated about 25% less CFU compared to WT in the presence of hemoglobin, a statistically significant value ($p \leq 0.05$). This result highlights the importance of HSP30 in the context of hemoglobin utilization by *Paracoccidioides* spp.

Despite all of these findings, some questions still demand elucidation: is the interaction between hemoglobin and HSP30 transient? If HSP30 is a heme oxygenase, is the interaction of HSP30 with hemoglobin just one part of the iron uptake system? Noteworthy, the degradation of heme-by-heme oxygenases leads to the production of iron, biliverdin, and carbon monoxide in a reaction dependent on NADPH: cytochrome *p*-450 reductase. [79]. Does the iron released from hemoglobin by the action of HSP30 feed the fungal reductive iron uptake pathway or is captured by siderophores? Could HSP30 also have a cytoprotective function, as demonstrated for human heme oxygenase [80]? Interestingly, the heme group presents toxic potential because it is able to produce reactive oxygen species [81]. Cytochrome c peroxidase is related to the defense against oxidative stress [82] and was one of the up-regulated proteins identified in the proteome in the presence of hemoglobin. Considering the toxic potential of the heme group, the upregulation of cytochrome c peroxidase and the possibility of HSP30 being a heme oxygenase, led us to infer that *Paracoccidioides* spp. employs mechanisms to counteract the toxicity caused by the heme group and thus enable the use of the molecule as a source of iron.

Additionally, if HSP30 acts as heme oxygenase, does its function dependent on an ancillary protein, and what protein would that be? Considering the production of carbon monoxide, could the HSP30 promote immunomodulatory effects as described for the *C. albicans* heme oxygenase [83]? It is notable that the present work opens perspectives for promising future investigations. Our results demonstrated that upregulation of potential adhesins occurs at the cell surface when the fungus is exposed to hemoglobin, which was confirmed by flow cytometry. We also confirmed the increased ability of the fungus to interact with macrophages. In addition, HSP30 of *Paracoccidioides* spp. is a novel hemoglobin-binding protein, silencing this gene decreases the ability of *P. brasiliensis* to use hemoglobin as a nutrient source. Henceforth, additional studies are needed to establish HSP30 as a virulence factor, which could support the development of new therapeutic and/or diagnostic approaches to PCM.

Supplementary Materials: The following are available online at https://www.mdpi.com/2309-608X/7/1/21/s1, Table S1: Oligonucleotide sequences for RT-qPCR used in the present study. Figure S1: Quality analysis of the obtained proteome. Table S2: Up-regulated proteins identified in Fraction 1 (F1) of the cell wall, extracted by treatment with SDS after Paracoccidioides lutzii yeast cells exposition to hemoglobin for 48 h. Figure S2: Expression and purification of PbHSP30 and production of polyclonal antibodies. Table S3: Analysis of all-atom contacts and geometry of the HSP30-hemoglobin complex. Figure S3: Ramachandran plots evaluation. Figure S4: Molecular Dynamics assessment. Figure S5: Sequence and structural alignment of HSP30 (PAAG_00871) and heme oxygenase 1 (P09601).

Author Contributions: C.M.d.A.S., A.F.d.S., M.V.T., J.D.P. and R.A.G. conceived and designed the experiments. A.F.d.S., M.V.T., J.S.d.C., C.A.P., L.C.B., J.D.P. and R.A.G. performed the experiments. K.S.F.eS. and M.P. performed the molecular dynamics analyses. C.M.d.A.S., M.P. and F.R. contributed with reagents and materials. A.F.d.S., M.V.T., K.S.F.eS., J.S.d.C., C.A.P., R.A.G. and C.M.d.A.S. wrote the manuscript. A.F.d.S. and M.V.T. contributed equally to this work. All authors have read and agreed to the published version of the manuscript.

Funding: We thank CAPES: CNPq and FAPEG for providing fellowships to A.F.d.S, M.V.T., K.S.F.eS., J.S.d.C, C.A.P., L.C.B., J.D.P. and R.A.G., F.R. was supported by the Northern Portugal Regional Operational Programme (NORTE 2020), under the Portugal 2020 Partnership Agreement, through the European Regional Development Fund (FEDER) (NORTE-01-0145-FEDER-000013). C.M.d.A.S. and M.P. belong to the Conselho Nacional de Desenvolvimento Científico e Tecnológico (CNPq). This work was supported by grants from Conselho Nacional de Desenvolvimento Científico e Tecnológico (CNPq) and Fundação de Amparo à Pesquisa do Estado de Goiás (FAPEG), Instituto Nacional de Ciência e Tecnologia (INCT) de Estratégias de Interação Patógeno-Hospedeiro (grant number 201810267000022/INCT-FAPEG).

Institutional Review Board Statement: We added this information in the materials and methods section. Thus, we believe that it is not necessary the Institutional Review Board Statement.

Informed Consent Statement: Not applicable.

Data Availability Statement: Not applicable.

Conflicts of Interest: The authors declare no conflict of interest. The funders had no role in the design of the study, nor in the collection, analyses, interpretation of data, in the writing of the manuscript or in the decision to publish the results.

References

1. Nairz, M.; Schroll, A.; Sonnweber, T.; Weiss, G. The struggle for iron—A metal at the host-pathogen interface. *Cell. Microbiol.* **2010**, *12*, 1691–1702. [CrossRef] [PubMed]
2. Núñez, G.; Sakamoto, K.; Soares, M.P. Innate nutritional immunity. *J. Immunol.* **2018**, *201*, 11–18. [CrossRef] [PubMed]
3. Ganz, T. Iron and infection. *Int. J. Hematol.* **2018**, *107*, 7–15. [CrossRef] [PubMed]
4. Nevitt, T. War-Fe-re: Iron at the core of fungal virulence and host immunity. *Biometals* **2011**, *24*, 547–558. [CrossRef] [PubMed]
5. Bairwa, G.; Jung, W.H.; Kronstad, J.W. Iron acquisition in fungal pathogens of humans. *Metallomics* **2017**, *9*, 215–227. [CrossRef] [PubMed]
6. Bailão, E.F.L.C.; Parente, A.F.A.; Parente, J.A.; Silva-Bailão, M.G.; de Castro, K.P.; Kmetzsch, L.; Staats, C.C.; Schrank, A.; Vainstein, M.H.; Borges, C.L.; et al. Metal acquisition and homeostasis in fungi. *Curr. Fungal Infect. Rep.* **2012**, *6*, 257–266. [CrossRef]
7. Caza, M.; Kronstad, J.W. Shared and distinct mechanisms of iron acquisition by bacterial and fungal pathogens of humans. *Front. Cell. Infect. Microbiol.* **2013**, *3*, 1–23. [CrossRef]
8. Roy, U.; Kornitzer, D. Heme-iron acquisition in fungi. *Curr. Opin. Microbiol.* **2019**, *52*, 77–83. [CrossRef]
9. Weissman, Z.; Shemer, R.; Conibear, E.; Kornitzer, D. An endocytic mechanism for haemoglobin-iron acquisition in *Candida albicans*. *Mol. Microbiol.* **2008**, *69*, 201–217. [CrossRef]
10. Kuznets, G.; Vigonsky, E.; Weissman, Z.; Lalli, D.; Gildor, T.; Kauffman, S.J.; Turano, P.; Becker, J.; Lewinson, O.; Kornitzer, D. A relay network of extracellular heme-binding proteins drives *C. albicans* iron acquisition from hemoglobin. *PLoS Pathog.* **2014**, *10*, 1–15. [CrossRef]
11. Weissman, Z.; Kornitzer, D. A family of *Candida* cell surface haem-binding proteins involved in haemin and haemoglobin-iron utilization. *Mol. Microbiol.* **2004**, *53*, 1209–1220. [CrossRef] [PubMed]
12. Okamoto-Shibayama, K.; Kikuchi, Y.; Kokubu, E.; Sato, Y.; Ishihara, K. Csa2, a member of the Rbt5 protein family, is involved in the utilization of iron from human hemoglobin during *Candida albicans* hyphal growth. *FEMS Yeast Res.* **2014**, *14*, 674–677. [CrossRef] [PubMed]
13. Nasser, L.; Weissman, Z.; Pinsky, M.; Amartely, H.; Dvir, H.; Kornitzer, D. Structural basis of haem-iron acquisition by fungal pathogens. *Nat. Microbiol.* **2016**, *1*, 16156. [CrossRef] [PubMed]
14. Cadieux, B.; Lian, T.; Hu, G.; Wang, J.; Biondo, C.; Teti, G.; Liu, V.; Murphy, M.E.P.; Creagh, A.L.; Kronstad, J.W. The mannoprotein cig1 supports iron acquisition from heme and virulence in the pathogenic fungus *Cryptococcus neoformans*. *J. Infect. Dis.* **2013**, *207*, 1339–1347. [CrossRef]
15. Hu, G.; Caza, M.; Cadieux, B.; Chan, V.; Liu, V.; Kronstad, J. *Cryptococcus neoformans* requires the ESCRT protein Vps23 for iron acquisition from heme, for capsule formation, and for virulence. *Infect. Immun.* **2013**, *81*, 292–302. [CrossRef]
16. Hu, G.; Caza, M.; Cadieux, B.; Bakkeren, E.; Do, E.; Jung, W.H.; Kronstad, J.W. The endosomal sorting complex required for transport machinery influences haem uptake and capsule elaboration in *Cryptococcus neoformans*. *Mol. Microbiol.* **2015**, *96*, 973–992. [CrossRef]

17. Bairwa, G.; Caza, M.; Horianopoulos, L.; Hu, G.; Kronstad, J. Role of clathrin-mediated endocytosis in the use of heme and hemoglobin by the fungal pathogen *Cryptococcus neoformans*. *Cell. Microbiol.* **2019**, *21*, 1–42. [CrossRef]
18. Rappleye, C.A.; Goldman, W.E. Defining virulence genes in the dimorphic fungi. *Annu. Rev. Microbiol.* **2006**, *60*, 281–303. [CrossRef]
19. Brummer, E.; Castaneda, E.; Restrepo, A. Paracoccidioidomycosis: An update. *Clin. Microbiol. Rev.* **1993**, *6*, 89–117. [CrossRef]
20. San-blas, G.; Niño-Vega, G.; Iturriaga, T. *Paracoccidioides brasiliensis* and paracoccidioidomycosis: Molecular approaches to morphogenesis, diagnosis, epidemiology, taxonomy and genetics. *Med. Mycol.* **2002**, *40*, 225–242. [CrossRef]
21. Teixeira, M.M.; Theodoro, R.C.; de Carvalho, M.J.A.; Fernandes, L.; Paes, H.C.; Hahn, R.C.; Mendoza, L.; Bagagli, E.; San-Blas, G.; Felipe, M.S.S. Phylogenetic analysis reveals a high level of speciation in the *Paracoccidioides* genus. *Mol. Phylogenet. Evol.* **2009**, *52*, 273–283. [CrossRef] [PubMed]
22. Turissini, D.A.; Gomez, O.M.; Teixeira, M.M.; Mcewen, J.G.; Matute, D.R. Species boundaries in the human pathogen *Paracoccidioides*. *Fungal Genet. Biol.* **2017**, *106*, 9–25. [CrossRef] [PubMed]
23. Restrepo, A.; McEwen, J.G.; Castañeda, E. The habitat of *Paracoccidioides brasiliensis*: How far from solving the riddle? *Med. Mycol.* **2001**, *39*, 233–241. [CrossRef] [PubMed]
24. Parente, A.F.A.; Bailão, A.M.; Borges, C.L.; Parente, J.A.; Magalhães, A.D.; Ricart, C.A.O.; Soares, C.M.A. Proteomic analysis reveals that iron availability alters the metabolic status of the pathogenic fungus *Paracoccidioides brasiliensis*. *PLoS ONE* **2011**, *6*. [CrossRef] [PubMed]
25. Silva-Bailão, M.G.; Bailão, E.F.L.C.; Lechner, B.E.; Gauthier, G.M.; Lindner, H.; Bailão, A.M.; Haas, H.; de Almeida Soares, C.M. Hydroxamate production as a high affinity iron acquisition mechanism in *Paracoccidioides* spp. *PLoS ONE* **2014**, *9*, 1–14. [CrossRef] [PubMed]
26. Bailão, E.F.L.C.; de Sousa Lima, P.; Silva-Bailão, M.G.; Bailão, A.M.; da Rocha Fernandes, G.; Kosman, D.J.; de Almeida Soares, C.M. *Paracoccidioides* spp. ferrous and ferric iron assimilation pathways. *Front. Microbiol.* **2015**, *6*, 1–12. [CrossRef]
27. Bailão, E.F.L.C.; Parente, J.A.; Pigosso, L.L.; de Castro, K.P.; Fonseca, F.L.; Silva-Bailão, M.G.; Báo, S.N.; Bailão, A.M.; Rodrigues, M.L.; Hernandez, O.; et al. Hemoglobin uptake by *Paracoccidioides* spp. is receptor-mediated. *PLoS Negl. Trop. Dis.* **2014**, *8*, 1–20. [CrossRef]
28. Araújo, D.S.; de Sousa Lima, P.; Baeza, L.C.; Parente, A.F.A.; Bailão, A.B.; Borges, C.L.; de Almeida Soares, C.M. Employing proteomic analysis to compare *Paracoccidioides lutzii* yeast and mycelium cell wall proteins. *BBA Proteins Proteom.* **2017**, *1865*, 1304–1314. [CrossRef]
29. Borges, C.L.; Pereira, M.; Felipe, M.S.S.; de Faria, F.P.; Gomez, F.J.; Deepe, G.S.; Soares, C.M.A. The antigenic and catalytically active formamidase of *Paracoccidioides brasiliensis*: Protein characterization, cDNA and gene cloning, heterologous expression and functional analysis of the recombinant protein. *Microbes Infect.* **2005**, *7*, 66–77. [CrossRef]
30. Pereira, L.A.; Báo, S.N.; Barbosa, M.S.; da Silva, M.J.L.; Felipe, M.S.S.; Santana, J.M.; Mendes-Giannini, M.J.S.; de Almeida Soares, C.M. Analysis of the *Paracoccidioides brasiliensis* triosephosphate isomerase suggests the potential for adhesin function. *FEMS Yeast Res.* **2007**, *7*, 1381–1388. [CrossRef]
31. Nogueira, S.V.; Fonseca, F.L.; Rodrigues, M.L.; Mundodi, V.; Abi-Chacra, E.A.; Winters, M.S.; Alderete, J.F.; de Almeida Soares, C.M. *Paracoccidioides brasiliensis* enolase is a surface protein that binds plasminogen and mediates interaction of yeast forms with host cells. *Infect. Immun.* **2010**, *78*, 4040–4050. [CrossRef] [PubMed]
32. Bailão, A.M.; Nogueira, S.V.; Bonfim, S.M.R.C.; de Castro, K.P.; da Silva, J.D.F.; Mendes Giannini, M.J.S.; Pereira, M.; de Almeida Soares, C.M. Comparative transcriptome analysis of *Paracoccidioides brasiliensis* during in vitro adhesion to type I collagen and fibronectin: Identification of potential adhesins. *Res. Microbiol.* **2012**, *163*, 182–191. [CrossRef] [PubMed]
33. De Sousa Lima, P.; Bailão, E.F.L.C.; Silva, M.G.; Castro, N.D.S.; Báo, S.N.; Orlandi, I.; Vai, M.; de Almeida Soares, C.M. Characterization of the *Paracoccidioides* beta-1,3-glucanosyltransferase family. *FEMS Yeast Res.* **2012**, *12*, 685–702. [CrossRef] [PubMed]
34. Tomazett, M.V.; Baeza, L.C.; Paccez, J.D.; Parente-Rocha, J.A.; Ribeiro-Dias, F.; de Almeida Soares, C.M. Identification and characterization of *Paracoccidioides lutzii* proteins interacting with macrophages. *Microbes Infect.* **2019**, 1–11. [CrossRef]
35. Restrepo, A.; Jiménez, B.E. Growth of *Paracoccidioides brasiliensis* yeast phase in a chemically defined culture medium. *J. Clin. Microbiol.* **1980**, *12*, 279–281. [CrossRef]
36. Pitarch, A.; Nombela, C.; Gil, C. Cell wall fractionation for yeast and fungal proteomics. *Methods Mol. Biol.* **2008**, *425*, 217–239. [CrossRef]
37. Geromanos, S.J.; Vissers, J.P.C.; Silva, J.C.; Dorschel, C.A.; Li, G.Z.; Gorenstein, M.V.; Bateman, R.H.; Langridge, J.I. The detection, correlation, and comparison of peptide precursor and product ions from data independent LC-MS with data dependant LC-MS/MS. *Proteomics* **2009**, *9*, 1683–1695. [CrossRef]
38. Chaves, E.A.C.; Weber, S.S.; Báo, S.N.; Pereira, L.A.; Bailão, A.B.; Borges, C.L.; de Almeida Soares, C.M. Analysis of *Paracoccidioides* secreted proteins reveals fructose 1,6-bisphosphate aldolase as a plasminogen-binding protein. *BMC Microbiol.* **2015**, *15*, 1–14. [CrossRef]
39. D'Agostino, R.B.; Chase, W.; Belanger, A. The appropriateness of some common procedures for testing the equality of two independent binomial populations. *Am. Stat.* **1988**, *42*, 198–202. [CrossRef]
40. Larkin, M.A.; Blackshields, G.; Brown, N.P.; Chenna, R.; Mcgettigan, P.A.; McWilliam, H.; Valentin, F.; Wallace, I.M.; Wilm, A.; Lopez, R.; et al. Clustal W and Clustal X version 2.0. *Bioinformatics* **2007**, *23*, 2947–2948. [CrossRef]

41. Zhang, Y.; Skolnick, J. TM-align: A protein structure alignment algorithm based on the TM-score. *Nucleic Acids Res.* **2005**, *33*, 2302–2309. [CrossRef] [PubMed]
42. Roy, A.; Kucukural, A.; Zhang, Y. I-TASSER: A unified platform for automated protein structure and function prediction. *Nat. Protoc.* **2010**, *5*, 725–738. [CrossRef] [PubMed]
43. Kozakov, D.; Hall, D.R.; Xia, B.; Porter, K.A.; Padhorny, D.; Yueh, C.; Beglov, D.; Vajda, S. The ClusPro web server for protein-protein docking. *Nat. Protoc.* **2017**, *12*, 255–278. [CrossRef] [PubMed]
44. Zhu, X.; Mitchell, J.C. KFC2: A knowledge-based hot spot prediction method based on interface solvation, atomic density, and plasticity features. *Proteins Struct. Funct. Bioinform.* **2011**, *79*, 2671–2683. [CrossRef]
45. Pronk, S.; Páll, S.; Schulz, R.; Larsson, P.; Bjelkmar, P.; Apostolov, R.; Shirts, M.R.; Smith, J.C.; Kasson, P.M.; van der Spoel, D.; et al. GROMACS 4.5: A high-throughput and highly parallel open source molecular simulation toolkit. *Bioinformatics* **2013**, *29*, 845–854. [CrossRef]
46. Eichenberger, A.P.; Allison, J.R.; Dolenc, J.; Geerke, D.P.; Horta, B.A.C.; Meier, K.; Oostenbrink, C.; Schmid, N.; Steiner, D.; Wang, D.; et al. GROMOS++ software for the analysis of biomolecular simulation trajectories. *J. Chem. Theory Comput.* **2011**, *7*, 3379–3390. [CrossRef]
47. Parente-rocha, J.A.; Flávia, A.; Parente, A.; Baeza, L.C.; Bail, M.; Taborda, C.P.; Borges, C.L.; De, C.M. Macrophage interaction with *Paracoccidioides brasiliensis* yeast cells modulates fungal metabolism and generates a response to oxidative stress. *PLoS ONE* **2015**, 1–18. [CrossRef]
48. Silva, M.G.; de Curcio, J.S.; Silva-Bailão, M.G.; Lima, R.M.; Tomazett, M.V.; de Souza, A.F.; Cruz-Leite, V.R.M.; Sbaraini, N.; Bailão, A.M.; Rodrigues, F.; et al. Molecular characterization of siderophore biosynthesis in *Paracoccidioides brasiliensis*. *IMA Fungus* **2020**, *11*, 1–14. [CrossRef]
49. Rappleye, C.A.; Engle, J.T.; Goldman, W.E. RNA interference in *Histoplasma capsulatum* demonstrates a role for α-(1,3)-glucan in virulence. *Mol. Microbiol.* **2004**, *53*, 153–165. [CrossRef]
50. De Groot, M.J.A.; Bundock, P.; Hooykaas, P.J.J.; Beijersbergen, A.G.M. *Agrobacterium tumefaciens*-mediated transformation of filamentous fungi. *Nat. Biotechnol.* **1998**, *16*, 839–842. [CrossRef]
51. Andersen, C.L.; Jensen, J.L.; Ørntoft, T.F. Normalization of real-time quantitative reverse transcription-PCR data: A model-based variance estimation approach to identify genes suited for normalization, applied to bladder and colon cancer data sets. *Cancer Res.* **2004**, *64*, 5245–5250. [CrossRef] [PubMed]
52. Dias-Melicio, L.A.; Calvi, S.A.; Peraçoli, M.T.S.; Soares, Â.M.V.D.C. Inhibitory effect of deferoxamine on *Paracoccidioides brasiliensis* survival in human monocytes: Reversal by holotransferrin not by apotransferrin. *Rev. Inst. Med. Trop. Sao Paulo* **2005**, *47*, 263–266. [CrossRef] [PubMed]
53. Dias-melicio, L.A.; Moreira, A.P.; Calvi, S.A.; Maria, A.; De Campos, V. Chloroquine inhibits *Paracoccidioides brasiliensis* survival within human monocytes by limiting the availability of intracellular iron. *Microbiol. Immunol.* **2006**, *50*, 307–314. [CrossRef] [PubMed]
54. Sorgo, A.G.; Brul, S.; de Koster, C.G.; de Koning, L.J.; Klis, F.M. Iron restriction-induced adaptations in the wall proteome of *Candida albicans*. *Microbiology* **2013**, *159*, 1673–1682. [CrossRef]
55. Pitarch, A.; Sánchez, M.; Nombela, C.; Gil, C. Sequential fractionation and two-dimensional gel analysis unravels the complexity of the dimorphic fungus *Candida albicans* cell wall proteome. *Mol. Cell. Proteom.* **2002**, *1*, 967–982. [CrossRef]
56. Longo, L.V.G.; da Cunha, J.P.C.; Sobreira, T.J.P.; Puccia, R. Proteome of cell wall-extracts from pathogenic *Paracoccidioides brasiliensis*: Comparison among morphological phases, isolates, and reported fungal extracellular vesicle proteins. *EuPA Open Proteom.* **2014**, *3*, 216–228. [CrossRef]
57. Nombela, C.; Gil, C.; Chaffin, W.L. Non-conventional protein secretion in yeast. *Trends Microbiol.* **2006**, *14*, 15–21. [CrossRef]
58. Karkowska-Kuleta, J.; Kozik, A. Cell wall proteome of pathogenic fungi. *Acta Biochim. Pol.* **2015**, *62*, 339–351. [CrossRef]
59. Bendtsen, J.D.; Jensen, L.J.; Blom, N.; von Heijne, G.; Brunak, S. Feature-based prediction of non-classical and leaderless protein secretion. *Protein Eng. Des. Sel.* **2004**, *17*, 349–356. [CrossRef]
60. Marcos, C.M.; de Oliveira, H.C.; da Silva, J.D.F.; Assato, P.A.; Yamazaki, D.S.; da Silva, R.A.M.; Santos, C.T.; Santos-Filho, N.A.; Portuondo, D.L.; Mendes-Giannini, M.J.S.; et al. Identification and characterisation of elongation factor Tu, a novel protein involved in *Paracoccidioides brasiliensis*-host interaction. *FEMS Yeast Res.* **2016**, *16*. [CrossRef]
61. Gonzalez, A.; Hernandez, O. New insights into a complex fungal pathogen: The case of *Paracoccidioides* spp. *Yeast* **2016**, *33*, 113–128. [CrossRef] [PubMed]
62. Ewing, J.F.; Maines, M.D. Histochemical localization of heme oxygenase-2 protein and mRNA expression in rat brain. *Brain Res. Protoc.* **1997**, *1*, 165–174. [CrossRef]
63. Bidmon, H.J.; Emde, B.; Oermann, E.; Kubitz, R.; Witte, O.W.; Zilles, K. Heme oxygenase-1 (HSP-32) and heme oxygenase-2 induction in neurons and glial cells of cerebral regions and its relation to iron accumulation after focal cortical photothrombosis. *Exp. Neurol.* **2001**, *168*, 1–22. [CrossRef] [PubMed]
64. Maines, M.D.; Trakshel, G.M.; Kutty, R.K. Characterization of two constitutive forms of rat liver microsomal heme oxygenase. *J. Biol. Chem.* **1986**, *261*, 411–419.
65. Maines, M.D. Heme oxygenase: Function, multiplicity, regulatory mechanisms, and clinical applications. *FASEB J.* **1988**, *2*, 2557–2568. [CrossRef]

66. Lathrop, J.T.; Timko, M.P. Regulation by heme of mitochondrial protein transport through a conserved amino acid motif. *Science* **1993**, *259*, 522–525. [CrossRef]
67. Zhang, L.; Guarente, L. Heme binds to a short sequence that serves a regulatory function in diverse proteins. *EMBO J.* **1995**, *14*, 313–320. [CrossRef]
68. Brewitz, H.H.; Goradia, N.; Schubert, E.; Galler, K.; Kühl, T.; Syllwasschy, B.; Popp, J.; Neugebauer, U.; Hagelueken, G.; Schiemann, O.; et al. Heme interacts with histidine- and tyrosine-based protein motifs and inhibits enzymatic activity of chloramphenicol acetyltransferase from *Escherichia coli*. *Biochim. Biophys. Acta Gen. Subj.* **2016**, *1860*, 1343–1353. [CrossRef]
69. Almeida, A.J.; Carmona, J.A.; Cunha, C.; Carvalho, A.; Rappleye, C.A.; Goldman, W.E.; Hooykaas, P.J.; Leão, C.; Ludovico, P.; Rodrigues, F. Towards a molecular genetic system for the pathogenic fungus *Paracoccidioides brasiliensis*. *Fungal Genet. Biol.* **2007**, *44*, 1387–1398. [CrossRef]
70. Almeida, A.J.; Cunha, C.; Carmona, J.A.; Sampaio-Marques, B.; Carvalho, A.; Malavazi, I.; Steensma, H.Y.; Johnson, D.I.; Leão, C.; Logarinho, E.; et al. Cdc42p controls yeast-cell shape and virulence of *Paracoccidioides brasiliensis*. *Fungal Genet. Biol.* **2009**, *46*, 919–926. [CrossRef]
71. Menino, J.F.; Saraiva, M.; Gomes-Rezende, J.; Sturme, M.; Pedrosa, J.; Castro, A.G.; Ludovico, P.; Goldman, G.H.; Rodrigues, F.P. *brasiliensis* Virulence is affected by SconC, the negative regulator of inorganic sulfur assimilation. *PLoS ONE* **2013**, *8*, 1–14. [CrossRef] [PubMed]
72. Torres, I.; Hernandez, O.; Tamayo, D.; Muñoz, J.F.; García, A.M.; Gómez, B.L.; Restrepo, A.; McEwen, J.G. *Paracoccidioides brasiliensis PbP27* gene: Knockdown procedures and functional characterization. *FEMS Yeast Res.* **2014**, *14*, 270–280. [CrossRef] [PubMed]
73. Torres, I.; Hernandez, O.; Tamayo, D.; Muñoz, J.F.; Leitão, N.P.; García, A.M.; Restrepo, A.; Puccia, R.; McEwen, J.G. Inhibition of PbGP43 expression may suggest that gp43 is a virulence factor in *Paracoccidioides brasiliensis*. *PLoS ONE* **2013**, *8*. [CrossRef] [PubMed]
74. Tamayo, D.; Muñoz, J.F.; Torres, I.; Almeida, A.J.; Restrepo, A.; McEwen, J.G.; Hernández, O. Involvement of the 90kDa heat shock protein during adaptation of *Paracoccidioides brasiliensis* to different environmental conditions. *Fungal Genet. Biol.* **2013**, *51*, 34–41. [CrossRef]
75. Goes, T.; Bailão, E.F.L.C.; Correa, C.R.; Bozzi, A.; Santos, L.I.; Gomes, D.A.; Soares, C.M.A.; Goes, A.M. New developments of RNAi in *Paracoccidioides brasiliensis*: Prospects for high-throughput, genome-wide, functional genomics. *PLoS Negl. Trop. Dis.* **2014**, *8*. [CrossRef]
76. Fernandes, F.F.; Oliveira, A.F.; Landgraf, T.N.; Cunha, C.; Carvalho, A.; Vendruscolo, P.E.; Gonçales, R.A.; Almeida, F.; da Silva, T.A.; Rodrigues, F.; et al. Impact of paracoccin gene silencing on *Paracoccidioides brasiliensis* virulence. *MBio* **2017**, *8*, 1–12. [CrossRef]
77. Nora, L.C.; Gonçales, R.A.; Martins-Santana, L.; Ferreira, B.H.; Rodrigues, F.; Silva-Rocha, R. Synthetic and minimalist vectors for *Agrobacterium tumefaciens*-mediated transformation of fungi. *Genet. Mol. Biol.* **2019**, *42*, 395–398. [CrossRef]
78. Oliveira, L.N.; Gonçales, R.A.; Silva, M.G.; Lima, R.M.; Tomazett, M.V.; de Curcio, J.S.; Paccez, J.D.; Cruz-Leite, V.R.M.; Rodrigues, F.; de Sousa Lima, P.; et al. Characterization of a heme-protein responsive to hypoxia in *Paracoccidioides brasiliensis*. *Fungal Genet. Biol.* **2020**, *144*, 1–11. [CrossRef]
79. Ryter, S.W.; Kvam, E.; Tyrrel, R.M. Heme oxygenase activity. In *Methods in Molecular Biology*; Humana Press: Totowa, NJ, USA, 2000; Volume 99, pp. 369–391.
80. Vile, G.F.; Basu-Modak, S.; Waltner, C.; Tyrrell, R.M. Heme oxygenase 1 mediates an adaptive response to oxidative stress in human skin fibroblasts. *Proc. Natl. Acad. Sci. USA* **1994**, *91*, 2607–2610. [CrossRef]
81. Ascenzi, P.; Bocedi, A.; Visca, P.; Altruda, F.; Tolosano, E.; Beringhelli, T.; Fasano, M. Hemoglobin and heme scavenging. *IUBMB Life* **2005**, *57*, 749–759. [CrossRef]
82. Dantas, A.S.; Andrade, R.V.; de Carvalho, M.J.; Felipe, M.S.S.; Campos, É.G. Oxidative stress response in *Paracoccidioides brasiliensis*: Assessing catalase and cytochrome c peroxidase. *Mycol. Res.* **2008**, *112*, 747–756. [CrossRef] [PubMed]
83. Navarathna, D.H.M.L.P.; Roberts, D.D. Candida albicans heme oxygenase and its product CO contribute to pathogenesis of candidemia and alter systemic chemokine and cytokine expression. *Free Radic. Biol. Med.* **2010**, *49*, 1561–1573. [CrossRef] [PubMed]

Supplementary Table 1. Oligonucleotide sequences for RT-qPCR used in the present study

Genes	Forward sequences (5′-3′)	Reverse sequence (5′-3′)
HSP30	ACTATGAAAGCCACCGCTCC	TCTGAGAATCTGTGAACTCGAT
GAPDH	CATGCGGGTGCCCACTGC	AGAATAGCCGAGAATGCCCTT

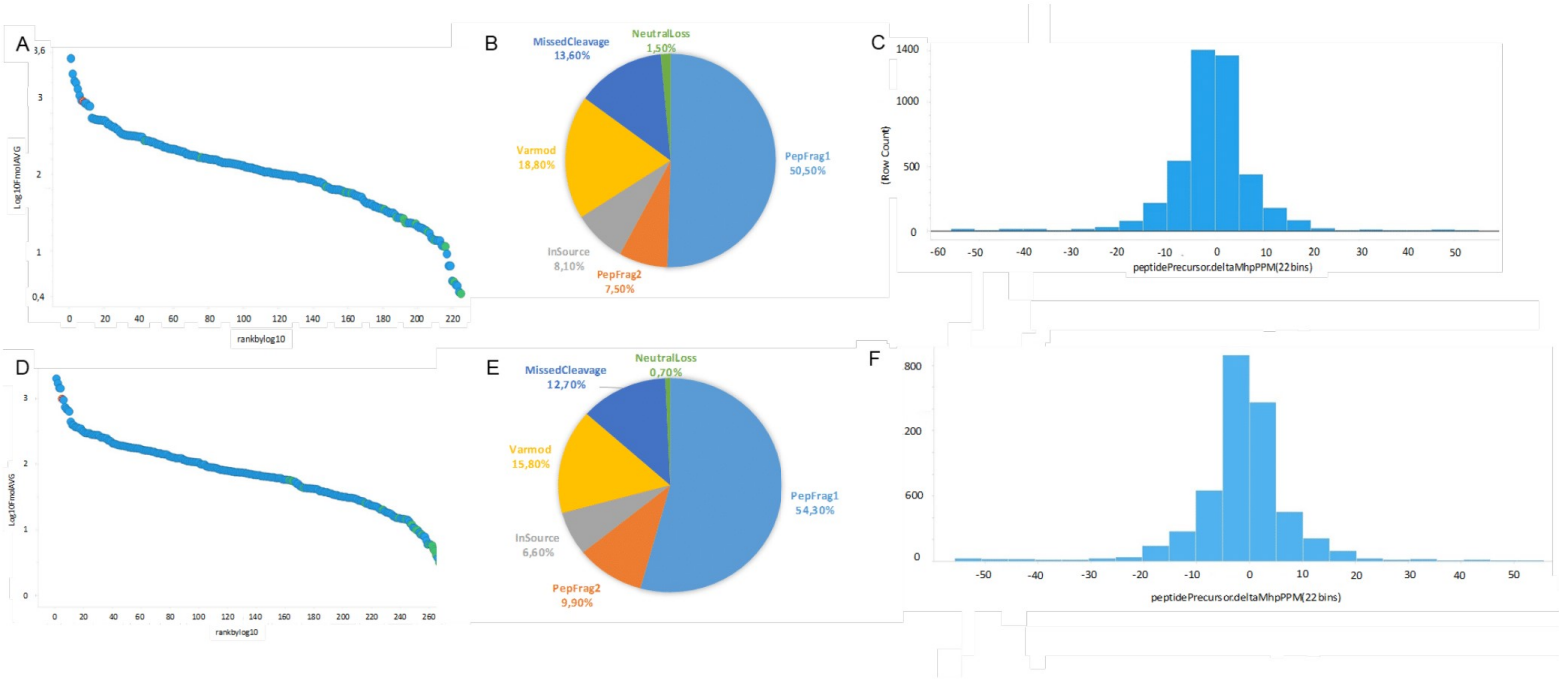

Supplementary Figure 1. Quality analysis of the obtained proteome. Quality charts of the proteomic analysis related to *P. lutzii* cell wall Fraction 1 obtained in the presence of hemoglobin (**A**) or BPS (**D**): Dynamic range of proteins detection, considering their abundance and molecular weight. Blue circle: proteins identified on a regular basis. Green circle: proteins identified in reverse. Red circle: standard (PHB). Type of peptides detection (**B**) (Hb) and (**E**) (BPS): PepFrag1 and PepFrag2: mode of identification in the *Paracoccidoides* database by PLGS. VarMod: variable modifications. InSource: fragmentation occurred at the ionization source. MissedCleavage: loss of cleavage by trypsin. NeutralLoss: loss of precursors of water, ammonia and / or phosphoric acid. Mass Accuracy (**C**) (Hb) and (**F**) (BPS): The graph shows accuracy in the detection of peptide masses, in which 61.9% of the peptides identified in haemoglobin condition and 62,2% of the peptides identified in BPS condition had a mass error of 5 ppm. Additional analysis showed false positives in 0.63% of the detected peptides from haemoglobin condition, low value that allows proteomic analysis to be performed. False positives were not identified in the BPS condition. Analysis based on (GEROMANOS et al., 2009).

Supplementary Table 2. Upregulated proteins identified in Fraction 1 (F1) of cell wall, extracted by treatment with SDS, after *Paracoccidioides lutzii* yeast cells exposition to hemoglobin for 48 hours

Accession Number[a]	**Description**[b]	**Score**[c]	**Expression levels Ratio (Hb/BPS)**[d]	**SignalP**[e]	**SecretomeP**[f]
PAAG_00435	(R)-benzylsuccinyl-CoA dehydrogenase	1048,6	1.92	-	-
PAAG_00773	14-3-3 family protein epsilon	2559,6	1.75	-	-
PAAG_00871	30 kDa heat shock protein	754,8	*	-	0.786
PAAG_01870	3-oxoacyl-[acyl-carrier protein] reductase	483,2	1.86	-	-
PAAG_02111	40S ribosomal protein S0	3130,3	1.55	-	-
PAAG_08955	40S ribosomal protein S1	672,2	1.62	-	0.720
PAAG_06367	40S ribosomal protein S11	3734,9	1.68	-	-
PAAG_08634	40S ribosomal protein S12	1542,5	1.80	-	-
PAAG_01413	40S ribosomal protein S17	1850,1	*	-	0.738
PAAG_09043	40S ribosomal protein S2	982,0	2.01	-	-
PAAG_03322	40S ribosomal protein S20	1303,5	1.63	-	0.750

PAAG_07847	40S ribosomal protein S26E	409,6	*	-	0.613
PAAG_02634	40S ribosomal protein S6-A	3851,9	1.65	-	-
PAAG_00468	4-aminobutyrate aminotransferase	977,2	1.75	-	0.601
PAAG_00724	60S ribosomal protein L11	2233,1	1.51	-	-
PAAG_00969	60S ribosomal protein L15	4374,1	1.60	-	-
PAAG_00430	60S ribosomal protein L2	360,1	1.55	-	0.853
PAAG_00952	60S ribosomal protein L20	1022,6	1.67	-	0.712
PAAG_01050	60S ribosomal protein L30	3630,4	1.67	-	-
PAAG_01178	6-phosphogluconate dehydrogenase. decarboxylating 1	1568,3	1.73	-	-
PAAG_07786	Acetyl-CoA acetyltransferase	1043,1	4.10	-	0.655
PAAG_03532	Actin	3976,5	1.70	-	-
PAAG_08620	ADP, ATP carrier protein	7031,9	1.63	-	-
PAAG_00403	Alcohol dehydrogenase 1	562,0	2.89	-	-
PAAG_05249	Aldehyde dehydrogenase	1357,1	1.86	-	-
PAAG_02603	Aspartate aminotransferase	303,7	1.92	-	-

PAAG_05117	Aspartate-tRNA(Asn) ligase	565,1	5.53	-	0.609
PAAG_04838	ATP synthase subunit 4, mitochondrial	663,4	1.51	-	0.781
PAAG_04820	ATP synthase subunit alpha, mitochondrial	1625,2	1.93	-	-
PAAG_04570	ATP synthase subunit D, mitochondrial	2347,4	1.54	-	-
PAAG_00689	ATP-dependent RNA helicase eIF4A	3109,0	1.92	-	-
PAAG_04511	ATP-dependent RNA helicase SUB2	2259,1	1.60	-	0.722
PAAG_03701	BAR domain-containing protein	844,8	2.48	-	0.614
PAAG_00731	Bifunctional purine biosynthesis protein ADE17	767,5	1.72	-	-
PAAG_05518	Cell division control protein 48	295,9	1.63	-	-
PAAG_00797	Chaperone DnaJ	1577,9	1.99	-	-
PAAG_01262	Chaperone DnaK	2982,3	1.57	0.864	-
PAAG_08075	Citrate synthase. mitochondrial	730,3	1.99	-	-
PAAG_08088	Cytochrome b-c1 complex subunit 2	603,4	1.54	-	-
PAAG_03292	Cytochrome c peroxidase, mitochondrial	3045,4	1.60	-	0.809
PAAG_06751	DNA damage checkpoint protein rad24	1203,8	2.05	-	-

PAAG_00173	Electron transfer flavoprotein subunit alpha	465,5	1.88	-	0.642
PAAG_03556	Elongation factor 1 gamma domain-containing protein	998,9	1.77	-	-
PAAG_11418	Elongation factor 1-alpha	14708,7	1.79	-	-
PAAG_00594	Elongation factor 2	3787,4	1.51	-	-
PAAG_00850	Glutamine-fructose-6-phosphate transaminase (isomerizing)	1305,8	1.65	-	0.693
PAAG_08093	GTP-binding protein ypt3	690,3	2.05	-	-
PAAG_03900	GTP-binding protein YPT52	440,3	*	-	-
PAAG_06811	Heat shock protein STI1	379,4	*	-	-
PAAG_07098	Histone H4.1	4254,4	1.62	-	-
PAAG_00126	Histone H4.2	4337,0	1.62	0.792	-
PAAG_08003	HSP72-like protein	4380,2	1.73	-	-
PAAG_07775	HSP75-like protein	472,9	2.10	-	-
PAAG_05679	HSP90-like protein	8089,5	1.68	-	-
PAAG_02130	HSP98-like protein	572,8	2.08	-	-

PAAG_00053	Malate dehydrogenase, NAD-dependent	1037,2	1.62	-	0.651
PAAG_02718	Mannose-1-phosphate guanyltransferase	427,5	2.18	-	-
PAAG_00481	Membrane biogenesis protein Yop1	922,3	1.93	-	0.902
PAAG_01861	Membrane-associated progesterone receptor component 1	443,0	*	-	0.735
PAAG_02265	Mitochondrial F1F0 ATP synthase subunit	1739,0	1.99	-	-
PAAG_12425	Mitochondrial outer membrane protein porin	1423,3	1.93	-	-
PAAG_06891	mRNA binding post-transcriptional regulator (Csx1)	1068,9	2.23	-	-
PAAG_12076	NAD(P)H:quinone oxidoreductase, type IV	1770,3	1.55	0.718	-
PAAG_00953	NADH-cytochrome b5 reductase 2	544,5	1.62	-	-
PAAG_05735	NADH-ubiquinone oxidoreductase 49 kDa subunit, mitochondrial	668,4	2.05	-	0.675
PAAG_08100	O-acetylhomoserine (thiol)-lyase	313,5	2.29	-	-
PAAG_01321	Oxidoreductase 2-nitropropane dioxygenase family	2254,9	1.79	-	0.707
PAAG_00739	Peptidyl-prolyl cis-trans isomerase B	583,7	1.65	0.641	-

PAAG_03334	Peptidyl-prolyl cis-trans isomerase D	4124,6	1.99	-	-
PAAG_01454	Peroxisomal catalase	2765,8	2.29	-	-
PAAG_08859	Peroxisomal multifunctional enzyme	460,3	1.80	-	-
PAAG_08082	Plasma membrane ATPase	738,9	1.93	-	0.712
PAAG_07957	Pre-mRNA splicing factor	539,9	2.69	-	0.801
PAAG_04458	Prohibitin-1	1883,9	1.62	-	-
PAAG_11504	Protein disulfide-isomerase domain	364,5	*	-	0.783
PAAG_00986	Protein disulfide-isomerase domain	585,2	1.90	-	-
PAAG_02050	Pyruvate decarboxylase	1078,4	1.84	-	-
PAAG_02769	Pyruvate dehydrogenase protein X component	325,5	*	-	0.685
PAAG_00417	Succinyl-CoA ligase subunit alpha	1400,3	1.88	-	0.624
PAAG_02921	Translation elongation factor Tu	990,0	1.70	-	0.773
PAAG_03031	Tubulin beta chain	1417,8	1.63	-	-
PAAG_04901	Ubiquitin-conjugating enzyme	555,9	1.79	-	0.883
PAAG_12424	Voltage-dependent anion channel protein 1	2827,7	1.54	-	0.761

[a]Protein accession number in NCBI, available at https://www.ncbi.nlm.nih.gov/protein.

[b]Description of the protein in the *Paracoccidioides* spp. databank, available in https://www.uniprot.org/uniprot/?query=paracoccidioides+lutzii&sort=score.
[c]Score that points to the quality of protein identification. Only proteins with satisfactory score values were included in the analysis.
[d]Ratio between quantification of proteins identified in hemoglobin/iron deprivation. Values ≥ 1.5 indicate upregulated proteins; (*) indicates that the protein was identified only upon hemoglobin treatment.
[e]Prediction of signal peptide presence; score must be ≥ 0.45; prediction performed by SignalP 4.1 available at http://www.cbs.dtu.dk/services/SignalP/. (-) indicates that the signal peptide was not identified.
[f]Prediction of protein secretion by non-classical pathways. whose score must be ≥ 0.6; prediction performed by SecretomeP 2.0 available at http://www.cbs.dtu.dk/services/SecretomeP/. (-) indicates that the protein was not predicted as secreted.

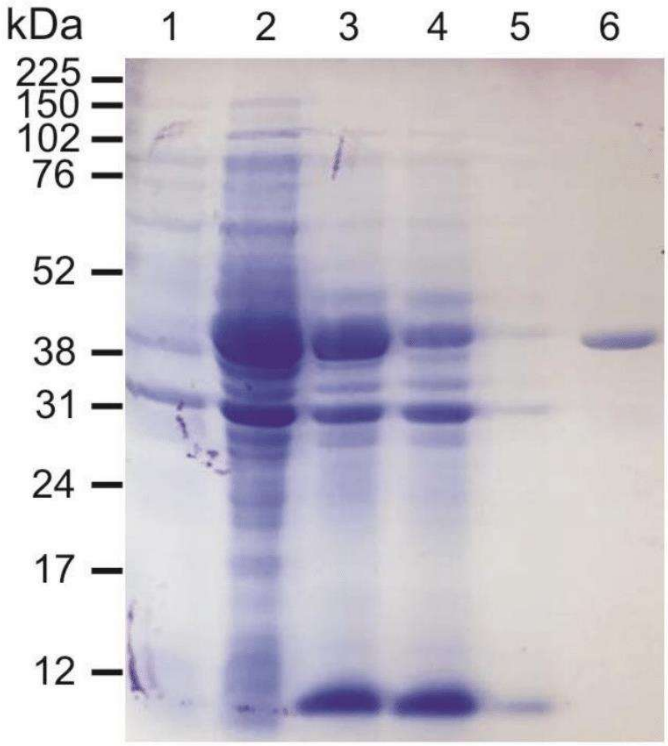

Supplementary Figure 2. Expression and purification of *Pb*HSP30. Heterologous expression of *Pb*HSP30. 1 – *E. coli* C43 bacteria harbouring the plasmid pET-32a containing the *HSP30* coding sequence without the addition of IPTG. 2 – Induction of HSP30 expression with IPTG 0.1 mM for 16 h in the bacteria *E. coli* C43 harbouring the plasmid pET-32a containing the *HSP30* coding sequence. 3 – Pellet of the protein extract from HSP30 induction after sarcosyl treatment. 4 – supernatants of the protein extract from HSP30 induction after sarcosyl treatment. 5 - nickel resin washing. 6 – purification of the HSP30 recombinant protein through nickel resin. The estimated molecular weight of the recombinant protein is 46 kDa.

Supplementary Table 3. Analysis of all-atom contacts and geometry of the HSP30-hemoglobin complex

Protein Geometry	Before DM	Percentage	After DM	Percentage
Poor rotamers	85	19.50%	14	2.13%
Favored rotamers	300	68.81%	600	91.19%
Ramachandran outliers	29	7.53%	10	1.25%
Ramachandran favored	293	76.10%	726	90.41%
Bad bonds	103	1.60%	0	0.00%
Twisted peptides	11	2.14%	5	0.62%

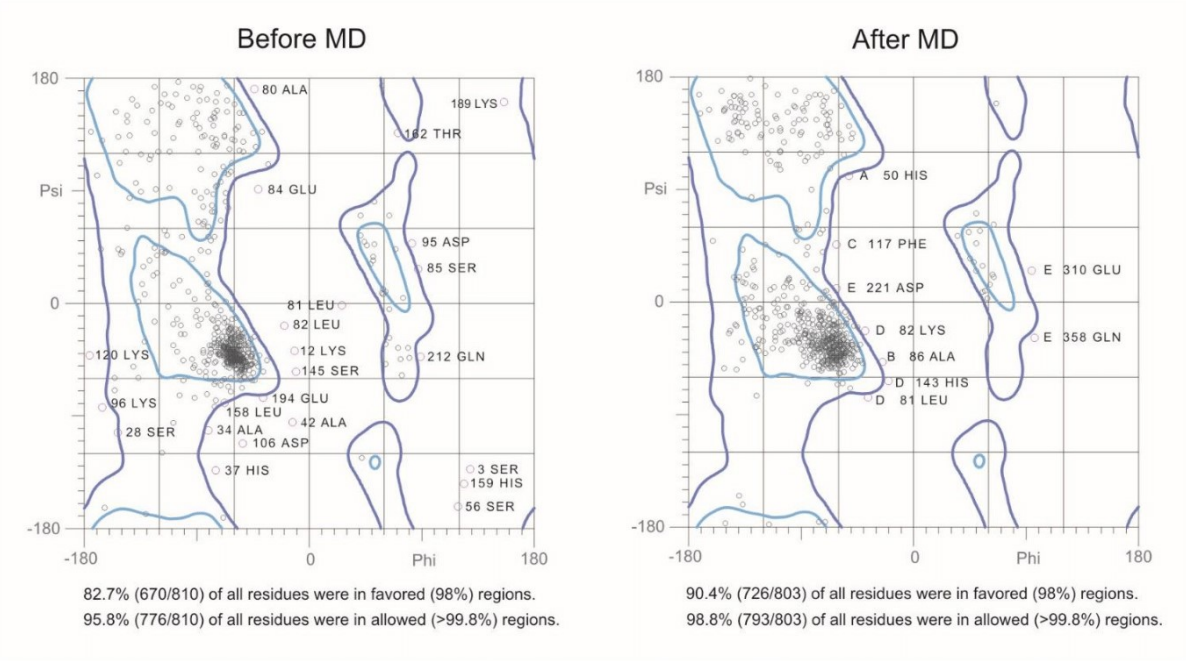

Supplementary Figure 3. Ramachandran plots evaluation. Ramachandran plots showing the analysis of residues in allowed, favored and forbidden regions (**A**) before and (**B**) after the HSP30-hemoglobin complex molecular dynamics. The light blue lines represent favorable regions, and the dark blue lines represent allowed regions. Regions outside blue lines represent forbidden regions and may characterize very flexible regions of either HSP30 or hemoglobin. The plots show that stereochemistry of the complex improved considerably after molecular dynamics.

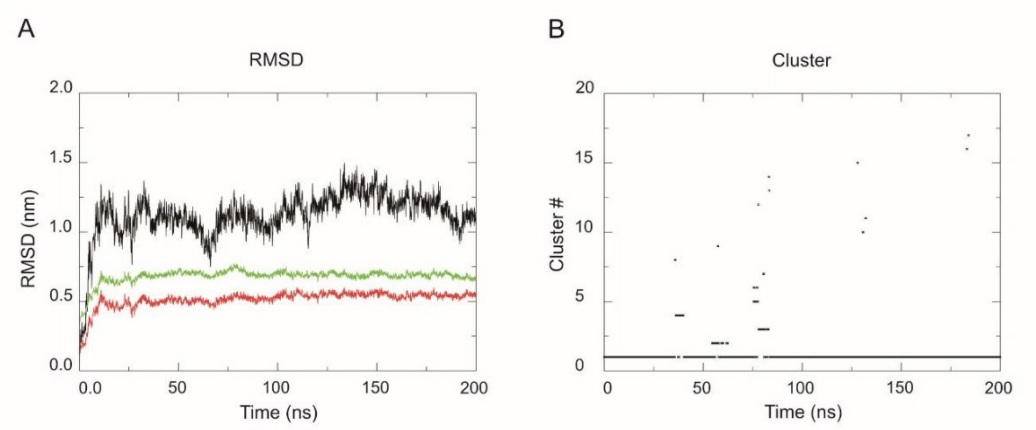

Supplementary Figure 4. Molecular Dynamics assessment. (**A**) RMSD (root mean square deviation) trajectories over 200 ns of the complex simulation. The complex formed by the interaction between HSP30 and hemoglobin achieved stability around 0.5 nm (green); hemoglobin achieved stability around 0.6 nm (red) and HSP30 conformation stabilized around 1.2 nm (black). The conformational structure of the complex is more stable than the proteins involved in the interaction taken individually. (**B**) The cluster plot shows eighteen sets of conformations along the HSP30-hemoglobin complex trajectories and the first cluster shows the most stable conformation persisting throughout the simulation.

A

```
P.lutzii HSP30          MFSRRAIRSPLKASRLPSQPTSSAYRISKFSSGAIPHIYPSATTTLSNINQARNMSFFPR
Human heme oxygenase1   MERPQPDSMPQDLSEALKEATKEVH--TQAENAEFMRNFQKGQVTRDGFKLVMASLYHIY
                        *   :.   * . *.  .:.*...:  :: ... : : : .. .* ..:: .    :.

P.lutzii HSP30          LPTGDFTPLFRLLDDYESHRSGVESSSHLGGMRTFAPRFDVREAKDAYHLDGELPGINQK
Human heme oxygenase1   VALEEEIERNKESPVFAPVYFPEELHRKAALEQDLAFWYGP-RWQEVIPYTPAMQRYVKR
                        :.  :     :    : .     *   : .  : :*  :.  . ::.      :    ::

P.lutzii HSP30          DIEIEFTDSQTLVIKGRSEREYTSSSNGEPGDKGQKKLHQPTVEDESSTSMTKTGGSSQE
Human heme oxygenase1   LHEVGRTEPELLVAH-----AYTRYLGDLSGGQVLKKIAQKALDLPSSG----EGLAFFT
                          *:  *:.: ** :      **   .. .*.:  **: * :::  **      * :

P.lutzii HSP30          VGSVREGVKYWVSERS-VGEFSRTFSFPTRVDQNAVKASLKNGILSVIIPKMSAPTSKKI
Human heme oxygenase1   FPNIASATKFKQLYRSRMNSLEMTPAVRQRVIEEAKTAFLLNIQLFEELQELLTHDTKDQ
                        . .: ...*:    ** :..:. * :.  ** ::* .* * *  *   : :: :  :*.

P.lutzii HSP30          TIE--
Human heme oxygenase1   SPSRA
                        : .
```

B

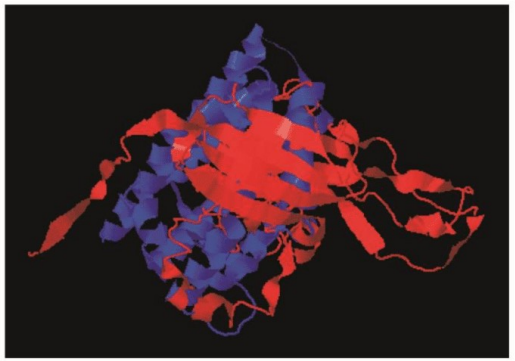

Supplementary Figure 5. Sequence and structural alignment of HSP30 (PAAG_00871) and heme oxygenase 1 (P09601). (**A**) The alignment was obtained by ClustalX 2.1 program. Asterisks (*) indicates position of complete identity, a colon (:) indicates conserved substitutions and a dot (.) indicates a semi-conserved substitution of amino acid residues. (**B**) Structural alignment was obtained by TM-align (https://zhanglab.ccmb.med.umich.edu/TM-align/). This algorithm is used to construct the best structural alignment between protein pairs according to the rotation of the alpha-carbons in amino acid residues.

Fungos do gênero *Paracoccidioides* têm sido alvo de estudos que visam elucidar a biologia do patógeno e as consequentes formas de adaptação do microrganismo a eventos estressores diversos, incluindo a privação de metais como cobre, zinco e ferro (Parente *et al.*, 2013; Parente, Ana F A *et al.*, 2011; Petito *et al.*, 2020). Especialmente em relação ao micronutriente Fe, a literatura apresenta algumas formas como o patógeno responde à privação do metal, utilizando para tanto proteínas do hospedeiro que contêm Fe, como a hemoglobina, sintetizando e captando sideróforos e utilizando um via redutiva de assimilação de Fe (Bailão *et al.*, 2014; 2015; Silva-Bailão *et al.*, 2014; Silva *et al.*, 2020). Apesar da robusta contribuição desses trabalhos, ainda há aspectos em relação ao evento *Paracoccidioides*-privação de Fe que demandam elucidação. No presente trabalho alvos de estudo que demandam investigação foram definidos e uma nova proteína ligante de hemoglobina, HSP30, foi descoberta.

A biossíntese e secreção de sideróforos, bem como a captação destas moléculas já são eventos estabelecidos na literatura de *Paracoccidioides* spp. (Silva-Bailão *et al.*, 2014; Silva *et al*, 2020). Entretanto, fungos deste gênero apresentam pelo menos três possíveis receptores de sideróforos, a saber Sit1, MirB e MirC (Silva *et al.*, 2011). Não está claro por qual motivo o fungo apresenta diferentes receptores de sideróforos se o patógeno é capaz de sintetizar apenas sideróforos do tipo hidroxamato (Silva-Bailão *et al*., 2014). O presente trabalho demonstrou que uma possibilidade é que o fungo é capaz de captar sideróforos de outras classes moleculares, como carboxilatos e catecolatos, o que foi apontado por simulações computacionais e parcialmente confirmado por RT-qPCR que Sit1 interage preferencialmente com Ferrioxamina B (FOB) (Souza *et al.*, 2020). Investigar a interação dos demais receptores com diferentes classes de sideróforos é sobremaneira relevante para entender a biologia do patógeno.

Paracoccidioides spp. é capaz de utilizar hemoglobina como fonte de Fe (bem como fonte de protoporfirina e aminoácidos) e este evento está diretamente relacionado com o receptor Rbt5, presente na parede celular fúngica (Bailão *et al.*, 2014), que contém o domínio CFEM, que em *C. albicans* foi apontado como porção do hemóforo Csa2 que interage com heme (Nasser *et al.*, 2016). Todavia, fungos do gênero *Paracoccidioides* não apresentam apenas a proteína Rbt5 com domínio CFEM. Há pelo menos quatro sequências no genoma de diferentes espécies do gênero que codificam para proteínas com esse domínio (Souza *et al.*, 2020). Estudar estas proteínas é um feito relevante, pois pode

expandir a compreensão do processo de utilização de heme/hemoglobina pelo patógeno, bem como possivelmente descobrir outras funções desempenhadas por elas.

Ainda com relação à utilização de hemoglobina por *Paracoccidioides* spp., o presente trabalho levou à bioprospecção de HSP30 como proteína que interage com hemoglobina (Souza *et al.*, 2021). Há a hipótese de que HSP30 atue como uma heme oxigenase, o que faz levantar diversas questões: A interação HSP30-Hb é transiente? HSP30 faz parte de um sistema de captação de heme/hemoglobina? HSP30 tem função citoprotetora? Será a função de HSP30 dependente de uma proteína ancilar? Se HSP30 atuar como heme oxigenase, o monóxido de carbono produzido apresenta efeitos imunomodulatórios? Todas essas são questões que demandam elucidação e abrem perspectivas para descobertas sobremaneira relevantes.

Outra questão apontada no presente trabalho é o fato de que expor *Paracoccidioides* spp. à presença de hemoglobina promove aumento da capacidade de adesão do fungo a macrófagos (Souza *et al.*, 2021). Isso aponta para mudanças qualitativas e quatitativas do proteoma em nível de parede celular do patógeno e levanta importantes questionamentos sobre a capacidade de adaptação do fungo.

O presente trabalho também destacou proteínas presentes no exoproteoma de *P. brasiliensis* que são reguladas positivamente quando o fungo é submetido à privação de Fe. Uma questão pungente fica em aberto: proteínas como Citocromo b5, altamente regulada na condição de privação do metal, atuam na resposta do fungo ao ambiente escasso do metal? Abordagens metodológicas que conduzam a essa resposta devem ser empregadas de forma a permitir elucidar o processo.

Não obstante, o presente trabalho abre perspectivas para investigações bastante significativas e que certamente irão contribuir para a compreensão de como *Paracoccidioides* spp. responde à privação de Fe. Tal conhecimento, apesar de básico, pode servir como cerne para o desenvolvimento de aplicações em diagnóstico diferencial e terapia da PCM.

O presente trabalho permitiu que novos alvos de estudo no contexto *Paracoccidioides*-privação de Fe fossem determinado. O estudo de proteínas com domínio CFEM e o estudo da especificidade dos transportadores de sideróforos de *Paracoccidioides* spp. ainda são pontos a serem investigado. Adicionalmente, conclui-se que a exposição de *Paracoccidioides* spp. a hemoglobina promove alterações em nível proteômico de parede celular, o que é refletido na capacidade aumentada do fungo interagir com macrófagos. Ainda neste contexto, foi determinada como ligante de hemoglobina a proteína HSP30, a qual é induzida na presença desta fonte de Fe e está presente na superfície celular fúngica. O silenciamento de *hsp30* promove capacidade reduzida do fungo crescer após exposição à hemoglobina. Estudos adicionais são requeridos para determinar se HSP30 apresenta atividade de heme oxigenase. A observação detalhada destas questões, ainda em aberto, pode promover a expansão do conhecimento sobre a biologia de *Paracoccidioides* spp. e, consequentemente, promover a bioprospecção de novos alvos para diagnóstico diferencial e/ou terapia da PCM.

REFERÊNCIAS

ALMEIDA, R. S.; BRUNKE, S.; ALBRECHT, A.; THEWES, S.; LAUE, M.; EDWARDS, J. E.; FILLER, S. G.; HUBE, B. The hyphal-associated adhesin and invasin Als3 of *Candida albicans* mediates iron acquisition from host ferritin. **PLoS Pathogens**, v. 4, p. 1–17, 2008.

ASEHNOUNE, K.; VILLADANGOS, J.; HOTCHKISS, R. S. Understanding host–pathogen interaction. **Intensive Care Medicine**, v. 42, n. 12, p. 2084–2086, 2016.

BAILÃO, A. M.; SCHRANK, A.; BORGES, C. L.; DUTRA, V.; MOLINARI-MADLUM, E. E. W. I.; FELIPE, M. S. S.; MENDES-GIANINI, M. J. S.; MARTINS, W. S.; PEREIRA, M.; SOARES, C. M. DE A. Differential gene expression by *Paracoccidioides brasiliensis* in host interaction conditions : Representational difference analysis identifies candidate genes associated with fungal pathogenesis. **Microbes and Infection**, v. 8, p. 2686–2697, 2006.

BAILÃO, A. M.; SHRANK, A.; BORGES, C. L.; PARENTE, J. A.; DUTRA, V.; FELIPE, M. S. S.; FIÚZA, R. B.; PEREIRA, M.; SOARES, C. M. D. A.; SOARES, A. The transcriptional profile of *Paracoccidioides brasiliensis* yeast cells is influenced by human plasma. **FEMS Immunology and Medical Microbiology**, v. 51, n. 1, p. 43–57, 2007.

BAILÃO, E. F. L. C. *et al.* Metal Acquisition and Homeostasis in Fungi. **Current Fungal Infection Reports**, v. 6, p. 257–266, 2012.

Bailão EFLC, Parente JA, Pigosso LL, de Castro KP, Fonseca FL, Silva-Bailão MG, et al. Hemoglobin Uptake by *Paracoccidioides* spp. Is Receptor-Mediated. **PLoS Negl Trop Dis.**; 8(5), 2014.

BAILÃO, E. F. L. C.; LIMA, P. DE S.; SILVA-BAILÃO, M. G.; BAILÃO, A. M.; FERNANDES, G. DA R.; KOSMAN, D. J.; SOARES, C. M. DE A. *Paracoccidioides* spp. ferrous and ferric iron assimilation pathways. **Frontiers in Microbiology**, v. 6, n. JUL, p. 1–12, 2015.

BAKER, H. M.; ANDERSON, B. F.; BAKER, E. N. Dealing with iron: common structural principles in proteins that transport iron and heme. **Proceedings of the National Academy of Sciences of the United States of America**, v. 100, p. 3579–3583, 2003.

BRADFORD, M. M. A rapid and sensitive method for the quantitation of microgram quantities of protein utilizing the principle of protein-dye binding. **Analytical Biochemistry**, v. 72, n. 1–2, p. 248–254, 1976.

BRUMMER, E.; CASTANEDA, E.; RESTREPO, A. Paracoccidioidomycosis: an update. **Clinical Microbiology Reviews**, v. 6, n. 4, p. 89–117, 1993.

BURGER, E. Paracoccidioidomycosis protective immunity. **Journal of Fungi**, v. 7, n. 2, p. 1–26, 2021.

CADIEUX, B.; LIAN, T.; HU, G.; WANG, J.; BIONDO, C.; TETI, G.; LIU, V.; MURPHY, M. E. P.; CREAGH, A. L.; KRONSTAD, J. W. The mannoprotein cig1

supports iron acquisition from heme and virulence in the pathogenic fungus *Cryptococcus neoformans*. **Journal of Infectious Diseases**, v. 207, n. 8, p. 1339–1347, 2013.

CAZA, M.; KRONSTAD, J. W. Shared and distinct mechanisms of iron acquisition by bacterial and fungal pathogens of humans. **Frontiers in Celullar and Infection Microbiology**, v. 3, p. 1–23, 2013.

CHAVES, E. A. C.; WEBER, S. S.; BÁO, S. N.; PEREIRA, L. A.; BAILÃO, A. B.; BORGES, C. L.; SOARES, C. M. DE A. Analysis of *Paracoccidioides* secreted proteins reveals fructose 1,6-bisphosphate aldolase as a plasminogen-binding protein. **BMC Microbiology**, v. 15, p. 1–14, 2015.

CURCIO, J. S. DE; OLIVEIRA, L. N.; BATISTA, M. P.; NOVAES, E.; ALMEIDA SOARES, C. M. DE. MiRNAs regulate iron homeostasis in *Paracoccidioides brasiliensis*. **Microbes and Infection**, 2020.

DLOUHY, A. C.; OUTTEN, C. E. The Iron Methallome in Eukaryotic Organisms. **Metal Ions in Life Sciences**, v. 12, p. 241–278, 2013.

FOSTER, L.-A. A. Utilization and cell-surface binding of hemin by *Histoplasma capsulatum*. **Canadian journal of microbiology**, v. 48, n. 5, p. 437–442, 2002.

GEROMANOS, S. J.; VISSERS, J. P. C.; SILVA, J. C.; DORSCHEL, C. A.; LI, G. Z.; GORENSTEIN, M. V.; BATEMAN, R. H.; LANGRIDGE, J. I. The detection, correlation, and comparison of peptide precursor and product ions from data independent LC-MS with data dependant LC-MS/MS. **Proteomics**, v. 9, n. 6, p. 1683–1695, 2009.

GONZALEZ, A.; HERNANDEZ, O. New insights into a complex fungal pathogen: the case of *Paracoccidioides* spp. **Yeast**, v. 33, p. 113–128, 2016.

GUANGGAN, H.; CAZA, M.; CADIEUX, B.; BAKKEREN, E.; DO, E.; JUNG, W. H.; KRONSTAD, J. W. The ESCRT machinery influences haem uptake and capsule elaboration in *Cryptococcus neoformans*. **Molecular Microbiology**, v. 96, n. 5, p. 973–992, 2015.

HAAS, H.; SCHOESER, M.; LESUISSE, E.; ERNST, J. F.; PARSON, W.; ABT, B.; WINKELMANN, G.; OBEREGGER, H. Characterization of the *Aspergillus nidulans* transporters for the siderophores enterobactin and triacetylfusarinine C. **The Biochemical journal**, v. 371, p. 505–513, 2003.

HENTZE, M. W.; MUCKENTHALER, M. U.; ANDREWS, N. C. Balancing Acts: Molecular Control of Mammalian Iron Metabolism. **Cell**, v. 117, p. 285–297, 2004.

HEYMANN, P.; GERADS, M.; SCHALLER, M.; DROMER, F.; WINKELMANN, G.; ERNST, J. F. The siderophore iron transporter of *Candida albicans* (Sit1p/Arn1p) mediates uptake of ferrichrome-type siderophores and is required for epithelial invasion. **Infection and Immunity**, v. 70, p. 5246–5255, 2002.

HISSEN, A. H. T.; CHOW, J. M. T.; PINTO, L. J.; MOORE, M. M. Survival of *Aspergillus fumigatus* in Serum Involves Removal of Iron from Transferrin: The Role of Siderophores. **Infection and Immunity**, v. 72, n. 3, p. 1402–1408, 2004.

HU, G.; CAZA, M.; CADIEUX, B.; CHAN, V.; LIU, V.; KRONSTAD, J. *Cryptococcus neoformans* requires the ESCRT protein Vps23 for iron acquisition from heme, for

capsule formation, and for virulence. **Infection and Immunity**, v. 81, n. 1, p. 292–302, 2013.

JUNG, W. H.; HU, G.; KUO, W.; KRONSTAD, J. W. Role of ferroxidases in iron uptake and virulence of *Cryptococcus neoformans*. **Eukaryotic Cell**, v. 8, p. 1511–1520, 2009.

JUNG, W. H.; KRONSTAD, J. W. Iron and fungal pathogenesis: A case study with *Cryptococcus neoformans*. **Cellular Microbiology**, v. 10, p. 277–284, 2008.

JUNG, W. H.; SHAM, A.; LIAN, T.; SINGH, A.; KOSMAN, D. J.; KRONSTAD, J. W. Iron source preference and regulation of iron uptake in *Cryptococcus neoformans*. **PLoS pathogens**, v. 4, p. 1–14, 2008.

KNIGHT, S. A B.; VILAIRE, G.; LESUISSE, E.; DANCIS, A. Iron Acquisition from Transferrin by *Candida albicans* Depends on the Reductive Pathway. **Infec**, v. 73, p. 5482–5492, 2005.

KOSMAN, D. J. Iron metabolism in aerobes: managing ferric iron hydrolysis and ferrous iron autoxidation. **Coordination Chemistry Reviews**, v. 257, n. 1, p. 1–24, 2013.

Kosman, D.J. A holistic view of mammalian (vertebrate) cellular iron uptake. **Metallomics**. 12(9):1–20. 2020.

KULKARNI, R. D.; KELKAR, H. S.; DEAN, R. A. An eight-cysteine-containig CFEM domain unique to a group of fungal membrane proteins. **Trends in Biochemical Sciences**, v. 28, p. 118–121, 2003.

KUZNETS, G.; VIGONSKY, E.; WEISSMAN, Z.; LALLI, D.; GILDOR, T.; KAUFFMAN, S. J.; TURANO, P.; BECKER, J.; LEWINSON, O.; KORNITZER, D. A Relay Network of Extracellular Heme-Binding Proteins Drives *C. albicans* Iron Acquisition from Hemoglobin. **PLoS Pathogens**, v. 10, n. 10, p. 1–15, 2014.

MACEDO, P. M. DE; FREITAS, D. F. S.; VARON, A. G.; LAMAS, C. DA C.; FERREIRA, L. C. F.; FREITAS, A. D.; FERREIRA, M. T.; NUNES, E. P.; SIQUEIRA, M. M.; VELOSO, V. G.; VALLE, A. C. F. DO. COVID-19 and acute juvenile paracoccidioidomycosis coinfection. **PLoS Neglected Tropical Diseases**, v. 14, n. 8, p. 1–7, 2020.

MANNS, J. M.; MOSSER, D. M.; BUCKLEY, H. R. Production of a hemolytic factor by *Candida albicans*. **Infection and Immunity**, v. 62, n. 11, p. 5154–5156, 1994.

MOORS, M. A; STULL, T. L.; BLANK, K. J.; BUCKLEY, H. R.; MOSSER, D. M. A role for complement receptor-like molecules in iron acquisition by *Candida albicans*. **The Journal of Experimental Medicine**, v. 175, n. June, p. 1643–1651, 1992.

MOREIRA, A. L. E.; OLIVEIRA, M. A. P.; SILVA, L. O. S.; INÁCIO, M. M.; BAILÃO, A. M.; PARENTE-ROCHA, J. A.; CRUZ-LEITE, V. R. M.; PACCEZ, J. D.; ALMEIDA SOARES, C. M. DE; WEBER, S. S.; BORGES, C. L. Immunoproteomic Approach of Extracellular Antigens From *Paracoccidioides* Species Reveals Exclusive B-Cell Epitopes. **Frontiers in Microbiology**, v. 10, n. January, 2020.

MUÑOZ, J. F. *et al.* Genome Diversity, Recombination, and Virulence across the Major Lineages of *Paracoccidioides*. **mSphere**, v. 1, n. 5, p. 1–18, 2016.

MURAD, A. M.; SOUZA, G. H. M. F.; GARCIA, J. S.; RECH, E. L. Detection and

expression analysis of recombinant proteins in plant-derived complex mixtures using nanoUPLC-MS^{E}. **Journal of Separation Science**, v. 34, n. 19, p. 2618–2630, 2011.

NASSER, L.; WEISSMAN, Z.; PINSKY, M.; AMARTELY, H.; DVIR, H.; KORNITZER, D. Structural basis of haem-iron acquisition by fungal pathogens. **Nature Microbiology**, v. 1, n. September, p. 16156, 2016.

NEILANDS, J. B. Siderophores. **Arquives of Biochemistry and Biophysics**, v. 302, p. 1–3, 1993.

NEMETH, E.; RIVERA, S.; GABAYAN, V.; KELLER, C.; TAUDORF, S.; PEDERSEN, B. K.; GANZ, T. IL-6 Mediates Hypoferremia of Inflammation by Inducing the Synthesis of Iron Regulatory Hormone Hepcidin. **The Journal of Clinical Investigation**, v. 113, p. 1271–1276, 2004.

NICOLA, A. M.; ANDRADE, R. V.; SILVA-PEREIRA, I. Molecular chaperones in the *Paracoccidioides brasiliensis* transcriptome. **Genetics and molecular research : GMR**, v. 4, n. 2, p. 346–357, 2005.

NÚÑEZ, G.; SAKAMOTO, K.; SOARES, M. P. Innate Nutritional Immunity. **The Journal of Immunology**, v. 201, n. 1, p. 11–18, 2018.

OKAMOTO-SHIBAYAMA, K.; KIKUCHI, Y.; KOKUBU, E.; SATO, Y.; ISHIHARA, K. Csa2, a member of the Rbt5 protein family, is involved in the utilization of iron from human hemoglobin during *Candida albicans* hyphal growth. **FEMS Yeast Research**, v. 14, n. 4, p. 674–677, 2014.

PAPANIKOLAOU, G.; PANTOPOULOS, K. Iron Metabolism and Toxicity. **Toxicology and Applied Pharmacology**, v. 202, p. 199–211, 2005.

PARENTE, ANA F. A.; BAILÃO, A. M.; BORGES, C. L.; PARENTE, J. A.; MAGALHÃES, A. D.; RICART, C. A. O.; SOARES, C. M. A. Proteomic analysis reveals that iron availability alters the metabolic status of the pathogenic fungus *Paracoccidioides brasiliensis*. **PLoS ONE**, v. 6, n. 7, 2011.

PARENTE, ANA F A; BAILÃO, A. M.; BORGES, C. L.; PARENTE, J. A.; MAGALHÃES, A. D.; RICART, C. A. O.; SOARES, C. M. A. Proteomic analysis reveals that iron availability alters the metabolic status of the pathogenic fungus *Paracoccidioides brasiliensis*. **PLoS ONE**, v. 6, n. 7, 2011.

PARENTE, A. F. A.; REZENDE, T. C. V. DE; CASTRO, K. P. DE; BAILÃO, A. M.; PARENTE, J. A.; BORGES, C. L.; SILVA, L. P.; SOARES, C. M. DE A. A proteomic view of the response of *Paracoccidioides* yeast cells to zinc deprivation. **Fungal Biology**, v. 7, p. 399–410, 2013.

PENDRAK, M. L.; CHAO, M. P.; YAN, S. S.; ROBERTS, D. D. Heme Oxygenase in *Candida albicans* Is Regulated by Hemoglobin and Is Necessary for Metabolism of Exogenous Heme and Hemoglobin to α-Biliverdin. **Journal of Biological Chemistry**, v. 279, n. 5, p. 3426–3433, 2004.

PENDRAK, M. L.; ROBERTS, D. D. Hemoglobin is an effective inducer of hyphal differentiation in *Candida albicans*. **Medical mycology**, v. 45, n. 1, p. 61–71, 2007.

PETITO, G.; CURCIO, J. S. DE; PEREIRA, M.; BAILÃO, A. M.; PACCEZ, J. D.;

MORAES, C. O. B. DE; SANTOS JÚNIOR, A. D. C. M. DOS; FONTES, W.; RICART, C. A. O.; SOARES, C. M. DE A. Metabolic adaptation of *Paracoccidioides brasiliensis* in response to in vitro copper deprivation. **Frontiers in Microbiology**, v. 11, n. August, p. 1834, 2020.

PIGOSSO, L. L.; BAEZA, L. C.; TOMAZETT, M. V.; FALEIRO, M. B. R.; MOURA, V. M. B. DE; BAILÃO, A. M.; BORGES, C. L.; PARENTE-ROCHA, J. A.; FERNANDES, G. DA R.; GAUTHIER, G. M.; SOARES, C. M. DE A. *Paracoccidioides brasiliensis* presents metabolic reprogramming and secretes a serine proteinase during murine infection. **Virulence**, v. 8, n. 7, p. 1417–1434, 2017.

PINSKY, M.; ROY, U.; MOSHE, S.; WEISSMAN, Z.; KORNITZER, D. Human Serum Albumin Facilitates Heme-Iron Utilization by Fungi. **mBio**, v. 11, n. 2, p. 1–14, 2020.

RAMANAN, N.; WANG, Y. A high-affinity iron permease essential for *Candida albicans* virulence. **Science**, v. 288, p. 1062–1064, 2000.

RAYMOND-BOUCHARD, I.; CARROLL, C. S.; NESBITT, J. R.; HENRY, K. A.; PINTO, L. J.; MOINZADEH, M.; SCOTT, J. K.; MOORE, M. M. Structural requirements for the activity of the MirB ferrisiderophore transporter of *Aspergillus fumigatus*. **Eukaryotic Cell**, v. 11, n. 11, p. 1333–1344, 2012.

RESTREPO, A.; JIMÉNEZ, B. E. Growth of *Paracoccidioides brasiliensis* yeast phase in a chemically defined culture medium. **Journal of Clinical Microbiology**, v. 12, n. 2, p. 279–81, 1980.

RODRIGUES, A.; OLIVEIRA, D.; NOJOSA, L.; SOARES, D. A.; PARENTE-ROCHA, J. A.; BAEZA, L. C. Characterization of extracellular proteins in members of the *Paracoccidioides* complex. **Fungal Biology**, v. 122, p. 738–751, 2018.

ROY, U.; KORNITZER, D. Heme-iron acquisition in fungi. **Current Opinion in Microbiology**, v. 52, p. 77–83, 2019.

SANTOS, R. P.; TOMICH, L. G. M. DE M.; CALÁBRIA, M. F. O.; SCARPELLIN, F.; GODOY, C. S. DE M.; SOARES, R. DE B. A. COINFECÇÃO POR LEISHMANIOSE E PARACOCCIDIOIDOMICOSE E COMPLICACÇÕES TROMBÓTICAS GRAVES POR COVID-19: RELATO DE CASO. **The Brazilian Journal of Infectious Diseases**, n. January, 2021.

SCHRETTL, M. *et al.* HapX-Mediated adaption to iron starvation is crucial for virulence of *Aspergillus fumigatus*. **PLoS Pathogens**, v. 6, n. 9, 2010.

SCHRETTL, M.; BIGNELL, E.; KRAGL, C.; SABIHA, Y.; LOSS, O.; EISENDLE, M.; WALLNER, A.; ARST, H. N.; HAYNES, K.; HAAS, H. Distinct roles for intra- and extracellular siderophores during *Aspergillus fumigatus* infection. **PLoS Pathogens**, v. 3, p. 1195–1207, 2007.

SHIKANAI-YASUDA, M. A.; MENDES, R. P.; COLOMBO, A. L.; QUEIROZ-TELLES, F. DE; SATIE, A.; KONO, G.; PANIAGO, A. M.; NATHAN, A.; CARLOS, A.; BAGAGLI, E. Ahead of Print Brazilian guidelines for the clinical management of paracoccidioidomycosis. n. June, 2017.

SILVA-BAILÃO, M. G.; BAILÃO, E. F. L. C.; LECHNER, B. E.; GAUTHIER, G. M.; LINDNER, H.; BAILÃO, A. M.; HAAS, H.; SOARES, C. M. D. A. Hydroxamate

production as a high affinity iron acquisition mechanism in *Paracoccidioides* Spp. **PLoS ONE**, v. 9, n. 8, 2014.

SILVA, M. G. *et al.* The homeostasis of iron, copper, and zinc in P*aracoccidioides brasiliensis*, *Cryptococcus neoformans var. Grubii*, and *Cryptococcus gattii*: A comparative analysis. **Frontiers in Microbiology**, v. 2, n. MAR, p. 1–19, 2011.

SILVA, M. G. *et al.* Molecular characterization of siderophore biosynthesis in *Paracoccidioides brasiliensis*. **IMA Fungus**, v. 11, n. 11, p. 1–14, 2020.

SOARES, C. M. A. .; MOLLINARI MADLUN, E. E. W. I. .; SILVA, S. P. .; PEREIRA, M. .; FELIPE, M. S. S. Characterization of *Paracoccidioides brasiliensis* Isolates by Random Amplified Polymorphic DNA Analysis. **Journal of Clinical Microbiology**, v. 33, n. 2, p. 505–507, 1995.

SOARES, M. P.; WEISS, G. The Iron age of host – microbe interactions. **EMBO Reports**, v. 16, n. 11, p. 1482–1500, 2015.

SORGO, A. G.; HEILMANN, C. J.; DEKKER, H. L.; BRUL, S.; KOSTER, C. G.; KLIS, F. M. Mass spectrometric analysis of the secretome of *Candida albicans*. **Yeast**, v. 27, p. 661–672, 2010.

SOUZA, A. F. DE; PAULA, M. S. DE; LIMA, R. M.; SILVA, M. G.; CURCIO, J. S. DE; PEREIRA, M.; SOARES, C. M. DE A. The"little iron waltz": The ternary response of *Paracoccidioides* spp. to iron deprivation. **Journal of Fungi**, v. 6, n. 4, p. 1–12, 2020.

SOUZA, A. F. DE; TOMAZETT, M. V.; SILVA, K. S. F. E; CURCIO, J. S. DE; PEREIRA, C. A.; BAEZA, L. C.; PACCEZ, J. D.; GONÇALES, R. A.; RODRIGUES, F.; PEREIRA, M.; SOARES, C. M. DE A. Interacting with Hemoglobin : *Paracoccidioides* spp. Recruits hsp30 on Its Cell Surface for Enhanced Ability to Use This Iron Source. **Journal of Fungi**, v. 7, n. 21, p. 1–21, 2021.

TAMAYO, D.; MUÑOZ, J. F.; TORRES, I.; ALMEIDA, A. J.; RESTREPO, A.; MCEWEN, J. G.; HERNÁNDEZ, O. Involvement of the 90kDa heat shock protein during adaptation of *Paracoccidioides brasiliensis* to different environmental conditions. **Fungal Genetics and Biology**, v. 51, n. 1, p. 34–41, 2013.

TANAKA, W. T. H.; NAKAO, N.; MIKAMI, T.; MATSUMOTO, T. Hemoglobin Is Utilized by *Candida albicans* in the Hyphal Form but Not Yeast Form. **Biochemical and Biophysical Research Communications**, v. 232, n. 2, p. 350–353, 1997.

TANDARA, L.; SALAMUNIC, I. Iron metabolism: current facts and future directions. **Biochemia Medica**, v. 22, n. 3, p. 311–328, 2012.

TANGEN, K. L.; JUNG, W. H.; SHAM, A. P.; LIAN, T.; KRONSTAD, J. W. The iron- and cAMP-regulated gene SIT1 influences ferrioxamine B utilization, melanization and cell wall structure in *Cryptococcus neoformans.* **Microbiology**, v. 153, n. 1, p. 29–41, 2007.

TOMAZETT, M. V.; BAEZA, L. C.; PACCEZ, J. D.; PARENTE-ROCHA, J. A.; RIBEIRO-DIAS, F.; SOARES, C. M. DE A. Identification and characterization of *Paracoccidioides lutzii* proteins interacting with macrophages. **Microbes and Infection**, p. 1–11, 2019.

TRISTÃO, G. B.; ASSUNÇÃO, L. P.; SANTOS, L. P. A. DOS; BORGES, C. L.; SILVA-BAILÃO, M. G.; ALMEIDA SOARES, C. M. DE; CAVALLARO, G.; BAILÃO, A. M. Predicting copper-, iron-, and zinc-binding proteins in pathogenic species of the *Paracoccidioides* genus. **Frontiers in Microbiology**, v. 6, n. JAN, p. 1–11, 2015.

TURISSINI, D. A.; GOMEZ, O. M.; TEIXEIRA, M. M.; MCEWEN, J. G.; MATUTE, D. R. Species boundaries in the human pathogen *Paracoccidioides*. **Fungal Genetics and Biology**, v. 106, n. January, p. 9–25, 2017.

VALLEJO, M. C.; NAKAYASU, E.; MATSUO, A.; SOBREIRA, T.; LONGO, L.; GANIKO, L.; ALMEIDA, I.; PUCCIA, R. Vesicle and Vesicle-Free Extracelullar Proteome of *Paracoccidioides brasiliensis*: Comparative Analysis with other Pathogenic Fungi. **J Proteomics**, v. 11, n. 3, p. 1676–1685, 2012.

WALLNER, A.; BLATZER, M.; SCHRETTL, M.; SARG, B.; LINDNER, H.; HAAS, H. Ferricrocin, a siderophore involved in intra- and transcellular iron distribution in *Aspergillus fumigatus*. **Applied and Environmental Microbiology**, v. 75, p. 4194–4196, 2009.

WANG, L.; CHERARYIL, B. J. Ironing out the Wrinkles in Host Defense: Interections beween Iron Homeostasis and Innate Immunity. **Journal of Innate Immunity**, v. 1, p. 455–464, 2009.

WATANABE, T.; TAKANO, M.; MURAKAMI, M.; TANAKA, H.; MATSUHISA, A.; NAKAO, N.; MIKAMI, T.; SUZUKI, M.; MATSUMOTO, T. Characterization of a haemolytic factor from *Candida albicans*. **Microbiology**, v. 145, n. 3, p. 689–694, 1999.

WEBER, S. S.; PARENTE, A. F. A.; BORGES, C. L.; PARENTE, J. A.; BAILÃO, A. M.; ALMEIDA SOARES, C. M. DE. Analysis of the Secretomes of *Paracoccidioides* Mycelia and Yeast Cells. **PLoS ONE**, v. 7, n. 12, 2012.

WEINBERG, E. D. Nutritional Immunity. **The Journal of the American Mecical Association**, v. 231, n. 1, p. 39–41, 1975.

WEISSMAN, Z.; KORNITZER, D. A family of *Candida* cell surface haem-binding proteins involved in haemin and haemoglobin-iron utilization. **Molecular Microbiology**, v. 53, n. 4, p. 1209–1220, 2004.

WEISSMAN, Z.; SHEMER, R.; CONIBEAR, E.; KORNITZER, D. An endocytic mechanism for haemoglobin-iron acquisition in *Candida albicans*. **Molecular Microbiology**, v. 69, p. 201–217, 2008.

WHITLEY, D.; GOLDBERG, S. P.; JORDAN, W. D. Heat shock proteins: A review of the molecular chaperones. **Journal of Vascular Surgery**, v. 29, n. 4, p. 748–751, 1999.

ZARNOWSKI, R.; COOPER, K. G.; BRUNOLD, L. S.; CALAYCAY, J.; WOODS, J. P. *Histoplasma capsulatum* secreted γ-glutamyltransferase reduces iron by generating an efficient ferric reductant. **Molecular Microbiology**, v. 70, n. 2, p. 352–368, 2008.

ZARNOWSKI, R.; WOODS, J. P. Glutathione-dependent extracellular ferric reductase activities in dimorphic zoopathogenic fungi. **Microbiology**, v. 151, n. Pt 7, p. 2233–2240, 2005.

ZHANG, Z.-N.; WU, Q.-Y.; ZHANG, G.-Z.; ZHU, Y.-Y.; MURPHY, R. W.; LIU, Z.; ZOU, C.-G. Systematic analyses reveal uniqueness and origin of the CFEM domain in fungi. **Scientific reports**, v. 5, p. 13032, 2015.

Anexo 1. Colaboração em artigo original publicado no *IMA Fungus*

Silva *et al. IMA Fungus* (2020) 11:11
https://doi.org/10.1186/s43008-020-00035-x

IMA Fungus

RESEARCH Open Access

Molecular characterization of siderophore biosynthesis in *Paracoccidioides brasiliensis*

Marielle Garcia Silva[1,2†], Juliana Santana de Curcio[1†], Mirelle Garcia Silva-Bailão[1], Raisa Melo Lima[1], Mariana Vieira Tomazett[1], Aparecido Ferreira de Souza[1], Vanessa Rafaela Milhomem Cruz-Leite[1], Nicolau Sbaraini[3], Alexandre Melo Bailão[1], Fernando Rodrigues[4,5], Maristela Pereira[1], Relber Aguiar Gonçales[4,5] and Célia Maria de Almeida Soares[1*]

Abstract

Iron is an essential nutrient for all organisms. For pathogenic fungi, iron is essential for the success of infection. Thus, these organisms have developed high affinity iron uptake mechanisms to deal with metal deprivation imposed by the host. Siderophore production is one of the mechanisms that fungal pathogens employ for iron acquisition. *Paracoccidioides* spp. present orthologous genes encoding the enzymes necessary for the biosynthesis of hydroxamates, and plasma membrane proteins related to the transport of these molecules. All these genes are induced in iron deprivation. In addition, it has been observed that *Paracoccidioides* spp. are able to use siderophores to scavenge iron. Here we observed that addition of the xenosiderophore ferrioxamine B FOB) to *P. brasiliensis* culture medium results in repression (at RNA and protein levels) of the SidA, the first enzyme of the siderophore biosynthesis pathway. Furthermore, SidA activity was reduced in the presence of FOB, suggesting that *P. brasiliensis* blocks siderophores biosynthesis and can explore siderophores in the environment to scavenge iron. In order to support the importance of siderophores on *Paracoccidioides* sp. life and infection cycle, silenced mutants for the *sidA* gene were obtained by antisense RNA technology. The obtained *AsSidA* strains displayed decreased siderophore biosynthesis in iron deprivation conditions and reduced virulence to an invertebrate model.

Keywords: Iron, SidA, RNA interference

INTRODUCTION

Iron is an essential nutrient for growth and development of living organisms. Due to iron redox properties, this metal occurs in two oxidation states, ferrous ion (Fe^{+2}) and ferric ion (Fe^{+3}), which are influenced by pH and oxygen (Sanchez et al. 2017). Fe^{+2} spontaneously convert to Fe^{+3} in the presence of oxygen (Halliwell and Gutteridge 1984). Iron is indispensable for a variety of cellular processes such as respiration, although, the excess or incorrect storage of this metal by cells is harmful. The reduced form of iron (Fe^{+2}) catalyzes the production of reactive oxygen species (ROS) through the Fenton/Haber Weiss reaction (Halliwell and Gutteridge 1984; Haber and Weiss 1934). In this way, the maintenance of the homeostasis of this micronutrient is essential. Proper iron homeostasis is achieved through fine-tuned regulation of iron acquisition, use and storage (Ganz 2009).

Nutritional immunity (i.e., host deprivation of metals, such Fe, Cu, Mn and Zn) is an important mechanism employed by the host to control the development of pathogenic organisms, to overcome the low availability of iron imposed by the host, microorganisms developed high affinity mechanisms for iron uptake (Raymond et al. 2003). In fungal pathogens these mechanisms include: the reduction of Fe^{+3} to Fe^{+2}, the acquisition of the iron bound to the heme group, and the solubilization of Fe^{+3} promoted by siderophores (Kornitzer 2009; Bailão et al.

* Correspondence: cmasoares@gmail.com
†Marielle Garcia Silva and Juliana Santana de Curcio contributed equally to this work.
[1]Laboratório de Biologia Molecular, Instituto de Ciências Biológicas, ICB II, Campus II, Universidade Federal de Goiás, Goiânia, GO, Brazil
Full list of author information is available at the end of the article

2012; Canessa and Larrondo 2013). The last strategy, also known as non-reductive iron uptake, is characterized by the use of siderophores, which are low molecular weight compounds that bind Fe^{+3} with high affinity making it available for consumption (Neilands 1993).

Fungal siderophore biosynthesis is well characterized in *Aspergillus fumigatus* (Blatzer et al. 2011; Schrettl et al. 2004; Schrettl et al. 2007) and internalization of the siderophore-iron complex is performed by Siderophore Iron Transporters (SIT), such as Sit, MirA, MirB and MirC, located on the cell surface, as described in *Candida glabrata* and *Aspergillus nidulans* (Nevitt and Thiele 2011; Haas 2003; Haas et al. 2003). Siderophores are also produced by fungi of the *Paracoccidioides* genus that cause paracoccidioidomycosis (PCM) (Restrepo 1985), a disease restricted to Latin America (San-Blas et al. 2002) with high rates in Brazil (Restrepo et al. 2001). *Paracoccidioides* spp. grow as mycelia in the environment and as yeast cells in host tissues (Restrepo 1985). After inhalation of conidia or mycelial propagules, these reach the pulmonary alveoli of the host and differentiate into yeast cells, thus initiating the infectious process (McEwen et al. 1987).

Fungi of the *Paracoccidioides* genus can use reductive (Fe^{+3} to Fe^{+2}) and siderophore uptake pathways to acquire iron under conditions of metal shortage (Silva et al. 2011; Silva-Bailao et al. 2014; Bailao et al. 2015). We have demonstrated that *Paracoccidioides* spp. present putative orthologue genes to those related to hydroxamate siderophore production (*sidA*, *sidF*, *sidC*, *sidD*, *SidH* and *sidI*) as well as siderophore uptake (*sit1*, *mirB* and *mirC*) (Silva et al. 2011; Silva-Bailao et al. 2014). All of them are up-regulated in iron restriction and, in such condition, hydroxamate siderophores are produced (Silva-Bailao et al. 2014, Parente et al. 2011). Furthermore, *Paracoccidioides* spp. can also explore siderophores from other organisms to scavenge iron, as dimerumic acid and ferrioxamine B (FOB). Additionally, prior exposure of *P. brasiliensis* to FOB increases fungus survival to phagocytosis by activated macrophages (Silva-Bailao et al. 2014).

Considering those findings, we sought to investigate the adaptation of *P. brasiliensis* after FOB exposure as well as the functional role of SidA, the first enzyme in the siderophore production, in this fungus. Moreover, knockdown strains for *sidA* were generated employing antisense RNA technology and *Agrobacterium tumefaciens*-mediated transformation (ATMT) (Almeida et al. 2007; Menino et al. 2012; Bailao et al. 2014). Notably, upon FOB exposure, *P. brasiliensis' sidA* was down regulated at transcriptional and translational levels, which was accompanied by reduced enzymatic activity. Furthermore, the knockdown of *sidA* (*AsSidA*) led to reduced siderophore production by *P. brasiliensis* and decreased fungal virulence to *Tenebrio molitor* an invertebrate model, suggesting an essential role of siderophores in the infection cycle of *P. brasiliensis*.

MATERIAL AND METHODS

Ethics statement

Mouse manipulation was carried out in accordance with the ethical principles of animal research adopted by the Brazilian Society of Laboratory Animal Science and a Brazilian Federal Law 11.749 (October 2008). Male BALB/c mice aged between 6 to 8 weeks were purchased from the Animal house of the Instituto de Patologia Tropical e Saúde Pública – UFG and were maintained in the Animal Facilities at the Laboratório de Biologia Molecular, Universidade Federal de Goiás. Animal experimentation was approved by institutional Ethics Commission on Animal Use of the Universidade Federal de Goiás – UFG (reference number 089/17).

Strains and culture conditions

Yeast cells of *P. brasiliensis*, *Pb*18 (ATCC32069) were used in all the experiments. Cells were maintained in brain heart infusion (BHI) solid medium added of 4% (w/v) glucose for 4 days, at 36 °C. For experiments, cells were grown in liquid BHI for 72 h at 36 °C, 150 rpm, in order to reach the exponential growth phase (10^7 cells per ml). Afterward, the cells were centrifuged at 1200 x *g* for 10 min at 4 °C and washed twice with Phosphate Buffered Saline (PBS) 1X. Cells were then incubated in McVeigh/Morton liquid medium (MMcM) (Restrepo and Jimenez 1980) containing: 4% (w/v) glucose, 0.15% (w/v) KH_2PO_4, 0.05% (w/v) $MgSO_4.7H_2O$, 0.015% (w/v) $CaCl_2.2H_2O$, 0.2% (w/v) $(NH_4)_2SO_4$, 0.2% (w/v) L-asparagine, 0.02% (w/v) L-cystine, 1% (v/v) of vitamin supplement (0.006% [w/v] thiamine, 0.006% [w/v] niacin B3, 0.006% [w/v] Ca^{+2} pantothenate, 0.001% [w/v] inositol B7, 0.0001% [w/v] biotin B8, 0.001% [w/v] riboflavin, 0.01% [w/v] folic acid B9, 0.01% [w/v] choline chloride, 0.01% [w/v] pyridoxine) and 0.1% (v/v) of trace elements supplement (0.0057% [w/v] H_3BO_3, 0.0081% [w/v] $MnSO_4.14H_2O$, 0.0036% [w/v] $(NH_4)_6MO_7O_{24}.4H_2O$, 0.0157% [w/v] $CuSO_4.H_2O$, 0.1404% [w/v] $Fe(NH_4)_2(SO_4)_2.6H_2O$) (Restrepo and Jimenez 1980) supplemented with 50 μM of bathophenanthroline-disulfonic acid (BPS; Sigma-Aldrich, Germany), a ferrous iron-specific chelator, for 24 h at 36 °C with shaking at 150 rpm (Parente et al. 2011, Silva-Bailao et al. 2014). Cells were centrifuged and washed twice with PBS 1X and cell viability was determined using trypan blue. A total of 10^7 cells per mL were transferred to MMcM medium containing 50 μM of BPS or 10 μM of ferrioxamine B with iron loaded (FOB; Sigma-Aldrich, Saint louis, USA) (Silva-Bailao et al. 2014). Yeast cells were incubated at 36 °C for 6 and 24 h, 150 rpm. For culture in MMcM medium

all the glassware was acid treated to remove residual traces of iron (Cox 1994).

RNA extraction and quantitative real time PCR (RT-qPCR)

Total RNA extraction was accomplished using TRIzol (TRI Reagent, Sigma-Aldrich, St. Louis, MO) and mechanical cell rupture (Mini-Beadbeater – Biospec Products Inc., Bartlesville, OK). The mRNA was reverse-transcribed using Super-Script III First-Strand Synthesis SuperMix (Invitrogen, Life Technologies). qRT-PCR was performed employing a QuantStudio5 real-time PCR system (Applied Biosystems Inc.) and SYBER green PCR master mix was used in the reaction mixture (Applied Biosystems, Foster City, CA). The sequences of forward and reverse oligonucleotides are listed in (Additional file 1: Table S1). The data were normalized with the 28 kDa ribonucleoprotein (GenBank accession number XP_015701336). The relative expression levels of transcripts of interest were calculated using the standard curve method for relative quantification (Bookout et al. 2006).

L-ornithine-N^5-oxygenase enzymatic assay

The enzymatic activity of L-ornithine-N^5-oxygenase (SidA) was evaluated as previously described by Zhou et al. (1998) and Haas et al. (1999) with few modifications. Briefly, *P. brasiliensis* yeast cells were collected and suspended in 0.5 mM potassium phosphate buffer (pH 8.0). The suspension was transferred to tubes containing glass beads (425–600 μm) and submitted to vigorous mixing in a bead beater apparatus (BioSpec) for 5 cycles with intervals of 30 s on ice. The samples were centrifuged 10,000 x *g* for 15 min and the protein concentration in supernatants was determined with the (Bradford) reagent. To measure the enzymatic activity of SidA, equal amounts of proteins (50 μg) of both conditions, yeast cells incubated with (BPS) or (FOB), were used. The reaction mixture containing 40 μl of 0.5 mM potassium phosphate pH 8.0, 10 μl of 10 mM NADPH, 2 μl of 0.5 mM FAD, 50 μg of cell extract, 30 μl of 10 mM L-ornithine was incubated at 30 °C for 2 h and added of 100 μl of 0.2 M perchloric acid to stop the reaction. For control, the same amount of perchloric acid was added to one sample before incubation. The samples were centrifuged and the supernatants were used to determine the absorbance at 340 nm.

Molecular modeling of SidA

The amino acid sequence of the *P. brasiliensis* SidA (PADG_00097) was modeled with ITASSER algorithm (Yang and Zhang 2015) available at (https://zhanglab.ccmb.med.umich.edu/). To predict protonation states of the model, the PDB2PQR server (http://nbcr-222.ucsd.edu/pdb2pqr_2.0.0/) at pH 7 was used. Pymol visualizer was used to perform the structural analysis (Rigsby and Parker 2016).

The MD simulation was performed by the GROMACS 4.5.5 package, using the AMBER force field (ff99SB-ILDM) in the presence of water TIP3P. The protein was subjected to the simulation of 100 ns, temperature of 300 K, pressure of 1 atm and time interval of 2 fentoseconds, without restriction of the conformation (Pronk et al. 2013).

Analysis of Clusters, Root Mean Square Deviation (RMSD) and Root Mean Square Fluctuations (RMSF) were performed using the software of the GROMACS package. The quality analysis and the Ramachandran diagram of the final MD model were performed using the MolProbity server (http://molprobity.biochem.duke.edu/) (Chen et al. 2010).

Heterologous expression of recombinant SidA

Primers used for amplification of *SidA* cDNA were listed in (Additional file 1: Table S1). The PCR product was sub cloned into the *Bam*HI/*Eco*RI sites of pGEX-4 T3 vector (GE Healthcare Life Sciences). Transformation of *Escherichia coli* Rosetta (DE3) was carried out using standard procedures. For protein expression, transformed cells were cultured in LB medium supplemented with ampicillin (100 μg/ml) for 16 h at 37 °C. The induction of the recombinant protein was performed by addition of Isopropyl β-D-1-thiogalactopyranoside (IPTG; Sigma-Aldrich, St Louis, MO, USA) at a final concentration of 1 mM for 2 h. The size and identity of the recombinant protein SidA (rSidA) was evaluated using SDS-PAGE and in-gel protein digestion (Rezende et al. 2011) followed by LC-MS/MS (Lima Pde et al. 2015).

Polyclonal antibodies production and immunoblotting assay

rSidA was used in the production of specific mouse polyclonal antibodies. Pre-immune sera were obtained and stored at − 20 °C. The rSidA was extracted from the SDS-PAGE polyacrylamide gel, and subsequently injected into mouse three times at 15 days intervals. The obtained sera were sampled and stored at − 20 °C.

A total of 40 μg of the protein extract was loaded on 12% SDS-PAGE, stained with (Coomassie Blue R) or transferred to Hybond ECL membrane (GE Healthcare) as described by Lima and colleagues (Lima Pde et al. 2015). Blocked membranes were incubated with anti-SidA polyclonal antibodies diluted 1:150 for 2 h. After incubation, the membrane was washed and incubated with anti-mouse secondary antibody alkaline phosphatase conjugated (1:20000). The reaction was developed using 5-bromo-4-chloro-3-indolylphosphate/nitroblue tetrazolium (BCIP/NBT). As a load control was employed anti-enolase polyclonal antibodies (Nogueira et al. 2010). The pixel intensity

of the bands was analyzed using the ImageJ 1.51 software (Schneider et al. 2012) and expressed as arbitrary units.

Extraction and digestion of proteins for nano-ESI-UPLC-MS^E acquisition

Protein extraction was performed by protocol described by Baeza and coleagues (Baeza et al. 2017). The protein concentration in the supernatant was determined using the Bradford reagent (Bradford 1976). Bovine serum albumin was used as a standard. Integrity of the proteins was verified using a 12% SDS-PAGE. A total of 150 μg of cytoplasmic protein was prepared for nanoUPLC-MS^E analysis, as previously described (Lima Pde et al. 2015; Murad et al. 2011). After digestion, the peptides were ressuspended in 30 μl of ultrapure water and subsequently purified in ZipTip C18 Pipette Tips (Millipore, MA, USA) and dried in a speed vacuum. The obtained peptides were suspended in 80 μl of a solution containing 20 mM of ammonium formiate and 200 fmol/μL of PHB (MassPREP™ protein). After solubilization, peptides were transferred to a Waters Total Recovery vial (Waters Corporation, MA, USA). For separation of tryptic peptides, Nanoscale LC was performed using an ACQUITY UPLC® M-Class system (Waters Corporation, MA, USA) (Tomazett et al. 2019).

Data processing and protein identification

Data processing were performed as previously described (Lima Pde et al. 2015). In brief, for proteomic analyzes of the data obtained from the LC-MS^E, the ProteinLynx Global Server version 3.0.2 (Waters, Manchester, UK) was employed. The processed spectra were searched against *P. brasiliensis* (*Pb*18) protein sequences (https://www.uniprot.org/proteomes/). The protein identification criteria also included the detection of at least 2 fragment ions per peptide, 5 fragments per protein and the determination of at least 1 peptide per protein. A protein that showed a variance coefficient of 0.057 and that was detected in all replicates was used to normalize the protein expression levels in the samples (PADG_04570). Expression^E informatics v.3.0.2 was used for quantitative comparisons. The mathematical model used to calculate the ratios was part of the Expression^E algorithm inside the PLGS software from the Waters Corporation (Geromanos et al. 2009). The minimum repeat rate for each protein in all replicates was 2. Protein tables generated by ProteinLynx Global Server were merged, and the dynamic range of the experiment was calculated using the software program MassPivot v1.0.1. The data obtained by NanoUPLC-MS^E were subjected to in silico analysis to identify functional classification. For this analysis, it was used FungiDB-database (https://fungidb.org/fungidb/).

Construction and characterization of the *P. brasiliensis* SidA antisense-RNA strain

The functional evaluation of SidA was performed by antisense RNA technique, as described by Bailão and colleagues (Bailao et al. 2014) and Parente-Rocha et al. (2015). *A. tumefaciens* strain LBA 1100 was used for *P. brasiliensis* genetic transformation experiments. The cells from *A. tumefaciens* were cultured in induction medium (IM) for co-cultivation. Transformants were selected in BHI medium containing hygromycin 75 μg/mL (w/v) and randomly selected clones were confirmed for silencing by qRT- PCR. RNA extraction, cDNA synthesis and real-time PCR procedure were performed.

P. brasiliensis wild type (WT), empty vector (EV) and silenced for *sidA* gene (*AsSidA*) were cultured in liquid MMcM at 36 °C and 180 rpm in the presence of iron. Cell growth was evaluated by optical density at a wavelength of 600 nm every 24 h. Cell viability analysis was evaluated by staining with 1 μg/mL (wt/vol) propidium iodide (Sigma Aldrich). The samples were analyzed in a fluorescence microscope (Zeiss Axiocam MRc – Scope A1) (Zambuzzi-Carvalho et al. 2013).

Siderophore production assayed by chrome azurol (CAS)

Siderophore production was analyzed as described previously (Silva-Bailao et al. 2014). For the overlay CAS (O-CAS) assay, 10^6 yeast cells were grown in solid MMcM medium with no iron supplementation for 5 days. After that, 15 ml of CAS solution (Schwyn and Neilands 1987) were applied over the plates. The ternary complex Chrome Azurol S/Fe^{3+}/hexadecyltrimetyl ammonium bromide (HDTMA) acts as an indicator of siderophore production, since it is originally blue and turns orange in presence of siderophores (Perez-Miranda et al. 2007).

The percentage of siderophores production was also determined (Machuca and Milagres 2003). Briefly, 10^6 yeast cells were grown in MMcM liquid medium with no iron supplementation or with different concentrations of ammonium ferrous sulfate (2.5 μm, 5 μm, 10 μm and 30 μm). After 5 days of growth, the culture supernatants were collected by centrifugation at 10,000 x *g* for 1 min and 400 μl were incubated with the same volume of CAS liquid medium (Schwyn and Neilands 1987). The reference sample was prepared by adding 400 μL of sterile MMcM without iron or with different iron concentrations to 400 μL of CAS liquid medium. After 1 h of incubation at room temperature in the dark, the absorbance at 630 nm (Ultraspec 2000 UV/Visible Spectrophotometer Pharmacia Biotech) was determined. The percentage of siderophore activity was calculated by subtracting the sample absorbance values from the reference according to the following formula [(Ar−As/Ar)] × 100, in which Ar means absorbance of reference and As absorbance of sample.

Standardization of *Tenebrio molitor* larvae as an infection model for *P. brasiliensis*

T. molitor larvae were acquired from a local supplier and maintained in oatmeal diet until experimentation. *P. brasiliensis* yeast cells were cultured in BHI as previously described, collected through centrifugation, washed three times with PBS 1X and resuspended in PBS. The cells were repeatedly passed through a 18-gauge needle coupled to a 5 mL syringe and later strained through a 40 μm nylon filter to obtain a homogenous cell suspension. The cells were counted with a hemocytometer and diluted to specific concentrations with PBS. Hemocoel injection was performed with a Hamilton syringe (Sigma-Aldrich) in *T. molitor* larvae weighing between 150 and 200 mg, showing light and uniform color and absence of pigmented spots. The infection was performed in the ventral part of the larva, in the second segment after the paws and the volume of cell suspension was 5 μL (e.g., harboring 1×10^5, 1×10^6 or 2×10^6 cells). The larvae were kept in Petri dishes at 37 °C. The number of dead larvae was evaluated every 24 h for 10 days and deceased larvae were removed from the plate. As a control, the larvae were inoculated under the same conditions described above with PBS 1X. The experiments were performed with a total of 30 larvae per group.

Evaluation of *AsSidA* virulence in *T. molitor* larvae

P. brasiliensis yeast cells of WT, EV and *AsSidA* mutants were cultured and prepared as previously described. The infection was performed as previously described, employing 2×10^6 cells. The larvae were kept in Petri plates at 37 °C and the amount of dead larvae was evaluated every 24 h for 10 days. As a control, the larvae were inoculated under the same conditions described above with PBS 1X. The experiments were performed with a total of 30 larvae per group.

Statistical analysis

Student's *t*-test was used for the statistical analysis of the following experiments, enzymatic activity, qRT-PCR, immunobloting analysis and siderophores production. The following *P* values: $p \leq 0.0005$, $p \leq 0.005$ and $p \leq 0.05$ were considered statistically significant, for each cited experiments, respectively. For the experiments in *T. molitor* the GraphPad Prism 5 program was used to generate the survival curve (using the Kaplan – Meier method) and for statistical analysis (Log-rank [Mantel-Cox]). p value < 0.05 was considered significant (de Souza et al. 2015; de Souza et al. 2018a, 2018b).

RESULTS

Molecular modeling of SidA demonstrates its interaction with substrates for the first step in siderophore biosynthesis

Although *P. brasiliensis* has orthologs for the all the components for siderophore biosynthesis, the functionality of this pathway still remains elusive. Therefore, we employ molecular modeling to describe in silico the structural characteristics of SidA and its possible ligands. The described SidA proteins harbor a conserved domain of the superfamily of oxygenases (Pfam 13,434; This domain is conserved in the putative SidA of *P. brasiliensis*) and require NADPH and FAD as cofactors. The crystallized protein with the most similar three-dimensional structure corresponds to *A. fumigatus* SidA, with 47% identity (PDBID: 4B63) (Franceschini et al. 2012; Krithika et al. 2006). Thus, molecular modeling of *P. brasiliensis* putative SidA was employed, in order to support and identify amino acid residues that hypothetically bind to FAD, NADPH and L-ornithine. The molecular modeling and three-dimensional structure comparison was based on *A. fumigatus* SidA (i.e, already crystallized protein; PDBID: 4B63) displaying 47% identity with *P. brasiliensis* putative SidA ortholog.

The (Additional file 2: Fig. S1 A) shows the alignment of *A. fumigatus* SidA (gray) and *P. brasiliensis* SidA (blue) showing a preserved site of interaction with L-ornithine, FAD and NADPH. The amino acid residues that interact with L-ornithine in *A. fumigatus* are LYS107, ASN323 and SER469, which in the *P. brasiliensis* model correspond to LYS88, ASN306 and SER448, respectively (Additional file 2: Fig. S1 B). The interaction between NADPH and FAD occurs through a triad of amino acids GLN102, VAL168 and ARG279 in the crystal of *A. fumigatus*, corresponding to GLN83, VAL149 and LYS262 in *P. brasiliensis* (Additional file 2: Fig. S1 C).

P. brasiliensis SidA was subjected to molecular dynamics (MD) simulation and the Clusters and RMSD analyzes showed that the equilibration phase started in 20 ns and stabilized in approximately 60 ns (Additional file 3: Fig. S2 A and B). Cluster 1 was the most relevant, as it remained between 20 ns until the end of the simulation, with no significant differences between the conformational models during this simulation period.

The quality parameters generated through clashscore and MolProbity showed high values for the model prior to MD 12.28 and 3.18, respectively. After the MD, the values were 0 and 1.28, respectively, showing a significant improvement in the quality of the structure, mainly considering the reduction of shocks between the atoms (Additional file 4: Table S2). In the Ramachandran diagrams (Additional file 3: Fig. S2 C and D) we observed a decrease in amino acid residues in non-permitted regions (according to the *phi* and *psi* angles).

The most flexible regions of *P. brasiliensis* SidA, according to the RMSF analysis, and the SidA pockets are shown (Additional file 3: Fig. S2 E and F). It is worth mentioning that the unstable regions highlighted in the RMSF do not correspond to the regions of the catalytic site. As the structural analyzes showed a high-quality for *P. brasiliensis* SidA model, this structure could be used for other structure-based approaches. Thus, the analysis

of the molecular structure, suggests that SidA binds to L-ornithine as a substrate, and this reaction depends on NADPH and FAD.

Expression and enzyme activity of SidA upon FOB exposure

Once the functionally of *P. brasiliensis* SidA was supported through molecular modelling, the effects of FOB treatment over *P. brasiliensis* was thorough examined. The transcript levels of *sidA* were evaluated in the presence of FOB. Notably, *sidA* transcripts were down regulated at 6 and 24 h in FOB condition when compared to to iron starvation condition (BPS) (Fig. 1a). Additionally, the enzymatic activity of SidA decreased in *P. brasiliensis* yeast cells grown in the presence of FOB (iron loaded siderophore) (Fig. 1b), poiting for a correlation between transcript levels and enzyme amount. The data strongly suggested that the presence of an exogenous siderophore represses the biosynthesis of endogenous siderophores, since the fungus can be using Fe^{3+} attached to the xenosiderophore as an alternative iron source.

SidA recombinant protein and polyclonal antibodies production allows the identification of SidA in yeast cells

The levels of SidA in *P. brasiliensis* cells were evaluated by western blotting with antibodies raised against recombinant SidA (rSidA). *P. brasiliensis* SidA protein was expressed in *E. coli* Rosetta (DE3) and rendered a protein with molecular mass of 79.5 kDa, corresponding to 53.5 kDa of SidA fused to 26 kDa of GST-tag (Fig. 2a). Following induction with IPTG, polyacrylamide gel pieces containing the recombinant protein were subjected to in-gel protein digestion for identification by LC-MS/MS approach; that confirmed the recombinant protein as SidA (Additional file 5: Fig. S3 and Additional file 6: Table S3). Immunoblotting results showed a decreased level of SidA in FOB-treated yeast cells when compared to BPS (Fig. 2b), corroborating the results obtained at transcript level. For loading control, membranes containing the same samples as in B were incubated with anti-*Pb*enolase polyclonal antibodies (Fig. 2c).

Label free proteomic analysis reveals that SidA is repressed in yeast cells grown in the presence of FOB

Proteomic analysis of *P. brasiliensis* yeast cells in presence of FOB and BPS was performed to evaluate alterations in the protein profile between both conditions. It was identified 431 and 475 proteins in BPS or FOB, respectively, in both time points, of 6 and 24 h (data not shown). Table 1 features the identified proteins, related to the synthesis of siderophores, which include those down and non-regulated. Proteins such as arginase (PADG_00637), ornithine aminotransferase (PADG_01328), glutamate-5-semialdehyde dehydrogenase (PADG_05337), NADP-specific glutamate dehydrogenase (PADG_04516), arginosuccinate synthase (PADG_00888), hydroxymethylglutaryl-CoA lyase (PADG_07031) and acetyl-CoA acetyltransferase (PADG_2751), which are related to the synthesis of ornithine, arginine and acetyl-CoA, respectively, were identified in the proteome. Notably, only SidA was down regulated after 24 h of incubation with FOB (Fig. 3 and Table 1).

Characterization of *sidA* silenced strains

The data obtained from gene expression, enzymatic activity, proteome and molecular modeling of SidA point to the function of this protein in *P. brasiliensis* as an

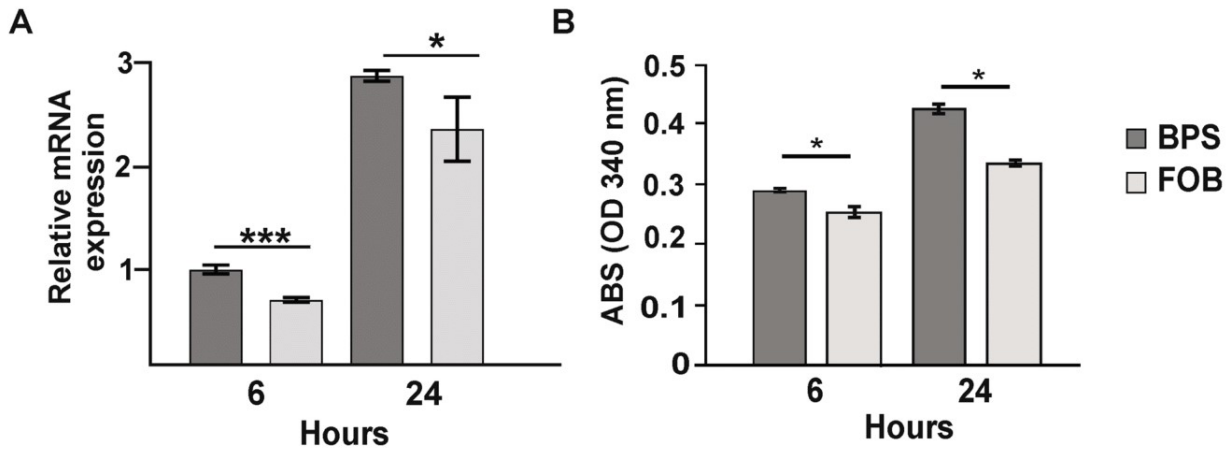

Fig. 1 Expression of the transcript and enzymatic activity of *P. brasiliensis* SidA. **a** Relative expression of the *sidA* was analyzed in *P. brasiliensis* yeast cells grown for 6 and 24 h in presence of FOB (10 μM) or BPS (50 μM). Data were normalized to the gene encoding the 28 kDa ribonucleoprotein (GenBank XP_015701336). **b** To determine expression in the presence of FOB the enzymatic activity of SidA (L-ornithine-N^5-oxygenase) was evaluated after growth of *P. brasiliensis* yeast cells in the presence of FOB or BPS. Results were obtained by absorbance at 340 nm. Student's t test was used for statistical comparisons in both assays. Error bars represent standard deviation of three experimental replicates while *** demonstrate $p \leq 0.0005$ and * represents $p \leq 0.05$

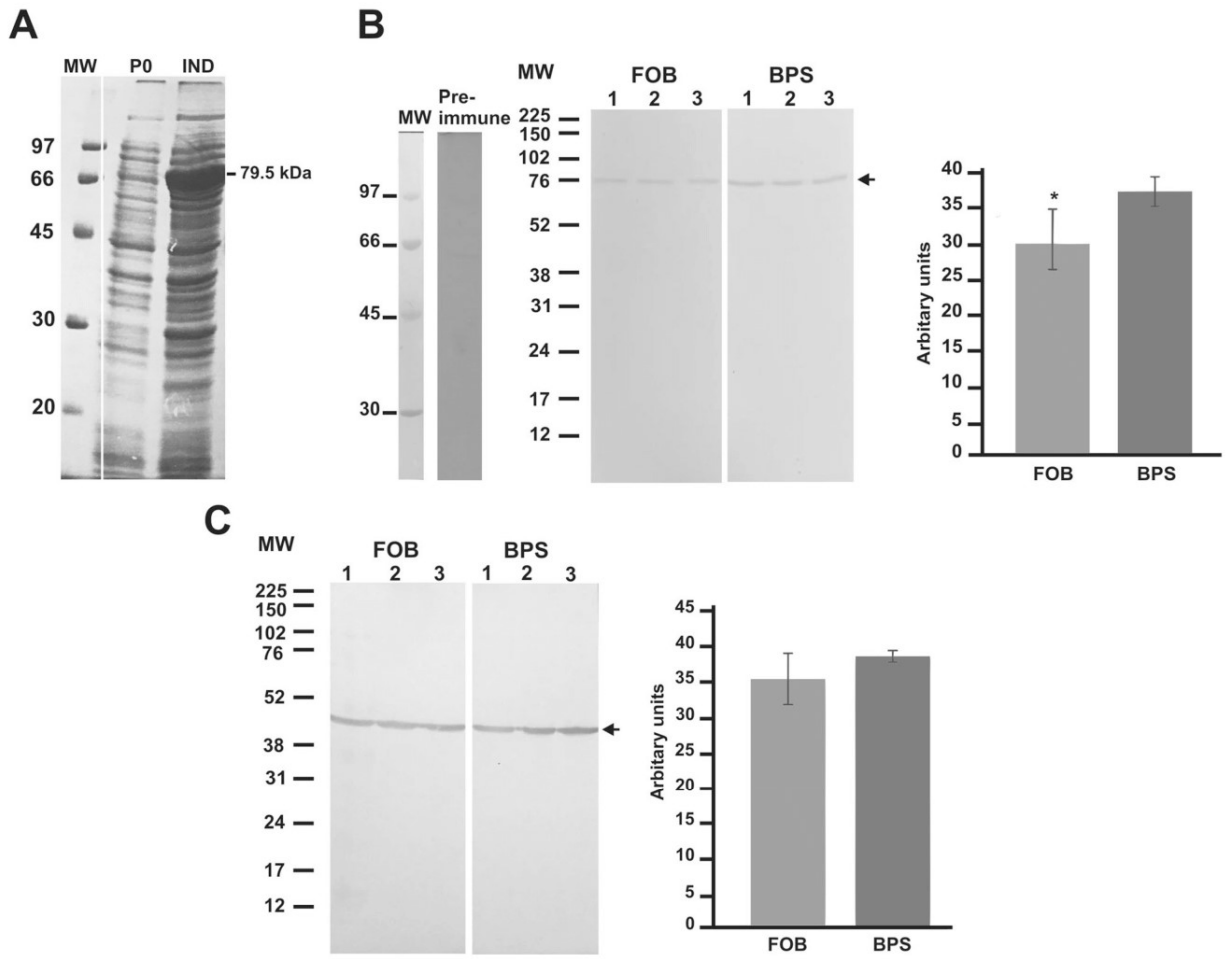

Fig. 2 Expression of the recombinant protein SidA and immunoblotting analysis. **a** SDS-PAGE of SidA expression by *E. coli* Rosetta (DE3). 79.5 kDa corresponds to 53.5 kDa of SidA fused to 26 kDa of GST-tag. **b** Membranes containing extracts of cytoplasmic proteins of *P. brasiliensis* cultivated in FOB or BPS for 24 h were incubated with pre-immune sera and anti-*Pb*SidA polyclonal antibodies. The native SidA protein presents a molecular mass of 53.5 kDa (black arrow). **c** Membranes with the same extracts described above were incubated with anti-*Pb*enolase polyclonal antibodies. The pixel intensity of the immunoblotting bands was analyzed using the ImageJ 1.51 software and expressed as arbitrary units. The Student's t test was used for statistical analysis. Error bars represent standard deviation of the experimental triplicate* $p \leq 0.05$. MW: molecular weight marker. P0: *E. coli* before IPTG induction. IND: *E. coli* after IPTG induction (1 mM IPTG for 2 h)

enzyme directly involved with the production of siderophores. Therefore, knockdown strains were constructed to determine the SidA role in *P. brasiliensis*. For that, it was used the antisense RNA technology, Fig. 4a depicts the *sidA* knockdown T-DNA cassette. This methodological approach provided *sidA*-knocked-down strains in *P. brasiliensis* yeast cells as demonstrated by qRT-PCR (Fig. 4b). The silencing percentage of six randomly selected clones ranged from 78 to 91% compared to those transformed with empty vector. *AsSidA* mutants grow similarly to the wild type and empty vector clones in MMcM medium supplemented with iron until 192 h. In addition, cells remained viable during the entire time growth (Fig. 4c).

sidA silenced strains present reduced siderophore production

Silenced clones were subjected to iron deprivation and subsequently subjected to O-CAS assay. As expected, in iron scarcity, WT and EV strains are still able to produce siderophores, while theknockdown strains (*AsSidA4* and *AsSidA5*) displayed a reduced production of these compounds (Fig. 5a). Furthermore, the siderophore production was evaluated in WT and *AsSidA5* strains after 5 days of growth in iron deprivation and in different iron concentrations (Fig. 5b). There was a pronounced decrease in siderophores production in *AsSidA5* strain in presence and absence of iron.

Table 1 Proteins related to the biosynthesis of siderophores identified in proteomic analysis

Accession number[a]	Description[b]	Time Point[c]	Score[d]
PADG_00637	Arginase (325 aa)	6 h	1131.29
PADG_00637	Arginase (325 aa)	24 h	1171.88
PADG_01328	Ornithine aminotransferase (461 aa)	6 h	2299.86
PADG_01328	Ornithine aminotransferase (461 aa)	24 h	1175.4
PADG_00888	Argininosuccinate synthase (416 aa)	6 h	3507.13
PADG_00888	Argininosuccinate synthase (416 aa)	24 h	4840.6
PADG_07031	Hydroxymethylglutaryl-CoA lyase (357 aa)	6 h	2406.52
PADG_07031	Hydroxymethylglutaryl-CoA lyase (357 aa)	24 h	2627.2
PADG_05337	Glutamate-5-semialdehyde dehydrogenase (457 aa)	6 h	1209.7
PADG_05337	Glutamate-5-semialdehyde dehydrogenase (457 aa)	24 h	771.05
PADG_04516	NADP-specific glutamate dehydrogenase (460 aa)	24 h	501.85
PADG_02751	Acetyl-CoA acetyltransferase (400 aa)	6 h	4328.06
PADG_02751	Acetyl-CoA acetyltransferase (400 aa)	24 h	3019.16
PADG_00097	L-ornithine-N^5-monooxigenase (475 aa)[e]	24 h	360.99

[a, b] Accession number and description of protein according to database of *Paracoccidioides* spp.(http://www.uniprot.proteomes/)
[c] Time of treatment with FOB
[d] Protein score obtained from MS data using the PLGS
[e] Regulated Protein

SidA can be a putative virulence factor in *P. brasiliensis*

Since it was the first virulence study of the effects of *P. brasiliensis* over *T. molitor* through intra-hemocoel injection, it was necessary to standardize the amount of cells needed to accomplish a successful infection in the larvae. First, only yeast cells of WT strain were employed to perform the standardization, followed by mutant analysis (EV and *AsSidA* strains). Thus, different concentrations of *P. brasiliensis* cells (1×10^5, 1×10^6 or 2×10^6) were inoculated in *T. molitor* larvae. As expected, larvae inoculated with *P. brasiliensis* cells showed an increase in the mortality rate as the fungus concentration also increased. The concentrations of 1×10^5 cells was not enough to kill all *T. molitor* larvae, which showed a survival rate of 75% after 10 days of infection. Furthermore, 1×10^6 cells of *P. brasiliensis* were not able to kill all larvae, presenting a survival rate of 57% after 10 days. In light of these results, an ideal concentration of 2×10^6 cells was chosen. This concentration led to 100% mortality after 7 days post infection (Fig. 6a).

Once the ideal cell concentration was established, the ability of the *AsSidA* strains (*AsSidA4* and *AsSidA5*) to kill the *T. molitor* larvae was evaluated, comparing with WT and EV strains (Fig. 6b). Larvae infected with EV had a survival rate of only 4% after 10 days of infection, while larvae infected with *AsSidA* mutant strains had a

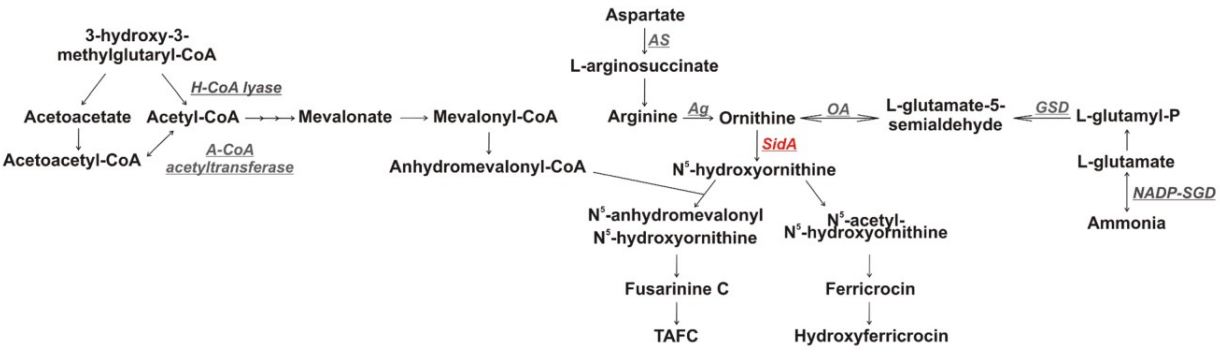

Fig. 3 Proteins related to siderophore synthesis identified in the proteome. AS**:** Argininosuccinate synthase (PADG_00888). Ag: Arginase (PADG_00637). OA: Ornithine aminotransferase (PADG_01328). GSD: Glutamate-5-semialdehyde dehydrogenase (PADG_05337). NADP-SGD: NADP-specific glutamate dehydrogenase (PADG_04516). H-CoA L: Hydroxymethylglutaryl-CoA lyase (PADG_07031). A-CoA AT: Acetyl-CoA acetyltransferase (PADG_02751). SidA: L-ornithine-N^5-monooxigenase (PADG_00097). The red color represents the repressed enzyme

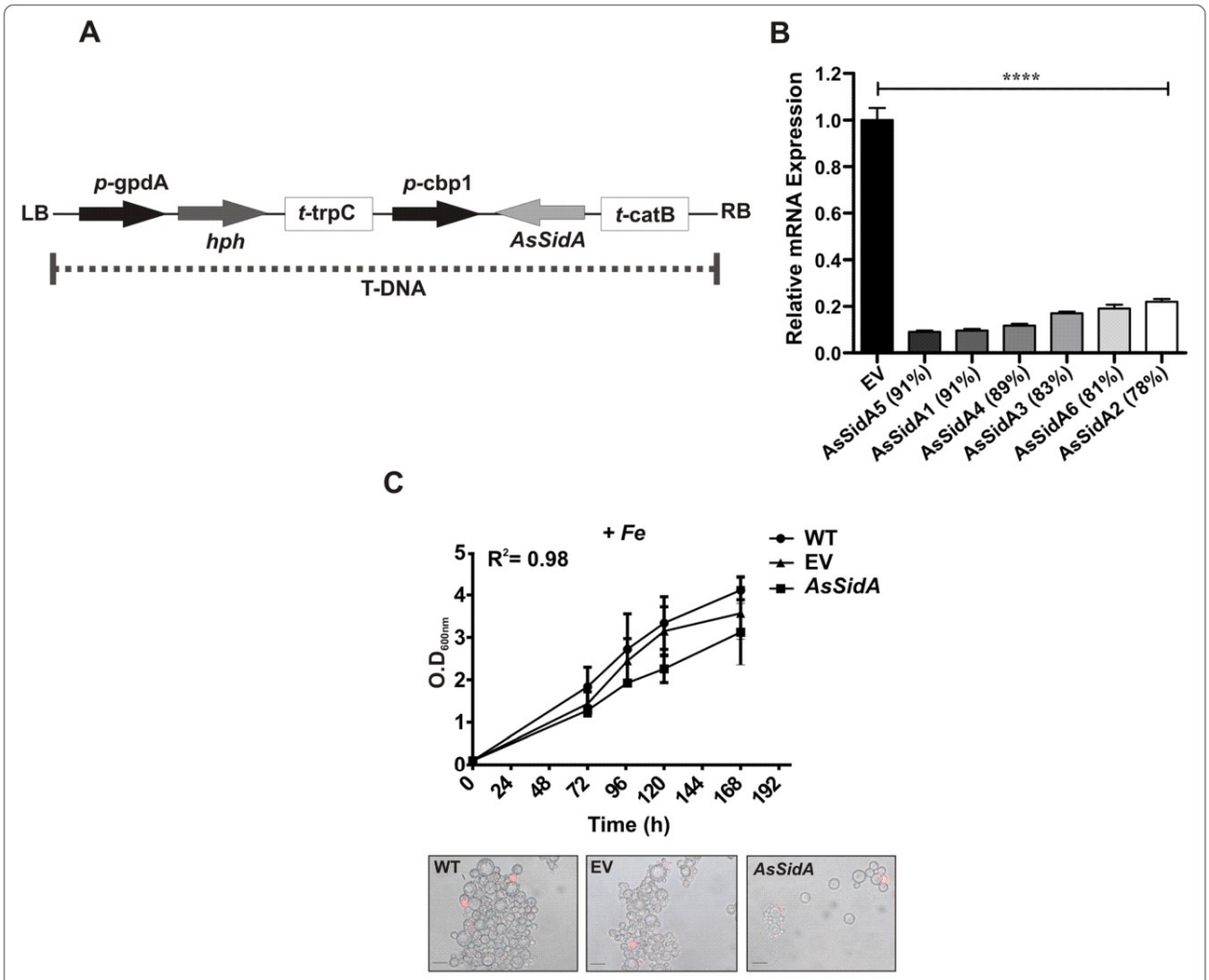

Fig. 4 aRNA silencing of *sidA* gene via *A. tumefaciens*-mediated transformation (ATMT) in *P. brasiliensis*. **a** Schematic representation of the T-DNA cassette. The cassette is as following: *sidA* antisense fragment was placed under control of the calcium binding protein (*p*-cbp1) promoter of *H. capsulatum* and the terminator (*t*-catB) of *A. fumigatus*. The selection marker, was hygromycin B phosphotransferase (HPH), under control of glyceraldehyde 3-phosphate dehydrogenase of *A. nidulans* (*p*-gpdA) with the terminator (*t*-trpC) of *A. nidulans*. **b** Relative quantification performed by qRT-PCR to confirm the gene silencing level in clones transformed with *Pb*SidA-aRNA. The transcript level of *Pb*WT transformed with the empty vector (EV) was also quantified and used as control. The actin gene (XP_010761942) was used as the endogenous control. The Student's t-test was used for statistical comparisons. **** $p < 0.0005$. **c** Growth and viability of *P. brasiliensis* WT, EV and *AsSidA* strains. Yeasts strains were cultivated in McMM supplemented with 30 μM $FeSO_4$ at 37 °C for 192 h. Growth curve profiles were determined by optical density, at a wavelength of 660 nm. Viability was accessed by staining of yeast cells with propidium iodide at 1 μg/ml on the last day of the growth curve. The images were obtained using an Axioscope A1 microscope (Carl Zeiss AG, Germany) and photographed at 493/636 nm

statistically significant reduction in larvae mortality, with a survival rate of 16 and 18%, respectively. These results point that the silencing of *SidA* affects the pathogenesis of *P. brasiliensis*, further supporting the role of siderophores on *Paracoccidioides* infection process.

DISCUSSION

SidA is an enzyme specific for hydroxylation of ornithine, a precursor molecule of ferricrome siderophores biosynthesis (Chocklett and Sobrado 2010). The three-dimensional structure of SidA in *A. fumigatus* demonstrates the presence of amino acid residues essential for both NAPDH association and ornithine binding and hydroxylation (Robinson et al. 2015; Robinson et al. 2014). In this sense, SidA structure from *P. brasiliensis* was studied since the capacity of ornithine hydroxylation and use of NADPH as cofactor are specific to this enzyme (Chocklett and Sobrado 2010), which are influenced by the amino acids present in its structure (Robinson et al. 2014; Robinson et al. 2015). The characterization of the three-dimensional SidA structure of *P. brasiliensis* was performed by molecular modeling based on *A. fumigatus* crystal, which is most similar structure available (Sanchez

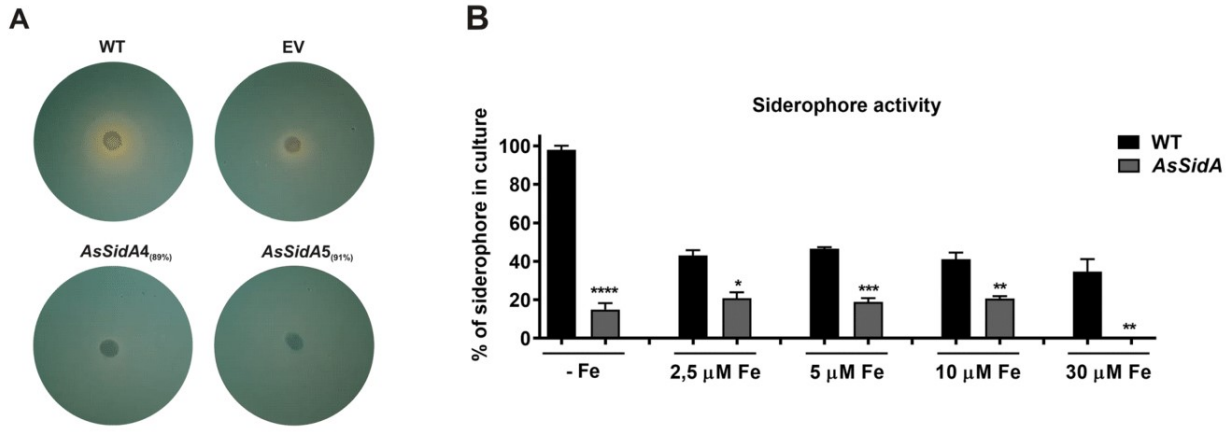

Fig. 5 Production of siderophores in *sidA* silenced strains. **a** Wild type (WT), empty vector (EV) and silenced sidA (*AsSid4* and *AsSid5*) strains were grown in iron limited MMcM for 5 days. Following, the O-CAS plate assay was performed. The presence of secreted siderophores induces the formation of an orange halo. **b** After 5 days of growth in iron limited MMcM liquid medium or in MMcM added of different concentrations of inorganic iron, the percentage of siderophores produced by different strains was verified by the CAS liquid assay. Control of the reaction was performed by incubating the culture medium with CAS without fungal cells. The presence of siderophores was compared spectrophotometrically with the values obtained in the control by the values obtained from the supernatant of the different cultures. The results were presented in percentage. Statistical analysis was performed by Student's t test. Error bars represent standard deviation of three experimental replicates while *** demonstrates $p \leq 0.0005$, ** $p \leq 0.005$ and * $p \leq 0.05$

et al. 2017). The amino acids from the active site ASN, SER and LYS coordinate L-ornithine in the pocket so that it can interact with NADPH and FAD. In *A. fumigatus*, mutations targeting residues in the L-ornithine binding site altered the substrate coupling and the kinetic parameters of the reaction. Among all mutations analyzed, alterations in LYS107, which corresponds to LYS88 in *P. brasiliensis*, led to important changes in the enzymatic kinetics and, therefore, it was considered the most important amino acid involved in enzymatic kinetics (Kosman 2003). Thus, molecular structure data confirm that the active site of *P. brasiliensis* SidA is conserved and has similar interaction residues when compared to *A. fumigatus* SidA.

We have previously demonstrated that members of the *Paracoccidioides* complex can use the heterologous siderophore ferrioxamine B (FOB) as an iron source and produce siderophores when grown in iron starvation conditions (Silva-Bailao et al. 2014). In an attempt to investigate the connection between siderophore biosynthesis and FOB utilization, experiments were conducted to demonstrate the repression of *sidA* when *P. brasiliensis* was incubated with FOB. In addition, SidA accumulation, at both transcriptional and proteomic level, and the cognate enzymatic activity were reduced in cells cultured in the presence of FOB, when compared to cells growing

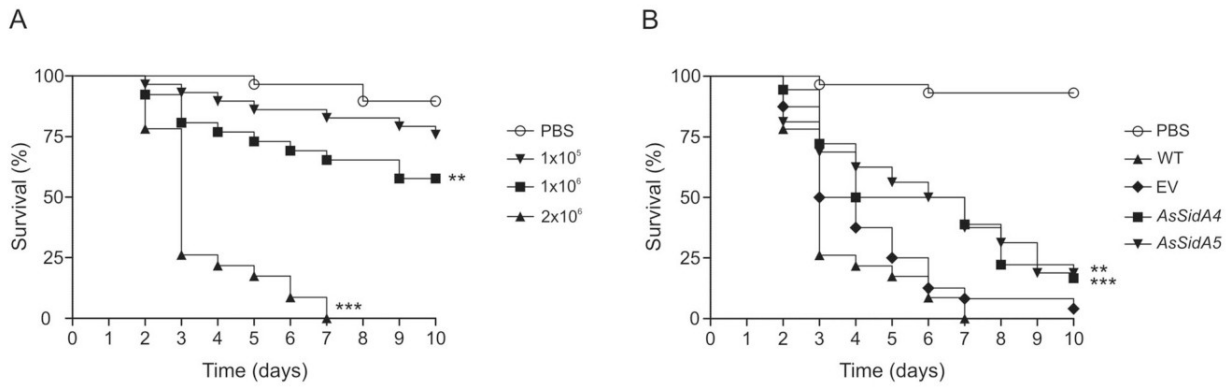

Fig. 6 Survival curves of *T. molitor* infected with *P. brasiliensis* yeast strains. *T. molitor* larvae were infected with different concentrations of *P. brasiliensis* yeast cells of WT strain (**a**) and with 2×10^6 yeast cells of the WT, EV and *AsSidA* mutant strains (*AsSidA4* and *AsSidA5*) (**b**). As a control, the larvae were inoculated with PBS only. The experiments were carried with a total of 30 larvae for each condition analyzed in a period of 10 days. The survival of *T. molitor* larvae is shown as a percentage. (*** $p < 0.0005$, ** $p < 0.005$ and * $p < 0.05$)

in iron depleted medium. Similar results employing xenosiderophores were described for *Candida albicans, Saccharomyces cerevisiae* and *A. nidulans* (Heymann et al. 2002; Haas 2003; Philpott and Protchenko 2008).

In order to better explore the impact of FOB over *P. brasiliensis* growth a proteomic analysis was performed. Data allowed the identification of several proteins involved in siderophores biosynthesis. Notably, the decrease of SidA levels in presence of FOB was the most glaring result. Thus, all the data obtained in this study demonstrate that, in the presence of FOB, SidA is repressed both transcriptionally and translationally, and evidences the siderophore biosynthesis pathway in *P. brasiliensis*.

To confirm the function of SidA in the production of siderophores and the role of this protein in the biology of *P. brasiliensis*, we silenced the *sidA* gene by using antisense RNA technique. The same system was already reported to obtain *P. brasiliensis* silenced clones for proteins playing relevant roles in the fungal pathobiology, e.g., Cdc42p (Almeida et al. 2009), *Pb*HAD32 (Hernandez et al. 2010), *Pb*Rbt5 (Bailao et al. 2014), *Pb*ccp (Parente-Rocha et al. 2015), *Pb*14–3-3 (Marcos et al. 2016), and *Pb*PCN (Fernandes et al. 2017). Here we have successfully obtained knockdown strains for *PbsidA*, as demonstrated by qRT-PCR.

As silencing of *sidA* gene did not impair fungal growth in regular culture media, the phenotypic characterization of this gene was performed employing iron deprivation conditions. The qualitative O-CAS assay showed that production of siderophores in the knockdown strains was diminished when compared to the WT and EV strains. Furthermore, a semi-quantitative CAS liquid assay also highlighted the diminished production of siderophores with and without iron.

Although murine models are valuable tools for in vivo infection studies, invertebrate models are becoming prominent alternatives. The ethical reasons linked to vertebrate models, as well as the high costs for animal management have propelled the examination of viable substitutes (Wilson-Sanders 2011). Several studies have demonstrated the use of *Galleria mellonella* larvae to characterize the infection process in pathogenic fungi, such as *Histoplasma capsulatum, C. albicans, Cryptococcus neoformans* and *P. brasiliensis* (Thomaz et al. 2013; Vargas et al. 2015; Bouklas et al. 2015; Scorzoni et al. 2015; Marcos et al. 2019). However, *G. mellonella* is an animal that requires almost daily handling, as well as these insects are not sold worldwide (Jorjao et al. 2018). An alternative that has been explored are larvae of *T. molitor*, an animal that is easy to handle, is marketed by several suppliers and is a low cost insect. Furthermore, the *T. molitor* larvae have been standardized as an in vivo infection model for several fungal pathogens as *C. albicans, C. neoformans, Malassezia furfur* and *Fonsecaea pedrosoi* (de Souza et al. 2015; Silva et al. 2018; Fornari et al. 2018). Here, we explored the application of *T. molitor* as an invertebrate infection model for *P. brasiliensis*. Noteworthy, increasing the viable cell concentration in the inoculum also increases *T. molitor* larvae mortality. The same observations can be draw for *C. albicans* and *C. neoformans*, demonstrating that this model is efficient for assessing the virulence of pathogenic fungi (de Souza et al. 2015).

Metal restriction is one of the several mechanisms employed by host cells to inhibit microbial development (Ganz 2016; Ganz 2018; Brechting and Rappleye 2019). Thus, the presence of a high affinity iron acquisition systems appears to be an essential strategy to circumvent the absence of this metal during growth in a hostile environment (McDonagh et al. 2008; Hilty et al. 2011; Pasricha et al. 2016; Kalidasan et al. 2018). In several fungal pathogens, siderophores are important for virulence and host-pathogen interaction (Heymann et al. 2002; Schrettl et al. 2004; Schrettl et al. 2010; Nevitt and Thiele 2011). For example, in *H. capsulatum*, the deletion of *sid1*, the homologue of *sidA* of *A. fumigatus*, promoted decreasing of siderophore production, resulting in diminished proliferation inside macrophages and murine pulmonary colonization (Hwang et al. 2008). Similarly, previous results pointed for a putative role of these molecules in pathogenesis of *P. brasiliensis*, since the expression of sidA was highly induced during fungal infection to macrophages (Silva-Bailao et al. 2014). The bioassays conducted here with *AsSidA* mutants support a main role of siderophores in the infection process of *Paracoccidioides* species. *AsSidA* mutants presented reduced virulence to *T. molitor* larvae, reasserting the importance of iron for host colonization.

CONCLUSIONS

Although previous results pointed that *P. brasiliensis* harbors a complete pathway for siderophore production several aspects about SidA regulation and activity were still to be determined. The molecular modelling, here employed, helped to highlight structural similarities between *A. fumigatus* SidA and *P. brasiliensis* SidA. Furthermore, the expression of SidA is repressed, at transcriptional and translational levels, in the presence of a xenosiderophore FOB. Moreover, *sidA* silencing in blocks the production of siderophores and promotes decrease in fungal virulence *P. brasiliensis*. Due to the relevance of iron for fungal survival inside the host, strategies aiming to block siderophore biosynthesis can be successful, helping to eliminate the infection. In this way, future studies will focus on molecules capable to block SidA activity.

Supplementary information

Supplementary information accompanies this paper at https://doi.org/10.1186/s43008-020-00035-x.

Additional file 1: Figure S1. Molecular structure of L-ornithine-N^5-monooxygenase. (A) *Af*SidA from *Aspergillus fumigatus* PDBID: 4B63 (gray)

and *Pb*SidA (blue) alignment using the Pymol viewer, evidencing the interactions among L-ornithine, FAD and NADPH. (B) Amino acid residues of *P. brasiliensis* SidA described as mainly involved in the interaction with L-ornithine and (C) cofactors are essential for the maintenance of them in the active site.

Additional file 2: Figure S2. Molecular dynamics of *P. brasiliensis* SidA. (A) Cluster and (B) RMSD graphs. It is observed that the stability starts at approximately 20 ns and that the most representative conformational mode of the trajectory is cluster 1. (C) Ramachandran diagrams of the three-dimensional model of SidA before molecular dynamics and (D) after molecular dynamics. (E) RMSF graph showing the more flexible residues (red) along the molecular dynamics. (F**)** Three-dimensional structure of SidA showing the most flexible regions (red) and pockets of the active site (green and orange).

Additional file 3: Figure S3. Characterization of the recombinant protein. MS/MS spectrum of the recombinant protein SidA identified by mass spectrometry.

Additional file 4: Table S1. Oligonucleotides used in this study.

Additional file 5: Table S2. Analysis of the quality of the SidA models through the Molprobity server.

Additional file 6: Table S3.

Acknowledgements
We thank the CAPES, CNPq and FAPEG for providing fellowships to MG Silva JS de Curcio, MV Tomazett, AF Souza, VRMC Leite and RM Lima. We also thank Dr. Augusto Schrank for the helpful suggestions.

Adherence to national and international regulations
Not applicable.

Authors' contributions
CMA Soares and MG Silva conceived and designed the experiments. MG Silva, JS de Curcio, MV Tomazett, AF Souza, VRMC Leite, RM Lima, N Sbaraini and RA Gonçales performed the experiments. MG Silva, JS de Curcio, MGS Bailão, AM Bailão, and CMA Soares analyzed and/or interpreted the data. M Pereira, F Rodrigues and CMA Soares contributed with reagents and materials. MG Silva, JS de Curcio, MGS Bailão and CMA Soares wrote the manuscript. The authors read and approved the final manuscript.

Funding
CMAS and MP are fellows from Conselho Nacional de Desenvolvimento Científico e Tecnológico (CNPq). MT and VRMCL is a fellow from Fundação de Amparo à Pesquisa do Estado de Goiás (FAPEG). RAG was supported by Coordenação de Aperfeiçoamento de Pessoal de Nível Superior (CAPES; grant: 88887.333726/2019–00). FR was supported by the Northern Portugal Regional Operational Programme (NORTE 2020), under the Portugal 2020 Partnership Agreement, through the European Regional Development Fund (FEDER) (NORTE-01-0145-FEDER-000013). This work was supported by grants from Conselho Nacional de Desenvolvimento Científico e Tecnológico (CNPq) and Fundação de Amparo à Pesquisa do Estado de Goiás (FAPEG)-Instituto Nacional de Ciência e Tecnologia (INCT) de Estratégias de Interação Patógeno-Hospedeiro.

Availability of data and materials
Not applicable.

Ethics approval and consent to participate
All the animal work carried out in accordance with the ethical principles of animal research adopted by the Brazilian Society of Laboratory Animal Science and a Brazilian Federal Law 11.749 (October 2008).

Consent for publication
Not applicable.

Competing interests
The authors declare that they have no competing interests.

Author details
[1]Laboratório de Biologia Molecular, Instituto de Ciências Biológicas, ICB II, Campus II, Universidade Federal de Goiás, Goiânia, GO, Brazil. [2]Programa de Pós-graduação em Patologia Molecular, Faculdade de Medicina, Universidade de Brasília, Brasília, DF 70910-900, Brazil. [3]Centro de Biotecnologia, Programa de Pós-graduação em Biologia Celular e Molecular, Universidade Federal do Rio Grande do Sul, Porto Alegre, RS, Brazil. [4]Life and Health Sciences Research Institute (ICVS), School of Medicine, University of Minho, Braga, Portugal. [5]ICVS/3B's - PT Government Associate Laboratory, Braga/Guimarães, Portugal.

Received: 30 January 2020 Accepted: 11 June 2020
Published online: 29 June 2020

References
Almeida AJ, Carmona JA, Cunha C, Carvalho A, Rappleye CA, Goldman WE et al (2007) Towards a molecular genetic system for the pathogenic fungus *Paracoccidioides brasiliensis*. Fungal Genet Biol 44(12):1387–1398

Almeida AJ, Cunha C, Carmona JA, Sampaio-Marques B, Carvalho A, Malavazi I et al (2009) Cdc42p controls yeast-cell shape and virulence of *Paracoccidioides brasiliensis*. Fungal Genet Biol 46(12):919–926

Baeza LC, da Mata FR, Pigosso LL, Pereira M, de Souza G, Coelho ASG et al (2017) Differential metabolism of a two-carbon substrate by members of the *Paracoccidioides* genus. Front Microbiol 8:2308

Bailao EF, de Lima PS, Silva-Bailao MG, Bailao AM, Fernandes Gda R, Kosman DJ et al (2015) *Paracoccidioides* spp. ferrous and ferric iron assimilation pathways. Front Microbiol 6:821

Bailao EF, Parente JA, Pigosso LL, Castro KP, Fonseca FL, Silva-Bailao MG et al (2014) Hemoglobin uptake by *Paracoccidioides* spp. is receptor-mediated. PLoS Negl Trop Dis 8(5):e2856

Bailão EFLC, Parente AFA, Parente JA, Silva-Bailão MGS, Castro KP, Kmetzsch L et al (2012) Metal acquisition and homeostasis in fungi. Curr Fungal Infect Rep 6:257–266

Blatzer M, Schrettl M, Sarg B, Lindner HH, Pfaller K, Haas H (2011) SidL, an *Aspergillus fumigatus* transacetylase involved in biosynthesis of the siderophores ferricrocin and hydroxyferricrocin. Appl Environ Microbiol 77(14):4959–4966

Bookout AL, Cummins CL, Mangelsdorf DJ, Pesola JM, Kramer MF (2006) High-throughput real-time quantitative reverse transcription PCR. Curr Protoc Mol Biol Chapter 15(15.8):1–28

Bouklas T, Diago-Navarro E, Wang X, Fenster M, Fries BC (2015) Characterization of the virulence of *Cryptococcus neoformans* strains in an insect model. Virulence 6(8):809–813

Bradford MM (1976) A rapid and sensitive method for the quantitation of microgram quantities of protein utilizing the principle of protein-dye binding. Anal Biochem 72:248–254

Brechting PJ, Rappleye CA (2019) Histoplasma responses to nutritional immunity imposed by macrophage activation. J Fungi (Basel) 5(2):45

Canessa P, Larrondo LF (2013) Environmental responses and the control of iron homeostasis in fungal systems. Appl Microbiol Biotechnol 97(3):939–955

Chen VB, Arendall WB 3rd, Headd JJ, Keedy DA, Immormino RM, Kapral GJ et al (2010) MolProbity: all-atom structure validation for macromolecular crystallography. Acta Crystallogr D Biol Crystallogr 66(Pt 1):12–21

Chocklett SW, Sobrado P (2010) *Aspergillus fumigatus* SidA is a highly specific ornithine hydroxylase with bound flavin cofactor. Biochemistry 49(31):6777–6783

Cox CD (1994) Deferration of laboratory media and assays for ferric and ferrous ions. Methods Enzymol 235:315–329

de Souza P, Custodio Caloni C, Wilson D, Sergio Almeida R (2018) An invertebrate host to study fungal infections, mycotoxins and antifungal drugs: *Tenebrio molitor*. J Fungi (Basel) 4(4):125

de Souza PC, Morey AT, Castanheira GM, Bocate KP, Panagio LA, Ito FA et al (2015) *Tenebrio molitor* (Coleoptera: Tenebrionidae) as an alternative host to study fungal infections. J Microbiol Methods 118:182–186

Fernandes FF, Oliveira AF, Landgraf TN, Cunha C, Carvalho A, Vendruscolo PE et al (2017) Impact of Paracoccin gene silencing on *Paracoccidioides brasiliensis* virulence. MBio 8(4):e00537–e00517

Fornari G, Gomes RR, Degenhardt-Goldbach J, Dos Santos SS, de Almeida SR, Dos Santos GD et al (2018) A model for trans-kingdom pathogenicity in *Fonsecaea* agents of human Chromoblastomycosis. Front Microbiol 9:2211

Franceschini S, Fedkenheuer M, Vogelaar NJ, Robinson HH, Sobrado P, Mattevi A (2012) Structural insight into the mechanism of oxygen activation and substrate selectivity of flavin-dependent N-hydroxylating monooxygenases. Biochemistry 51(36):7043–7045
Ganz T (2009) Iron in innate immunity: starve the invaders. Curr Opin Immunol 21(1):63–67
Ganz T (2016) Macrophages and iron metabolism. Microbiol Spectr 4(5):1–10
Ganz T (2018) Iron and infection. Int J Hematol 107(1):7–15
Geromanos SJ, Vissers JP, Silva JC, Dorschel CA, Li GZ, Gorenstein MV et al (2009) The detection, correlation, and comparison of peptide precursor and product ions from data independent LC-MS with data dependant LC-MS/MS. Proteomics 9(6):1683–1695
Haas H (2003) Molecular genetics of fungal siderophore biosynthesis and uptake: the role of siderophores in iron uptake and storage. Appl Microbiol Biotechnol 62(4):316–330
Haas H, Schoeser M, Lesuisse E, Ernst JF, Parson W, Abt B et al (2003) Characterization of the *Aspergillus nidulans* transporters for the siderophores enterobactin and triacetylfusarinine C. Biochem J 371(Pt 2):505–513
Haas H, Zadra I, Stoffler G, Angermayr K (1999) The *Aspergillus nidulans* GATA factor SREA is involved in regulation of siderophore biosynthesis and control of iron uptake. J Biol Chem 274(8):4613–4619
Haber F, Weiss J (1934) The catalytic decomposition of hydrogen peroxide by iron salts. Proc Royal Soc London 147:332–351
Halliwell B, Gutteridge JM (1984) Oxygen toxicity, oxygen radicals, transition metals and disease. Biochem J 219(1):1–14
Hernandez O, Almeida AJ, Gonzalez A, Garcia AM, Tamayo D, Cano LE et al (2010) A 32-kilodalton hydrolase plays an important role in *Paracoccidioides brasiliensis* adherence to host cells and influences pathogenicity. Infect Immun 78(12):5280–5286
Heymann P, Gerads M, Schaller M, Dromer F, Winkelmann G, Ernst JF (2002) The siderophore iron transporter of *Candida albicans* (Sit1p/Arn1p) mediates uptake of ferrichrome-type siderophores and is required for epithelial invasion. Infect Immun 70(9):5246–5255
Hilty J, George Smulian A, Newman SL (2011) *Histoplasma capsulatum* utilizes siderophores for intracellular iron acquisition in macrophages. Med Mycol 49(6):633–642
Hwang LH, Mayfield JA, Rine J, Sil A (2008) *Histoplasma* requires *SID1*, a member of an iron-regulated siderophore gene cluster, for host colonization. PLoS Pathog 4(4):e1000044
Jorjao AL, Oliveira LD, Scorzoni L, Figueiredo-Godoi LMA, Cristina APM, Jorge AOC et al (2018) From moths to caterpillars: ideal conditions for *Galleria mellonella* rearing for in vivo microbiological studies. Virulence 9(1):383–389
Kalidasan V, Azman A, Joseph N, Kumar S, Awang Hamat R, Neela VK (2018) Putative iron Acquisition Systems in *Stenotrophomonas maltophilia*. Molecules 23(8):2048
Kornitzer D (2009) Fungal mechanisms for host iron acquisition. Curr Opin Microbiol 12(4):377–383
Kosman DJ (2003) Molecular mechanisms of iron uptake in fungi. Mol Microbiol 47(5):1185–1197
Krithika R, Marathe U, Saxena P, Ansari MZ, Mohanty D, Gokhale RS (2006) A genetic locus required for iron acquisition in *Mycobacterium tuberculosis*. Proc Natl Acad Sci U S A 103(7):2069–2074
Lima Pde S, Chung D, Bailao AM, Cramer RA, Soares CM (2015) Characterization of the *Paracoccidioides* hypoxia response reveals new insights into pathogenesis mechanisms of this important human pathogenic fungus. PLoS Negl Trop Dis 9(12):e0004282
Machuca A, Milagres AM (2003) Use of CAS-agar plate modified to study the effect of different variables on the siderophore production by *Aspergillus*. Lett Appl Microbiol 36(3):177–181
Marcos CM, de Silva JF, Oliveira HC, Assato PA, Singulani Jde L, Lopez AM et al (2016) Decreased expression of 14-3-3 in *Paracoccidioides brasiliensis* confirms its involvement in fungal pathogenesis. Virulence 7(2):72–84
Marcos CM, Tamer G, de Oliveira HC, Assato PA, Scorzoni L, Santos CT et al (2019) Down-regulation of TUFM impairs host cell interaction and virulence by *Paracoccidioides brasiliensis*. Sci Rep 9(1):17206
McDonagh A, Fedorova ND, Crabtree J, Yu Y, Kim S, Chen D et al (2008) Sub-telomere directed gene expression during initiation of invasive aspergillosis. PLoS Pathog 4(9):e1000154
McEwen JG, Bedoya V, Patino MM, Salazar ME, Restrepo A (1987) Experimental murine paracoccidiodomycosis induced by the inhalation of conidia. J Med Vet Mycol 25(3):165–175
Menino JF, Almeida AJ, Rodrigues F (2012) Gene knockdown in *Paracoccidioides brasiliensis* using antisense RNA. Methods Mol Biol 845:187–198
Murad AM, Souza GH, Garcia JS, Rech EL (2011) Detection and expression analysis of recombinant proteins in plant-derived complex mixtures using nanoUPLC-MS(E). J Sep Sci 34(19):2618–2630
Neilands JB (1993) Siderophores. Arch Biochem Biophys 302(1):1–3
Nevitt T, Thiele DJ (2011) Host iron withholding demands siderophore utilization for *Candida glabrata* to survive macrophage killing. PLoS Pathog 7(3): e1001322
Nogueira SV, Fonseca FL, Rodrigues ML, Mundodi V, Abi-Chacra EA, Winters MS et al (2010) *Paracoccidioides brasiliensis* enolase is a surface protein that binds plasminogen and mediates interaction of yeast forms with host cells. Infect Immun 78(9):4040–4050
Parente AF, Bailao AM, Borges CL, Parente JA, Magalhaes AD, Ricart CA et al (2011) Proteomic analysis reveals that iron availability alters the metabolic status of the pathogenic fungus *Paracoccidioides brasiliensis*. PLoS One 6(7): e22810
Parente-Rocha JA, Parente AF, Baeza LC, Bonfim SM, Hernandez O, McEwen JG et al (2015) Macrophage interaction with *Paracoccidioides brasiliensis* yeast cells modulates fungal metabolism and generates a response to oxidative stress. PLoS One 10(9):e0137619
Pasricha S, Schafferer L, Lindner H, Joanne Boyce K, Haas H, Andrianopoulos A (2016) Differentially regulated high-affinity iron assimilation systems support growth of the various cell types in the dimorphic pathogen *Talaromyces marneffei*. Mol Microbiol 102(4):715–737
Perez-Miranda S, Cabirol N, George-Tellez R, Zamudio-Rivera LS, Fernandez FJ (2007) O-CAS, a fast and universal method for siderophore detection. J Microbiol Methods 70(1):127–131
Philpott CC, Protchenko O (2008) Response to iron deprivation in *Saccharomyces cerevisiae*. Eukaryot Cell 7(1):20–27
Pronk S, Pall S, Schulz R, Larsson P, Bjelkmar P, Apostolov R et al (2013) GROMACS 4.5: a high-throughput and highly parallel open source molecular simulation toolkit. Bioinformatics 29(7):845–854
Raymond KN, Dertz EA, Kim SS (2003) Enterobactin: an archetype for microbial iron transport. Proc Natl Acad Sci U S A 100(7):3584–3588
Restrepo A (1985) The ecology of *Paracoccidioides brasiliensis*: a puzzle still unsolved. Sabouraudia 23(5):323–334
Restrepo A, Jimenez BE (1980) Growth of *Paracoccidioides brasiliensis* yeast phase in a chemically defined culture medium. J Clin Microbiol 12(2):279–281
Restrepo A, McEwen JG, Castaneda E (2001) The habitat of *Paracoccidioides brasiliensis*: how far from solving the riddle? Med Mycol 39(3):233–241
Rezende TC, Borges CL, Magalhaes AD, de Sousa MV, Ricart CA, Bailao AM et al (2011) A quantitative view of the morphological phases of *Paracoccidioides brasiliensis* using proteomics. J Proteomics 75(2):572–587
Rigsby RE, Parker AB (2016) Using the PyMOL application to reinforce visual understanding of protein structure. Biochem Mol Biol Educ 44(5):433–437
Robinson R, Franceschini S, Fedkenheuer M, Rodriguez PJ, Ellerbrock J, Romero E et al (2014) Arg279 is the key regulator of coenzyme selectivity in the flavin-dependent ornithine monooxygenase SidA. Biochim Biophys Acta 1844(4): 778–784
Robinson R, Qureshi IA, Klancher CA, Rodriguez PJ, Tanner JJ, Sobrado P (2015) Contribution to catalysis of ornithine binding residues in ornithine N5-monooxygenase. Arch Biochem Biophys 585:25–31
San-Blas G, Nino-Vega G, Iturriaga T (2002) *Paracoccidioides brasiliensis* and paracoccidioidomycosis: molecular approaches to morphogenesis, diagnosis, epidemiology, taxonomy and genetics. Med Mycol 40(3):225–242
Sanchez M, Sabio L, Galvez N, Capdevila M, Dominguez-Vera JM (2017) Iron chemistry at the service of life. IUBMB Life 69(6):382–388
Schneider CA, Rasband WS, Eliceiri KW (2012) NIH image to ImageJ: 25 years of image analysis. Nat Methods 9(7):671–675
Schrettl M, Bignell E, Kragl C, Joechl C, Rogers T, Arst HN Jr et al (2004) Siderophore biosynthesis but not reductive iron assimilation is essential for *Aspergillus fumigatus* virulence. J Exp Med 200(9):1213–1219
Schrettl M, Bignell E, Kragl C, Sabiha Y, Loss O, Eisendle M et al (2007) Distinct roles for intra- and extracellular siderophores during *Aspergillus fumigatus* infection. PLoS Pathog 3(9):1195–1207
Schrettl M, Ibrahim-Granet O, Droin S, Huerre M, Latge JP, Haas H (2010) The crucial role of the *Aspergillus fumigatus* siderophore system in interaction with alveolar macrophages. Microbes Infect 12(12–13):1035–1041
Schwyn B, Neilands JB (1987) Universal chemical assay for the detection and determination of siderophores. Anal Biochem 160(1):47–56

Scorzoni L, de Paula e Silva AC, de Singulani JL, Leite FS, de Oliveira HC, da Silva RA et al (2015) Comparison of virulence between *Paracoccidioides brasiliensis* and *Paracoccidioides lutzii* using *Galleria mellonella* as a host model. Virulence 6(8):766–776

Silva APRV, A. D, Viana RO, Ricoy A, C. DS, Johann S, Alves VDS (2018) *Caenorhabditis elegans* and *Tenebrio molitor* - new tools to investigate *Malassezia species* Preprints 1

Silva MG, Schrank A, Bailao EF, Bailao AM, Borges CL, Staats CC et al (2011) The homeostasis of iron, copper, and zinc in *Paracoccidioides brasiliensis*, *Cryptococcus neoformans* var. *grubii*, and *Cryptococcus gattii*: a comparative analysis. Front Microbiol 2:49

Silva-Bailao MG, Bailao EF, Lechner BE, Gauthier GM, Lindner H, Bailao AM et al (2014) Hydroxamate production as a high affinity iron acquisition mechanism in *Paracoccidioides* spp. PLoS One 9(8):e105805

Thomaz L, Garcia-Rodas R, Guimaraes AJ, Taborda CP, Zaragoza O, Nosanchuk JD (2013) Galleria mellonella as a model host to study *Paracoccidioides lutzii* and *Histoplasma capsulatum*. Virulence 4(2):139–146

Tomazett MV, Baeza LC, Paccez JD, Parente-Rocha JA, Ribeiro-Dias F, Soares CMA (2019) Identification and characterization of *Paracoccidioides lutzii* proteins interacting with macrophages. Microbes Infect S1286–4579(19):30046–30042[pii]. https://doi.org/10.1016/j.micinf.2019.03.002

Vargas G, Rocha JD, Oliveira DL, Albuquerque PC, Frases S, Santos SS et al (2015) Compositional and immunobiological analyses of extracellular vesicles released by *Candida albicans*. Cell Microbiol 17(3):389–407

Wilson-Sanders SE (2011) Invertebrate models for biomedical research, testing, and education. ILAR J 52(2):126–152

Yang J, Zhang Y (2015) Protein structure and function prediction using I-TASSER. Curr Protoc Bioinformatics 52:581–515

Zambuzzi-Carvalho PF, Tomazett PK, Santos SC, Ferri PH, Borges CL, Martins WS et al (2013) Transcriptional profile of *Paracoccidioides* induced by oenothein B, a potential antifungal agent from the Brazilian Cerrado plant Eugenia uniflora. BMC Microbiol 13:227

Zhou LW, Haas H, Marzluf GA (1998) Isolation and characterization of a new gene, sre, which encodes a GATA-type regulatory protein that controls iron transport in *Neurospora crassa*. Mol Gen Genet 259(5):532–540

Publisher's Note

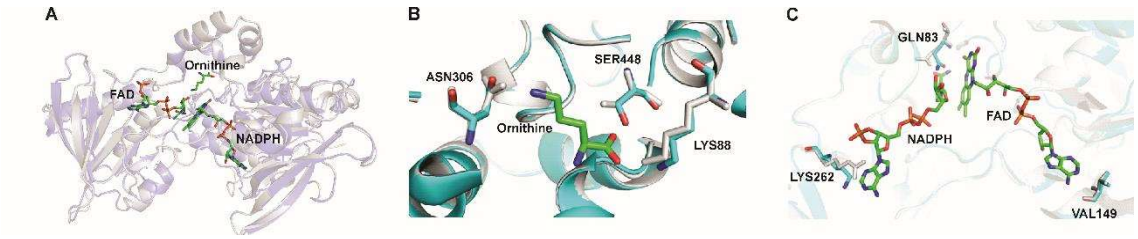

Figure S1: Molecular structure of L-ornithine-N^5-monooxygenase. (A) *Af*SidA from *Aspergillus fumigatus* PDBID: 4B63 (gray) and *Pb*SidA (blue) alignment using the Pymol viewer, evidencing the interactions among L-ornithine, FAD and NADPH. (B) Amino acid residues of *P. brasiliensis* SidA described as mainly involved in the interaction with L-ornithine and (C) cofactors are essential for the maintenance of them in the active site.

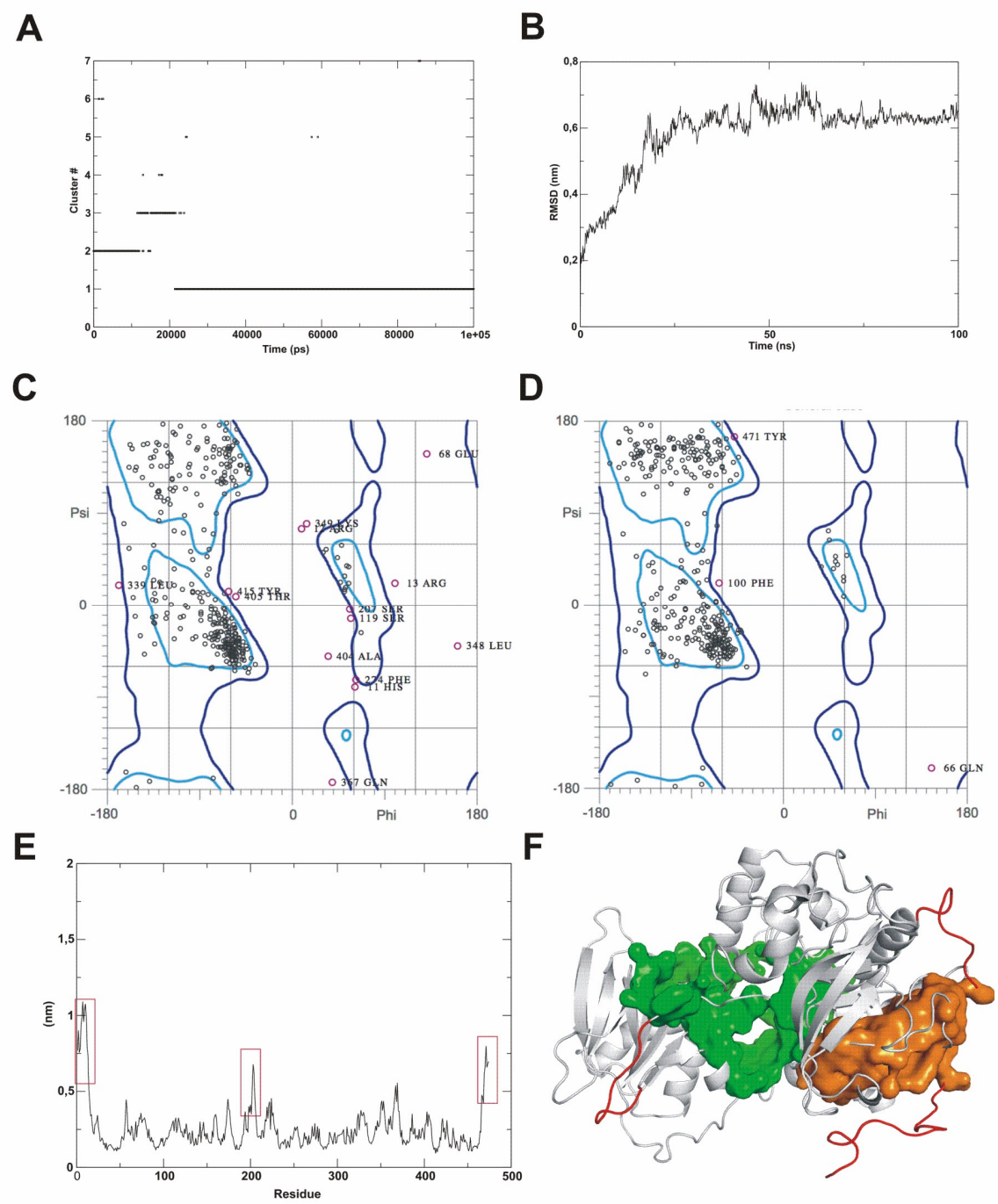

Figure S2: Molecular dynamics of *P, brasiliensis* SidA. **(A)** Cluster and **(B)** RMSD graphs. It is observed that the stability starts at approximately 20 ns and that the most representative conformational mode of the trajectory is cluster 1. **(C)** Ramachandran diagrams of the three-dimensional model of SidA before molecular dynamics and **(D)** after molecular dynamics. **(E)** RMSF graph showing the more flexible residues (red) along the molecular dynamics. **(F)** Three-dimensional structure of SidA showing the most flexible regions (red) and pockets of the active site (green and orange)

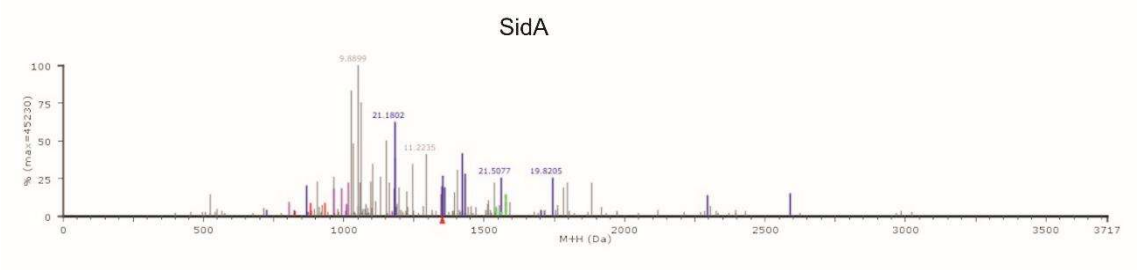

Figure S3: Characterization of the recombinant protein, MS/MS spectrum of the recombinant protein SidA identified by mass spectrometry.

Table S1 Oligonucleotides used in this study

Accession number[a]	Sequence
sidA (PADG_00097)	Foward: 5’ GCGACGATAGCCCATTTGTC 3’
	Reverse: 5’ATTAGCAGGATTAGGATCAAGG 3’
Actin (XP_010761942)	Foward: 5’ CGTCCTCGCCATCATGGTAT 3’
	Reverse: 5’ TCTCCATATCATCCCAGTTCG 3’
28 kDa	Foward: 5’ GAAAGGGTTCGGCTACGTTG 3’
ribonucleoportein	Reverse: 5’ ATCTCTGGGGGCAGCATTTG 3’
(XP_015701336)	
rSidA* (PADG_00097)	Foward:
	5’ GGTTCCGCGTGGATCCATGGAGACCGTTATCAAGAA 3’
	Reverse:
	5’ GTCGACCCGGGAATTCCTATAGTCGTGCGTAATTCT 3’

[a] Accession numbers according to database of *Paracoccidioides* spp,. (https://blast,ncbi,nlm,nih,gov/Blast,cgi)

*Primers used for obtaining the recombinant SidA protein

Table S2 Analysis of the quality of the SidA models through the Molprobity server

	SidA model before MD*	SidA model after MD*
Clashscore	12.28	0
Molprobity score	3.18	1.28
Ramachandran outliers	26 aa	3 aa

*Molecular dynamics

Table S3 Identification of recombinant SidA by mass spectrometry

Accession number[a]	Description[b]	mW (Da)[c]	pI[d]	Protein Score[e]	Peptides[f]	Peptides sequence[g]	Coverage (%)[h]
PADG_00097	Hypothetical protein (475aa)	53505	7,0854	1805,296	18	RSSELLDSILASSKR RYDVVVLATGYTRN KFLDPNPANWSLRL RLSLLESVYEKL KELPNNQVELHVKD KRAENYARL REFGWHTGMLLPGSKM KMQISFIKD RELSNEPLPSTVIHSSVYLESEQ KF RELSAKH RRVLFLERQ KWCASHFDDWVQYKQ RAENYARL KDTQSGQIESSGERY RERGGSYRF KQEVLSVAAAEARPGWPAEHF KV AENYARL REFGWHTGMLLPGSKM	44,3038

[a] Available at NCBI database (https://www,ncbi,nlm,nih,gov).

[b] Protein annotation of the *Paracoccidioides* genome database.

[c] Molecular Weight.

[d] Isoelectric point.

[e] Protein score obtained from MS data using the PLGS.

[f] Number of peptides identified.

[g] Sequence of identified peptides.

[h] Average coverage.

CERTIFICADO

Certificamos que **Aparecido Ferreira de Souza**, participou do evento **I Workshop do Laboratório de Biologia Molecular da Universidade Federal de Goiás** realizado de 29/03/2021 a 31/03/2021, ministrando a Apresentação de Trabalho " Ampliando horizontes: expansão do conhecimento sobre como Paracoccidioides spp. responde à privação de Fe".

Goiânia, 31 de Março de 2021.

Profa. Dra. Célia Maria de Almeida Soares
Coordenadora LBM - UFG

Profa. Dra. Mirelle Garcia Silva Bailão
Organizadora do Workshop

INCT/IPH
Instituto Nacional de Ciência e Tecnologia de Estratégias de Interação Patógeno - Hospedeiro (IPH)

LBM

ICB

UFG
UNIVERSIDADE FEDERAL DE GOIÁS


29º CBM | 2017
29º Congresso Brasileiro
de Microbiologia
De22 a 25 de Outubro de 2017/ Foz do Iguaçu-Paraná-Brasil
"60 anos da Sociedade Brasileira de Microbiologia"
Certificado
Certificamos que o trabalho intitulado HEMOGLOBIN INDUCES THE EXPRESSION OF ADHESINS AND ENZYMES RELATED TO DEFENSE AGAINST OXIDATIVE STRESS IN PARACOCCIDIOIDES LUTZII CELL WALL com a autoria de: SOUZA, A.F., BAEZA, L.C., PACCEZ, J.D., SOARES, C.M.A. foi apresentado na forma de pôster durante o XIII INTERNATIONAL MEETING ON PARACOCCIDIOIDOMYCOSIS - PCM realizado no Rafain Palace Hotel e Convention Center, na cidade de Foz do Iguaçu, PR, no período de 22 a 25 de outubro de 2017.
Prof. Dr. Carlos Pelleschi Taborda
Presidente da SBM
Prof. Dr. Jorge Luiz Mello Sampaio
1º Secretário da SBM
ORGANIZAÇÃO E REALIZAÇÃO:
SBM
APOIO:
CNPq
Pfizer
INSTITUT MERIEUX
MICROGEO
ADUBAÇÃO BIOLÓGICA
BD
FAPESP
AMERICAN SOCIETY FOR MICROBIOLOGY
Organização Pan-Americana da Saúde
Organização Mundial da Saúde

International Symposium on Fungal Stress

ISFUS

Certificate

Goiania, GO, Brazil - May 8 to 11, 2017

in recognition of your poster presentation

Utilization of heme by *Paracoccidioides lutzii*: analysis of the cell wall proteome after exposure to hemoglobin and heterologous expression of Pga7, a probable hemoglobin receptor – *Aparecido Souza, Juliano Paccez, Celia Soares*

[redacted]

Dr. Drauzio Eduardo Naretto Rangel
Symposium Chair

[redacted]

Dr. Flávia Aparecida de Oliveira
Director of IPTSP/UFG

[redacted]

Alene Alder-Rangel
Symposium Co-chair

IPTSP
INSTITUTO DE PATOLOGIA TROPICAL E SAÚDE PÚBLICA

UFG
UNIVERSIDADE FEDERAL DE GOIÁS

65 anos CAPES

ELSEVIER

FAPEG
Fundação de Amparo à Pesquisa do Estado de Goiás

MATERIAL E MÉTODOS

Isolado e condições de cultivo

O isolado de *P. brasiliensis Pb*18 foi utilizado no presente estudo. A forma leveduriforme do fungo foi mantida cultivando-o em meio Fava Netto semi-sólido [peptona 1% (p/v), extrato de levedura 0,5% (p/v), proteose peptona 0,3% (p/v), extrato de carne 0,5% (p/v), NaCl 0,5% (p/v); ágar bacteriológico 1% (p/v), pH 7,2] suplementado com glicose 4% (p/v), na temperatura de 36º C. Para a obtenção de exoproteomas de *P. brasiliensis* sob depleção de Fe, células cultivadas por 5 dias em meio Fava Netto semi-sólido foram inoculadas em 250 mL de meio Fava Netto líquido suplementado com glicose 4% (p/v) e mantidas por 72 h, sob agitação constante (120 rpm), na temperatura de 36º C.

Após, as células fúngicas foram lavadas 2 vezes (800 *g*, 5 min, 4º C) com PBS 1X (solução salina tamponada com fosfato 1x; KH_2PO_4 1,4 mM, Na_2HPO_4 8 mM, NaCl 140 mM, KCl 2,7 mM; pH 7,2), a viabilidade celular foi verificada pelo método de azul de tripano e 10^6 células viáveis/mL foram transferidas para 250 mL de meio quimicamente definido MMcM modificado, sem Fe (Restrepo e Jiménez, 1980). As células foram mantidas por 48 h sob agitação constante (120 rpm), na temperatura de 36º C.

Para a condição de depleção de Fe (tratamento), foram adicionados 50 µM do quelante de Fe ácido batofenantrolino disulfônico (BPS - Sigma-Aldrich, St, Louis, MO, USA), uma vez que em trabalho anteriormente publicado, o cultivo em MMcM de *P.* brasiliensis exposto a esta molaridade de quelante por 48 h não afetou a viabilidade do fungo (Parente, Ana F. A. *et al.*, 2011). Para a condição controle, 10 µM de $Fe(NH_4)_2(SO_4)_2$ foram adicionados ao meio. Para os experimentos de depleção de Fe, todos os meios e soluções foram preparados com água ultrapura. Todas as vidrarias utilizadas para o preparo de meios e soluções foram previamente tratadas com HCl 5N por 1 hora e após, lavadas extensivamente com água ultrapura, como estratégia para minimizar a contaminação por metais, incluindo o Fe.

Obtenção de exoproteoma de *P. brasiliensis*

Para a obtenção de exoproteoma de *P.* brasiliensis sob depleção de Fe, foi seguida a estratégia descrita por (Weber *et al.*, 2012), com algumas modificações: os sobrenadantes de culturas foram coletados (800 *g*, 15 min, 4º C) e, para minimizar a possibilidade de contaminação por eventuais células fúngicas em suspensão, os sobrenadantes foram filtrados por membranas com póros de 0,22 µm. Posteriormente, os sobrenadantes filtrados foram concentrados 250 vezes através de membranas com nível de exclusão de 10 kDa (Amicon Ultra centrifugal filter, Millipore, Bedford, MA, USA) e lavados 3 vezes com tampão NH_4HCO_3 50 mM, pH 8,5. Todos os processos de concentração e manejo da amostra foram realizados em temperaturas baixas (≤ 4º C) para minimizar a atividade de proteases. As amostras obtidas foram estocadas a -20º C até o momento de serem utilizadas.

Preparo de amostras para nanoUPLC-MS^E

As amostras de exoproteomas obtidas foram quantificadas pelo método de Bradford (Bradford, 1976). Após, 150 µg de proteínas de cada réplica biológica foram individualmente preparados para serem submetidos a cromatografia líquida de alta resolução, em nano escala, acoplada à espectrometria de massas com aquisição independente de dados (nanoUPLC-MS^E), conforme descrito anteriormente (Murad *et al.*, 2011). Inicialmente, 10 µL de NH_4HCO_3 50 mM, pH 8,5, foram adicionados às amostras. Em seguida, como agente surfactante, foram adicionados 75 µL de uma solução de RapiGEST^{TM} 0,2% (p/v) (Waters, EUA) e a mistura foi incubada a 80º C, por 15 min. Após este período de incubação, 2,5 µL de DTT 100 mM, um agente redutor de pontes dissulfeto, foram adicionados e nova incubação, a 60º C, por 30 min, foi realizada. Ao fim do período de incubação, aguardou-se que as amostras atingissem temperatura ambiente e 2,5 µL de Iodoacetamida 300 mM, um agente alquilante, foram adicionados e a mistura permaneceu em repouso por 30 min à temperatura ambiente, ao abrigo da luz. Em seguida, as amostras foram submetidas a digestão tríptica. Para tanto, foram adicionados 30 µL de uma solução de tripsina 0,05µg/µL (Promega, EUA) e incubação a 37º C por 16 h foi realizada. Posteriormente, para a precipitação do agente surfactante, foram adicionados 30 µL de ácido trifluoroacético 5% (v/v) e incubação a 37º C foi realizada por mais 90 min. Em seguida, as amostras foram centrifugadas 13000 *g* por 30 min, a 4º C e os sobrenadantes foram transferidos para microtubos novos. O processo de

centrifugação foi repetido até que não houvesse mais a formação de precipitados. As amostras foram concentradas a vácuo. Os peptídeos obtidos de cada amostra foram ressuspendidos em 80 µL de uma solução contendo formiato de amônio 20 mM, pH 10 e 200 fmol/µL de PHB (*Rabbit Phosphorylase B*) (Waters Corporation, Manchester, UK) (MassPREP^{TM} protein). PHB foi utilizada como padrão interno para a quantificação posterior dos peptídeos obtidos.

Cromatografia líquida de alta resolução, em nano escala, acoplada à espectrometria de massas

As amostras que passaram pelo tratamento de digestão tríptica descrito na sessão anterior foram submetidas a cromatografia líquida de alta resolução, em nano escala, por meio do sistema *ACQUITY UPLC® M-Class* (Waters Corporation, USA). O fracionamento dos peptídeos foi realizado em uma pré-coluna de fase reversa *XBridge® Peptide 5 µm BEH130 C18 300 µm x 50 mm* (Waters, USA), sistema que foi mantido em fluxo de 0,5 µL/min com uma condição inicial de acetonitrila (ACN) de 3%, o que consistiu na primeira dimensão. Os peptídeos foram submetidos a 5 fracionamentos (F1-F5), propiciados pelo emprego de diferentes gradientes lineares de concentrações de ACN (F1-11,4%; F2-14,7%; F3-17,4%; F4-20,7% e F5-50%). Para a realização da segunda dimensão, cada fração foi eluída em coluna de aprisionamento *Trap, 2D Symmetry® 5 µm BEH100 C18,* 180 µm x 20mm (Waters, USA) e passaram por separação em coluna analítica *Peptide CSH™ BEH130 C18* 1,7 µm, 100 µm x 100 mm (Waters, USA), em fluxo de 0,4 µL/min a 40º C. A proteína *[Glu1]-Fibronopeptide B human* (GFP - Sigma-Aldrich, EUA) foi utilizada para calibração de massa, a qual foi mensurada a cada 30 segundos e em fluxo constante de 0,5 µL/min. GFP foi utilizada na concentração de 200 fmol/µL. A identificação e quantificação dos peptídeos foram realizadas por um espectrômetro de massas *Synapt G1 MS^{TM}* (Waters, USA) equipado com uma fonte de *NanoElectronSpray* e dois analisadores de massa [um primeiro quadrupolo e o segundo tempo de vôo (TOF) operando em modo V], operando em modo MS^{E}, que faz a troca entre energia baixa (6V) e energia alta (40V) em cada modo de aquisição a cada 0,4 s. Três réplicas experimentais foram realizadas para as réplicas biológicas Fe A, Fe B, BPS A e BPS B. Duas réplicas experimentais foram realizadas para as réplicas biológicas Fe C e BPS C. Desta forma, um total de oito réplicas experimentais foram realizadas, fato que aponta para a robustez dos dados proteômicos obtidos.

Processamento de espectros e análises proteômicas

Após nanoUPLC-MS^E, o processamento de dados foi realizado através do *software ProteinLynx Global Server version 3,0,2* (PLGS) (Waters, Manchester, UK), o qual permitiu a determinação do tempo de retenção de massa exata (EMRT) dos peptídeos bem como inferir o peso molecular destes, através da razão massa/carga (*m/z*). Para a identificação de peptídeos, os espectros obtidos (juntamente com sequências reversas) foram comparados com sequências do banco de dados de *P. brasiliensis* (https://www,uniprot,org/uniprot/?query=paracoccidioides+brasiliensis+strain+pb18&sort=score). Os critérios de identificação de proteínas incluíram: (i) detecção de no mínimo dois íons por fragmentos de peptídeos, (ii) cinco por fragmentos de proteínas, (iii) determinação de pelo menos um peptídeo por proteína, (iv) taxa de detecção de falso positivo de no máximo 4%, (v) carbamidometilação da cisteína, (vi) oxidação da metionina, (vii) fosforilação de serina, treonina e tirosina, (viii) e um sítio de clivagem perdida por tripsina foi permitido. O *Microsoft Office Excel* (Microsoft®, USA) foi utilizado para o manejo de tabelas. Foram incluídas nas análises subsequentes proteínas presentes em pelo menos duas das três réplicas experimentais de cada réplica biológica.

Inicialmente, as proteínas que apresentaram menor coeficiente de variância e que foram detectadas em todas as réplicas foram utilizadas para normalização de intensidade. Após, o Algoritmo de Expressão (Expression^E), que faz parte do *software* PLGS (Geromanos *et al.*, 2009), foi utilizado para as análises de expressão diferencial. Foram consideradas reguladas proteínas com diferenças ± 1,0 entre a quantificação no extrato obtido na depleção de Fe x presença de Fe. Foi realizada investigação de homologia de proteínas hipotéticas identificadas através da ferramenta *online BLASTp* (*Basic Local Alignment Search Tool* - https://blast.ncbi.nlm.nih.gov/Blast.cgi?PAGE=Proteins). Informações sobre função molecular das proteínas identificadas foram obtidas na *Paracoccidioides database* (disponível em http://paracoccidioides.com/). As sequências proteicas foram submetidas a análises *in silico* adicionais para a verificação da presença de peptídeo sinal pela da ferramenta *online* SignalP 4.1 Server (disponível em http://www.cbs.dtu.dk/services/SignalP-4.1/). Para a predição de proteínas secretadas por vias não-clássicas, foi utilizada a ferramenta *online* SecretomeP 2.0 (disponível em http://www.cbs.dtu.dk/services/SecretomeP/). Os dados obtidos também foram comparados com dados de trabalhos previamente publicados que acessaram o exoproteoma de *Paracoccidioides* spp. A Figura Suplementar1 consiste numa

representação do "*workflow*" empregado para as análises proteômicas. Após, seguem as tabelas resultantes.

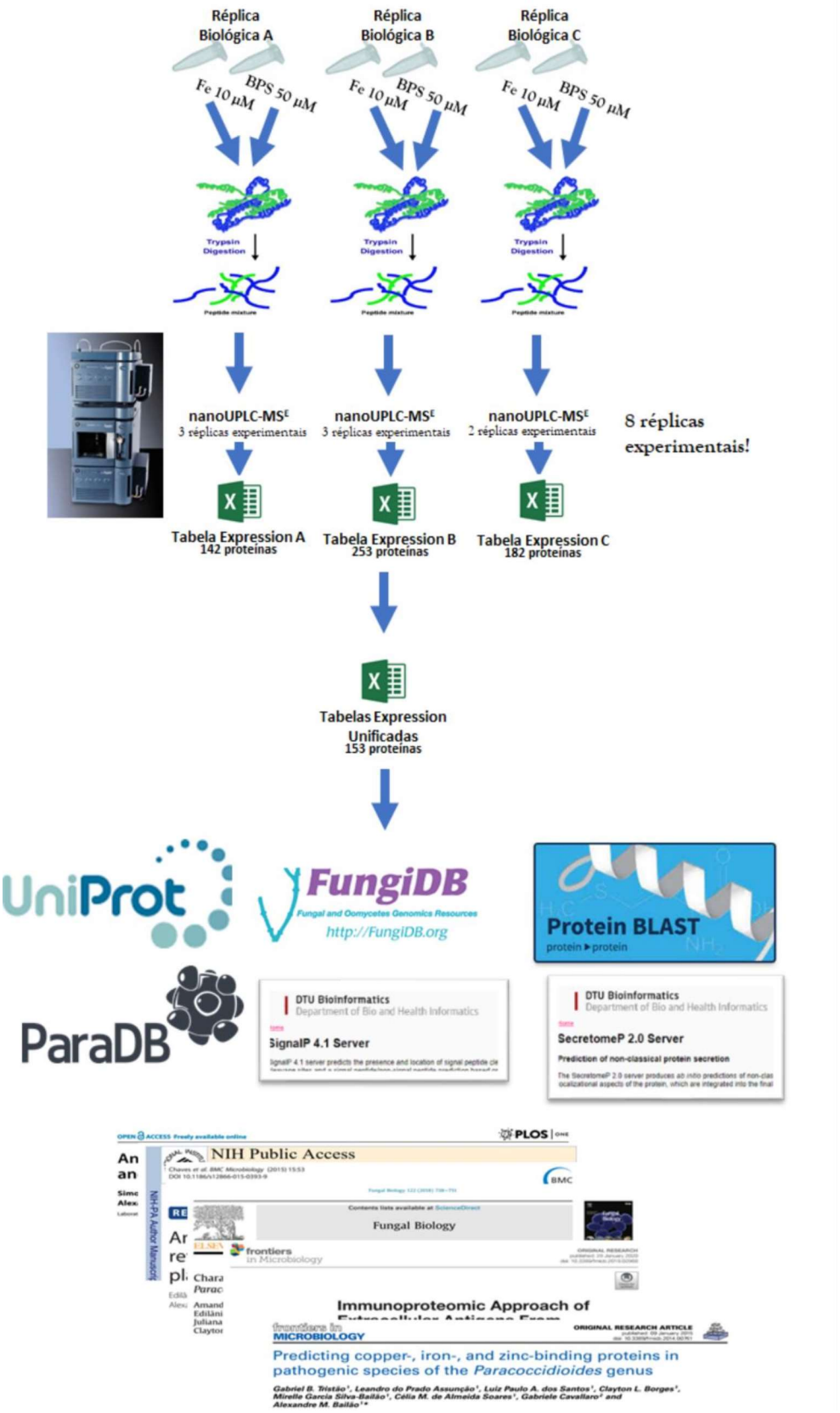

Figura I. *Workflow* das análises proteômicas.

Tabela I. Exoproteoma de *P. brasiliensis* (*Pb*18) identificado após cultura de células leveduriformes por 48 horas a 37º C em meio líquido MMcM com privação de Fe (BPS 50 μM) x suplementação de Fe [Fe $(NH_4)_2$ $(SO_4)_2$,$6H_2O$ 10 μM]

Código de acesso[a]	Descrição[b]	Score[c]	BPS:Fe Ratio[d]	Função molecular[e]	Ligante de FE? Tristão *et al.*, 2015[f]
PADG_01366	NADH desidrogenase (ubiquinona) 1 alfa subcomplexo 5 •	7336	0,16	Atividade de oxidorredutase, atuando em NAD(P)H	**
PADG_07891	Proteína ribossômica Ubiquitina-60S L40 •	5805	0,24	Constituinte estrutural do ribossomo	**
PADG_01372	Manitol-1-fosfato 5-desidrogenase	4989	0,25	Atividade de manitol-1-fosfato 5-desidrogenase, ligação de coenzima	**
PADG_02022	Cadeia leve de clatrina	2841	0,29	Atividade de molécula estrutural	**
PADG_05837	E3 ubiquitina ligase subunidade SCF sconC	14726	0,35	Ligação da origem de replicação do DNA, atividade da ligase, atividade da proteína ubiquitina ligase	**
PADG_08406	O-acetylhomoserine (thiol)-liase	3946	0,39	Atividade de transferase, transferência de grupos alquil ou aril (diferente de metil), atividade de liase, ligação de piridoxal fosfato	**
PADG_04604	Transcetolase	1997	0,52	Atividade de transcetolase	**
PADG_02056	Proteína ribossomal L7 / L12 •	8637	0,56	Constituinte estrutural do ribossomo	**
PADG_11379	Proteína ribossomal L5 60S •	3386	0,59	Constituinte estrutural do ribossomo, ligação de rRNA 5S, atividade de hidrolase	**
PADG_02761	Proteína semelhante a Hsp75	2135	0,61	Ligação de ATP	**
PADG_04730	Subunidade alfa do complexo associado ao polipeptídeo nascente	6273	0,71	Ligação de fosfatidilinositol-3-fosfato, ligação de fosfatidilinositol-4-fosfato, ligação de ácido fosfatídico, ligação de fosfatidilinositol-3,5-bifosfato	**
PADG_00674	Proteína hipotética •	2139	0,73	NDA	**
PADG_02967	Proteína hipotética	3922	0,77	NDA	**
PADG_07749	NAD(P)H: quinona oxidoredutase, tipo IV •	15726	0,78	Atividade de NAD(P)H desidrogenase (quinona), ligação a FMN	**

PADG_06906	Triosefosfato isomerase	11326	0,84	Atividade de triosefosfato isomerase	**
PADG_07213	Complexo piruvato desidrogenase dihidrolipoamida acetiltransferase	2736	0,84	Atividade de acetiltransferase de resíduo de dihidrolipoilisina	**
PADG_01010	Proteína contendo domínio AMPK1_CBM	3455	0,85	NDA	**
PADG_08615	Tropomiosina-1	11021	0,87	NDA	**
PADG_03562	Chaperona DnaK	6962	0,89	Ligação de ATP, atividade de ATPase	**
PADG_00183	Profilina	19317	0,90	NDA	**
PADG_07715	Proteína semelhante a Hsp90	3526	0,93	Ligação de ATP	**
PADG_06992	Homóloga de proteína GrpE •	3945	0,95	Atividade de fator de troca de adenil-nucleotídeo	**
PADG_01363	Proteína de ligação de Acil-CoA	11793	1,00	Ligação de acil-CoA graxo	**
PADG_04056	Proteína 14-3-3 da família epsilon •	10435	1,01	NDA	**
PADG_06488	Peptidil-prolil cis-trans isomerase D	17659	1,02	Atividade de peptidil-prolil cis-trans isomerase	**
PADG_02726	Cisteína sintase	18233	1,16	NDA	**
PADG_00430	Proteína semelhante a Hsp7	15295	1,17	Ligação de ATP	**
PADG_05922	Glutamato carboxipeptidase	1312	1,17	Atividade de dipeptidase	**
PADG_00784	Proteína ribossomal S0 40S •	1850	1,20	Constituinte estrutural do ribossomo	**
PADG_00995	Proteína ribossomal S27a Ubiquitina-40S •	5556	1,22	Constituinte estrutural do ribossomo	**
PADG_02555	Proteína de ligação de ácido nucléico	4268	1,22	Ligação de nucleotídeo, ligação de ácido nucleico	**
PADG_07418	Superóxido dismutase [Cu-Zn]	12014	1,25	Atividade de superóxido dismutase, ligação de íons metálicos	**
PADG_02652	Grp1p	5794	1,27	Ligação de nucleotídeo, ligação de DNA telomérico de fita simples	**
PADG_01407	Proteína ribossomal 40S	9378	1,28	Ligação de RNA, constituinte estrutural do ribossomo	**
PADG_06515	Suaprga1 •	22754	1,32	NDA	**
PADG_02017	Calmodulina	43048	1,35	Ligação de íon cálcio	**
PADG_08369	Proteína semelhante a Hsp60	17604	1,41	Ligação de origem de replicação de DNA, ligação de DNA de fita simples, ligação de ATP, atividade de ATPase	**
PADG_05160	Dipeptidil peptidase 3	2563	1,44	Atividade de dipeptidil-peptidase, ligação de íon metálico	**
PADG_07524	Nucleosídeo difosfato quinase	37920	1,47	Atividade de nucleosídeo difosfato quinase, ligação de ATP	**

PADG_01605	Poliubiquitina	4911	1,48	NDA	**
PADG_03149	Aminopeptidase	2712	1,49	Atividade de metalopeptidase, ligação de íon zinco	**
PADG_03841	Proteína com domínio de dissulfeto-isomerase	22371	1,60	Atividade de proteína dissulfeto isomerase	**
PADG_07782	Desoxiuridina 5-trifosfato nucleotidohidrolase	7471	1,61	atividade dUTP difosfatase	**
PADG_07420	Transaldolase	7105	1,63	Sedoheptulose-7-fosfato: D-gliceraldeído-3-fosfato gliceronetransferase atividade	**
PADG_04148	Alfa manosidase vacuolar	5961	1,70	Atividade de alfa-manosidase, ligação de íon zinco, ligação de carboidrato	**
PADG_08054	Malato desidrogenase, dependente de NAD	4526	1,81	Atividade de L-malato desidrogenase	**
PADG_02785	Proteína de choque térmico Hsp88	5877	1,83	Ligação de ATP	**
PADG_00688	Subunidade H de transporte de H + ATPase tipo F	8080	1,96	NDA	**
PADG_05032	Co-chaperona de ligação Hsp90 (Sba1)	8142	2,14	NDA	**
PADG_01479	Gama-glutamiltransferase	6243	2,43	Atividade de gama-glutamiltransferase	**
PADG_00921	Proteína hipotética •	3213	2,51	NDA	**
PADG_04059	Enolase	9477	2,52	Ligação de íons de magnésio, atividade de fosfopiruvato hidratase	**
PADG_01711	Co-chaperona Hsp90 AHA1	11850	2,54	Atividade de ativador ATPase	**
PADG_01706	Frutose-1,6-bisfosfatase	13110	2,58	Atividade de frutose 1,6-bisfosfato 1-fosfatase	**
PADG_04710	2-metilcitrato sintase, mitocondrial	17077	2,84	Atividade de citrato (Si)-sintase, atividade de 2-metilcitrato sintase	**
PADG_02343	Proteína MYG1 •	7766	2,95	NDA	**
PADG_07422	Serino Proteinase	3358	3,06	Atividade de endopeptidase em resíduos de serina	**
PADG_06490	Formamidase	12362	3,15	Atividade de hidrolase, atuando nas ligações carbono-nitrogênio (mas não no peptídeo), em amidas lineares	**
PADG_02446	Proteína ribossomal ácida P2 60S	29077	3,61	Constituinte estrutural do ribossomo	**
PADG_02735	Componente de proteassomo PRE6	13436	3,91	Atividade de endopeptidase em resíduos de treonina	**
PADG_04288	Endoribonuclease L-PSP	31240	3,94	NDA	**
PADG_08118	Proteína semelhante a Hsp72	49968	3,97	Ligação de ATP	**
PADG_05855	Lactonohidrolase	8467	4,07	NDA	**

PADG_11950	Subunidade TFIID / TFIIF do fator de iniciação da transcrição •	13634	4,72	NDA	**
PADG_05750	Subunidade putativa VIa de citocromo c oxidase	23847	5,07	Atividade de citocromo-c oxidase	**
PADG_00663	Homosserina desidrogenase	7981	5,12	Atividade da homosserina desidrogenase, ligação a NADP	**
PADG_06494	Diidrolipoil desidrogenase	32031	5,37	Atividade de diidrolipoil desidrogenase, atividade de glicina desidrogenase (descarboxilação), atividade de oxoglutarato desidrogenase (transferência de succinila), atividade de piruvato desidrogenase, ligação de flavina adenina dinucleotídeo	**
PADG_05798	Proteína da família de ligação de fita simples de DNA	41240	7,76	Ligação de DNA de fita simples	**
PADG_03559	Citocromo b5 #	17493	30,67	Ligação ao heme, ligação de íon metálico	**
PADG_00026	Citidina desaminase •	4546	BPS	Atividade de citidina desaminase, ligação de íon zinco	**
PADG_00060	Proteína MGS207 •	1122	BPS	NDA	**
PADG_00210	Glicina desidrogenase	1077	BPS	Atividade da glicina desidrogenase (descarboxilação)	**
PADG_00211	Proteína que contém domínio DUF427 •	3310	BPS	NDA	**
PADG_00220	Fator de transcrição da família CBF/NF-Y •	1323	BPS	Ligação do promotor do núcleo, atividade do fator de transcrição da RNA polimerase II, ligação da proteína da classe TBP, envolvida na montagem do complexo de pré-iniciação, ligação da cromatina, atividade do coativador da transcrição, atividade do corepressor da transcrição	**
PADG_00451	Glicose-6-fosfato isomerase	1011	BPS	Atividade de glicose-6-fosfato isomerase	**
PADG_00514	Proteína ribossomal L16 60S •	1435	BPS	Constituinte estrutural do ribossomo	**
PADG_00615	Subunidade de proteassomo tipo alfa C7	1010	BPS	Atividade de endopeptidase em resíduos de treonina	**
PADG_00676	Fator de degradação RNAPII def1	1191	BPS	NDA	**
PADG_00809	Enzima de conjugação de ubiquitina •	2155	BPS	NDA	**
PADG_00822	Glutaminase A	786	BPS	NDA	**
PADG_00888	Argininosuccinato sintase •	804	BPS	Atividade de argininosuccinato sintase, ligação de ATP	**
PADG_00912	UDP-galactopiranose mutase	1287	BPS	Atividade de oxidorredutase	**
PADG_00988	Ribonuclease T2 •	923	BPS	Ligação de RNA, atividade de ribonuclease T2	**

PADG_01404	Aspartato aminotransferase	740	BPS	L-aspartato: atividade de 2-oxoglutarato aminotransferase, ligação de fosfato de piridoxal, L-fenilalanina: atividade de 2-oxoglutarato aminotransferase	**
PADG_01626	Proteína doadora de ferro CyaY •#	5703	BPS	Atividade de ferroxidase, ligação de ferro férrico	**
PADG_01644	Proteína v-SNARE vti1 de transporte de vesículas •	1227	BPS	NDA	**
PADG_01654	Proteína ribossômica 40S S6-A •	1333	BPS	Constituinte estrutural do ribossomo	**
PADG_01665	Quinurenina-oxoglutarato transaminase •	1278	BPS	Atividade de quinurenina-oxoglutarato transaminase, ligação de fosfato de piridoxal, atividade de 2-aminoadipato transaminase	**
PADG_01871	3-oxoacil-(Acil-carreadora-proteína) redutase •	1652	BPS	NDA	**
PADG_01949	Fator de alongamento de tradução Tu •	2648	BPS	Atividade de fator de alongamento de tradução, atividade de GTPase, ligação de GTP	**
PADG_02260	Succinato-CoA ligase [formadora de ADP] subunidade alfa, mitocondrial	2156	BPS	Atividade de ligase, ligação de cofator	**
PADG_02561	ATP sintase subunidade alfa, mitocondrial	2772	BPS	Ligação de ATP, atividade de ATP sintase de transporte de prótons, mecanismo de rotação	**
PADG_02763	Subunidade reguladora de quinase dependente de ciclina •	3528	BPS	Atividade de quinase, atividade reguladora de proteína serina/treonina quinase dependente de ciclina	**
PADG_02845	Proteína de manutenção de estado diplóide chpA •	1291	BPS	NDA	**
PADG_02862	Glucano 1,3-beta-glucosidase	1997	BPS	Atividade de 1,3-beta-glucanosiltransferase, atividade de glucano endo-1,3-beta-D-glucosidase	**
PADG_03121	Proteína hipotética •	1070	BPS	NDA	**
PADG_03278	Inositol-3-fosfato sintase •	885	BPS	Atividade de inositol-3-fosfato sintase	**
PADG_03526	Proteína com repetição de M •	637	BPS	NDA	**
PADG_03778	Proteína ribossomal 60S L10-A •	1463	BPS	Constituinte estrutural do ribossomo	**
PADG_03830	Proteína que interage com actina	637	BPS	NDA	**
PADG_03852	Proteína membro da família LiPid Depleted •#	779	BPS	Ligação de íons de ferro, ligação de cluster de ferro-enxofre	Sim

PADG_03856	Proteína ribossomal L15 60S •	1833	BPS	Constituinte estrutural do ribossomo	**
PADG_04030	Proteína ribossomal ácida 60S P0	1335	BPS	Constituinte estrutural do ribossomo, ligação de rRNA de subunidade ribossômica grande	**
PADG_04242	Sulfidril oxidase •	5011	BPS	Atividade de tiol oxidase	**
PADG_04475	Proteína ribossomal S36, mitocondrial •	3489	BPS	NDA	**
PADG_04516	Glutamato desidrogenase NADP-específica	1563	BPS	Atividade de glutamato desidrogenase (NAD +)	**
PADG_04588	Proteína ribossomal L22 60S	3027	BPS	Constituinte estrutural do ribossomo	**
PADG_04934	Proteína com domínio RNP	919	BPS	Ligação de nucleotídeo, ligação de ácido nucleico	**
PADG_05239	Cofator A de ligação à tubulina •	2900	BPS	NDA	**
PADG_05277	Serina hidroximetiltransferase	655	BPS	Atividade de glicina hidroximetiltransferase, ligação piridoxal fosfato	**
PADG_05321	Nuclease mitocondrial #	1132	BPS	Atividade de endodeoxirribonuclease de DNA de fita simples, ligação de ácido nucleico, atividade de endoribonuclease, ligação de íon metálico	**
PADG_05683	Proteína de controle de divisão celular 48•	1683	BPS	Ligação de ATP, atividade reguladora de proteína fosfatase tipo 1, atividade de ATPase	**
PADG_06155	Palmitoil-proteína tioesterase	1632	BPS	Atividade de palmitoil-(proteína) hidrolase	**
PADG_06273	Calcineurina subunidade B •	2812	BPS	Atividade de fosfoproteína fosfatase, ligação de íons de cálcio, atividade reguladora de proteína serina / treonina fosfatase dependente de cálcio	**
PADG_06382	3-metil-2-oxobutanoato hidroximetiltransferase •	711	BPS	Atividade de transferase, transferência de grupos acil diferentes dos grupos amino-acil	**
PADG_06671	3-isopropilmalato desidrogenase A	1032	BPS	Ligação de íons de magnésio, atividade de 3-isopropilmalato desidrogenase, ligação de NAD	**
PADG_06726	Proteína ribossomal L17 60S •	1694	BPS	Constituinte estrutural do ribossomo	**
PADG_06838	Proteína ribossomal S5 40S	3023	BPS	Ligação de RNA, constituinte estrutural do ribossomo	**

PADG_06997	Proteína de ligação ao cap nuclear •	2485	BPS	Ligação de nucleotídeo, ligação de ácido nucleico, atividade de peptidil-prolil cis-trans isomerase	**
PADG_07264	Proteína de domínio barrel A/B responsiva ao estresse •	3637	BPS	NDA	**
PADG_07870	Proteína ribossomal S7 30S •	1112	BPS	Constituinte estrutural do ribossomo	**
PADG_07888	Fator de iniciação da tradução eucariótica 5A	4225	BPS	Atividade do fator de iniciação da tradução, atividade do fator de alongamento da tradução, ligação ao ribossomo	**
PADG_08045	Aminotransferase de aminoácidos de cadeia ramificada •	795	BPS	Atividade de transaminase de aminoácidos de cadeia ramificada	**
PADG_08098	Adenilato quinase 1•	1995	BPS	Atividade de adenilato quinase, ligação de ATP	**
PADG_08108	Coproporphyrinogen III oxidase •#	1114	BPS	Coproporfirinogênio III oxidase	**
PADG_08212	Proteína hipotética •	4444	BPS	NDA	**
PADG_08244	Proteína ribossomal ácida P1 60S	14,12	BPS	Constituinte estrutural do ribossomo	**
PADG_08270	Proteína contendo domínio UBX •#	1143	BPS	Ligação de íons metálicos	**
PADG_08328	5-metiltetrahidropteroiltriglutamato-homocisteína S-metiltransferase •	756	BPS	Atividade de 5-metiltetrahidropteroiltriglutamato-homocisteína S-metiltransferase, ligação de íon zinco	**
PADG_08376	Aspartato-semialdeído desidrogenase	2046	BPS	Atividade de N-acetil-gama-glutamil-fosfato redutase, atividade de aspartato-semialdeído desidrogenase, ligação de NADP, ligação de NAD	**
PADG_08391	ATPase da membrana plasmática #	517	BPS	Ligação de ATP, atividade de ATPase de exportação de hidrogênio, mecanismo fosforilativo, ligação de íons metálicos	**
PADG_08466	Homogentisato 1,2-dioxigenase #	784	BPS	Atividade de homogentisado 1,2-dioxigenase	Sim
PADG_08468	4-hidroxifenilpiruvato dioxigenase •#	897	BPS	Atividade 4-hidroxifenilpiruvato dioxigenase, ligação de íons metálicos	Sim
PADG_08587	Proteína de ligação a FK506	3833	BPS	NDA	**
PADG_08599	Proteína com domínio DnaJ •	1141	BPS	NDA	**
PADG_11679	Antígeno nuclear de célula em proliferação (pcna)	1358	BPS	Ligação ao DNA, atividade do fator de processabilidade da DNA polimerase	**
PADG_11711	RNA helicase dependente de ATP eIF4A •	1151	BPS	Ligação de ácido nucleico, atividade de helicase, ligação de ATP	**
PADG_12077	Actina	1073	BPS	Constituinte estrutural do citoesqueleto, ligação de ATP	**

PADG_12252	Proteína da família de enzimas fosfotransferases •	987	BPS	NDA	**
PADG_12253	Proteína ribossomal L3 60S	1229	BPS	Constituinte estrutural do ribossomo, atividade de carbono-enxofre liase	**
PADG_12365	Proteína ribossomal 40S S8-A •	890	BPS	Constituinte estrutural do ribossomo	**

A tabela foi organizada em ordem crescente dos valores da razão BPS: Fe;

[a]Código de acesso da proteína no NCBI, disponível em https://www.ncbi.nlm.nih.gov/protein;

[b]Descrição da proteína no banco de dados de *Paracoccidioides* spp, disponível em https://www.uniprot.org/proteomes/?query=paracoccidioides&sort=score;

•Aponta que a proteína foi identificada exclusivamente no presente trabalho;

#Aponta que a proteína potencialmente liga-se a Fe;

[c]O número de *score* de identificação de proteínas é obtido por um processo em múltiplas etapas, realizado pelo PLGS; somente dados com nível de confiança ≥ 95% e *false discovery ratio* ≤ 4% foram utilizados no presente estudo;

[d]Razão entre a quantificação de proteínas identificadas na condição de privação de Fe/presença de Fe. Valores ≥ 2,0 indicam proteínas reguladas positivamente; valores ≤ 0,5 indicam proteínas reguladas negativamente; BPS indica que a proteína foi identificada somente na condição de privação de Fe;

[e]Função molecular descrita no ParaDB, disponível em http://paracoccidioides.com/. NDA indica que não há informações disponíveis em relação às funções moleculares da referida proteína nessa base de dados;

[f]Proteínas preditas como ligantes de Fe de acordo com trabalho de (Tristão *et al.*, 2015), disponível em https://doi.org/10.3389/fmicb.2014,00761. (**) indica que a proteína não foi predita como ligante de Fe no trabalho citado.

Tabela II. Proteínas preditas como secretadas no exoproteoma de *P. brasiliensis* (*Pb*18) identificadas após cultura de cél
meio líquido MMcM com privação de Fe (BPS 50 µM) x suplementação de Fe [Fe $(NH_4)_2$ $(SO_4)_2$,$6H_2O$ 10 µM]

Código de acesso[a]	Descrição[b]	Score[c]	BPS:Fe Ratio[d]	SignalP ≥ 0,45[e]	SecretomeP ≥ 0,6[f]	Evidência de secreção na liteatura de *Paracoccidioides* spp.[g]	Função molecular[h]
PADG_01366	NADH desidrogenase (ubiquinona) 1 alfa subcomplexo 5 •	7336	0,16	***	0,657	-	Atividade de oxidorredutase, atuando em NAD(P)H
PADG_01372	Manitol-1-fosfato 5-desidrogenase	4989	0,25	***	0,670	-	Atividade de manitol-1-fosfato 5-desidrogenase, ligação de coenzima
PADG_02022	Cadeia leve de clatrina	2841	0,29	***	0,775	-	Atividade de molécula estrutural
PADG_05837	E3 ubiquitina ligase subunidade SCF sconC	14726	0,35	***	0,706	-	Ligação da origem de replicação do DNA, atividade da ligase, atividade da proteína ubiquitina ligase
PADG_04604	Transcetolase	1997	0,52	***	0,650	-	Atividade de transcetolase
PADG_02056	Proteína ribossomal L7 / L12 •	8637	0,56	***	0,752	-	Constituinte estrutural do ribossomo
PADG_04730	Subunidade alfa do complexo associado ao polipeptídeo nascente	6273	0,71	***	0,797	-	Ligação de fosfatidilinositol-3-fosfato, ligação de fosfatidilinositol-4-fosfato, ligação de ácido fosfatídico, ligação de fosfatidilinositol-3,5-bifosfato
PADG_07749	NAD(P)H: quinona oxidoredutase, tipo IV •	15726	0,78	***	0,623	-	Atividade de NAD(P)H desidrogenase (quinona), ligação a FMN
PADG_06906	Triosefosfato isomerase	11326	0,84	***	0,623	-	Atividade de triosefosfato isomerase
PADG_07213	Complexo piruvato desidrogenase dihidrolipoamida acetiltransferase	2736	0,84	***	0,635	-	Atividade de acetiltransferase de resíduo de dihidrolipoilisina
PADG_08615	Tropomiosina-1	11021	0,87	***	0,793	-	NDA
PADG_03562	Chaperona DnaK	6962	0,89	0,864	***		- ão de ATP, atividade de ATPase
PADG_00183	Profilina	19317	0,90	***	0,889	-	NDA
PADG_06992	Homóloga de proteína GrpE •	3945	0,95	***	0,846	-	Atividade de fator de troca de adenil-nucleotídeo

PADG_01363	Proteína de ligação de Acil-CoA	11793	1,00	***	0,873	-	Ligação de acil-CoA graxo
PADG_02726	Cisteína sintase	18233	1,16	***	0,621	-	NDA
PADG_05922	Glutamato carboxipeptidase	1312	1,17	***	0,630	-	Atividade de dipeptidase
PADG_00995	Proteína ribossomal S27a Ubiquitina-40S •	5556	1,22	***	0,834	-	Constituinte estrutural do ribossomo
PADG_02555	Proteína de ligação de ácido nucléico	4268	1,22	***	0,654	-	Ligação de nucleotídeo, ligação de ácido nucleico
PADG_02652	Grp1p	5794	1,27	***	0,839	-	Ligação de nucleotídeo, ligação de DNA telomérico de fita simples
PADG_06515	Suaprga1 •	22754	1,32	***	0,754	-	NDA
PADG_02017	Calmodulina	43048	1,35	***	0,744	-	Ligação de íon cálcio
PADG_03841	Proteína com domínio de dissulfeto-isomerase	22371	1,60	0,726	***	-	Atividade de proteína dissulfeto isomerase
PADG_07782	Desoxiuridina 5-trifosfato nucleotidohidrolase	7471	1,61	***	0,601	-	atividade dUTP difosfatase
PADG_00688	Subunidade H de transporte de H + ATPase tipo F	8080	1,96	***	0,827	-	NDA
PADG_01479	Gama-glutamiltransferase	6243	2,43	***	***	Bailão *et al*., 2015	Atividade de gama-glutamiltransferase
PADG_04059	Enolase	9477	2,52	***	***	Donofrio *et a.*,, 2009; Nogueira *et al*., 2010; Marcos *et al*., 2012	Ligação de íons de magnésio, atividade de fosfopiruvato hidratase
PADG_07422	Serino Proteinase	3358	3,06	0,669	***	Parente *et al*., 2010; Pigosso *et al*., 2017	Atividade de endopeptidase em resíduos de serina
PADG_06490	Formamidase	12362	3,15	***	***	Borges *et al*., 2010	Atividade de hidrolase, atuando nas ligações carbono-nitrogênio (mas não no peptídeo), em amidas lineares
PADG_04288	Endoribonuclease L-PSP	31240	3,94	***	0,874	-	NDA
PADG_05750	Subunidade putativa VIa de citocromo c oxidase	23847	5,07	***	0,722	-	Atividade de citocromo-c oxidase
PADG_00663	Homosserina desidrogenase	7981	5,12	***	0,651	-	Atividade da homosserina desidrogenase, ligação a NADP
PADG_06494	Diidrolipoil desidrogenase	32031	5,37	***	***	Landgraf *et al*., 2017	Atividade de diidrolipoil desidrogenase, atividade de glicina desidrogenase (descarboxilação), atividade de oxoglutarato desidrogenase (transferência de succinila), atividade de piruvato desidrogenase, ligação de flavina adenina dinucleotídeo

PADG_05798	Proteína da família de ligação de fita simples de DNA				41240		7,76 *** 0,809	-
PADG_03559	Citocromo b5 #	17493	30,67	***	0,688	-	Ligação ao heme, ligação de íon metálico	
PADG_00451	Glicose-6-fosfato isomerase	1011	BPS	***	***	-	Atividade de glicose-6-fosfato isomerase	
PADG_00514	Proteína ribossomal L16 60S •	1435	BPS	***	***	-	Constituinte estrutural do ribossomo	
PADG_00615	Subunidade de proteassomo tipo alfa C7	1010	BPS	***	***	-	Atividade de endopeptidase em resíduos de treonina	
PADG_00676	Fator de degradação RNAPII def1	1191	BPS	***	***	-	NDA	
PADG_00809	Enzima de conjugação de ubiquitina •	2155	BPS	***	0,825	-	NDA	
PADG_00822	Glutaminase A	786	BPS	0,730	***	-	NDA	
PADG_00988	Ribonuclease T2 •	923	BPS	***	0,614	-	Ligação de RNA, atividade de ribonuclease T2	
PADG_01404	Aspartato aminotransferase	740	BPS	***	0,662	-	L-aspartato: atividade de 2-oxoglutarato aminotransferase, ligação de fosfato de piridoxal, L-fenilalanina: atividade de 2-oxoglutarato aminotransferase	
PADG_01871	3-oxoacil-(Acil-carreadora-proteína) redutase •	1652	BPS	***	0,895	-	NDA	
PADG_01949	Fator de alongamento de tradução Tu •	2648	BPS	***	0,751	Marcos *et al.*, 2016; Marcos *et al.*, 2019	Atividade de fator de alongamento de tradução, atividade de GTPase, ligação de GTP	
PADG_02260	Succinato-CoA ligase [formadora de ADP] subunidade alfa, mitocondrial	2156	BPS	***	0,644	-	Atividade de ligase, ligação de cofator	
PADG_02763	Subunidade reguladora de quinase dependente de ciclina •	3528	BPS	***	0,773	-	Atividade de quinase, atividade reguladora de proteína serina/treonina quinase dependente de ciclina	
PADG_02845	Proteína de manutenção de estado diplóide chpA •	1291	BPS	***	0,829	-	NDA	
PADG_02862	Glucano 1,3-beta-glucosidase	1997	BPS	0,871	***	-	Atividade de 1,3-beta-glucanosiltransferase, atividade de glucano endo-1,3-beta-D-glucosidase	
PADG_03121	Proteína hipotética •	1070	BPS	***	0,811	-	NDA	
PADG_03278	Inositol-3-fosfato sintase •	885	BPS	***	0,640	-	Atividade de inositol-3-fosfato sintase	

PADG_03778	Proteína ribossomal 60S L10-A •	1463	BPS	***	0,678	-	Constituinte estrutural do ribossomo
PADG_03852	Proteína membro da família LiPid Depleted •#	779	BPS	***	0,692	-	Ligação de íons de ferro, ligação de cluster de ferro-enxofre
PADG_04475	Proteína ribossomal S36, mitocondrial •	3489	BPS	***	0,791	-	NDA
PADG_06155	Palmitoil-proteína tioesterase	1632	BPS	0,808	***	-	Atividade de palmitoil-(proteína) hidrolase
PADG_06382	3-metil-2-oxobutanoato hidroximetiltransferase •	711	BPS	***	0,685	-	Atividade de transferase, transferência de grupos acil diferentes dos grupos amino-acil
PADG_06726	Proteína ribossomal L17 60S •	1694	BPS	***	0,869	-	Constituinte estrutural do ribossomo
PADG_06838	Proteína ribossomal S5 40S	3023	BPS	***	0,632	-	Ligação de RNA, constituinte estrutural do ribossomo
PADG_06997	Proteína de ligação ao cap nuclear •	2485	BPS	***	0,665	-	Ligação de nucleotídeo, ligação de ácido nucleico, atividade de peptidil-prolil cis-trans isomerase
PADG_08045	Aminotransferase de aminoácidos de cadeia ramificada •	795	BPS	***	0,682	-	Atividade de transaminase de aminoácidos de cadeia ramificada
PADG_08098	Adenilato quinase 1•	1995	BPS	***	0,666	-	Atividade de adenilato quinase, ligação de ATP
PADG_08212	Proteína hipotética •	4444	BPS	***	0,637	-	NDA
PADG_08270	Proteína contendo domínio UBX •#	1143	BPS	***	0,891	-	Ligação de íons metálicos
PADG_08376	Aspartato-semialdeído desidrogenase	2046	BPS	***	0,618	-	Atividade de N-acetil-gama-glutamil-fosfato redutase, atividade de aspartato-semialdeído desidrogenase, ligação de NADP, ligação de NAD
PADG_08391	ATPase da membrana plasmática #	517	BPS	***	0,715	-	Ligação de ATP, atividade de ATPase de exportação de hidrogênio, mecanismo fosforilativo, ligação de íons metálicos
PADG_08466	Homogentisato 1,2-dioxigenase #	784	BPS	***	0,601	-	Atividade de homogentisado 1,2-dioxigenase
PADG_08587	Proteína de ligação a FK506	3833	BPS	0,869	***	-	NDA
PADG_12365	Proteína ribossomal 40S S8-A •	890	BPS	***	0,792	-	Constituinte estrutural do ribossomo

A tabela foi organizada em ordem crescente dos valores da razão BPS: Fe;

[a]Código de acesso da proteína no NCBI, disponível em https://www.ncbi.nlm.nih.gov/protein;

[b]Descrição da proteína no banco de dados de *Paracoccidioides* spp, disponível em https://www.uniprot.org/proteomes/?query=paracoccidioides&sort=score;

•Aponta que a proteína foi identificada exclusivamente no presente trabalho;

#Aponta que a proteína potencialmente liga-se a Fe;

[c]O número de *score* de identificação de proteínas é obtido por um processo em múltiplas etapas, realizado pelo PLGS; somente dados com nível de confiança ≥ 95% e *false discovery ratio* ≤ 4% foram utilizados no presente estudo;

[d]Razão entre a quantificação de proteínas identificadas na condição de privação de Fe/presença de Fe. Valores ≥ 2,0 indicam proteínas reguladas positivamente; valores ≤ 0,5 indicam proteínas reguladas negativamente; BPS indica que a proteína foi identificada somente na condição de privação de Fe;

[e]Predição da presença de peptídeo sinal; cujo valor *score* deve ser ≥ 0,45; predição realizada pela ferramenta on-line SignalP 4.1 disponível em http://www.cbs.dtu.dk/services/SignalP-4.1/; (***) indica que não houve predição de presença peptídeo sinal;

[f]Predição de secreção de proteínas por vias não-clássicas, cujo valor de *score* deve ser ≥ 0,6; predição realizada pela ferramenta on-line SecretomeP 2.0 disponível em http://www.cbs.dtu.dk/services/SecretomeP/. (***) indica que a proteína não foi predita como secretada;

[g]Evidência de secreção de proteínas na literatura de *Paracoccidioides* spp. Buscas foram realizadas no repositório de dados PUBMED no período entre 07/2019 – 05/2021. Os termos utilizados nas buscas foram aqueles presentes na coluna "descrição" + Paracoccidioides, (-) indica que evidências de secreção da proteína em questão não foram encontradas na literatura;

[h]Função molecular descrita no ParaDB, disponível em http://paracoccidioides.com/. NDA indica que não há informações disponíveis em relação às funções moleculares da referida proteína nessa base de dados;

Tabela III. Análise comparativa de proteínas identificadas no presente trabalho e proteínas reportadas em trabalhos prévios como presentes no exoproteoma de *Paracoccidioides* spp.

Código de acesso[a]	Descrição[b]	Score[c]	BPS:Fe Ratio[d]	Função molecular[e]	Weber *et al.*, 2012[f]	Vallejo *et al.*, 2012[g]	Chaves *et al.*, 2015[h]	Rodrigues *et al.*, 2018[i]	Moreira *et al.*, 2020[j]	Ligante de FE? Trisião *et al.*, 2015[k]
PADG_01372	Manitol-1-fosfato 5-desidrogenase	4989	0,25	Atividade de manitol-1-fosfato 5-desidrogenase, ligação de coenzima	Sim	Sim	*	Sim	Sim	**
PADG_02022	Cadeia leve de clatrina	2841	0,29	Atividade de molécula estrutural	*	Sim	*	*	*	**
PADG_05837	E3 ubiquitina ligase subunidade SCF sconC	14726	0,35	Ligação da origem de replicação do DNA, atividade da ligase, atividade da proteína ubiquitina ligase	*	Sim	*	*	*	**
PADG_08406	O-acetylhomoserine (thiol)-liase	3946	0,39	Atividade de transferase, transferência de grupos alquil ou aril (diferente de metil), atividade de liase, ligação de piridoxal fosfato	Sim	*	*	*	*	**
PADG_04604	Transcetolase	1997	0,52	Atividade de transcetolase	*	Sim	*	*	*	**
PADG_02761	Proteína semelhante a Hsp75	2135	0,61	Ligação de ATP	*	Sim	*	*	*	**
PADG_04730	Subunidade alfa do complexo associado ao polipeptídeo nascente	6273	0,71	Ligação de fosfatidilinositol-3-fosfato, ligação de fosfatidilinositol-4-fosfato, ligação de ácido	*	Sim	*	Sim	*	**

				fosfatídico, ligação de fosfatidilinositol-3,5-bifosfato						
PADG_02967	Proteína hipotética	3922	0,77	NDA	*	Sim	*	*	*	**
PADG_06906	Triosefosfato isomerase	11326	0,84	Atividade de triosefosfato isomerase	*	Sim	*	Sim	*	**
PADG_07213	Complexo piruvato desidrogenase dihidrolipoamida acetiltransferase	2736	0,84	Atividade de acetiltransferase de resíduo de dihidrolipoilisina	*	Sim	*	*	*	**
PADG_01010	Proteína contendo domínio AMPK1_CBM	3455	0,85	NDA	*	Sim	*	*	*	**
PADG_08615	Tropomiosina-1	11021	0,87	NDA	*	Sim	*	*	*	**
PADG_03562	Chaperona DnaK	6962	0,89	*	Sim	*	*	*	**	
PADG_00183	Profilina	19317	0,90	NDA	*	Sim	*	*	*	**
PADG_07715	Proteína semelhante a Hsp90	3526	0,93	Ligação de ATP	*	Sim	*	*	*	**
PADG_01363	Proteína de ligação de Acil-CoA	11793	1,00	Ligação de acil-CoA graxo	*	Sim	*	*	*	**
PADG_06488	Peptidil-prolil cis-trans isomerase D	17659	1,02	Atividade de peptidil-prolil cis-trans isomerase	Sim	Sim	*	Sim	*	**
PADG_02726	Cisteína sintase	18233	1,16	NDA	*	Sim	*	Sim	*	**
PADG_00430	Proteína semelhante a Hsp7	15295	1,17	Ligação de ATP	*	Sim	*	*	*	**
PADG_05922	Glutamato carboxypeptidase	1312	1,17	Atividade de dipeptidase	Sim	Sim	*	Sim	Sim	**
PADG_02555	Proteína de ligação de ácido nucléico	4268	1,22	Ligação de nucleotídeo, ligação de ácido nucleico	Sim	Sim	*	*	*	**
PADG_07418	Superóxido dismutase [Cu-Zn]	12014	1,25	Atividade de superóxido dismutase, ligação de íons metálicos	Sim	*	*	*	*	**
PADG_02652	Grp1p	5794	1,27	Ligação de nucleotídeo, ligação de DNA telomérico de fita simples	*	Sim	*	*	*	**
PADG_01407	Proteína ribossomal 40S	9378	1,28	Ligação de RNA, constituinte estrutural do ribossomo	*	Sim	*	*	*	**

PADG_02017	Calmodulina	43048	1,35	Ligação de íon cálcio	*	Sim	*	Sim	*	**
PADG_08369	Proteína semelhante a Hsp60	17604	1,41	Ligação de origem de replicação de DNA, ligação de DNA de fita simples, ligação de ATP, atividade de ATPase	Sim	Sim	*	*	*	**
PADG_05160	Dipeptidil peptidase 3	2563	1,44	Atividade de dipeptidil-peptidase, ligação de íon metálico	*	Sim	*	Sim	*	**
PADG_07524	Nucleosídeo difosfato quinase	37920	1,47	Atividade de nucleosídeo difosfato quinase, ligação de ATP	Sim	Sim	*	Sim	*	**
PADG_01605	Poliubiquitina	4911	1,48	NDA	*	Sim	*	*	*	**
PADG_03149	Aminopeptidase	2712	1,49	Atividade de metalopeptidase, ligação de íon zinco	*	Sim	*	Sim	Sim	**
PADG_03841	Proteína com domínio de dissulfeto-isomerase	22371	1,60	Atividade de proteína dissulfeto isomerase	*	Sim	*	*	*	**
PADG_07782	Desoxiuridina 5-trifosfato nucleotidohidrolase	7471	1,61	atividade dUTP difosfatase	*	Sim	*	*	*	**
PADG_07420	Transaldolase	7105	1,63	Sedoheptulose-7-fosfato: D-gliceraldeído-3-fosfato gliceronetransferase atividade	*	Sim	*	*	*	**
PADG_04148	Alfa manosidase vacuolar	5961	1,70	Atividade de alfa-manosidase, ligação de íon zinco, ligação de carboidrato	*	Sim	*	*	*	**
PADG_08054	Malato desidrogenase, dependente de NAD	4526	1,81	Atividade de L-malato desidrogenase	Sim	*	Sim	Sim	Sim	**
PADG_02785	Proteína de choque térmico Hsp88	5877	1,83	Ligação de ATP	Sim	Sim	*	Sim	*	**
PADG_00688	Subunidade H de transporte de H + ATPase tipo F	8080	1,96	NDA	*	Sim	*	*	*	**
PADG_05032	Co-chaperona de ligação Hsp90 (Sba1)	8142	2,14	NDA	Sim	*	*	Sim	*	**
PADG_01479	Gama-glutamiltransferase	6243	2,43	Atividade de gama-glutamiltransferase	Sim	*	*	*	*	**
PADG_04059	Enolase	9477	2,52	Ligação de íons de magnésio, atividade de fosfopiruvato hidratase	Sim	Sim	*	Sim	*	**
PADG_01711	Co-chaperona Hsp90 AHA1	11850	2,54	Atividade de ativador ATPase	*	Sim	*	Sim	*	**

PADG_01706	Frutose-1,6-bisfosfatase	13110	2,58	Atividade de frutose 1,6-bisfosfato 1-fosfatase	*	Sim	*	*	*	**
PADG_04710	2-metilcitrato sintase, mitochondrial	17077	2,84	Atividade de citrato (Si)-sintase, atividade de 2-metilcitrato sintase	Sim	Sim	Sim	Sim	Sim	**
PADG_07422	Serino Proteinase	3358	3,06	Atividade de endopeptidase em resíduos de serina	*	Sim	*	*	*	**
PADG_06490	Formamidase	12362	3,15	Atividade de hidrolase, atuando nas ligações carbono-nitrogênio (mas não no peptídeo), em amidas lineares	Sim	Sim	Sim	Sim	Sim	**
PADG_02446	Proteína ribossomal ácida P2 60S	29077	3,61	Constituinte estrutural do ribossomo	*	Sim	*	Sim	*	**
PADG_02735	Componente de proteassomo PRE6	13436	3,91	Atividade de endopeptidase em resíduos de treonina	*	Sim	*	*	*	**
PADG_04288	Endoribonuclease L-PSP	31240	3,94	NDA	*	Sim	*	Sim	Sim	**
PADG_08118	Proteína semelhante a Hsp72	49968	3,97	Ligação de ATP	*	Sim	*	*	Sim	**
PADG_05855	Lactonohidrolase	8467	4,07	NDA	*	*	*	*	*	**
PADG_05750	Subunidade putativa VIa de citocromo c oxidase	23847	5,07	Atividade de citocromo-c oxidase	Sim	Sim	*	*	*	**
PADG_00663	Homosserina desidrogenase	7981	5,12	Atividade da homosserina desidrogenase, ligação a NADP	*	Sim	*	Sim	*	**
PADG_06494	Diidrolipoil desidrogenase	32031	5,37	Atividade de diidrolipoil desidrogenase, atividade de glicina desidrogenase (descarboxilação), atividade de oxoglutarato desidrogenase (transferência de succinila), atividade de piruvato desidrogenase, ligação de flavina adenina dinucleotídeo	Sim	Sim	*	Sim	Sim	**

PADG_05798	Proteína da família de ligação de fita simples de DNA	41240	7,76	Ligação de DNA de fita simples	*	Sim	*	*	*	**
PADG_03559	Citocromo b5 #	17493	30,67	Ligação ao heme, ligação de íon metálico	*	Sim	*	*	*	**
PADG_00210	Glicina desidrogenase	1077	BPS	Atividade da glicina desidrogenase (descarboxilação)	*	Sim	*	*	*	**
PADG_00451	Glicose-6-fosfato isomerase	1011	BPS	Atividade de glicose-6-fosfato isomerase	*	Sim	*	*	*	**
PADG_00615	Subunidade de proteassomo tipo alfa C7	1010	BPS	Atividade de endopeptidase em resíduos de treonina	*	*	*	*	*	**
PADG_00676	Fator de degradação RNAPII def1	1191	BPS	NDA	*	Sim	*	*	*	**
PADG_00822	Glutaminase A	786	BPS	NDA	*	Sim	*	*	*	**
PADG_00912	UDP-galactopiranose mutase	1287	BPS	Atividade de oxidorredutase	*	Sim	*	*	*	**
PADG_01404	Aspartato aminotransferase	740	BPS	L-aspartato: atividade de 2-oxoglutarato aminotransferase, ligação de fosfato de piridoxal, L-fenilalanina: atividade de 2-oxoglutarato aminotransferase	*	Sim	*	*	*	**
PADG_02260	Succinato-CoA ligase [formadora de ADP] subunidade alfa, mitocondrial	2156	BPS	Atividade de ligase, ligação de cofator	*	Sim	*	*	*	**
PADG_02561	ATP sintase subunidade alfa, mitocondrial	2772	BPS	Ligação de ATP, atividade de ATP sintase de transporte de prótons, mecanismo de rotação	*	Sim	*	*	*	**
PADG_02862	Glucano 1,3-beta-glucosidase	1997	BPS	Atividade de 1,3-beta-glucanosiltransferase, atividade de glucano endo-1,3-beta-D-glucosidase	Sim	*	*	*	*	**
PADG_03830	Proteína que interage com actina	637	BPS	NDA	Sim	*	*	*	*	**

PADG_04030	Proteína ribossomal ácida 60S P0	1335	BPS	Constituinte estrutural do ribossomo, ligação de rRNA de subunidade ribossômica grande	*	Sim	*	*	*	**
PADG_04516	Glutamato desidrogenase NADP-específica	1563	BPS	Atividade de glutamato desidrogenase (NAD +)	*	*	Sim	*	*	**
PADG_04588	Proteína ribossomal L22 60S	3027	BPS	Constituinte estrutural do ribossomo	*	Sim	*	Sim	*	**
PADG_04934	Proteína com domínio RNP	919	BPS	Ligação de nucleotídeo, ligação de ácido nucleico	*	*	*	Sim	*	**
PADG_05277	Serina hidroximetiltransferase	655	BPS	Atividade de glicina hidroximetiltransferase, ligação piridoxal fosfato	Sim	*	*	*	*	**
PADG_05321	Nuclease mitocondrial #	1132	BPS	Atividade de endodeoxirribonuclease de DNA de fita simples, ligação de ácido nucleico, atividade de endoribonuclease, ligação de íon metálico	*	Sim	*	*	*	**
PADG_06155	Palmitoil-proteína tioesterase	1632	BPS	Atividade de palmitoil-(proteína) hidrolase	*	Sim	*	*	*	**
PADG_06671	3-isopropilmalato desidrogenase A	1032	BPS	Ligação de íons de magnésio, atividade de 3-isopropilmalato desidrogenase, ligação de NAD	*	Sim	*	*	*	**
PADG_06838	Proteína ribossomal S5 40S	3023	BPS	Ligação de RNA, constituinte estrutural do ribossomo	*	Sim	*	*	*	**
PADG_07888	Fator de iniciação da tradução eucariótica 5ª	4225	BPS	Atividade do fator de iniciação da tradução, atividade do fator de alongamento da tradução, ligação ao ribossomo	Sim	*	*	*	*	**

PADG_08244	Proteína ribossomal ácida P1 60S	14,128	BPS	Constituinte estrutural do ribossomo	*	Sim	*	*	*	**
PADG_08376	Aspartato-semialdeído desidrogenase	2046	BPS	Atividade de N-acetil-gama-glutamil-fosfato redutase, atividade de aspartato-semialdeído desidrogenase, ligação de NADP, ligação de NAD	*	Sim	*	*	*	**
PADG_08391	ATPase da membrana plasmática #	517	BPS	Ligação de ATP, atividade de ATPase de exportação de hidrogênio, mecanismo fosforilativo, ligação de íons metálicos	*	Sim	*	*	*	**
PADG_08466	Homogentisato 1,2-dioxigenase #	784	BPS	Atividade de homogentisado 1,2-dioxigenase	*	*	Sim	*	*	Sim
PADG_08587	Proteína de ligação a FK506	3833	BPS	NDA	*	Sim	*	*	*	**
PADG_11679	Antígeno nuclear de célula em proliferação (pcna)	1358	BPS	Ligação ao DNA, atividade do fator de processabilidade da DNA polimerase	*	Sim	*	*	*	**
PADG_12077	Actina	1073	BPS	Constituinte estrutural do citoesqueleto, ligação de ATP	*	Sim	*	*	*	**
PADG_12253	Proteína ribossomal L3 60S	1229	BPS	Constituinte estrutural do ribossomo, atividade de carbono-enxofre liase	*	Sim	*	*	*	**

A tabela foi organizada em ordem crescente dos valores da razão BPS: Fe;

[a]Código de acesso da proteína no NCBI, disponível em https://www.ncbi.nlm.nih.gov/protein;

[b]Descrição da proteína no banco de dados de *Paracoccidioides* spp., disponível em https://www.uniprot.org/proteomes/?query=paracoccidioides&sort=score;

#Aponta que a proteína potencialmente liga-se a Fe;

[c]O número de *score* de identificação de proteínas é obtido por um processo em múltiplas etapas, realizado pelo PLGS; somente dados com nível de confiança ≥ 95% e *false discovery ratio* ≤ 4% foram utilizados no presente estudo;

[d]Razão entre a quantificação de proteínas identificadas na condição de privação de Fe/presença de Fe. Valores ≥ 2,0 indicam proteínas reguladas positivamente; valores ≤ 0,5 indicam proteínas reguladas negativamente; BPS indica que a proteína foi identificada somente na condição de privação de Fe;

[e]Função molecular descrita no ParaDB, disponível em http://paracoccidioides.com/. NDA indica que não há informações disponíveis em relação às funções moleculares da referida proteína nessa base de dados;

[f]Proteínas identificadas no trabalho de (Weber *et al.*, 2012), disponível em https://journals.plos.org/plosone/article?id=10,1371/journal.pone.0052470. (*) indica que a proteína não foi identificada no estudo citado;

[g]Proteínas identificadas no trabalho de (Vallejo *et al.*, 2012), disponível em https://pubs.acs.org/doi/10.1021/pr200872s. (*) indica que a proteína não foi identificada no estudo citado;

[h]Proteínas identificadas no trabalho de (Chaves *et al.*, 2015), disponível em https://bmcmicrobiol.biomedcentral.com/articles/10.1186/s12866-015-0393-9. (*) indica que a proteína não foi identificada no estudo citado;

[i]Proteínas identificadas no trabalho de (Rodrigues *et al.*, 2018), disponível em https://www.sciencedirect.com/science/article/pii/S187861461830062X?via%3Dihub. (*) indica que a proteína não foi identificada no estudo citado;

[j]Proteínas identificadas no trabalho de (Moreira *et al.*, 2020), disponível em https://www.frontiersin.org/articles/10.3389/fmicb.2019.02968/full. (*) indica que a proteína não foi identificada no estudo citado;

[k]Proteínas preditas como ligantes de Fe de acordo com trabalho de (Tristão *et al.*, 2015), disponível em https://doi.org/10.3389/fmicb.2014,00761. (**) indica que a proteína não foi predita como ligante de Fe no trabalho citado.

Tabela IV. Proteínas reguladas positivamente identificadas no exoproteoma de *P. brasiliensis* (*Pb*18) após cultura de células leveduriformes por 48 horas a 37º C em meio líquido MMcM com privação de Fe (BPS 50 μM) x suplementação de Fe [Fe $(NH_4)_2$ $(SO_4)_2$,$6H_2O$ 10 μM]

Código de acesso[a]	Descrição[b]	Score[c]	BPS:Fe Ratio[d]	SignalP ≥ 0,45[e]	SecretomeP ≥ 0,6[f]	Evidência de secreção na liteatura de *Paracoccidioides* spp,[g]	Função molecular[h]	Weber *et al*., 2012[i]	Vallejo *et al*., 2012[j]	Chaves *et al*., 2015[k]	Rodrigues *et al*., 2018[l]	Moreira *et al*., 2020[m]	Ligante de FE? Tristão *et al*., 2015[n]
PADG_05032	Co-chaperona de ligação Hsp90 (Sba1)	8142	2,14	***	***	-	NDA	Sim	*	*	Sim	*	**
PADG_01479	Gama-glutamiltransferase	6243	2,43	***	***	Bailão *et al*., 2015	Atividade de gama-glutamiltransferase	Sim	*	*	*	*	**
PADG_00921	Proteína hipotética •	3213	2,51	***	***	-	NDA	*	*	*	*	*	**
PADG_04059	Enolase	9477	2,52	***	***	Donofrio *et a.*,, 2009; Nogueira *et al*., 2010; Marcos *et al*., 2012	Ligação de íons de magnésio, atividade de fosfopiruvato hidratase	Sim	Sim	*	Sim	*	**
PADG_01711	Co-chaperona Hsp90 AHA1	11850	2,54	***	***	-	Atividade de ativador ATPase	*	Sim	*	Sim	*	**
PADG_01706	Frutose-1,6-bisfosfatase	13110	2,58	***	***	-	Atividade de frutose 1,6-bisfosfato 1-fosfatase	*	Sim	*	*	*	**
PADG_04710	2-metilcitrato sintase, mitocondrial	17077	2,84	***	***	-	Atividade de citrato (Si)-sintase, atividade de 2-metilcitrato sintase	Sim	Sim	Sim	Sim	Sim	**
PADG_02343	Proteína MYG1 •	7766	2,95	***	***	-	NDA	*	*	*	*	*	**
PADG_07422	Serino Proteinase	3358	3,06	0,669	***	Parente *et al*., 2010; Pigosso *et al*., 2017	Atividade de endopeptidase em resíduos de serina	*	Sim	*	*	*	**
PADG_06490	Formamidase	12362	3,15	***	***	Borges *et al*., 2010	Atividade de hidrolase, atuando nas ligações carbono-nitrogênio (mas não no peptídeo), em amidas lineares	Sim	Sim	Sim	Sim	Sim	**
PADG_02446	Proteína ribossomal ácida P2 60S	29077	3,61	***	***	-	Constituinte estrutural do ribossomo	*	Sim	*	Sim	*	**
PADG_02735	Componente de proteassomo PRE6	13436	3,91	***	***	-	Atividade de endopeptidase em resíduos de treonina	*	Sim	*	*	*	**

PADG_04288	Endoribonuclease L-PSP	31240	3,94	***	0,874	-	NDA	*	Sim	*	Sim	Sim	**
PADG_08118	Proteína semelhante a Hsp72	49968	3,97	***	***	-	Ligação de ATP	*	Sim	*	*	Sim	**
PADG_05855	Lactonohidrolase	8467	4,07	***	***	-	NDA	*	*	*	*	*	**
PADG_11950	Subunidade TFIID / TFIIF do fator de iniciação da transcrição •	13634	4,72	***	***	-	NDA	*	*	*	*	*	**
PADG_05750	Subunidade putativa VIa de citocromo c oxidase	23847	5,07	***	0,722	-	Atividade de citocromo-c oxidase	Sim	Sim	*	*	*	**
PADG_00663	Homosserina desidrogenase	7981	5,12	***	0,651	-	Atividade da homosserina desidrogenase, ligação a NADP	*	Sim	*	Sim	*	**
PADG_06494	Diidrolipoil desidrogenase	32031	5,37	***	***	Landgraf *et al*., 2017	Atividade de diidrolipoil desidrogenase, atividade de glicina desidrogenase (descarboxilação), atividade de oxoglutarato desidrogenase (transferência de succinila), atividade de piruvato desidrogenase, ligação de flavina adenina dinucleotídeo	Sim	Sim	*	Sim	Sim	**
PADG_05798	Proteína da família de ligação de fita simples de DNA	41240	7,76	***	0,809	-	Ligação de DNA de fita simples	*	Sim	*	*	*	**
PADG_03559	Citocromo b5 #	17493	30,67	***	0,688	-	Ligação ao heme, ligação de íon metálico	*	Sim	*	*	*	**
PADG_00026	Citidina desaminase •	4546	BPS	***	***	-	Atividade de citidina desaminase, ligação de íon zinco	*	*	*	*	*	**
PADG_00060	Proteína MGS207 •	1122	BPS	***	***	-	NDA	*	*	*	*	*	**
PADG_00210	Glicina desidrogenase	1077	BPS	***	***	-	Atividade da glicina desidrogenase (descarboxilação)	*	Sim	*	*	*	**
PADG_00211	Proteína que contém domínio DUF427 •	3310	BPS	***	***	-	NDA	*	*	*	*	*	**

PADG_00220	Fator de transcrição da família CBF/NF-Y •	1323	BPS	***	***	-	Ligação do promotor do núcleo, atividade do fator de transcrição da RNA polimerase II, ligação da proteína da classe TBP, envolvida na montagem do complexo de pré-iniciação, ligação da cromatina, atividade do coativador da transcrição, atividade do corepressor da transcrição	*	*	*	*	*	**
PADG_00451	Glicose-6-fosfato isomerase	1011	BPS	***	***	-	Atividade de glicose-6-fosfato isomerase	*	Sim	*	*	*	**
PADG_00514	Proteína ribossomal L16 60S •	1435	BPS	***	***	-	Constituinte estrutural do ribossomo	*	*	*	*	*	**
PADG_00615	Subunidade de proteassomo tipo alfa C7	1010	BPS	***	***	-	Atividade de endopeptidase em resíduos de treonina	*	*	*	*	*	**
PADG_00676	Fator de degradação RNAPII def1	1191	BPS	***	***	-	NDA	*	Sim	*	*	*	**
PADG_00809	Enzima de conjugação de ubiquitina •	2155	BPS	***	0,825	-	NDA	*	*	*	*	*	**
PADG_00822	Glutaminase A	786	BPS	0,730	***	-	NDA	*	Sim	*	*	*	**
PADG_00888	Argininosuccinato sintase •	804	BPS	***	***	-	Atividade de argininosuccinato sintase, ligação de ATP	*	*	*	*	*	**
PADG_00912	UDP-galactopiranose mutase	1287	BPS	***	***	-	Atividade de oxidorredutase	*	Sim	*	*	*	**
PADG_00988	Ribonuclease T2 •	923	BPS	***	0,614	-	Ligação de RNA, atividade de ribonuclease T2	*	*	*	*	*	**
PADG_01404	Aspartato aminotransferase	740	BPS	***	0,662	-	L-aspartato: atividade de 2-oxoglutarato aminotransferase, ligação de fosfato de piridoxal, L-fenilalanina: atividade de 2-oxoglutarato aminotransferase	*	Sim	*	*	*	**

PADG_01626	Proteína doadora de ferro CyaY •#	5703	BPS	***	***	-	Atividade de ferroxidase, ligação de ferro férrico	*	*	*	*	*	**
PADG_01644	Proteína v-SNARE vti1 de transporte de vesículas •	1227	BPS	***	***	-	NDA	*	*	*	*	*	**
PADG_01654	Proteína ribossômica 40S S6-A •	1333	BPS	***	***	-	Constituinte estrutural do ribossomo	*	*	*	*	*	**
PADG_01665	Quinurenina-oxoglutarato transaminase •	1278	BPS	***	***	-	Atividade de quinurenina-oxoglutarato transaminase, ligação de fosfato de piridoxal, atividade de 2-aminoadipato transaminase	*	*	*	*	*	**
PADG_01871	3-oxoacil-(Acil-carreadora-proteína) redutase •	1652	BPS	***	0,895	-	NDA	*	*	*	*	*	**
PADG_01949	Fator de alongamento de tradução Tu •	2648	BPS	***	0,751	Marcos *et al*., 2016; Marcos *et al*., 2019	Atividade de fator de alongamento de tradução, atividade de GTPase, ligação de GTP	*	*	*	*	*	**
PADG_02260	Succinato-CoA ligase [formadora de ADP] subunidade alfa, mitocondrial	2156	BPS	***	0,644	-	Atividade de ligase, ligação de cofator	*	Sim	*	*	*	**
PADG_02561	ATP sintase subunidade alfa, mitocondrial	2772	BPS	***	***	-	Ligação de ATP, atividade de ATP sintase de transporte de prótons, mecanismo de rotação	*	Sim	*	*	*	**
PADG_02763	Subunidade reguladora de quinase dependente de ciclina •	3528	BPS	***	0,773	-	Atividade de quinase, atividade reguladora de proteína serina/treonina quinase dependente de ciclina	*	*	*	*	*	**
PADG_02845	Proteína de manutenção de estado diplóide chpA •	1291	BPS	***	0,829	-	NDA	*	*	*	*	*	**
PADG_02862	Glucano 1,3-beta-glucosidase	1997	BPS	0,871	***	-	Atividade de 1,3-beta-glucanosiltransferase, atividade de glucano endo-1,3-beta-D-glucosidase	Sim	*	*	*	*	**
PADG_03121	Proteína hipotética •	1070	BPS	***	0,811	-	NDA	*	*	*	*	*	**
PADG_03278	Inositol-3-fosfato sintase •	885	BPS	***	0,640	-	Atividade de inositol-3-fosfato sintase	*	*	*	*	*	**
PADG_03526	Proteína com repetição de M •	637	BPS	***	***	-	NDA	*	*	*	*	*	**

PADG_03778	Proteína ribossomal 60S L10-A •	1463	BPS	***	0,678	-	Constituinte estrutural do ribossomo	*	*	*	*	*	**
PADG_03830	Proteína que interage com actina	637	BPS	***	***	-	NDA	Sim	*	*	*	*	**
PADG_03852	Proteína membro da família LiPid Depleted •#	779	BPS	***	0,692	-	Ligação de íons de ferro, ligação de cluster de ferro-enxofre	*	*	*	*	*	Sim
PADG_03856	Proteína ribossomal L15 60S •	1833	BPS	***	***	-	Constituinte estrutural do ribossomo	*	*	*	*	*	**
PADG_04030	Proteína ribossomal ácida 60S P0	1335	BPS	***	***	-	Constituinte estrutural do ribossomo, ligação de rRNA de subunidade ribossômica grande	*	Sim	*	*	*	**
PADG_04242	Sulfidril oxidase •	5011	BPS	***	***	-	Atividade de tiol oxidase	*	*	*	*	*	**
PADG_04475	Proteína ribossomal S36, mitocondrial •	3489	BPS	***	0,791	-	NDA	*	*	*	*	*	**
PADG_04516	Glutamato desidrogenase NADP-específica	1563	BPS	***	***	-	Atividade de glutamato desidrogenase (NAD +)	*	*	Sim	*	*	**
PADG_04588	Proteína ribossomal L22 60S	3027	BPS	***	***	-	Constituinte estrutural do ribossomo	*	Sim	*	Sim	*	**
PADG_04934	Proteína com domínio RNP	919	BPS	***	***	-	Ligação de nucleotídeo, ligação de ácido nucleico	*	*	*	Sim	*	**
PADG_05239	Cofator A de ligação à tubulina •	2900	BPS	***	***	-	NDA	*	*	*	*	*	**
PADG_05277	Serina hidroximetiltransferase	655	BPS	***	***	-	Atividade de glicina hidroximetiltransferase, ligação piridoxal fosfato	Sim	*	*	*	*	**
PADG_05321	Nuclease mitocondrial #	1132	BPS	***	***	-	Atividade de endodeoxirribonuclease de DNA de fita simples, ligação de ácido nucleico, atividade de endoribonuclease, ligação de íon metálico	*	Sim	*	*	*	**
PADG_05683	Proteína de controle de divisão celular 48•	1683	BPS	***	***	-	Ligação de ATP, atividade reguladora de proteína fosfatase tipo 1, atividade de ATPase	*	*	*	*	*	**
PADG_06155	Palmitoil-proteína tioesterase	1632	BPS	0,808	***	-	Atividade de palmitoil-(proteína) hidrolase	*	Sim	*	*	*	**

PADG_06273	Calcineurina subunidade B •	2812	BPS	***	***	-	Atividade de fosfoproteína fosfatase, ligação de íons de cálcio, atividade reguladora de proteína serina / treonina fosfatase dependente de cálcio	*	*	*	*	*	**
PADG_06382	3-metil-2-oxobutanoato hidroximetiltransferase •	711	BPS	***	0,685	-	Atividade de transferase, transferência de grupos acil diferentes dos grupos amino-acil	*	*	*	*	*	**
PADG_06671	3-isopropilmalato desidrogenase A	1032	BPS	***	***	-	Ligação de íons de magnésio, atividade de 3-isopropilmalato desidrogenase, ligação de NAD	*	Sim	*	*	*	**
PADG_06726	Proteína ribossomal L17 60S •	1694	BPS	***	0,869	-	Constituinte estrutural do ribossomo	*	*	*	*	*	**
PADG_06838	Proteína ribossomal S5 40S	3023	BPS	***	0,632	-	Ligação de RNA, constituinte estrutural do ribossomo	*	Sim	*	*	*	**
PADG_06997	Proteína de ligação ao cap nuclear •	2485	BPS	***	0,665	-	Ligação de nucleotídeo, ligação de ácido nucleico, atividade de peptidil-prolil cis-trans isomerase	*	*	*	*	*	**
PADG_07264	Proteína de domínio barrel A/B responsiva ao estresse •	3637	BPS	***	***	-	NDA	*	*	*	*	*	**
PADG_07870	Proteína ribossomal S7 30S •	1112	BPS	***	***	-	Constituinte estrutural do ribossomo	*	*	*	*	*	**
PADG_07888	Fator de iniciação da tradução eucariótica 5A	4225	BPS	***	***	-	Atividade do fator de iniciação da tradução, atividade do fator de alongamento da tradução, ligação ao ribossomo	Sim	*	*	*	*	**
PADG_08045	Aminotransferase de aminoácidos de cadeia ramificada •	795	BPS	***	0,682	-	Atividade de transaminase de aminoácidos de cadeia ramificada	*	*	*	*	*	**
PADG_08098	Adenilato quinase 1•	1995	BPS	***	0,666	-	Atividade de adenilato quinase, ligação de ATP	*	*	*	*	*	**

PADG_08108	Coproporphyrinogen III oxidase •#	1114	BPS	***	***	-	Coproporfirinogênio III oxidase	*	*	*	*	*	**
PADG_08212	Proteína hipotética •	4444	BPS	***	0,637	-	NDA	*	*	*	*	*	**
PADG_08244	Proteína ribossomal ácida P1 60S	14,128	BPS	***	***	-	Constituinte estrutural do ribossomo	*	Sim	*	*	*	**
PADG_08270	Proteína contendo domínio UBX •#	1143	BPS	***	0,891	-	Ligação de íons metálicos	*	*	*	*	*	**
PADG_08328	5-metiltetrahidropteroiltriglutamato-homocisteína S-metiltransferase •	756	BPS	***	***	-	Atividade de 5-metiltetrahidropteroiltriglutamato-homocisteína S-metiltransferase, ligação de íon zinco	*	*	*	*	*	**
PADG_08376	Aspartato-semialdeído desidrogenase	2046	BPS	***	0,618	-	Atividade de N-acetil-gama-glutamil-fosfato redutase, atividade de aspartato-semialdeído desidrogenase, ligação de NADP, ligação de NAD	*	Sim	*	*	*	**
PADG_08391	ATPase da membrana plasmática #	517	BPS	***	0,715	-	Ligação de ATP, atividade de ATPase de exportação de hidrogênio, mecanismo fosforilativo, ligação de íons metálicos	*	Sim	*	*	*	**
PADG_08466	Homogentisato 1,2-dioxigenase #	784	BPS	***	0,601	-	Atividade de homogentisado 1,2-dioxigenase	*	*	Sim	*	*	Sim
PADG_08468	4-hidroxifenilpiruvato dioxigenase •#	897	BPS	***	***	-	Atividade 4-hidroxifenilpiruvato dioxigenase, ligação de íons metálicos	*	*	*	*	*	Sim
PADG_08587	Proteína de ligação a FK506	3833	BPS	0,869	***	-	NDA	*	Sim	*	*	*	**
PADG_08599	Proteína com domínio DnaJ •	1141	BPS	***	***	-	NDA	*	*	*	*	*	**
PADG_11679	Antígeno nuclear de célula em proliferação (pcna)	1358	BPS	***	***	-	Ligação ao DNA, atividade do fator de processabilidade da DNA polimerase	*	Sim	*	*	*	**

PADG_11711	RNA helicase dependente de ATP eIF4A •	1151	BPS	***	***	-	Ligação de ácido nucleico, atividade de helicase, ligação de ATP	*	*	*	*	*	**
PADG_12077	Actina	1073	BPS	***	***	-	Constituinte estrutural do citoesqueleto, ligação de ATP	*	Sim	*	*	*	**
PADG_12252	Proteína da família de enzimas fosfotransferases •	987	BPS	***	***	-	NDA	*	*	*	*	*	**
PADG_12253	Proteína ribossomal L3 60S	1229	BPS	***	***	-	Constituinte estrutural do ribossomo, atividade de carbono-enxofre liase	*	Sim	*	*	*	**
PADG_12365	Proteína ribossomal 40S S8-A •	890	BPS	***	0,792	-	Constituinte estrutural do ribossomo	*	*	*	*	*	**

A tabela foi organizada em ordem crescente dos valores da razão BPS: Fe;

[a]Código de acesso da proteína no NCBI, disponível em https://www.ncbi.nlm.nih.gov/protein;

[b]Descrição da proteína no banco de dados de *Paracoccidioides* spp, disponível em https://www.uniprot.org/proteomes/?query=paracoccidioides&sort=score;

•Aponta que a proteína foi identificada exclusivamente no presente trabalho;

#Aponta que a proteína potencialmente liga-se a Fe;

[c]O número de *score* de identificação de proteínas é obtido por um processo em múltiplas etapas, realizado pelo PLGS; somente dados com nível de confiança ≥ 95% e *false discovery ratio* ≤ 4% foram utilizados no presente estudo;

[d]Razão entre a quantificação de proteínas identificadas na condição de privação de Fe/presença de Fe. Valores ≥ 2,0 indicam proteínas reguladas positivamente; BPS indica que a proteína foi identificada somente na condição de privação de Fe;

[e]Predição da presença de peptídeo sinal; cujo valor *score* deve ser ≥ 0,45; predição realizada pela ferramenta on-line SignalP 4.1 disponível em http://www.cbs.dtu.dk/services/SignalP-4.1/; (***) indica que não houve predição de presença peptídeo sinal;

[f]Predição de secreção de proteínas por vias não-clássicas, cujo valor de *score* deve ser ≥ 0,6; predição realizada pela ferramenta on-line SecretomeP 2.0 disponível em http://www.cbs.dtu.dk/services/SecretomeP/. (***) indica que a proteína não foi predita como secretada;

[g]Evidência de secreção de proteínas na literature de *Paracoccidioides* spp. Buscas foram realizadas no repositório de dados PUBMED no período entre 07/2019 – 05/2021. Os termos utilizados nas buscas foram aqueles presentes na coluna "descrição" + Paracoccidioides, (-) indica que evidências de secreção da proteína em questão não foram encontradas na literatura;

[h]Função molecular descrita no ParaDB, disponível em http://paracoccidioides.com/. NDA indica que não há informações disponíveis em relação às funções moleculares da referida proteína nessa base de dados;

[i]Proteínas identificadas no trabalho de (Weber *et al.*, 2012), disponível em https://journals.plos.org/plosone/article?id=10,1371/journal.pone.0052470. (*) indica que a proteína não foi identificada no estudo citado;

[j]Proteínas identificadas no trabalho de (Vallejo *et al.*, 2012), disponível em https://pubs.acs.org/doi/10.1021/pr200872s. (*) indica que a proteína não foi identificada no estudo citado;

[k]Proteínas identificadas no trabalho de (Chaves *et al.*, 2015), disponível em https://bmcmicrobiol.biomedcentral.com/articles/10.1186/s12866-015-0393-9. (*) indica que a proteína não foi identificada no estudo citado;

[l]Proteínas identificadas no trabalho de (Rodrigues *et al.*, 2018), disponível em https://www.sciencedirect.com/science/article/pii/S187861461830062X?via%3Dihub. (*) indica que a proteína não foi identificada no estudo citado;

[m]Proteínas identificadas no trabalho de (Moreira *et al.*, 2020), disponível em https://www.frontiersin.org/articles/10.3389/fmicb.2019.02968/full. (*) indica que a proteína não foi identificada no estudo citado;

[n]Proteínas preditas como ligantes de Fe de acordo com trabalho de (Tristão *et al.*, 2015), disponível em https://doi.org/10.3389/fmicb.2014,00761. (**) indica que a proteína não foi predita como ligante de Fe no trabalho citado.

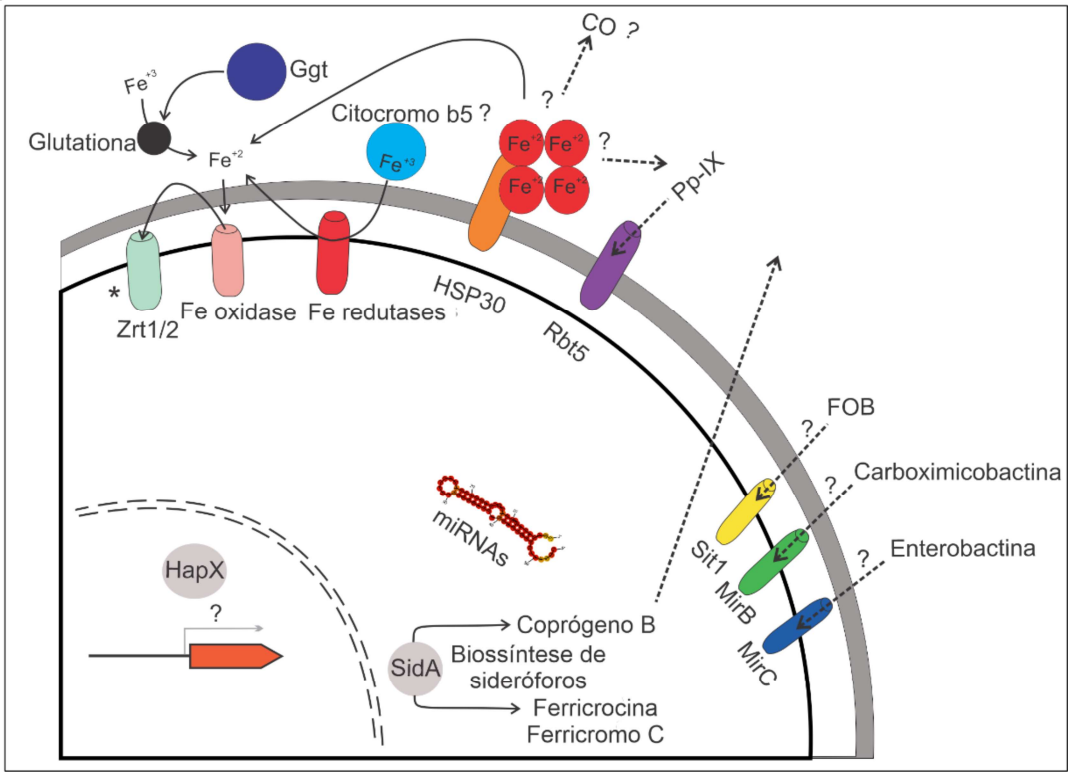

Representação esquemática de mecanismos de captação de Fe por *Paracoccidioides* spp. *Paracoccidioides* emprega como mecanismos de alta afinidade e especificidade para captação de Fe: (1) a captação de heme mediada pelo receptor Rbt5 (HSP30 atuaria como heme oxigenase atuando nos grupos heme contidos na hemoglobina, promovendo a liberação de Fe^{2+} para a via redutiva de assimilação de Fe, Pp-IX para internalização via Rbt5 e CO?); (2) a biossíntese e captação de sideróforos/xenosideróforos (os receptores de sideróforos Sit1, MirB e MirC possuem maior afinidade por diferentes classes moleculares de sideróforos?) e, (3) uma via redutiva não canônica (*por empregar Fe/Zn permeases e não uma Fe permeasse específica) de assimilação de Fe (seria esta via alimentada por proteínas secretadas reguladas positivamente na privação de Fe, como a Citocromo b5 identificada no exoproteoma?). Salienta-se que ainda faz-se necessário a definição de HapX como fator de transcrição regulador da resposta de *Paracoccidioides* spp. à privação de Fe. FOB: Ferrioxamina B. Ggt: Gama-glutamiltransferase. CO: Monóxido de carbono. Pp-IX: Protoporfirina IX. Adaptado de Souza *et al*., 2020.